REPORT NO.
UCB/EERC-88/01
JANUARY 1988

EARTHQUAKE ENGINEERING RESEARCH CENTER

SEISMIC BEHAVIOR OF CONCENTRICALLY BRACED STEEL FRAMES

by

IBRAHIM F. KHATIB
STEPHEN A. MAHIN
KARL S. PISTER

Report to the National Science Foundation

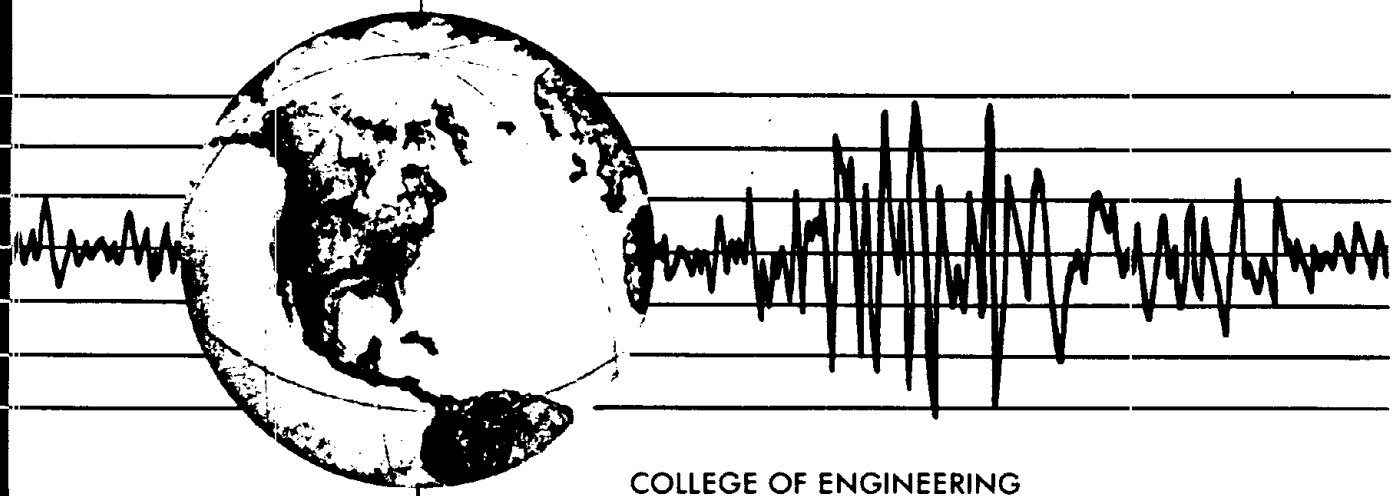

COLLEGE OF ENGINEERING

UNIVERSITY OF CALIFORNIA AT BERKELEY

For sale by the National Technical Information Service, U.S. Department of Commerce, Springfield, Virginia 22161

See back of report for up to date listing of EERC reports.

50272-101

REPORT DOCUMENTATION PAGE	1. REPORT NO. NSF/ENG-88040	2.	3. PB91-210898

4. Title and Subtitle
"Seismic Behavior of Concentrically Braced Steel Frames."

5. Report Date
January 1988

6.

7. Author(s)
I. Khatib, S. Mahin, and K. Pister

8. Performing Organization Rept. No.
UCB/EERC-88/01

9. Performing Organization Name and Address
Earthquake Engineering Research Center
University of California, Berkeley
1301 S 46th St.
Richmond, CA 94804

10. Project/Task/Work Unit No.

11. Contract(C) or Grant(G) No.
(C)
(G) CEE-8414904

12. Sponsoring Organization Name and Address
National Science Foundation
1800 G. St. NW
Washington, DC 20550

13. Type of Report & Period Covered

14.

15. Supplementary Notes

16. Abstract (Limit: 200 words)

Concentrically braced steel frames designed by conventional methods may exhibit several undesirable modes of behavior. Chevron-braced frames have an inelastic cyclic behavior that is often characterized by rapid redistribution of internal forces, a deterioration of strength, a tendency of form soft stories, and fracture due to excessive deformation demand. Parameters having a significant influence on these phenomena are identified. Recommendations are offered related to preferable ranges of brace slenderness, approaches for designing beams, and a simplified capacity design approach for proportioning columns and connections. Optimization techniques are applied to the design of chevron-braced to improve their seismic reponse. Further improvements related to changes in structural systems are presented. These include the use of double story X-braced framing, incorporation of a secondary moment resisting frame, and the use of braces in a V configuration. Each of these approaches has advantages in certain circumstances. Each has disadvantages which are examined using results of analytical parametric studies. The basis of a new structural system which incorporates vertical linkage elements in a conventional chevron-braced frame and appears to overcome in an economical and practical way many of the deficiencies of chevron-braced frames is examined and its effectiveness demonstrated.

17. Document Analysis a. Descriptors
concentrically braced
chevron-braced
X-braced
seismic

b. Identifiers/Open-Ended Terms
steel frames

c. COSATI Field/Group

18. Availability Statement
Release Unlimited

19. Security Class (This Report) unclassified

20. Security Class (This Page) unclassified

21. No. of Pages 230

22. Price

(See ANSI-Z39.18) *See Instructions on Reverse*

OPTIONAL FORM 272 (4-77)
(Formerly NTIS-35)
Department of Commerce

i.a

SEISMIC BEHAVIOR OF CONCENTRICALLY BRACED STEEL FRAMES

by

Ibrahim F. Khatib

Stephen A. Mahin

Karl S. Pister

A Report on Research Conducted
under Grant CEE-8414904 from
the National Science Foundation

Report No. UCB/EERC-88/01
Earthquake Engineering Research Center
University of California
Berkeley, California

January 1988

ABSTRACT

Concentrically braced steel frames designed by conventional methods may exhibit several undesirable modes of behavior. In particular, chevron-braced frames have an inelastic cyclic behavior that is often characterized by a rapid redistribution of internal forces, a deterioration of strength, a tendency to form soft stories, and fracture due to excessive deformation demand. Through analytical studies and numerical simulations, parameters having a significant influence on these phenomena are identified. Recommendations are offered related to preferable ranges of brace slenderness, approaches for designing beams, and a simplified capacity design approach for proportioning columns and connections. Optimization techniques are applied to the design of chevron-braced frames to improve their seismic response. Further improvements related to changes in structural systems are presented and discussed. These include the use of double story X-braced framing, incorporation of a secondary moment resisting frame, and the use of braces in a V configuration. Each of these approaches has been investigated and each has advantages in certain circumstances. Each also has disadvantages which are examined using results of analytical parametric studies. A new structural system which incorporates vertical linkage elements in a conventional chevron-braced frame appears to overcome in an economical and practical way many of the deficiencies of chevron-braced frames. The basis of this system is examined, its effectiveness is demonstrated using analytical results, and finally, further research directions are outlined.

ACKNOWLEDGEMENTS

The study reported herein was supported by the National Science Foundation grant CEE-8414904. This support is gratefully acknowledged. The views presented herein, however, are those of the authors and not necessarily those of the National Science Foundation.

TABLE OF CONTENTS

NOTATION

A	=	Cross sectional area
E	=	Modulus of elasticity
F_c	=	Story shear at impending buckling
H_i	=	Story height above base
I	=	Moment of inertia of cross-section
K_0	=	Story stiffness
K_{bb}	=	Buckled brace contribution to story stiffness
K_{bm}	=	Beam stiffness at midspan
K_{br}	=	Brace contribution to story stiffness
K_{fr}	=	Frame contribution to story drift stiffness
K_e	=	Story stiffness with one brace buckled
L	=	Member length
M_o	=	Story overturning moment
M_p	=	Plastic moment of beam
$\bar{P}$	=	Mean peak column compression
P_c	=	Brace buckling load
P_{ct}	=	Column tension
P_{CAP}	=	Yield compression strength of column
P_D	=	Dynamic unbalance component of braced bay column compression
P_g	=	Gravity component of braced bay column compression
P_{gi}	=	Midspan conc. load equiv. to uniform gravity loads at story i
P_o	=	Overturning moment component of braced bay column compression
P_T	=	Total estimated column compression (SRSS approach)
P_{ud_i}	=	Upper bound on dyn. unb. force from braces of story i
P_{un}	=	Unbalance load at beam midspan
P_y	=	Tension yield force
d	=	Depth of section
k	=	Effective length factor of the brace
r	=	Governing radius of gyration of cross-section
w_g	=	Total distributed gravity service load at story i
γ	=	New cross-section factor
η	=	Shape factor of cross-section
λ	=	Brace slenderness
Θ	=	Angle of inclination of brace

CHAPTER 1

INTRODUCTION

1.1. NATURE OF THE PROBLEM

Concentrically braced steel frames are often used in the construction of multistory high rise buildings. Compared with moment resisting frames, braced frames are more efficient in providing the strength required to resist lateral loads and the stiffness needed to limit story drifts. The technique used for their design is usually an allowable stress approach. It consists of a static elastic analysis for distributed lateral loads in addition to the service level vertical gravity loads. Structural elements are then proportioned on the basis of allowable stresses. Initially developed to account for wind loading, this design technique is also used for earthquake resistant design. Even though significant inelastic deformations are anticipated in braced frames in the event of major earthquake shaking, this design approach has not been seriously questioned until recently; most seismically resistant design codes still recommend equivalent static lateral loads corresponding to the elastic range of behavior.

Studies on the seismic response of braced frames progressed slowly until the 1970's. The expansion of offshore oil exploration in regions of seismic risk stimulated analytical and experimental investigations of the inelastic cyclic response of tubular steel braced structures [6]. At the same time, evidence was accumulating that buildings with braced frames were being damaged during major earthquakes in the United States [74], Japan [85] and more recently in Mexico [8]. These events motivated an increasing number of studies on the inelastic behavior of steel braced frames both analytically and experimentally. A good deal of this research effort has focused on the study of individual brace behavior. Braced frames, when studied, were often simple one bay one story structures, and were used to explore the effect of end restraints on the behavior of braces. Comparatively fewer studies have been oriented towards understanding the behavior of multistory braced frames acting as a system. Consequently, numerous questions still exist regarding the influence of various design parameters on the response of steel braced frames and many uncertainties remain regarding the adequacy of current design methods.

In the remainder of this chapter some results of the most relevant analytical and experimental studies concerning braces and concentrically braced building frames are reviewed, and their influence on current code provisions is examined. After summarizing the points on which all studies agree, conflicting and controversial items are

identified. These unresolved items form the basis of the research objectives for this study. A detailed research plan is presented at the end of this chapter.

1.2. ANALYTICAL STUDIES

In one of the first analytical studies of frame response Workman [94] analyzed a ten story X braced, single bay building frame using an elasto-plastic tension only model to represent brace behavior. This model roughly approximated the hysteretic behavior of very slender braces. Nonetheless it gave valuable insights into the differences between the elastic and inelastic response of simple braced frames.

Jain, Goel and Hanson [38] studied the response of seven story frames with X, chevron and eccentric (split-K) bracing. Two variants of the chevron-braced frames were investigated; one with "weak girders" and "strong braces" and one with "weak girders" and "weak braces". The quoted adjectives "weak" and "strong" are intended to emphasize the fact that different authors associate different meanings to these terms. For each type of bracing system, two brace slendernesses (60 and 120) were investigated. In the first phase of this investigation, only the elastic responses were compared. In the second phase, the inelastic responses were compared for a single triangular base acceleration pulse with a 1.5 g magnitude and a duration of 1/15 of the structures' fundamental periods. In the third phase, only the seismic inelastic response of eccentrically braced (split K) systems was studied. The comparison quantities were the maximum story displacements, the maximum story shears, axial forces in columns and braces, member ductilities, displacement and plastification histories. This study concluded that stocky braces of $\lambda \leq 60$ should be treated as having fixed ends, while slender braces of $\lambda \geq 120$ can be considered as pin-ended. It found that chevron-braced frames with "weak beams" suffer considerable plastification in columns and bracing members, irrespective of brace strength. In a subsequent study, Singh [77] used a single story, single bay, chevron-braced frame to compare the inelastic dynamic response obtained with various phenomenological models developed up to that time. He concluded that the response predictions are very sensitive to the type of model used.

Jain and Goel [39] studied the response of two seven story, chevron-braced frames subjected to a real and an artificial earthquake ground motion record. One frame was designed as having "weak girders" and braces with intermediate slenderness; the other had "strong beams" and "weak braces" (slender braces with a reduced buckling load). The study concluded that stocky braces increase the ductility demand in girders, columns and braces. They found that a "strong girder-weak

brace" design induces a better distribution of yielding over the height of the structure. They also found that braces rarely yield in tension. Story displacements were found to increase with increasing brace slenderness.

The response of several ten story, chevron-braced frames designed according to different philosophies were studied by Nilforoushan [55]. In one frame (C) the bracing members were considered as secondary elements ("strong beam-weak brace" design). In the second frame (F) the bracing members were considered as main elements statically supporting the beam at midspan ("weak beam-strong brace" design). The third frame (FM) was designed similar to the second, except that it did not take advantage of the 33% increase in allowable stresses for the braces for earthquake loads. An X braced frame was considered for comparison. Nilforoushan found that compared to a "strong beam-weak brace" design, the "weak beam-strong brace" design had lighter girders, but suffered larger story displacements and accelerations, and larger column axial forces in the upper stories. Braces in the "weak beam-strong brace" design never yielded in tension. Compared to the other two designs, the conservatively designed "weak beam-strong brace" (FM) frame had smaller story displacements, less energy dissipation in girders and braces, but greater column axial forces. Compared to the chevron-braced frames, the X braced frame had a longer fundamental period, more energy input, less energy dissipation, larger column ductility demands in lower floors and smaller beam ductility demands in the upper floors. Goel [28] studied the combined effect of horizontal and vertical ground excitation from the 1940 El Centro earthquake on six story frames using chevron and split X bracing. He concluded that split X systems are more sensitive to the vertical component of ground acceleration than chevron-braced systems. For horizontal excitation only, they induce less yielding than chevron bracing, but for combined vertical and horizontal input they cause more ductility demand in the columns.

Anderson [3] studied the inelastic response of three variants of a ten story chevron-braced frame designed according to the "weak beam-strong brace" concept. The first frame had a single chevron-braced bay over its entire height. The second frame was similar to the first except for the addition of a top hat truss. The third frame was similar to the first except for a soft first story obtained by deleting the bracing in the first story. He concluded that chevron bracing is effective in limiting story drift in the inelastic range. Inelastic deformations tended to concentrate in the soft stories (first story of the third frame). The outrigger truss improved the response by transfering overturning axial forces from the interior columns to the exterior ones. This increased the moment resisting capacity of the interior columns,

and the overturning moment capacity of the frame.

Ikeda [35] developed a "refined physical theory" brace model and used it to reproduce experimental results already obtained for an offshore platform model, and for a six story chevron-braced steel frame. He conducted parametric studies to select the best analysis strategy and to investigate the governing design parameters for chevron-braced frames. He found the response to be extremely sensitive to the characteristics of earthquake ground motions. In addition, the response was found sensitive to brace parameters in cases where a "weak" moment resisting frame was used; when inelastic deformations spread over braces, beams and columns. He noted that the effects of brace slenderness and of brace buckling strength could be separated. For example, at constant brace slenderness increasing the brace buckling load reduced the occurrence of inelastic behavior. At constant buckling capacity, large slenderness braces caused an increase in story stiffness and beams plastification, but they reduced the occurrence of tension yielding in braces. Small slenderness braces provided the structure with more ductility capacity.

Shibata and Wakabayashi [88] studied the response of a chevron-braced one story one bay frame to alternating cyclic deformation. They concluded that the strength deteriorates under constant amplitude repeated deformation. The rate of strength deterioration was linked to the stiffness of the beam and the slenderness of the braces, being larger for slender braces in combination with flexible beams, than for stocky braces and stiff beams. Most of the deterioration occurs in the first hysteresis cycle. Tsugawa et al [87] analysed chevron-braced frames of different proportions and concluded that a stiff beam allows story strength to increase after brace buckling, while with a flexible beam the ultimate strength is lower than that at first buckling. Sakamoto [70] conducted a Monte Carlo simulation of a three bay multistory X braced frame for four different brace slendernesses (λ = 0,46,93,183). Each frame was subjected to twenty artificial earthquake records. He concluded that except for displacements the response in general becomes more irregular with increasing frame contribution to the lateral load resisting system. However, he recommended that the frame participation be kept over 50%. Inoue [34] analyzed a ten story X braced frame proportioned by plastic design. He concluded that lateral story displacements become smaller and more uniform as brace slenderness increased. Fujiwara [24] studied the response of a seven story X braced frame subjected to five artificial earthquakes. He observed that maximum story drifts increased with increasing brace slenderness. He explained this phenomenon by the fact that the increased column compression that is associated with slender braces

favors a cantilever bending mode of deformation of the frame as a whole. He recommended a gradual reduction of brace stiffness over the height of the structure such that the top story braces have 30 to 40% the stiffness of the first story braces.

Design codes [6] for fixed offshore structures to be located in regions of seismic hazard stipulate that the inelastic response of the structure be explicitly calculated to demonstrate structural integrity during rare and unusually severe seismic events. Considerable research has been carried out to develop analytical tools to perform these computations, and numerous investigations of braced platform performance have been undertaken [95]. However, as these structures often differ in many significant ways from building frames, this material will not be reviewed herein.

1.3. EXPERIMENTAL STUDIES

Wakabayashi et al. [89] subjected a one story one bay X braced frame to alternating cyclic loading. They used various types of braces: H sections, tube sections and built up sections. They compared the hysteresis behavior of the different brace types and examined the effect of end restraints. They found that slender braces resulted in significantly pinched hysteresis loops for the structure as a whole. Takane and Tokyama [84] also tested a one story one bay chevron-braced frame subjected to alternating cyclic loading. For the stocky braces used, they concluded that unless the beam is very stiff, the maximum strength deteriorates with repeated cycling.

Fukuta et al. [25] subjected a three story, two bay chevron-braced frame to alternating cyclic deformation. They found that the composite (steel and concrete) beams were very ductile, and that the brace buckling load was correctly predicted by assuming the effective length factor (k) for the brace equal to unity. However, the shape of the hysteresis loops corresponded more to a k between 0.50 and 0.65. Takanashi and Ohi [83] carried shaking table tests on three story models of unbraced and X braced frames. They concluded that braces reduce story drift considerably even if they buckle. Ghanaat and Clough [26] performed shaking table tests on a moment resisting frame X braced with rods, pipes and double angles. They concluded that rods are undesirable for bracing. Even if pretensioned, they tend to slacken after a few cycles and impose impact loading on the frame as they pick up tension again. Their failure tends to be brittle (by fracture). Double angles and pipes are to be preferred for their good energy dissipation capacity, especially if they are of low slenderness ($Pc/Py > 0.5$). Astaneh-Asl, Goel and Hanson [10] observed that in an X-braced building frame the gusset plate joining braces at their

intersection causes uncertain end conditions for brace segments and hence unpredictable behavior in compression.

Clough and Ghanaat [27] performed shaking table tests on a 5/48 scale model of an X braced offshore platform frame made of tubular members. Quasistatic and pseudo-dynamic tests [95] of a similar X braced frame were also performed. These studies found that small brace slenderness and careful detailing provided full hysteresis loops. However, initiation of local buckling led to a rapid deterioration of brace stiffness and strength. In X braced panels, only one half of the compression strut tended to buckle instead of both segments, thereby increasing local deformation demands.

1.4. DISCUSSION

These studies have been of great value in revealing the many factors that influence the behavior of braced frames. All the references reviewed agree on the following points concerning the inelastic behavior of concentrically braced frames in general. Braced frames are very effective in reducing lateral deflections. Braces provide most of the lateral stiffness until they buckle. Since the strength of a moment resisting frame develops at a much slower rate than that of a braced frame, the inelastic behavior of braces governs the inelastic response of the entire frame. The large reduction in brace stiffness after brace buckling subjects braced frames to force redistributions that are more drastic than in ductile moment resisting frames (DMRF). Such force redistributions, undetectable by elastic analysis, can lead to premature loss of strength and to concentration of damage. Braced frames have less displacement ductility capacity than ductile moment resisting frames.

In addition, chevron-braced frames have several peculiarities of their own. Chevron-braced bays were found to fail in one of two mechanisms [74,92,84,87]:

1- A weak beam mechanism where the buckling of the compression brace causes an unbalance force to be applied on the beam and subsequently the formation of plastic hinges in the beam.

Weak beams lead to considerable plastification in columns, beams and braces, irrespective of brace slenderness. Slender braces increase the ductility demand in all remaining members, and rarely yield in tension.

2- A strong beam mechanism where buckling of the compression brace is followed by yielding of the tension brace, the beam being sufficiently strong to remain elastic despite the vertical unbalance force applied to it by the braces at midspan. Chevron-braced frames with strong beams and weak braces exhibit a

more uniform distribution of yielding with height than frames with weak beams and strong braces.

Nevertheless, these studies have been of limited value in formulating design recommendations concerning the member proportioning needed to obtain a satisfactory inelastic behavior. There are several reasons behind this shortcoming. Most of these studies have individually focused on only a few aspects of structural behavior. Similarly, the basic assumptions and terminology have varied from study to study. For example, in some studies the strength of an element refers actually to its stiffness while in others it means its yield strength, and in others its buckling strength. In some studies the slenderness of the brace varies while the cross-sectional area is kept constant; in other studies the brace slenderness and cross-sectional area vary such that the brace buckling load remains constant. Most of the early analytical studies were hampered by the lack of adequate brace models. An elasto-plastic model overestimates the energy dissipation capacity of the brace and cannot reproduce the global instability that accompanies buckling. Some early phenomenological models could not reproduce the observed reduction in buckling load following inelastic cycling. In many studies the inelastic analysis was based on only one or two ground motions of similar characteristics. These studies do not account for the strong sensitivity of the inelastic response to the characteristics of the ground motion.

As a result it is not surprising to see different studies conclude with conflicting recommendations. For example, SEAOC [74] discourages the use of chevron-braced frames by requiring larger equivalent lateral forces in their design, and the New Zealand code [93] does not allow their use in structures more than five stories high. On the other hand, the Japanese code [5] expects frame and bracing to resist loads in proportion to their elastic stiffness, and requires the frame to have an ultimate strength that is a fraction of that of the braced bay. Meanwhile, Cheng and Juang [20], based on an optimization study of elastic structural systems, conclude that chevron-braced frames are the most efficient concentric bracing system. Moreover, most researchers [18,26,89,56,5] favor the use of low slenderness braces over braces of large slenderness because the former have "full" and "stable" hysteresis loops, allowing them to dissipate more energy for a given displacement amplitude. They discount slender braces on the basis of their low buckling load, their pinched hysteresis loops (leading to "creeping" collapse), the impact loading when straightened out (leading to fracture in connections), and the high axial forces they induce in columns. Yet others [38,76,34] prefer slender braces on the basis that early compression buckling will cause the tension brace to yield and dissipate energy

in tension. They argue that this energy dissipation mechanism is more reliable than that of plastic hinge rotation in inelastic buckling of stocky braces which are likely to fail prematurely by local buckling of the flanges.

In the case of chevron-braced frames it is not evident from the data in the literature which collapse mechanism is preferable. The weak beam mechanism concentrates the energy dissipation in the beams which are better energy dissipators than the braces. However, it causes a deteriorating force deformation curve which leads to more energy dissipation demand. The strong beam mechanism provides a tri-linear force deformation characteristic which is believed by many [53,68,69,88] to be an ideal force deformation characteristic. On the other hand, it concentrates the energy dissipation in the braces (the least capable elements) and may require unreasonably stiff and strong beams. In addition, it increases the maximum column compression and hence the danger of column buckling. This is a very undesirable situation for it might lead to column failure, soft story formation, or incremental collapse.

As for code recommendations concerning the design of steel braced frames, detailing requirements for connections based on capacity design are well founded. However, most codes still proceed on the basis of elastic analyses under reduced equivalent lateral loads. The complex inelastic behavior of braced frames and the limited energy dissipation capacity of braces make rational selection of design load factors difficult. Use of small load reduction factors reduces the probability of inelastic behavior. However, given the complexity of braced frame behavior and the diversity of the factors influencing this behavior, it is not clear whether current code provisions provide the same degree of safety as for moment resisting frames or whether they are unduly conservative.

1.5. OBJECTIVES

In view of these observations , this research aims at investigating the inelastic behavior of chevron-braced frames, and more specifically:

(1)- To investigate the parameters that affect the inelastic force redistributions in chevron-braced frames.

(2)- To trace the sensitivity of their response to these parameters.

(3)- To look for optimal proportioning rules that can improve the response of these frames.

(4)- To evaluate different design variants of chevron-braced frames.

(5)- To formulate design recommendations in a form that might be included in

design codes or their commentaries.

In carrying out this investigation, certain basic precepts were considered. For example, in assessing the merits of each design variant it is desired to distribute the energy dissipation demand in proportion to the energy dissipation capacity of the elements involved. Thus, careful attention must be paid to the post-buckling and failure characteristics of braces. Moreover, since the magnitude of the extreme seismic loading is uncertain, it is desirable to make the structure's behavior as predictable and as insensitive to the characteristics of the ground motion as possible. Consequently, the statistical nature of the response to a wide variety of excitations should be considered. Similarly, because of the significant post-buckling force redistributions associated with braced systems, design recommendations concerned with member proportioning and detailing formulae should be based on capacity design concepts.

1.6. SCOPE

To achieve these objectives, the research proceeds in several steps. Chapter 2 reviews available analytical models for braces. Since inelastic brace behavior dominates the inelastic response of braced frames, the first step is to determine which parameters control the postbuckling behavior of a brace. An analytic study, limited to monotonic loading, identified several parameters that were later found useful in numerical simulations of cyclic and dynamic loading.

Chapter 3 builds on the results of Chapter 2 and identifies those parameters at the structure level which govern the inelastic deformation (collapse) mechanism and attendant force redistributions in chevron-braced frames. The results of several numerical simulations illustrate the importance of the parameters identified on the magnitude of the force redistributions and on the overall inelastic characteristics of the structure.

In Chapter 4 the dynamic inelastic behavior of a single story chevron-braced frame is compared to that of a moment resisting frame of same dynamic characteristics and strength level. The effect of the deteriorating hysteresis loop characteristics associated with braces of differing slenderness on displacement and energy ductility demand is assessed.

In Chapter 5 a systematic parametric study of realistic multistory braced frames is carried out to reassess the importance of the various parameters identified in the previous chapters. Braced frames are compared with dual systems where the frame participates in resisting the lateral load in different proportions. The effects of low

slenderness braces are compared to those of intermediate slenderness braces. The comparisons are limited to the inelastic regime. A realistic physical brace model [35] is used in all the brace simulations. Important dynamic interactions are discovered that were not predictable or observable from the simplified analyses and models used in the previous chapters.

Two approaches were taken to improve the behavior of chevron-braced frames. Chapter 6 describes the use of optimization procedures in the seismic resistant design of chevron-braced frames. The implications of the results concerning design recommendations and member proportioning are discussed. Problems in using optimization techniques for such complex systems are also examined.

Chapter 7 examines the performance of several alternative bracing configurations. Systems considered included those with V, split X, and Tie-Bars-To-Ground configurations as well as a new variant devised during this research program (the Zipper configuration). Computer simulations of this latter variant showed that it is highly effective in distributing the energy dissipation over the whole frame in a way that is relatively insensitive to ground motion characteristics.

In Chapter 8, results and conclusions are summarized. Based on these results, basic design recommendations are formulated for each of the systems considered. Directions for further research are also pointed out. Detailed design recommendations and examples are presented in the Appendices.

CHAPTER 2

HYSTERETIC BEHAVIOR OF BRACES

2.1. INTRODUCTION

Research [45,80,21] has shown that inelastic structural response to earthquake loading depends mainly on the period, strength level, hysteretic characteristics of the structure and on the dynamic characteristics of the excitation. Since braces confer most of the strength and stiffness to braced structures, a study of the dynamic inelastic behavior of braced frames should start with an examination of the inelastic behavior of braces. In studying the inelastic behavior of braces, one needs to look specifically at the rate of deterioration of strength with increasing deformation, the deformation capacity, as well as the energy dissipation demand and capacity.

This chapter starts with a review of experimental and analytical research on brace behavior to identify assumptions that are appropriate for subsequent analytical studies. Next, a dimensionless model of inelastic brace behavior is developed to help evaluate the sensitivity of brace response to the various parameters. Then, a simple model for brace deformation and energy dissipation capacities is developed. Finally, the observed dependencies and their implications for structural design are summarized.

2.2. EXPERIMENTAL PROGRAMS

Many experiments have been conducted by various researchers to investigate the effects of slenderness ratio $\lambda = kL/r$, section shape and end-restraints on the strength of braces and on the "fullness" of their hysteresis loops. These tests have employed scale models as well as full size elements.

The effective brace slenderness has been found to be the major parameter controlling the characteristics of the hysteresis loop [18,38,66,91]. Hysteresis loops become pinched for slender braces and tend to be fuller for stocky braces. Compared to stocky braces, slender braces also tend to suffer more strength reduction from cycle to cycle.

The effect of section shape has been studied independently by several groups of investigators. Jain, Goel and Hanson [37] tested small tubes of square section, angles and bars of rectangular cross-section. They concluded that differences in the hysteresis loop characteristics of different section types can be attributed to their different susceptibility to local buckling; thin walled sections being more likely to fail

prematurely by early local buckling. Closed sections are less likely to suffer torsional buckling, but their strength deteriorates faster with cycling because of the distortion of the cross-section. Popov et al. [18] tested a variety of full sized steel sections (wide-flanges, double angles, channels, T sections, pipes, and square tubes) with slenderness values equal to 40, 80 and 120). They noted that cyclic loading reduces the buckling strength of braces, and that the effect of cross section shape on hysteresis characteristics is most noticeable in small slenderness sections where occurrence of local buckling is predominant. Gugerli [30] tested the effect of section shape and scale effect on the hysteretic characteristics of rectangular tube and wide flange sections. He found that the hysteresis loops of both section types were similar, but that fracture was more critical than local buckling in limiting the resistance and energy dissipating capacity of braces. The fracture life of tubes was smaller than that of wide flanges in his experiments.

Astaneh-Asl [10] investigated the effectiveness of gusset plates in restraining double angle braces. He found that for buckling in the plane of the gusset plates, the effective length factor can be taken as 0.5. Plastic hinges then form at midspan in the braces and at their connections with the gusset plates. For out-of-plane buckling, an effective length factor of one was found to be satisfactory. Plastic hinges form at midspan in the braces and in the gusset plates. Astaneh proposed new detailing specifications for the gusset plates to avoid local buckling and fracture there, and improved stitching details for built-up members. Wakabayashi et al. [90] tested small scale elements with flexible end restraints. They found that compared to pin ended braces of the same effective slenderness , end-restrained braces have more energy dissipating capacity (because of two additional plastic hinges). Jain [36,37,38] tested small rectangular tubes with gusset plates and concluded that the ratio of bending stiffness of brace to gusset plate is more important than their strength ratio in determining the effective end restraint.

Kahn and Hanson [40] performed tests to assess the effect of rate of loading. They found no appreciable difference between quasistatic strain rates and those usually encountered in seismic situations.

2.3. ANALYTICAL BRACE MODELS

The earliest analytical brace model is the so-called slip model. It is a bilinear elastic model in compression with a compression yield force set equal to the elastic buckling load of the brace. Bilinear hysteretic behavior is assumed in tension. While this model is sufficient to capture the initial nonlinearity that follows brace

buckling, it is unable to reproduce the strength deterioration with increasing deformation and the softening observed with repeated cycles. As experimental work in brace behavior has progressed, many improved analytical models have been developed to predict their cyclic inelastic behavior. These models can be classified into one of three categories [96]:

2.3.1. Physical models (force driven):

This category of brace models incorporates a simplified analytical description of certain aspects of the physical buckling and yielding processes involved. In most of these models the axial compression force is the independent variable and the deformation is the dependent variable. However, most structural analysis techniques supply the model with deformation increments and request the corresponding axial force (total or change). Determination of the axial force P corresponding to a specified displacement increment must then be accomplished by iteration. Convergence is checked by comparing the displacement increment compatible with the assumed value of P with the specified displacement increment. Many researchers have worked on improving the iterative schemes (choice of iteration variables, recasting of the equations, etc...). The determination of the axial force P remains computationally expensive and sometimes not robust (i.e., may fail to converge to the correct value).

One of the first physical brace models was developed by Higginbotham [31] and featured a point plastic hinge, a provision for a yield surface involving the interaction of axial force P and moment M, and a formulation for large lateral deformation involving elliptical integrals. This model was adequate for braces of intermediate to large slenderness. The next model, developed by Nonaka [91], consisted of a point plastic hinge, provision for inelastic axial and flexural deformations in the plastic hinge, and rigid sections for the remainder of the brace. This model was adequate for braces of small to intermediate slenderness. Igarashi [33] improved Nonaka's model by using a more refined yield function. Then, Pragthuangsit [67] investigated the effect of end restraints, namely fixed ends, pinned ends, elastic restraints. Singh [77] introduced a new model by using trigonometric functions instead of the elliptic integrals used by Higginbotham. Gugerli [30] refined Singh's model by including the residual deformation Δ_p and an empirical provision for the reduction in maximum compressive strength after cycling. Ikeda [35] improved Gugerli's model by adding a reduction of the modulus of elasticity upon cycling, "material nonlinearity" in the elastic range, and gradual

plastification of the plastic hinge. Moreover, Ikeda developed numerical techniques that substantially reduced the need for iteration, thereby facilitating the use of this model in inelastic dynamic analyses of complete structures.

2.3.2. Kinematic models (displacement driven):

Comparatively little effort has been devoted to displacement driven models. In these models, a tangent stiffness matrix is formed based on material properties, the current state of strain and some parameter(s) measuring accumulated damage. Given the displacement increment from the analysis program and the tangent stiffness matrix a member force increment is computed and added to the current axial force P. These models have the advantage of eliminating the iterations at element level [46]. However, the rapid changes in brace post-buckling tangent stiffnesses often require very small load increments and increase the number of iterations at the global level. Fujimoto [23] used a finite element model to simulate the spread of the inelastic zone. However, he used a linear elastic perfectly plastic material property assumption. Chen [19] and Zayas [96] each developed a displacement driven model. These models were not very successful in reproducing the degradation in strength and stiffness of braces under cyclic loading.

2.3.3. Phenomenological models (empirical rules and parameters):

These types of models are often favored for their computational economy, especially when the structure analyzed contains many inelastic braces. These models are governed by a set of empirical rules derived from experimental observations and contain parameters depending on material and geometric properties. Phenomenological models are restricted in use to conditions similar to those from which the rules and parameters were derived. One must often run some preliminary analyses in conjunction with one of the other models (physical or kinematic) to fine tune some of the input parameters. Almost every researcher [77,67,91] who has worked on a physical model has also developed an alternate phenomenological model with a set of parameters to approximate the results obtained with physical models and experimental data.

2.4. DIMENSIONLESS BRACE MODEL

In order to identify the most important parameters governing the inelastic behavior of braces, a physical brace model will be studied whose equations realistically describe the actual behavior of the brace. Presenting the results in

dimensionless form makes them more compact, easier to grasp and more generally applicable.

2.4.1. Assumptions:

Based on the review of existing physical brace models and of experimental results, the following assumptions will be used in developing the dimensionless brace model:

(1)- Every cross section along the axis retains its shape (no section distortion or local buckling).

(2)- The effects of shearing stresses and strains are disregarded.

(3)- Plane sections remain plane.

(4)- Only wide flange sections bent about their minor principal axis are considered. The web stress contribution is assumed negligible compared with that of the flanges.

(5)- The lateral deflections and the corresponding slopes are relatively small (first order deformations).

(6)- The plastic deformations at the plastic hinge are determined on the basis of an associative flow rule.

(7)- The effective member length kL is used in place of the member length L for determining buckling characteristics.

(8)- The initial buckling stress is computed using the AISC [2] formula with the factors of safety removed.

(9)- The analytic study is limited in this chapter to a monotonically increasing compressive deformation.

2.4.2. Terminology:

Brace slenderness λ is defined as $\lambda = kL/r$ where k is the effective length factor, L is the clear span of the brace and r is the governing radius of gyration (such that the ratio k/r is maximum). Large slenderness is defined here as that for which the elastic buckling stress is less than half the yield stress. That is $\lambda \geq 770 / \sqrt{F_y}$ where F_y is in kips per square inch (ksi). For A36 steel large slenderness is equivalent to $\lambda > 130$. Small slenderness is defined here as that for which yielding and local buckling phenomena become predominant. The exact value depends on the ratio of width to thickness of the flange and the restraint provided by the web [59,60]. For A36 steel and the usual AISC compact sections used for braces, small slenderness is equivalent to $\lambda \leq 60$, approximately. Intermediate slenderness is that

for which local buckling phenomena are less critical than inelastic buckling. For A36 steel intermediate slenderness is equivalent to $60<\lambda<130$. The distinction between small slenderness braces and intermediate slenderness braces is an important one. In small slenderness braces large lateral displacements initiated by yielding or local buckling of a flange (wide flange sections) or plate (rectangular tube sections) trigger global buckling of the brace. For compact sections, the buckling stress is very close to the yield stress. Intermediate slenderness braces experience column buckling. However, the effective buckling stress is reduced because of residual fabrication stresses.

2.4.3. Normalization:

In the following analyses of brace behavior, the brace buckling load P_c is held to a constant value. There are several reasons for normalizing behavior with respect to P_c instead of the brace yield load P_y (as is usually done), the most important of which is that brace buckling, not brace yielding, is the first likely inelastic event in a braced steel frame. Furthermore, whether in an allowable stress approach or in cases where serviceability or damageability limit states are considered, the structure is assumed to resist its loading elastically. The design forces corresponding to these cases define a lower limit for the brace buckling load, not its tension yield load. It is interesting to note that these forces are often specified independently from the brace slenderness.

2.4.4. Post buckling behavior of brace:

In this section a simple expression is developed that relates the axial deformation to the axial compression in a brace. The relation is in non-dimensional terms. The next two sections will use the results obtained herein to derive expressions for the tangent stiffness and energy dissipation demand as a function of brace deformation and other relevant brace parameters. Referring to Figure 2-1 and the notation in Appendix A, the deflection of the buckled brace is

$$y(x) = A\cos\left(\frac{\pi}{2}\sqrt{\frac{P}{P_c}}x\right) + B\sin\left(\frac{\pi}{2}\sqrt{\frac{P}{P_c}}x\right) \qquad 2\text{-}1$$

the boundary conditions being

$$y(0) = 0 \rightarrow A = 0 \qquad 2\text{-}2$$

$$y\left(\frac{L}{2}\right) = \frac{M_p(P)}{P} \rightarrow B = \frac{M_p(P)}{P\sin\left(\frac{\pi}{2}\sqrt{\frac{P}{P}}\right)} \qquad 2\text{-}3$$

The plastic rotation θ_p at the plastic hinge is given by

$$\theta_p = 2y'(\frac{L}{2}) = 2\frac{M_p}{P\sin(\frac{\pi}{2}\sqrt{\frac{P}{P_c}})}\frac{\pi}{L}\sqrt{\frac{P}{P_c}}\cos\frac{\pi}{2}\sqrt{\frac{P}{P_c}} \qquad 2\text{-}4$$

The axial deformation of the brace Δ has three components; elastic Δ_e , geometric Δ_g and plastic Δ_p:

$$\Delta = \Delta_e + \Delta_g + \Delta_p \qquad 2\text{-}5$$

where the elastic deformation is

$$\Delta_e = \frac{PL}{AE} \qquad 2\text{-}6$$

and the geometric deformation

$$\Delta_g = 2\int_0^{\frac{L}{2}} \frac{1}{2} y'^2 dx \qquad 2\text{-}7$$

and the plastic deformation

$$\Delta_p = -\frac{dM_p(P)}{dP}\theta_p\Big|_{P_c}^{P} + \int_{P_c}^{P}\frac{d^2M_p(P)}{dP^2}\theta_p(P)dP \qquad 2\text{-}8$$

Letting $M_p(P) = M_p(1 - \frac{P^2}{P_y^2})$ be a parabolic yield surface, then

$$\frac{M_p}{P_y} = 2\nu r\frac{r}{d} = 2\gamma r \qquad 2\text{-}9$$

in which a new section property $\gamma = \nu r/d$ is defined. For wide flange sections bent about their minor axis, γ has a narrow range of values (between 0.3 and 0.4; see Table 2-1). For notational simplicity, the following dimensionless pararneters are defined:

$$u = \frac{P}{P_y} \qquad 2\text{-}10\text{-}a$$

$$a = \frac{P_c}{P_y} = \begin{cases} 1 - \frac{1}{2}\frac{\lambda^2}{\lambda_c^2} & \lambda \le \lambda_c \\ \frac{1}{2}\frac{\lambda_c^2}{\lambda^2} & \lambda > \lambda_c \end{cases} \qquad 2\text{-}10\text{-}b$$

where $\lambda_c = \sqrt{2\pi^2/\epsilon_y}$

$$z = \pi\sqrt{\frac{P}{P_c}} = \pi\sqrt{\frac{u}{a}} \qquad 2\text{-}10\text{-}c$$

$$\eta = \frac{z}{2} \qquad 2\text{-}10\text{-}d$$

$$\lambda = \frac{L}{r} \qquad 2\text{-}10\text{-}e$$

Notice that $\eta = \pi/2\sqrt{u/a}$ can be recast to give $u = 4a\eta^2/\pi^2 = b\eta^2$ where $b = 4a/\pi^2$. Using series expansions from Abramowitcz [1] for some of the functions in Eq 2-1 to 2-8, and collecting terms, one obtains for the total deformation (details of the derivation are in Appendix A):

$$\frac{\Delta}{L} = \epsilon_y b\eta^2 + 8\frac{\gamma^2}{\lambda^2}\frac{1}{b^2}\left[\left(\frac{1}{\eta^4} + 2.16941e^{-2} + 6.112386e^{-3}\eta^2\right)\right. \qquad 2\text{-}11$$

$$+2(15.96334 - 22.432173\eta^{0.25} + 7.43265\eta^{0.50} - 0.29613\eta^2 - 9.50725e^{-2}\eta^4)$$

$$\left.-b^2(2.18817 + 2.59573\eta^4 - 1.68026\eta^6)\right]$$

Figure 2-3 shows the results for this equation assuming $\gamma = 0.3$. It is clear from that figure that at a constant buckling load, braces of intermediate slenderness have the most rapid strength deterioration with increasing deformation. Very stocky braces have practically elasto-plastic deformation characteristics while slender braces have a "long plateau" of elastic buckling before reaching the yield surface and experiencing a reduction in strength.

2.5. POST BUCKLING TANGENT STIFFNESS

Since Eq 2-11 expresses the deformation in terms of the applied force, the instantaneous tangent stiffness can be obtained relatively easily in terms of the force level by inverting the brace flexibility expressed as a function of axial load. Thus,

$$\frac{1}{K_{bt}} = \frac{\partial\Delta}{\partial\eta}\cdot\frac{\partial\eta}{\partial P} = \frac{\pi}{2}\frac{1}{\sqrt{PP_c}}\frac{\partial\Delta}{\partial\eta} \qquad 2\text{-}12$$

gives at $\eta = \pi/2$ (details of the derivation are in Appendix A)

$$\frac{K_{bt}(\frac{\pi}{2})}{K_0} = \frac{1}{2}\frac{1}{1+2\pi^2\frac{\gamma^2}{\epsilon_y\lambda^2 a^3}(2.93676a^4-2.18737a^2-0.7137)} \qquad 2\text{-}13$$

There are parameter combinations for which the ratio K_{bt}/K_0 is infinite or negative. This corresponds to the cases where the tangent stiffness is infinite or positive. This characteristic instability has been observed by other investigators as well [81]. To overcome these difficulties a "secant stiffness" with an origin at the buckling load will be used. This secant stiffness is defined as $K_s=(P_c-P(\Delta_y))/(\Delta_c-\Delta_y)$. Figure 2-3 shows the variation of K_s with brace slenderness and axial deformation. Intermediate slenderness braces have the largest ratio of $|K_s/K_0|$.

2.6. ENERGY DISSIPATION DEMAND

The inelastic energy dissipation demand E_{in} can be expressed as (Figure 2-4):

$$E_{in} = A_1-A_2+A_3 \qquad 2\text{-}14$$

where $A_1 = \int_{P_c}^{P}\Delta dP$, $A_2 = (P_c-P)1/2(\Delta_c+\Delta_c P/P_c)$, and $A_3 = P(\Delta-\Delta_c P/P_c)$. Since unloading will not in general follow the initial loading slope, the term for A_3 is only approximate. Using the dimensionless variables previously defined, we obtain

$$E_{in} = \frac{\epsilon_y b}{4}(\eta^4-6.08807) \qquad 2\text{-}15$$

$$+8\frac{\gamma^2}{\lambda^2}[\frac{1}{b^2}(-\frac{1}{2\eta^2}+\frac{1}{2}2.16941e^{-2}\eta^2+\frac{1}{4}6.112386e^{-3}\eta^4+0.08285)$$

$$+2(\frac{1}{2}0.99524\eta^2-\frac{1}{4}0.29613\eta^4-\frac{1}{6}9.50725e^{-2}\eta^6-\frac{1}{2}\eta^2(\ln\eta^2-1)-0.65855)$$

$$-b^2(\frac{1}{2}2.18817\eta^2+\frac{1}{6}2.59573\eta^6-\frac{1}{8}1.68026\eta^8-1.41350)]$$

The energy demand is normalized with respect to $P_c\Delta_c/2$. Figure 2-5 shows that for a given displacement ductility intermediate slenderness braces have the lowest relative energy dissipation capacity. Alternatively, Figure 2-6 shows that to achieve a given energy demand, braces of intermediate slenderness have to undergo the largest displacement ductility when compared to stocky and slender braces. Figure 2-7-a shows that there is a range of displacement ductility where a brace may dissipate more energy than an elasto-plastic system of same strength and undergoing the same

deformation. However this happens only for very stocky braces. Figure 2-7-b shows that this is possible when area A1 is larger than area A2.

2.7. ENERGY DISSIPATION CAPACITY

2.7.1. Damage index for braces:

Many of the analytical brace models available so far can satisfactorily reproduce the main hysteretic characteristics of braces, but none of them can predict when a brace will fail. Popov et al. [62,63,64,65], Mitani [47,50,51] and Kato [42] have done extensive cyclic loading tests on beams, columns and beam to column connections to determine their failure mode and their energy dissipating capacity for low cycle fatigue. This loading condition is characterized by a relatively low number of cycles of large amplitude extending well into the inelastic range. They found that such components fail by fracture. The fracture is usually the result of a crack starting at a weld or a re-entrant corner, that grows and propagates across the flange. Alternatively, it can be initiated by a local buckling leading to cracking and ultimately to fracture. Research has shown that for low cycle fatigue damage indices should be based on plastic strain cycles amplitude (Coffin-Manson [48]) or on cumulative hysteretic energy dissipation (Suidan and Eubanks [82], Srinivasan [78], Kato [41]). Krawinkler [44] proposed a low cycle fatigue model for beams bent about their major principal axis.

While some recent work has just been reported by Goel [86] on brace failure criteria, most research is still oriented at understanding the cyclic behavior of braces and at deriving models reproducing that behavior. There are several reasons that prevent extrapolation of results obtained for beams to braces. First, in beams bent about their major principal axis, flanges are uniformly stressed. In wide flange braces buckling about their minor principal axis, flanges are under a more complex stress distribution. Second, the plastic hinge length in a beam bent about its major principal axis is much shorter than that of a brace buckled about its minor principal axis (because of a smaller shape factor and a larger moment gradient in the beam). Third, in beam or column problems the bending moment and axial force are independent while in a buckled brace they are totally coupled through the deflected shape. Therefore, efforts are needed to develop failure criteria consistent with physical behavior and analytical models.

2.7.2. Assumptions for the energy dissipation capacity of braces:

Given the lack of knowledge about the energy dissipation capacity of braces, two simple bounds are herein proposed. In the absence of specific experimental data, the bounds developed should be considered as approximate. There are several assumptions made in developing these bounds. Material is assumed to be elastic-perfectly plastic. The energy dissipation capacity of the brace is limited by reaching the material's ultimate strain anywhere in the member under monotonically increasing axial compression deformation. The cumulative energy dissipation capacity under cyclic loading is assumed equal to that under monotonic loading [41]. Sequence effects and mean strain effects are neglected. The energy dissipation capacity under tension yielding is assumed to be substancially larger than that under inelastic buckling, and is therefore not critical.

The ultimate strain ϵ_u can be reached in one of two ways: either on the compression side of a brace in a global buckling mode, or on the compression side of a flange in local buckling mode. Accordingly, two energy dissipating mechanisms are considered: a global buckling mechanism where energy is dissipated in a point plastic hinge, and a local buckling mechanism where energy is dissipated in plastic yield lines in the flanges. Torsional buckling is neglected, and the derivations are limited to wide flange sections bent about their minor axis.

2.7.3. Upper Bound Solution 1; Global Buckling Mechanism:

Section curvatures are assumed to vary linearly between the first point on the brace to yield and the ultimate curvature point at the midspan. Similarly, a linear moment variation is assumed between these two points. These two assumptions imply that the moment-curvature relationship is linear between the first yield and the ultimate moments; however this implication later will be violated. The location of the neutral axis between its first yield position and its position assuming rigid plastic material is taken to be inversely proportional to the strain ductility. Energy dissipation is assumed to occur only in plastic hinge rotations; plastic axial deformations that are important in case of stocky braces are neglected.

The total energy dissipation capacity E_{in} is assumed to be

$$E_{in} = M_p(P)\theta_p \qquad 2\text{-}16$$

where the ultimate plastic hinge rotation

$$\theta_p = \bar{L}_p \varnothing_u \qquad 2\text{-}16\text{-a}$$

is estimated from the effective length of the plastic hinge $\bar{L}_p$ and the ultimate curvature $\varnothing_u$. The effective plastic moment M_p at the given axial compression P is given by

$$M_p = M_{p0}(1 - \frac{P^2}{P_y^2})(1 - \frac{1}{\nu\mu_s^2}) \qquad 2\text{-}16\text{-}b$$

and the effective length of the plastic hinge $\bar{L}_p$ is approximated by

$$\bar{L}_p = \frac{1}{2}L_p(\varnothing_y+\varnothing_u) \qquad 2\text{-}17$$

where

$$L_p = L(1 - \frac{M_{py}}{M_{pu}}) \qquad 2\text{-}18$$

$$= L[1 - \frac{\mu_s^2}{(\nu\mu_s^2 - 1)(1+P/P_y)}] \qquad 2\text{-}18\text{-}a$$

It can be shown (Figure 2-8) that

$$\varnothing_y = \frac{2\epsilon_y(1 - \frac{P}{P_y})}{d(1 - 2\frac{P}{P_y})} \qquad 2\text{-}19\text{-}a$$

and

$$\varnothing_u = \frac{\mu_s\epsilon_y}{yd} \qquad 2\text{-}19\text{-}b$$

where

$$y = \frac{1}{2(1 - P/P_y)}[\frac{1}{\mu_s^n}(1 - 2\frac{P}{P_y})+(1 - \frac{1}{\mu_s^n})(1 - \frac{P}{P_y})^2] \qquad 2\text{-}20$$

The parameter n in Figure 2-8 describes how rapidly the neutral axis migrates with increasing curvature. Setting n = 1 for simplicity, gives

$$E_{in} = 2\frac{\gamma^2}{\nu}P_y\epsilon_y\frac{L}{d}\frac{(1 - P/P_y)(1 - P^2/P_y^2)}{1 - 2P/P_y}[1 - \frac{1}{\nu\mu_s^2}] \qquad 2\text{-}21$$

$$[1+\frac{\mu_s^2}{1+\frac{(\mu-1)(1-P/P_y)^2}{1-2P/P_y}}][1 - \frac{\mu_s^2}{(\nu\mu_s^2-1)(1+P/P_y)}]$$

normalizing this with respect to $\frac{1}{2}P_c\Delta_c$ gives the desired normalized energy

dissipation capacity:

$$E_{in} = 4\frac{\gamma^2}{\nu}\left(\frac{P_c}{P_y}\right)^2\frac{(1-P_c/P_y)(1-P_c^2/P_y^2)}{1-2P_c/P_y}\left[1-\frac{1}{\nu\mu_s^2}\right] \qquad 2\text{-}22$$

$$\left[1+\frac{\mu_s^2}{1+\frac{(\mu_s-1)(1-P_c/P_y)^2}{1-2P_c/P_y}}\right]\left[1-\frac{\mu_s^2}{(\nu\mu_s^2-1)(1+P_c/P_y)}\right]$$

2.7.4. Upper Bound Solution 2; Local Buckling Mechanism:

Figure 2-9 indicates the kinematics assumed for the shape of the local buckles. In this derivation, several major assumptions are made. The web is considered to limit the yield lines to one side of the flange only; it is assumed to have no effect on axial force and moment capacity. A uniform stress distribution is assumed in the flanges. Although a triangular or trapezoidal stress distribution may be more appropriate at impending flange buckling, stress redistributions occur as buckling proceeds. These redistributions would tend to equalize the stresses across the flange. Moreover, considering the uncertainty due to residual stresses, a more sophisticated stress distribution is not warranted. The plastic yield lines are assumed to form simultaneously so that their plastic rotations can be kinematically related. Alternatively, the material can be assumed to be rigid plastic. The variation of moments and axial forces at yield lines as the plastic rotation increases is neglected. An effective modulus of elasticity corrected for residual stresses is used. That modulus decreases linearly from its full value at half the yield stress to zero at the yield stress [59,60].

The buckling stress is taken as the smallest of the global buckling stress for the brace and the local buckling stress of the flange. Recall that the global buckling stress $\sigma_c = a\sigma_y$ where a is obtained from Eq 2-10-b. The local buckling stress for the flange is

$$\sigma_c = \frac{\sigma'}{\left(\frac{\sigma'}{\sigma_y}+1\right)} \qquad 2\text{-}23$$

where

$$\sigma' = \frac{2k\pi^2E}{12(1-\nu^2)}\left(\frac{t_f}{b_f/2}\right)^2$$

and k=0.5 approximately [60].

The flange's plastic moment is

$$M_p = M_{p0}(1 - \frac{\sigma_c^2}{\sigma_y^2}) \qquad 2\text{-}24$$

and $M_{p0} = \frac{1}{4}\sigma_y t_f^2 \frac{b_f}{2}$.

The ultimate plastic hinge rotation is

$$\theta_p = \frac{\epsilon_u}{\frac{t_f}{2}(1 - \frac{\sigma_c}{\sigma_y})} L_p \qquad 2\text{-}25$$

where L_p can be taken either as

$$L_p = \min(\frac{3}{2}t_f , \frac{5}{2}b_f \frac{1 - 3\frac{\sigma_c^2}{\sigma_y^2}}{1 - \frac{\sigma_c^2}{\sigma_y^2}}) \qquad 2\text{-}26$$

The first value is an estimate, and the second is based on the assumption of linear moment variation between successive yield lines.

The energy dissipation capacity, assuming only two folds are formed, is

$$E_{in} = 8M_p\theta_p \qquad 2\text{-}27$$

which gives for the first definition of L_p

$$E_{in} = \min(3\sqrt{12}\sigma_y A_f L \epsilon_y \mu_s \frac{t_f}{b_f}\frac{1}{\lambda}(1+\frac{\sigma_c}{\sigma_y}) , 5\frac{\sqrt{12}}{6}\sigma_y A_f L \epsilon_y \mu_s \frac{1}{\lambda}\frac{1-3\frac{\sigma_c^2}{\sigma_y^2}}{1-\frac{\sigma_c}{\sigma_y}}) \qquad 2\text{-}28$$

Normalizing with respect to $1/2P_c\Delta_c$, one gets

$$\bar{E}_{in} = \min(6\sqrt{12}\frac{t_f}{b_f}\frac{1}{\lambda}(1+\frac{\sigma_c}{\sigma_y})(\frac{\sigma_y}{\sigma_c})^2\mu_s , \frac{10}{\sqrt{3}}\frac{1-3\frac{\sigma_c^2}{\sigma_y^2}}{1-\frac{\sigma_c}{\sigma_y}}\frac{1}{\lambda}(\frac{\sigma_y}{\sigma_c})^2\mu_s) \qquad 2\text{-}29$$

Figures 2-10-a to 2-10-d show the variation of allowable energy ductility for various material strain ductilities μ_s and flange thickness ratios b_f/t_f. It is evident that the allowable energy ductility increases with increasing material strain ductility and with decreasing flange thickness ratios. In all these cases the flange local buckling mechanism was governing. Again, intermediate slenderness braces exhibit the lowest energy ductility.

2.8. DISPLACEMENT DUCTILITY CAPACITY

It is also useful to know the displacement at which the energy capacity of the brace is exceeded. To facilitate comparisons, this will be normalized by the initial buckling displacement. In addition to the assumptions made in the previous sections, the assumption of point plastic hinge is reiterated. The required point plastic hinge rotation, based on equilibrium is

$$\theta_p = \frac{2\pi}{L}\frac{M_p(P)}{\sqrt{PP_c}}\cot\left(\frac{\pi}{2}\sqrt{\frac{P}{P_c}}\right) \qquad 2\text{-}30$$

On the other hand, the available plastic hinge rotation capacity based on a spread plastic hinge and a linear distribution of moment is

$$\theta_p = \epsilon_y\frac{L}{d}\frac{1-P/P_y}{1-2P/P_y}\left[1+\frac{\mu_s^2}{1+\frac{(\mu_s-1)(1-P/P_y)^2}{1-2P/P_y}}\right]\left[1-\frac{\mu_s^2}{(\nu\mu_s^2-1)(1+\frac{P}{P_y})}\right] \qquad 2\text{-}31$$

Equating both equations and rearranging terms, one obtains

$$\frac{\cot\eta}{\eta}(1+b\eta^2)(1-2b\eta^2) = \qquad 2\text{-}32$$

$$\frac{\epsilon_y b\lambda^2}{2\pi^2\sqrt{12\gamma}}\left[1+\frac{\mu_s^2}{1+\frac{(\mu_s-1)(1-b\eta^2)^2}{1-2b\eta^2}}\right]\left[1-\frac{\mu_s^2}{(\nu\mu_s^2-1)(1+b\eta^2)}\right]$$

where $\nu=\frac{M_p}{M_y}$ is the section shape factor, $\mu_s = \frac{\epsilon_u}{\epsilon_y}$ is th material strain ductility, and $b=4\pi b/\pi^2$. Equation 2-31 must be solved for η which is then substituted in Eq 2-11 for Δ. The ratio $\mu_b = \frac{\Delta}{\Delta_c}$ is then the brace displacement ductility capacity. The results of such an analysis are shown in Figure 2-11. The allowable displacement ductilities can be rather large. Once again, intermediate slenderness braces

have the lowest allowable displacement ductility.

2.9. CONCLUSIONS

The brace slenderness ratio λ is the single most important parameter governing the brace inelastic behavior. The section shape factor γ is almost equally important, but the limited range of values it can take makes it less critical for the response of wide flange braces. Braces of intermediate slenderness seem to have the most undesirable characteristics; namely, the fastest strength deterioration, the largest displacement demand for a given energy dissipation demand, and the smallest displacement and energy ductility capacity. It is interesting to note in this respect, that the recently proposed SEAOC design recommendations [75] limit the allowable brace slenderness values to the stocky and intermediate slenderness ranges. There is a displacement ductility range where stocky braces can dissipate more energy than an elasto-plastic system of same strength undergoing the same deformation. Local buckling seems to be the main limit to the energy dissipation capacity of braces. The energy dissipation capacity increases with increasing material strain ductility and decreasing flange slenderness. There is a need for experimental research in the energy dissipation capacity of braces.

CHAPTER 3

QUASISTATIC INELASTIC FORCE REDISTRIBUTIONS

3.1. INTRODUCTION

Braced steel frames are usually designed according to an allowable stress approach and using elastic analysis techniques. While their behavior in the elastic range may be satisfactory, these frames can collapse suddenly once the design lateral loads are exceeded. This apparent brittleness can be traced to the limited ductility of braces and to the lack of consideration for the force redistribution that occur in such frames. The previous chapter examined the parameters that control the energy dissipating capacity of braces. In this chapter, the inelastic force redistributions are studied analytically and the governing parameters are identified.

This chapter starts by an analytical study of the post-buckling stiffness of a simple chevron-braced bay (Figure 3-1). Parameters that affect the shape of the story hysteresis characteristics are identified. With the help of these parameters, it is possible to classify beams quantitatively as being stiff or flexible. This classification is essential in studying the different collapse mechanisms that are possible and in determining which one is likely to occur for a given structure. Two collapse mechanisms are studied in detail with three subcases considered for each. The characteristic postbuckling behavior and force redistribution pattern are identified for each subcase. Then, based on the results of numerical simulations, design recommendations are made to help improve the force-deformation characteristics of chevron-braced frames and their energy dissipation capacity.

3.2. POSTBUCKLING STORY LATERAL STIFFNESS

Consider a simple chevron-braced bay loaded by lateral forces as in Figure 3-1. A single braced panel from this frame will be considered as indicated in Figure 3-2 (to which all subsequent notation refers). It is assumed that beams are pin connected to the columns. No vertical loads are applied. Beams and columns are assumed to be axially inextensible. In the elastic range, the tension force in the brace B1 and the compression in the brace B2 are equal in magnitude. The maximum lateral resistance provided by the elastic braces is equal to

$$F_c = \max (T+C)\cos\Theta = 2P_c\cos\Theta \qquad 3\text{-}1$$

The net vertical component P_{un} of brace forces applied at the beam midspan is zero:

$$P_{un} = (T-C)\sin\Theta = 0 \qquad 3\text{-}2$$

The lateral story stiffness provided by the braces is given by

$$K_{br} = 2\left(\frac{AE}{L}\right)_{br}\cos^2\Theta \qquad 3\text{-}3$$

As soon as a compression brace buckles, the braced story stiffness drops and can be analytically modeled as in Figure 3-2 where the beam provides an elastic vertical restraint for the braces. As the lateral deformation is increased by Δ_t, the axial deformation in the compression brace is increased by Δ_{brc} while the tension brace axial elongation is increased by Δ_{brt} and the beam is deflected downward by: Δ_{bm}. From Figure 3-3 it can be shown that

$$\Delta_{brc} = \Delta_t\cos\Theta + \Delta_{bm}\sin\Theta \qquad 3\text{-}4\text{-}a$$

$$\Delta_{brt} = \Delta_t\cos\Theta - \Delta_{bm}\sin\Theta \qquad 3\text{-}4\text{-}b$$

The compression force in brace B2 decreases by

$$\Delta C = -\Delta_{brc}K_{bb} \qquad 3\text{-}5$$

where K_{bb} is the current tangent postbuckling stiffness of the brace. The tension force in B1 increases by

$$\Delta T = \Delta_{brt}K_{br} \qquad 3\text{-}6$$

where K_{bt} is the tensile tangent stiffness of brace B1. Since the absolute values of the force increments ΔT and ΔC in braces B1 and B2 are not equal, an unbalanced force is applied to the beam. The vertical component of this force will be referred to as the "unbalance-force" P_{un}. The vertical unbalance force on the beam changes by

$$\Delta P_{un} = \Delta_{bm}K_{bm} \qquad 3\text{-}7$$

where K_{bm} is the effective vertical stiffness provided by the beam at midspan. It is clear from equilibrium that the total increase in lateral resistance is

$$\Delta F = (\Delta T + \Delta C)\cos\Theta \qquad 3\text{-}8$$

and the vertical unbalance increment is

$$\Delta P_{un} = (\Delta T - \Delta C)\sin\Theta \qquad 3\text{-}9$$

To obtain the effective story drift tangent stiffness ($K_e = \Delta F/\Delta_t$) some manipulations are required.

Noting that

$$\Delta T - \Delta C = K_{br}\Delta_{brt} + K_{bb}\Delta_{brc} \qquad 3\text{-}10$$

$$= K_{br}\Delta_t\cos\Theta - K_{br}\Delta_{bm}\sin\Theta + K_{bb}\Delta t\cos\Theta + K_{bb}\Delta_{bm}\sin\Theta$$

Substituting this in Eq 3-9 gives

$$\Delta_{bm} = \Delta_t\sin\Theta\cos\Theta\frac{K_{br}+K_{bb}}{K_{bm}+(K_{br}-K_{bb})\sin^2\Theta} \qquad 3\text{-}11$$

Similarly

$$\Delta T + \Delta C = K_{br}\Delta_{brt} - K_{bb}\Delta_{brc} \qquad 3\text{-}12$$

$$= [(K_{br}-K_{bb})\cos\Theta - \frac{(K_{br}+K_{bb})^2\sin^2\Theta\cos\Theta}{K_{bm}+(K_{br}-K_{bb})\sin^2\Theta}]\Delta_t \qquad 3\text{-}13$$

Substituting this in Eq 3-8 for $\Delta T + \Delta C$ gives

$$\Delta F = \Delta_t\cos^2\Theta[(K_{br}-K_{bb}) - \frac{(K_{br}+K_{bb})^2\sin^2\Theta}{K_{bm}+(K_{br}-K_{bb})\sin^2\Theta}] \qquad 3\text{-}14$$

The effective tangent lateral stiffness is then

$$K_e = \frac{\Delta F}{\Delta_t} = \cos^2\Theta[(K_{br}-K_{bb}) - \frac{(K_{br}+K_{bb})^2\sin^2\Theta}{K_{bm}+(K_{br}-K_{bb})\sin^2\Theta}] \qquad 3\text{-}15$$

Notice that for an infinitely stiff beam ($K_{bm} = \infty$) the effective stiffness reduces to

$$K_e = (K_{br}-K_{bb})\cos^2\Theta \qquad 3\text{-}16$$

And if $K_{bb} = 0$ (elastic brace buckling) K_e becomes

$$K_e = \frac{K_{br}\cos^2\Theta}{1+\frac{K_{br}}{K_{bm}}\sin^2\Theta} \qquad 3\text{-}17$$

In order to have $K_e > 0$ (assuming $K_{bb} < K_{br}$), the following relation from Eq 3-15 must be satisfied:

$$K_{br}-K_{bb} \geq \frac{(K_{br}+K_{bb})^2\sin^2\Theta}{K_{bm}+(K_{br}-K_{bb})\sin^2\Theta} \qquad 3\text{-}18$$

or

$$K_{bm} \geq 4\frac{K_{br}K_{bb}\sin^2\Theta}{(K_{br}-K_{bb})} \qquad 3\text{-}19$$

The same expression is obtained for $K_{bb} > K_{br}$. It should be noted that P−Δ effects have been disregarded. If gravity loads were considered, the limits on K_{bm} would become more stringent.

3.2.1. Classification of beams:

Equation 3-19 specifies the minimum stiffness for the vertical degree of freedom at the brace to beam connection to obtain a positive post-buckling tangent story stiffness. The vertical displacement stiffness provided elastically by the beam is

$$K_{bm} = 48\,\alpha\,(\frac{EI}{L^3})_{bm} \qquad 3\text{-}20$$

where α is a factor depending on boundary conditions. For fixed ends $\alpha = 4$ and for pinned ends $\alpha = 1$. The brace stiffness for lateral load is

$$K_{br} = (\frac{AE}{L})_{br}\cos^2\Theta \qquad 3\text{-}21$$

but $L_{br} = L_{bm}/2\cos\Theta$, therefore Eq 3-21 becomes

$$K_{br} = 2\frac{A_{br}E}{L_{bm}}\cos^3\Theta \qquad 3\text{-}22$$

Replacing K_{bm} and K_{br} in Eq 3-19 by their respective values from Eq 3-20 and 3-22

$$I_{bm} \geq \frac{1}{6\alpha}\frac{A_{br}L_{bm}^2\cos^3\Theta}{(\frac{K_{br}}{K_{bb}}-1)} \qquad 3\text{-}23$$

To avoid having to consider column stiffnesses it is possible to establish a beam classification based on flexural stiffness as follows:

A flexible beam fails to satisfy Eq 3-23 even if it had fixed ends ($\alpha = 4$). It is then characterized by

$$I_{bm} \leq \frac{1}{24}\frac{A_{br}L_{bm}^2\cos^3\Theta}{(\frac{K_{br}}{K_{bb}}-1)} \qquad 3\text{-}24$$

A stiff beam satisfies Eq 3-23 even if it were simply supported ($\alpha = 1$); it is characterized by

$$I_{bm} \geq \frac{1}{6}\frac{A_{br}L_{bm}^2\cos^3\Theta}{(\frac{K_{br}}{K_{bb}}-1)} \qquad 3\text{-}25$$

An intermediate stiffness beam has a moment of inertia falling between the limits defined by Eq 3-24 and 3-25:

$$\frac{1}{24}\frac{A_{br}L_{bm}^2\cos^3\Theta}{(\frac{K_{br}}{K_{bb}}-1)} \le I_{bm} \le \frac{1}{6}\frac{A_{br}L_{bm}^2\cos^3\Theta}{(\frac{K_{br}}{K_{bb}}-1)} \qquad 3\text{-}26$$

Notice that for the same moment of inertia, a given beam will be considered as stiff, intermediate or flexible as the area of the braces is increased from small to intermediate to large, respectively.

3.2.2. Vertical unbalance load on beams:

From Figure 3-2 and Eq 3-5, 3-6 and 3-9 the maximum unbalance load that can be statically applied to the beam can be approximated by

$$P_{un} = (K_{br}\Delta_{brt}+K_{bb}\Delta_{brc})\sin\Theta \qquad 3\text{-}27$$

or

$$P_{un} = (P_c-P_{cy}+K_{br}\Delta_{brt})\sin\Theta$$

where $\Delta_{brc} = \Delta_y-\Delta_c$ and $P_{cy} = P(\Delta = \Delta_y)$. Replacing Δ_{bm} in Equations 3-4-a and 3-4-b by its value from Equation 3-11, Equation 3-4-a now contains Δ_{brc} and Δ_t only. Further, replacing Δ_t in Equation 3-4-b by its value in Δ_{brc} obtained from Equation 3-4-a as modified hereabove, Equation 3-27 now becomes

$$P_{un} = \sin\Theta(P_c-P_{cy}+K_{br}\Delta_{brc})\frac{\cos\Theta-\dfrac{\sin^2\Theta(K_{br}+K_{bb})}{\sin^2\Theta(K_{br}-K_{bb})+K_{bm}}}{\cos\Theta+\dfrac{\sin^2\Theta(K_{br}+K_{bb})}{\sin^2\Theta(K_{br}-K_{bb})+K_{bm}}} \qquad 3\text{-}28.$$

Normalizing with respect to story shear at first buckling $V_c = 2P_c\cos\Theta$:

$$\frac{P_{un}}{F_c} = \frac{1}{2}\tan\Theta[1-\frac{P_{cy}}{P_c}+(\frac{P_y}{P_c}-1)]\frac{\cos\Theta-\dfrac{\sin^2\Theta(1+\frac{K_{bb}}{K_{br}})}{\sin^2\Theta(1-\frac{K_{bb}}{K_{br}})+\frac{K_{bm}}{K_{br}}}}{\cos\Theta+\dfrac{\sin^2\Theta(1+\frac{K_{bb}}{K_{br}})}{\sin^2\Theta(1-\frac{K_{bb}}{K_{br}})+\frac{K_{bm}}{K_{br}}}} \qquad 3\text{-}29$$

Figure 3-3-c illustrates the variation of the unbalance force with brace slenderness and relative beam stiffness. A beam will be considered as strong if it can sustain the maximum vertical unbalance force in addition to its normal gravity loading. A weak beam develops plastic hinges prior to the yielding of the tension braces. The collapse mechanism associated with such a case involves energy dissipation in the buckled braces and the plastic hinges of the beam only. In all cases beams are assumed to have sufficient shear strength to avoid failure by shear. The above mentioned classification of beam strength is independent of the stiffness classification previously established: a stiff beam could be strong or weak, as could be a flexible beam. However, in the remainder of this chapter all beams, stiff and flexible, will be assumed to be strong.

3.3. TYPES OF COLLAPSE MECHANISMS

Consider a typical chevron-braced panel from the structure in Figure 3-1. The static collapsed state of that panel corresponds to the state in which no increase in lateral load resistance can be obtained. If a strong-column weak-girder design approach is used, there are two possible collapse mechanisms. The first collapse mechanism is associated with a flexible beam and the second involves a stiff beam. As seen from the previous section, the effective post buckling stiffness is very sensitive to the stiffnesses of the beam and of the braces. Since there are three categories of brace slenderness (small, intermediate and large), there are three different cases for each collapse mechanism. Moreover, the beam may yield before or after the tension brace, leading to a total of twelve different mechanisms.

3.3.1. Flexible beam collapse mechanism:

For small brace slenderness the tension yield force P_y is only slightly larger than the buckling force magnitude (Figure 3-4-a). The unbalance force applied to the beam is then about equal to $(P_y - P_c)\sin\Theta$. Since $P_y \approx P_c$, this implies that the maximum unbalance is nearly zero. However the beam being very flexible, the tension force in B1 remains practically constant. Δ_{brt} increases less rapidly than Δ_{brc} (Figures 3-4-a).

For intermediate slenderness the tension force P_y is significantly larger than P_c. The maximum unbalance force that can be applied to the beam is thus larger. However, as for small slenderness braces, the beam being very flexible, the tension force in B1 remains almost constant (Figure 3-4-c). Since intermediate slenderness braces lose strength quickly with increasing deformation, the total lateral resisting force

will decrease significantly with increasing deformation. The overall behavior effect is then that of a buckling element: a sudden drop in resistance (Figure 3-4-d).

For large slenderness the tension yield force P_y is much larger than the buckling force P_c. The maximum unbalance force that can be applied to the beam is then quite large, but the beam being flexible, the tension force in brace B1 cannot not increase to P_y (Figure 3-4-e). Since the resistance of the compression brace decreases slowly with increasing deformation, the overall lateral resistance of the panel decreases slowly as the deformation is increased (Figure 3-4-f).

In all three cases the final collapse mechanism may occur when plastic hinges form at the beam ends, rather than by yielding of the tension brace. This weak beam case behaves similarly to the one with stronger beams but the onset of the collapse mechanism is sooner. Notice also that for all cases with a flexible beam, the resistance when a collapse mechanism forms is smaller than the resistance at first buckling.

3.3.2. Stiff beam collapse mechanism:

The second collapse mechanism is associated with a stiff beam. It is assumed that the beam's shear strength is sufficient to avoid shear failure. Equations 3-4 to 3-9 still apply in this case. However, the beam being stiff, the tension brace elongation Δ_{brt} is approximately equal in magnitude to the compression brace shortening Δ_{brc} (Figures 3-5-a,c,e). Again, one can distinguish three cases: small brace slenderness, intermediate brace slenderness and large brace slenderness.

For small slenderness the tension yield force P_y is only slightly larger than the buckling force P_c. The beam being very stiff, the tension force in brace B1 will keep increasing. The maximum unbalance force that can be applied to the beam is $(P_y - P_c)\sin\Theta$. If the beam is strong, according to our definition, the tension in brace B1 will reach P_y before the beam yields. From that point onward the resistance provided by the bracing cannot increase; in fact it drops slowly because the compression in brace B2 decreases slowly with deformation (Figure 3-5-a). For small slenderness the points where P_c and P_y occur are so close that they can be considered as a single event. The overall behavior is that of a deformation softening system (Figure 3-5-b).

For intermediate slenderness braces the tension yield force P_y is significantly larger than P_c, but cannot exceed $2P_c$. The maximum unbalance P_{un} that can be applied to the beam is larger than in the previous case. The tension force in brace

B1 will be increasing at the rate K_0, while the compression in brace B2 will be decreasing at the rate K_{bb}. For intermediate brace slenderness the buckled brace tangent stiffness K_{bb} is negative and starts with an absolute value larger than the elastic brace stiffness K_0. The magnitude of K_{bb} decreases rapidly to stabilize at a small fraction of K_0. The total effect is a sharp drop in story resisting force, followed by an increase at the rate K_e. Since P_y is less than $2P_c$, the ultimate story strength F_u is approximately equal to the strength at first buckling F_b (Figure 3-5-d). After brace B1 yields in tension, the total resistance starts dropping slowly.

For large slenderness the tension yield force P_y is much larger than P_c. The maximum unbalance P_{un} that can be applied to the beam is larger than in the previous case. The tension force in brace B1 will be increasing at the rate K_0, while the compression in brace B2 will be decreasing at the rate K_{bb} (Figure 3-5-e). For large slenderness K_{bb} is always numerically smaller than K_{br}, therefore K_e is always positive and the resisting force is always increasing. After brace B1 yields in tension, the total resistance starts dropping slowly. The overall behavior is that of trilinear system with a deformation softening final stage (Figure 3-5-f).

Again, as in the previous cases, beam yielding could precede yielding of the tension brace. The same overall force-deformation characteristics would be observed.

3.4. COMPUTER SIMULATIONS

To demonstrate the effect of brace buckling on load redistribution more quantitatively, a two-story chevron-braced structure is used as the basis of a series of computer simulations (Figure 3-1). In order to limit the number of parameters in this demonstration, all members are assumed pin jointed, and beams and columns are assumed to be inextensible and infinitely strong axially. Beams have a finite flexural stiffness but are assumed to remain elastic. A linear lateral force pattern is imposed quasistatically to permit comparison of results for cases with the same deformation history but different member proportions.

Both flexible and stiff beam configurations were investigated. Three different brace slenderness ratios, equal to 20, 100 and 200, were employed. The analyses are first carried out for braces having a constant buckling strength P_c (Section 3.4.1) and then are repeated for braces having constant yield force P_y (Section 3.4.2). Details of the structures considered are contained in Figure 3-1 and Table 3-1. The analysis was carried out using the structural analysis program ANSR [52], the braces

being modeled by Ikeda's brace element [35].

Several quantities were used for comparisons. Story shear versus story drift relationships are examined to study resistance characteristics of the structure following brace buckling. The internal forces of interest are the axial forces in the columns, and the vertical unbalance force at midspan for the beams. To examine the force redistribution process, results are plotted with respect to story drift. However, to assess the magnitude of the redistributed forces and of their importance, the variation of internal forces with story shear are also shown.

Results for stiff beams are compared to those obtained for flexible beams. In all the figures, a solid line denotes results for small brace slenderness (λ = 20). Long-dashed lines represent values for braces of intermediate slenderness (λ = 100), and short dashes are for large slenderness (λ = 200). All forces are normalized versus story shear at first buckling. Story drift is measured as a percentage of the story height.

3.4.1. Chevron-braced frames at constant P_c:

In all cases examined in this section braces have the same buckling load P_c (see Section 2.4.3). The quantitative results obtained are in complete agreement with the qualitative descriptions in Sections 3.1 and 3.2.

3.4.1.1. Story shear versus story drift: It can be seen from Figure 3-6 that small slenderness braces cause a bilinear softening behavior, whether the beam is stiff or flexible. An intermediate slenderness results in a degrading resistance-deformation curve. The strength deterioration is more important for flexible beams than for stiff ones. The resistance increases slowly with drift until the tension brace yields (beams are assumed to remain elastic in these examples). Yielding of the tension brace occurs sooner with stiff beams (0.5 % drift for λ=100) than with flexible beams (2.5 % drift for λ=100). For large slenderness braces and a flexible beam, the force-deformation curve has a narrow range of reduced stiffness corresponding to the elastic buckling strength plateau. This is followed by a strength degradation after the compression brace forms a plastic hinge. If a stiff beam is used then one obtains a trilinear hardening resistance-deformation curve.

Notice that the initial lateral stiffness increases with brace slenderness. This is due to the constraint of constant brace buckling strength adopted in this section. As brace slenderness increases the buckling stress drops (Eq 2-10-b). To maintain the same buckling strength, the brace cross sectional area must be increased with

increasing slenderness. This increases the brace axial stiffness which is a major component of the structure's lateral stiffness.

3.4.1.2. Beam unbalance load: As expected, the maximum unbalance force on the beam increases with brace slenderness. For the same brace slenderness, the unbalance force is larger and occurs earlier for stiff beams than for flexible beams (except for the stocky braces where the results are similar). Unbalance forces occur at a smaller drift for larger brace slenderness (Figure 3-7) because frames with slender braces have more lateral stiffness and hence reach the buckling strength at a smaller drift. The unbalance force keeps increasing until the tension brace yields. This happens sooner with stiff beams (0.5 % for $\lambda = 100$) than with flexible beams (2.5 % for $\lambda = 100$). The maximum unbalance force can be quite large compared to the story elastic shear strength F_c, especially in cases of stiff beams and slender braces. It may not be possible to economically design beams that are strong enough to resist such large unbalance forces.

The maximum unbalance force on the beam for a given story shear increases with brace slenderness (Figure 3-9). For the same brace slenderness, the maximum beam unbalance force is larger for stiff beams than for flexible beams.

3.4.1.3. Column axial forces: Axial forces in the columns originate from two sources: an overturning moment component, and a component due to the vertical unbalance load on the beam. Because of the geometry of the example frame and the use of pinned connections, the first source of axial force, the overturning component is most clearly displayed in the ground story columns for the case of stocky braces (λ = 20). For that case the vertical unbalance component is almost nonexistent with either flexible or stiff beams. The axial column forces on both sides of the structure are almost symmetric across the horizontal axis in Figure 3-8-a. Since the shapes of the base shear-lateral deflection relations for these cases (Figure 3-6) are nearly elasto-perfectly plastic, column axial forces follow the same relationship and have a maximum value as expected equal to 0.6 F_c. The second source of axial force results from the shear in the beam attached to the top of the column. In the elastic range this force is zero, but once a brace buckles in that story, the shear in the beam increases column compression by $P_{unbal} / 2$.

Both of these effects are combined in the first story columns. It is interesting to note that the two effects tend to cancel in the column that would normally be in tension. The unbalanced load is sufficient in many cases to induce net compression

forces in the tension column. Similarly, the compression forces can be significantly increased. The vertical unbalance component is most clearly displayed in Figure 3-8-b for the second story column axial forces. The overturning moment component for these columns is nil because the lateral load is directly picked up by the braces. It is evident in this case how the unbalance force developed in the beams after brace buckling (Figure 3-7) is transmitted to the columns. The axial force is zero until brace buckling occurs, and then it increases with brace slenderness, especially in presence of stiff beams. This is particularly significant in cases of slender braces with stiff beams where the maximum column compression may be quite large (up to three times the elastic story shear strength). Of course, beam yielding may limit these forces. However, beams may be stronger than intended due to composite action with slabs. Similarly, unbalance forces can be larger than expected due to use of braces larger than the required size, approximate effective length factors and initial imperfections (reducing P_c). If these possibilities are not accounted for at the design stage, column yielding or buckling may occur leading to sudden collapse of the whole structure. Consequently, it is important to consider the effect of brace slenderness ratio as well as of beam stiffness and strength on the post-buckling strength and redistribution of forces.

At any given story shear value after brace buckling has occurred, column compression is larger for slender braces than for stocky braces (Figure 3-10-a,b). The increase is not very large when flexible beams are used. At any brace slenderness and story shear, column compression is larger for a stiff beam than for a flexible beam. Moreover, in case of stiff beams and slender braces, the column axial compression after brace buckling increases with story shear at a faster rate than it did before brace buckling (Figure 3-10-a). The trend is even more evident in Figure 3-10-b for the second story columns. This implies that for such cases, as the actual loading increases beyond the story elastic shear strength column forces increase at a faster rate and hence may fail earlier than predicted by an extrapolation of elastic analysis results. Notice that the imposed displacement pattern yields the first story before the second, hence the complicated curves in Figure 3-10-a.

3.4.2. Chevron-braced frame at constant P_y:

Another series of simulations was considered where the tension yield force P_y was held constant for various brace slendernesses (λ = 20,100,and200) and beam stiffnesses (flexible and stiff). The objective was to compare the observations with those based on constant P_c. As for constant P_c cases, the two most important

parameters were found to be brace slenderness and ratio of beam stiffness to brace stiffness in the vertical direction.

3.4.2.1. Story shear versus story drift: Since the areas of the braces are the same in all of the cases considered, the initial elastic stiffnesses of the frames are identical (Figure 3-11). However, relative to the base shear capacity of a system with yielding rather than buckling braces, it is seen that the shear strength at which the first brace buckling occurs decreases with increasing brace slenderness. The strength reduces substantially following first buckling in all cases except for slender braces with stiff beams. A stiff beam increases the post-buckling strength for all brace slenderness cases.

3.4.2.2. Beam unbalance load: For stiff beams, the unbalance force applied to the beam occurs at smaller story drifts for large brace slenderness (Figure 3-12). That is because large slenderness braces buckle at a smaller load and hence at a smaller drift. Maximum beam unbalance force is largest for intermediate brace slenderness and stiff beams. For flexible beams, the unbalance force applied to the beam is practically independent of brace slenderness.

3.4.2.3. Column axial forces: For constant P_y the overturning moment component of column compression seems to be predominant over the vertical unbalance load component. For flexible beams as well as for stiff beams, maximum column compression in the first story decreases with increasing brace slenderness (Figure 3-13-a). Since the second story columns receive axial forces from the vertical unbalance force component only, their pattern of axial force variation with story drift is the same as that of the vertical unbalance force on the beam. With stiff beams, maximum column compression at any given story drift increases with brace slenderness (Figure 3-13-b). With flexible beams, maximum column compression is practically the same for all brace slendernesses.

Conclusions derived from comparisons at constant brace yield load are in general similar to those made from comparisons at constant brace buckling load. The most important difference concerns column axial forces. At constant brace yield force increasing the slenderness would reduce the columns axial forces, but it would also reduce the story strength at the first inelastic event. This conclusion is misleading because in practice the desired story strength would be determined first hence fixing the brace's buckling load. At constant brace buckling load increasing the

slenderness would increase column axial forces, especially if a stiff strong beam is used.

3.5. CONCLUSIONS

It has been shown that the post-buckling force redistributions in chevron-braced frames are extensive and are very sensitive to beam stiffness and to brace slenderness. These force redistributions are entirely unpredictable by elastic analysis (e.g., the vertical unbalance force on the beam) or are underestimated (e.g., the increased rate of column compression after brace buckling). Yet, to improve the ductility of such frames, it is essential to keep in mind these redistributions when proportioning the structural components. A classification for beams has been established according to their stiffness. With this classification along with that of braces (Chapter 2) it is possible to determine which collapse mechanism (flexible or stiff beam mechanism) is likely to occur for a given configuration. Alternatively, it becomes possible to proportion beams and braces to favor one collapse mechanism over another. With Equation 3-28 it is possible to predict the maximum unbalance force that the brace can apply to the beam. This unbalance force will be considered further in following chapters and appendices.

It is generally believed that a hardening post-yield force-deformation characteristic gives a better dynamic response than an elasto-plastic response which is still preferable to a deteriorating resistance characteristic. Stiff beams and slender braces are necessary to achieve a trilinear response. From Equation 3-25, a table of steel section properties and the usual braced bay dimensions, it is evident that it is difficult or impractical to achieve a stiff beam effect. Furthermore, Equation 3-29 implies that the columns in such a frame would then have to be designed for very large compression forces, if column yielding or buckling is to be avoided. Similarly, it appears that intermediate slenderness braces should be avoided because they induce the largest force redistributions. It appears from these static analysis results that stocky braces should therefore be used wherever possible.

CHAPTER 4

INELASTIC DYNAMIC RESPONSE OF A CHEVRON-BRACED PANEL

4.1. INTRODUCTION

As shown in the analyses of Chapter 3, it is possible to obtain six different modes of inelastic behavior in chevron-braced frames depending on the relative proportions of beams and braces. These quasi-static analyses are not sufficient by themselves to recommend one mode of behavior over another.

In this chapter, the dynamic inelastic response of each mode of chevron-braced frame behavior is analyzed for two kinds of idealized excitations: a pulse load and a sinusoidal excitation. The response of an elasto-plastic system of same strength, fundamental period and damping as the chevron-braced frame is used for comparison. Inelastic design spectra developed for chevron-braced systems subjected to various earthquake ground motions are compared to those for elasto-plastic systems. With these comparisons it is possible to assess some of the recent code recommendations for the design forces for braced systems.

4.2. SYSTEMS COMPARED

As shown in Figure 4-0, the structures used in the comparisons consist of one story, one bay, chevron-braced frames, and one story, one bay, moment resisting frames, proportioned to have the same fundamental period, viscous damping, and strength level at the first inelastic event. For each of the six cases for a chevron-braced system identified in Chapter 3, the brace and beam sections are chosen to maintain the same strength level at first brace buckling.

The response quantities utilized for the comparisons are the maximum displacement and the maximum energy dissipation demand. These are normalized with respect to the corresponding quantities for an equivalent elasto-plastic system of same strength level, fundamental period and viscous damping. Since the dynamic inelastic response of elasto-plastic systems has been widely researched and is thoroughly documented, it constitutes a good basis for comparison. The ductility demand for these elasto-plastic systems are shown in Figure 4-7 which is reproduced from Biggs [17].

4.3. RESPONSE COMPARISON FOR IDEALIZED EXCITATIONS

Earthquake excitations consist of a mix of pulses and of harmonic vibrations. The pulses often dominate in ground motions recorded close to the fault site while harmonic vibrations are most noticeable far away from the epicentre of the earthquake [54]. It is generally known that elasto-plastic systems are particularly vulnerable to excitations characterized by long pulses [14]. On the other hand, harmonic excitations can induce the most severe response in elastic systems and hence hasten the occurrence of yielding. They can also lead to problems of low cycle fatigue in yielding systems. Accordingly, two idealized loadings are used to study the dynamic inelastic response of chevron-braced systems. One excitation is a triangular pulse with equal rise and fall time T_r, and the other consists of five cycles of a sine wave of period T_f.

For each of the simulations, the amplitude P_{max} of the excitation ranges (Figure 4-0) from $0.2F_c$ to $2.0F_c$. For the pulse excitation the ratio T_r/T sweeps the range between 0.2 and 2.0. Similarly, for the sinusoidal excitation, the ratio T_f/T varies between 0.2 and 2.0. In all cases, the system is assumed to be initially at rest.

4.4. FINDINGS

The results of all simulations are shown in Figures 4.1 to 4.4. The peak ductility ratios are reported in Tables 4-1 and 4-2.

Figures 4-1-a to 4-1-f show the variation with T_r/T and P_{max}/F_c of the ratio of maximum displacements for the six cases. It is evident from these graphs that for the case of stocky braces, the beam stiffness does not appreciably affect the response. However, displacement ductility demands are amplified when $P_{max}/P_y \geq 1$. For the case of intermediate slenderness braces, the maximum displacement for a braced system can also be a lot larger than that of a corresponding elasto-plastic system. However, the use of a stiff beam reduces the magnitude of the peak displacement ratio (which still remains large). For slender braces, the use of a stiff beam can tremendously reduce the maximum displacement ratio, even to less than one. This is due to the trilinear deformation hardening characteristics.

Similarly, Figures 4-2-a to 4-2-f show the variation with T_r/T and P_{max}/F_c of the ratio of maximum energy dissipation for the same six cases. These figures dramatically show the relative sensitivity of the braced system with intermediate slenderness braces. The high sharp peaks reflect the cases where an elasto-plastic system barely yields while a braced system has to dissipate a large amount of energy.

The use of a stiff beam in all cases of brace slenderness does reduce the amount of energy dissipation demand, but that amount still remains high compared to that in an equivalent elasto-plastic system.

Figures 4-3-a to 4-3-f show the variation with T_f/T and P_{max}/F_c of the ratio of maximum displacements for the six cases. These figures differ markedly from those for the pulse excitation. The ratio of peak displacements are closer to one. In particular, the response of frames with stiff and flexible beams are comparable. In the case of stocky braces, the response is always larger than or equal to that of an equivalent elasto-plastic system (because of the deformation softening). Displacement ratios increase with increasing T_f/T and P_{max}/P_y. In the cases of slender and intermediate slenderness braces, the maximum displacement can in some cases be smaller than that of corresponding elasto-plastic system irrespective of the beam stiffness. This can be probably related to the existence of a range of displacement amplitudes where a braced system can dissipate more energy per cycle than a similar elasto-plastic system. However, the displacement ratios generally increase with increasing T_f/T for P_{max}/P_y less than unity.

Figures 4-4-a to 4-4-f show the variation with T_f/T and P_{max}/F_c of the ratio of energy dissipation demand for the harmonic loading cases. Although the ratio of energy dissipation demand is largest in the case of intermediate slenderness braces and flexible beams, it is much smaller than the corresponding ratio for pulse loading. The use of stiff beams reduces the maximum ratio of energy dissipation demand.

4.5. COMPARISON OF INELASTIC DESIGN SPECTRA

Inelastic design spectra have been developed for structures exhibiting elasto-plastic types of hysteresis loops [15,80]. These models represent the behavior of moment resisting frames, but they are not suitable for chevron-braced frames which exhibit a more complex hysteretic behavior. A special program (NOSPEC) was developed to generate inelastic response spectra for a variety of structural hysteresis models. One model in NOSPEC represents the buckling behavior of chevron-braced frames (Figure 4-5). Using this element, it is possible to generate inelastic design spectra for buckling type structures and to compare them with those of moment resisting structures. The design spectra are developed as follows. For every strength level, a mean response spectrum is obtained by averaging the results of six earthquake records (typical of the western United States, Table 4-3). The ductility demand curves at constant strength levels are back interpolated to obtain design strength levels $\eta = F_c/M\ddot{v}_{g_{max}}$ for constant ductility. The same procedure is repeated

for displacement and energy ductility demands.

Three cases were considered in generating the inelastic design spectra. Only chevron-braced systems of deteriorating strength type are considered because they are the most commonly encountered and the most critical. Data is available elsewhere for bilinear and trilinear hysteretic systems [15]. The systems considered are:

(1)- SNAP40: a braced system model with $K_b/K_0 = -0.5$, $K_f/K_0 = 0.001$ and $P_{min}/P_c = 0.40$. This case is an idealization of a chevron-braced system with intermediate slenderness braces and flexible beams.

(2)- SNAP70: a braced system model with $K_b/K_0 = -0.5$, $K_f/K_0 = 0.001$ and $P_{min}/P_c = 0.70$. This case is an idealization of a chevron-braced system with intermediate slenderness braces and flexible beams and enclosed within a moment resisting frame.

(3)- LEPP: a reference elasto-plastic model with $K_f/K_0 = 0.001$.

4.6. FINDINGS

Figures 4-6-a to 4-6-d show the ratio of design strength levels of chevron-braced systems to those of elasto-plastic systems, necessary to maintain the same ductility demands. It is evident from these results that the constraint of equal displacement ductility demand (Figures 4-6-a and 4-6-c) is more stringent than that of equal energy ductility demand (Figures 4-6-b and 4-6-d): it requires a higher strength level for either braced system considered. Assuming that the allowable displacement and energy ductility capacities of chevron-braced systems are arbitrarily three-fourth (3/4) of those for an elasto-plastic system, Table 4-4 shows that such braced systems must be designed for a force level 1.3 to 1.9. In that case the proposed SEAONC [75] code recommendations for chevron-braced frames appear to be on the conservative side: 1.5 * 12/ 8 = 2.25. The 12 and 8 are the design force reduction factors R_W specified by SEAONC for moment resisting and braced systems respectively, and the 1.50 factor is for the 50% increase in design forces for chevron-braced systems. These recommendations do not account for the different cases introduced here. However, before more general conclusions can be drawn on the adequacy of such recommendations more extensive studies on multidegree of freedom systems must be performed.

4.7. CONCLUSIONS

From comparing the results of pulse loading to those of harmonic excitation, it is evident that pulse loading is particularly damaging for braced systems. For both types of loading, the combination of stiff beam and slender braces has the most desirable overall dynamic response, followed by cases of stocky braces. The combination of flexible beam and intermediate slenderness braces has the most undesirable response characteristics, namely very large displacement and energy dissipation demands.

At the same strength level as a comparable elasto-plastic system, chevron-braced structures have to accommodate more displacement and energy dissipation demand. However, braced systems usually have a smaller reliable energy dissipation capacity, so that they must be designed for a higher strength level. The earthquake design spectra generated have confirmed the already accepted notion of designing concentrically braced frames for higher force levels. These results are strictly valid only for single degree of freedom systems. The next chapter will examine the validity of these conclusions for realistic multistory structure models.

CHAPTER 5

INELASTIC DYNAMIC RESPONSE OF MULTISTORY CHEVRON-BRACED FRAMES

5.1. INTRODUCTION

The last two chapters have dealt with the static and dynamic response characteristics of one story, one bay, chevron-braced structures. These were modeled as single degree of freedom systems for the dynamic analyses. These chapters contained several important conclusions which may not be directly applicable to multi-degree of freedom systems. As discussed in Chapter 1, multistory chevron-braced structures have been found to exhibit special problems, in particular a tendency to form soft stories.

This chapter explores the behavioral characteristics specific to multistory chevron-braced steel frames. It also examines the effectiveness of several design recommendations that are generally believed to improve their response; namely,

(1)- The use of stocky braces instead of intermediate slenderness braces.

(2)- The use of stiff beams instead of flexible beams.

(3)- An increase of frame participation in resisting lateral loads.

These investigations are carried out using numerical simulations. The first section of this chapter describes the simulation procedures and the response quantities monitored. Then, a detailed account of the results is examined, followed by a discussion of some of the dynamic effects characteristic of chevron-braced frames. Finally, conclusions are drawn regarding the effectiveness of the design recommendations considered, and the implications of the results observed.

5.2. STRUCTURAL MODELS

The primary design parameters considered for this study are the brace slenderness, the beam stiffness, and the frame participation in resisting the lateral load. A six story high by three bays wide chevron-braced steel frame is used to systematically study the effects of these parameters on the dynamic inelastic response.

The frames analyzed (Figure 5-1) are assumed to be an exterior frame of a six story building that is square in plan and that has three bays on each side. Frames are spaced at 20 ft (6.10 m) in each direction and only the exterior frames are assumed to be braced and to resist the lateral loads. The gravity loads assumed consist of uniformly distributed dead loads of 110 psf (5.27kN/m$^{2)}$ and live loads of 80 psf (3.83kN/m^2). The equivalent static lateral seismic loads are computed according

to 1985 UBC Zone 4 requirements. The factor K was taken equal to one (1) for all frames except those considered as dual systems for which K is set to 0.8 [32]. The importance factor I was set to one (1) and the product CS was controlled by the limit 0.12. Z being one (1) for zone 4, this leads to a base shear coefficient of 0.12 for the reference case KREG. Floor diaphragms are considered as rigid in plane and flexible out of plane. In designing the beams of the braced bays, the support provided by the braces at midspan is neglected. A weak beam-strong column philosophy is applied in selecting member proportions. A36 steel is used for all structural steel members. The inertial mass for the horizontal degree of freedom at each story is based on half the story dead load (there are two symmetric braced frames in each direction). For the vertical degrees of freedom, inertial mass is computed based on tributary area and dead load weight.

In all parameter variations for a given set of lateral loads the braces design buckling loads are kept constant. This corresponds to the typical design situation where equivalent lateral loads are specified and simplified analysis procedures are used in the design. Thus, brace sizes change with the assumed slenderness ratio so as to maintain the same buckling load. When choosing brace sections from the AISC tables, wide flange sections only were considered for braces except in one case where double angles were used.

To carry out the analyses a physical theory brace model developed by Ikeda [35] was used in the program ANSR [52]. The numerical time integration uses Newmark's average accceleration scheme, with an integration time step of 0.001 s to capture higher mode effects. Rayleigh type damping conforming to 3% in the first two modes was used. Constant stiffness iteration is used at each time step to insure convergence despite softening force-deformation characteristics.

5.3. CASES CONSIDERED

In conducting the parametric studies many cases were considered. To simplify their description, they can be classified into three sets:

5.3.1. The first set:

The first set looks at the sensitivity of the response in a chevron-braced frame to such factors as hinged versus fixed beam to column connections, brace slenderness, accidental brace understrength and overstrength, beam stiffness, and ground motion intensity. For all cases in this set the UBC coefficient K is set to one (1).

(1)- KREG is the reference chevron-braced frame as described above with

intermediate slenderness braces (λ = 92). The braced bay is sized to carry all the design lateral loads. However, all beams are connected to columns via moment resisting connections designed for gravity loading.

(2)- KPIN is a chevron-braced frame similar to KREG but with pinned beam-to-column connections outside the braced bays.

(3)- KELAS is a frame similar to KREG except that all members are assumed to remain elastic.

(4)- KSBM is a frame similar to KREG except that flexurally rigid infinitely strong beams in the braced bay.

(5)- KSTO is a frame similar to KREG except that it uses small slenderness braces (λ = 46) each with the same buckling load as the corresponding brace in KREG. These pin ended braces do not correspond to any real sections in the AISC tables; their cross sectional areas are given in Table 5-1.

(6)- KOVER is a frame similar to KREG except that it is analyzed assuming that the braces have an actual effective length of half the value assumed in the design (for example the design assumes the braces have pinned ends while the construction provides full fixity). The effective buckling strength of these braces is 25% larger than that of their counterparts in KREG, and their effective slenderness is 46.

(7)- KUNDER is a frame similar to KSTO except that it is analyzed assuming that the braces have an actual effective length of twice the value assumed in the design (for example the design assumes the braces to have fixed ends while the construction provides pinned end conditions). The effective buckling strength of these braces is 21% lower than that of their counterparts in KSTO and in KREG, and their effective slenderness is 92.

(8)- KREG30 is a frame similar to KREG except that the ground excitations are proportionately scaled downward such that the North-South component of the 1940 El Centro record has a peak acceleration of 0.30g.

(9)- KREG70 is a frame similar to KREG except that the ground excitations are proportionately scaled upward such that the North-South component of the 1940 El Centro record has a peak acceleration of 0.70g.

5.3.2. The second set:

The second set of studies looks at the effect of frame participation on the response characteristics. In this set, design frame participation took values of 0%, 25%, and 50% for intermediate slenderness braces and for stocky braces. Frame

participation in this context is the proportion of the static lateral design loads that is assigned to the moment resisting frame. All beam to column connections are moment resisting. All intermediate slenderness braces have a slenderness of 92 in the first four stories and of 115 in the top two stories. All small slenderness braces have a slenderness of 46 in the first four stories and of 57 in the top two stories. For all the cases in this set the UBC coefficient K is set to 0.8.

(1)- KD00 is a frame similar to KREG but designed using K=0.8 as for dual systems, even though the moment resisting frame is not sized for the design lateral loads. This case serves as a reference in determining the effect of frame participation (when compared to KD25 and KD50) and of design load magnitude (when compared with KREG). It should be noted however, that member sizes in the moment resisting frame are controlled by gravity loads and do not change as much as the braces. Braces do become smaller as a result of the smaller K factor (see Table 5-1).

(2)- KD25 is a dual system chevron-braced frame with intermediate slenderness braces and a moment resisting frame sized for 25% of the design lateral loads.

(3)- KS25 is a frame similar to KD25 except that it uses small slenderness braces (λ=46).

(4)- KD50 is a dual system chevron-braced frame with intermediate slenderness braces and a moment resistant frame sized for 50% of the design lateral loads.

(5)- KS50 is a frame similar to KD50 except that it uses small slenderness braces. The braces in KS25 and KS50 do not correspond to any sections in the AISC tables; their cross-sectional areas are reported in Table 5-1.

5.3.3. The third set:

The third set of studies evaluates the merits of a design based on an "improved strength and stiffness distribution". Such a distribution aims at achieving mean peak forces and energy dissipation demands that are proportional to member capacities. It is obtained as follows. An average power spectrum is derived for the earthquakes used in the simulations. The trial structures are analyzed using random vibration techniques for the input power spectrum determined above. The brace section sizes are changed by trial and error until the section size distribution becomes proportional to the expected elastic peak brace compression. Convergence to the "improved design" is quite fast; requiring two or three iterations only. Since the random vibration analysis technique used is applicable to elastic structures only, the section sizes finally obtained are scaled downward proportionately such that the first story brace

sizes equal those of the UBC based design. The section sizes in all other stories are imaginary in that they do not correspond to the size of any section in the AISC manual [2]. The required sizes of the imaginary sections reduce more rapidly with height than do those of the UBC design (Table 5-1). All the proportional braces have the same slenderness of 92 (Table B9). Only one structure was finally analyzed for this set (i.e. KPRO) which corresponds to the conditions assumed for KREG. Except for the braces, KPRO has the same member sizes as KREG (Table 5-1).

The range of fundamental periods is quite narrow, with KREG and KD50 at the low end around 0.6s and KSTO, KPIN and KPRO at the upper end around 0.7s.

5.4. EARTHQUAKE LOADING

The simulations are confined to severe ground motions only. That is because chevron-braced frames generally show an excellent response in the elastic range (corresponding to seismic excitations of moderate intensity). For the dynamic analysis each frame is subjected to the "worst ten seconds" of six earthquakes representative of the western United States (Table 5-2). The "worst ten seconds" from each earthquake are taken as those where there is a maximum increment in root mean square acceleration (Arias intensity [7]). To obtain the standard ground motion intensity, the ten second window extracted from the North-South component of the 1940 El Centro record is scaled to a peak ground acceleration of 0.5g. The remaining excitations are then scaled to the same root mean square acceleration (Figure 5-2-a). The overall mean of the peak ground acceleration for the excitations used is 0.56g. Figure 5-2-b shows the average input power spectrum of the scaled excitations. The T_{start} entry in Table 5-2 indicates the beginning of the 10 s window in the original earthquake record.

5.5. RESPONSE QUANTITIES

The response quantities used for evaluating seismic performance of the different cases include:

(1)- The **total energy dissipation demand** and its **distribution** over the individual stories. The total energy dissipation demand is a measure of the cumulative damage inflicted to the structure. The distribution over the individual stories is a measure of design effectiveness, based on the premise that the more uniform the distribution, the better the design. A distribution of energy

dissipation demand that is uniform or proportional to member strength distribution reflects the absence of soft stories and an "optimal" distribution of strength.

(2)- The **maximum story shears.** Maximum story shears give an indication of the ability of the structure to meet or exceed its strength capacity. Maximum story shears in conjunction with story ductility may be used heuristically to decide how much one should increase or decrease story strength to achieve a more uniform ductility demand over the structure.

(3)- The **maximum story drift** is another measure of damage incurred in the structure. Drifts should be kept below a certain limit (e.g. 1/75 or 1/50 of the story height) to avoid geometric instability [45].

(4)- The **maximum column compression** is a good indicator of the frame participation in the response and of force redistributions due to brace buckling. Beam moments are not retained for evaluation because the frames are proportioned according to weak beam-strong column design philosophy and moments are thus limited by the beam yield value.

To account for the variability of inelastic response in evaluating each system's performance, the mean and coefficient of variation (COV) of each response quantity must be considered. Mean values are used to show trends and COV should reflect the sensitivity of the response to the characteristics of the ground motion [4]. Ideal structural configurations have uniform mean values and small coefficients of variation, indicating a response that is relatively insensitive to the characteristics of the excitations.

Consider, for example, the graphs for KREG shown in Figure 5-3; the solid lines show the mean peak values, and the dashed lines a margin of plus and minus one standard deviation. There is a 50% chance that the response exceeds the mean peak value. The wider the band defined by the dashed lines, the more scattered the response is. Assuming a normally distributed response, the probability of the response falling within the band defined by the dashed lines is 33%. The narrow bands for story shear and column compression forces indicate that the maxima of these forces are controlled by the formation of collapse mechanisms. Hence, these forces can be well predicted by capacity design methods. The short dashed lines on the column compression plots show for comparison the axial forces present under service gravity loads. It should be noted that these graphs do not vary uniformly with height. This reflects the tendency of chevron-braced frames to form soft stories. Here, greater drifts and energy dissipation demands were concentrated in the bottom three stories and in the fifth story. The typical story hysteresis loop

shown in Figure 5-3 is for the shear-drift relation of the first story for the East-West component of the 1935 Helena record.

5.6. DESCRIPTION OF RESULTS

Results for the frames considered are shown in Figures 5-3 to 5-17 and Tables 5-3 to 5-17. The description of the observed results is divided into sections that emphasize the effect of the design parameters on the response quantities:

5.6.1. Elastic design versus inelastic design (KELAS vs KREG, Figures 5-5 and 5-3 and Tables 5-5 and 5-3):

Designing the frame to remain elastic would require accomodating mean peak force levels two to three times as large as in a frame designed according to UBC. Moreover, the COV of elastic forces is much larger than the corresponding COV in KREG (twenty to thirty times bigger). Compared to KREG, drifts in KELAS are smaller in the lower stories and larger in upper stories. The comparatively larger lower story drifts in KREG are due to the occurrence of soft stories there. The relatively larger upper story drifts in KELAS can be possibly traced to three causes: (1) higher mode effects in the elastic structure KELAS which are not limited by brace buckling, (2) the increased column axial deformations (because of the higher elastic forces) leading to an overall bending deformation of the frame (cantilever deflection), and (3) the yielding of the lower stories in the inelastic frame (KREG) may help isolate the upper stories from further excitation. However, it is interesting to note that the COV of story drifts for KELAS are smaller than those for KREF.

5.6.2. Pinned connections versus moment connections (KPIN vs KREG, Figures 5-4 and 5-3, Tables 5-4 and 5-3):

The maximum story shears in KPIN are slightly lower than those in KREG due to reduced frame participation. But they have larger COV except at the third and fifth floors. Maximum story drifts in KPIN are larger than those in KREG at all stories except the first. The distribution of mean peak energy dissipation shows the same trend for both cases, but with a slightly lower COV in the case of KPIN. Compared to KREG, KPIN must dissipate slightly more energy in the upper stories.

5.6.3. Stiff beams versus flexible beams (KSBM vs KREG, Figures 5-6 and 5-3, Tables 5-6 and 5-3):

The use of stiff and strong beams changes the hysteresis loop characteristics from a deteriorating one (Type 2 as in Fig. 3-4-d) to a trilinear one (Type 6 as in Fig. 3-5-f). Compared to KREG, story shears in KSBM are approximately 40% larger and have a smaller COV (except in the first two stories). However, the increased axial forces in the columns reduced the flexural capacities sufficiently to completely yield the first story interior columns in flexure, causing a soft story there. The first story experienced very large drifts, excessive energy dissipation demands in the braces and the frame elements, and a doubling of exterior columns compression (due to force redistribution to the moment resisting frame).

5.6.4. Stocky braces versus intermediate slenderness braces (KSTO vs KREG; Figures 5-7 and 5-3 and Tables 5-7 and 5-3, KS25 vs KD25; Figures 5-14 and 5-13 and Tables 5-14 and 5-13, KS50 vs KD50; Figures 5-16 and 5-15 and Tables 5-16 and 5-15):

Using small slenderness braces ($\lambda = 46$) instead of intermediate slenderness braces ($\lambda = 92$) reduced maximum story shears, brace energy dissipation demands, and interior column compressions. On the other hand story drifts and total energy dissipation demand remained practically unchanged, and exterior columns compression increased. All these symptoms indicate an increased participation of the frame in load resistance and in energy dissipation. The COVs of member forces and energy dissipation demand are noticeably smaller for small slenderness braces than for the intermediate slenderness braces.

5.6.5. Accidental variation in brace strength (KOVER vs KREG; Figures 5-8 and 5-3 and Tables 5-8 and 5-3, KUNDER vs KREG; Figures 5-9 and 5-3 and Tables 5-9 and 5-3):

Compared to KREG, frames with accidentally overstrong braces (KOVER) experience a different pattern of response. All maximum story shears are increased by 30% approximately. Maximum story drifts remain approximately the same, except at the top story where drift increases by 40% (due to the higher elastic forces corresponding to the higher yield level). Compared to KREG, the largest amplification in story drift COV occurs for KOVER at the top and bottom of the frame (1.9 and 2.1 respectively), and maximum attenuation occurs at mid-height (fourth story; 0.21). The increased variability of story drift in the first story is probably due to the

less frequent yielding there. This is confirmed by the lower mean peak energy dissipation demand there and its increased COV. The increased variability of story drift in the top story is caused apparently by the larger elastic forces and the larger yield levels in KOVER compared to KREG. Compared to KREG, the mean peak energy dissipation demand in KOVER increases and so does its COV. The location of maximum energy dissipation demand moves from the first story to the third. The increased brace capacities result in increased mean peak interior column forces (and COVs) everywhere except in the top floor. All exterior columns have increased compression but not to the same extent as the interior columns.

Maximum story shears are naturally smaller and story drifts larger in KUNDER than in KREG for all stories except the top and the bottom. Story shear COVs are much larger in KUNDER than in KREG in all stories except the top. The story drift COVs are smaller in KUNDER than in KREG in all stories except the top and the bottom. The story hysteretic loops in KUNDER are totally different from those of KREG. Whereas KREG stories exhibit a deteriorating force-deformation hysteresis (Type 2, Fig. 3-4-d) KUNDER stories have trilinear force deformation curves (Type 6, Fig. 3-5-f). The small section size of the originally stocky braces makes the beam behave as a stiff and strong one.

Although maximum story shears in KUNDER are smaller and the drifts are larger than those of KREG, the total energy dissipation demand is smaller, has less variance and has a more uniform distribution than in KREG. The moment resisting frame assumes a larger portion of the energy dissipation demand, mainly in the beams (Table 5-18). The KUNDER frame resists the lateral load following brace buckling through a cantilever mode which transfers loads from the braced core to the exterior columns by shear in the beams. This is confirmed by the energy dissipation demand in the beams and by the pattern of column axial forces. Mean peak column compression and their COVs are much smaller in the interior columns of KUNDER than in those of KREG, while the opposite is true for exterior columns.

5.6.6. Large versus small frame participation (KD25 vs KD00; Figures 5-13 and 5-12 and Tables 5-13 and 5-12, KD50 vs KD25; Figures 5-15 and 5-13 and Tables 5-15 and 5-13):

As the frame participation increases, maximum story shears and column compressions increase (a 15% increase for KD25 compared to KD00). The COVs of all response quantities increase in general. The energy dissipation demands, however, decrease. The locations of maximum story drift and of maximum energy

dissipation tend to shift to the story where the brace contribution to lateral story stiffness is largest (from the first to the second or third story in these cases).

5.6.7. Proportional brace design (KPRO vs KREG; Figures 5-17 and 5-3 and Tables 5-17 and 5-3):

Compared to KREG, maximum story shears in KPRO are smaller, especially in the upper stories. However they exhibit more variability, particularly in the lower stories. Maximum story drifts are smaller in KPRO than in KREG for the first three stories and larger for the last three stories. The smaller story drifts in KPRO are the consequence of reduced plastification in those stories. The larger story drifts in KPRO are due to larger elastic drifts (smaller brace sections) and increased inelastic activity in the upper stories. A comparison of the distribution of energy dissipation demand for KPRO and KREG confirms this observation. The ratio of energy dissipation demand of KPRO compared to that of KREG shows the same trend as the story drifts: smaller in the lower stories and larger in the top stories. The interior column compressions in KPRO are smaller than those in KREG, presumably because of the smaller brace sections in the top stories. On the other hand the exterior columns of KPRO have larger compressions than the corresponding columns in KREG. This indicates an increased frame participation caused by the lower overall strength and stiffness of the braced bay.

5.6.8. Effect of ground motion intensity (KREG30 vs KREG; Figures 5-10 and 5-3 and Tables 5-10 and 5-3, KREG70 vs KREG; Figures 5-11 and 5-3 and Tables 5-11 and 5-3):

For the reduced ground motion intensity (KREG30 versus KREG), one observes a reduction in story drifts and in energy dissipation demand. The reduction in drift is proportional to the ratio of earthquake intensities at the first floor, but top story drifts remain practically equal. The reduction in story energy dissipation demand is proportionally larger than the reduction in earthquake intensity. Maximum story shears and column compressions (interior and exterior) are practically unchanged. Coefficients of variation of most quantities are larger in the case of reduced earthquake intensity, compared to the reference case (KREG).

For the magnified ground motion intensity (KREG70 versus KREG), there is an increase in story drifts and energy dissipation demand. The increase in story drifts is largest at the lower three floors, story drifts of the top three stories remain practically unchanged. The increase in energy dissipation demand in KREG70

compared to KREG is larger than the increase in earthquake intensity. The maximum increase in energy dissipation demand is in the third story. The COVs of energy dissipation demand are noticeably reduced in all stories. Maximum column compression in interior and exterior columns are practically unchanged; brace and beam yielding effectively limit the amount of compression fed into the columns.

5.7. ANALYSIS OF RESULTS

This section attempts to determine from the observed results the underlying basic phenomena and to draw more general hypotheses and conclusions regarding the factors controlling the behavior of braced frames.

5.7.1. Energy dissipation demand:

The energy dissipation demand was concentrated mostly in the braces (Table 5-18). The columns practically remained elastic and the total energy dissipation demand in the beams was negligible compared to that in the braces. Since the energy dissipation capacity of the braces is much less than that of the beams, the discussion of energy dissipation demand is limited to that of the braces.

It can be noticed from the maximum story drifts in most figures that inelastic deformations are concentrated in a few soft stories near the bottom of the building. However, as the frame participation increases the maximum energy dissipation demand increases and tends to move upwards (from the first story to the second) or to where there are section changes (third and fifth stories). Similarly, as the braced bay beam stiffness and strength are increased the maximum energy dissipation demand increases and moves upward in the structure (to the third story). The COV of energy dissipation demand decreases with increasing frame participation, increasing beam stiffness, and decreasing brace slenderness. This trend is more acute when stocky braces are used.

It can be inferred that as frame participation is increased by increasing column sizes, frame stiffness and strength increase. The increase is most noticeable in the first story where the base fixity helps the columns to develop their full potential strength and stiffness. The increase is less noticeable in other stories where the development of strength and stiffness depends on joint fixity and the restraint provided by the beams. The first story being now relatively stronger, damage tends to concentrate in the second story. The aforementioned trend is even more noticeable when stocky braces, with smaller relative stiffness are used. This shift in the location of maximum energy dissipation demand is not necessarily detrimental. It might

be deliberately used to make the energy dissipation demand more uniform. It may also create problems if not taken into account.

5.7.2. Maximum story shear:

Dual systems have smaller maximum story shears by design. As frame participation increases, the COV of maximum story shear increases in the stories where inelastic activity occurs. For dual systems there is no definite increase in maximum story shear in going from intermediate slenderness braces to stocky braces.

The increase in COV with increasing frame participation and decreasing brace slenderness reflects the variability of the frame resistance mechanism. This mechanism depends to a large extent on the joint rotations at the column ends. If the joints at the ends of a column are rotating in the same direction while story drift occurs, column resistance is increased. If they are rotating in opposite directions, column resistance is decreased. This resistance mechanism is therefore sensitive to higher modes through their effect on joint rotations. On the other hand, in KREG maximum story shear is very simply linked to the buckling strength of the braces and the amount of interstory drift. It is therefore less sensitive to higher modes effects, at least in the absence of simultaneous vertical excitation.

5.7.3. Maximum story drift:

Maximum story drifts are larger for dual systems than for KREG because dual systems are designed for smaller lateral loads. Maximum story drifts increase when stocky braces are used instead of slender braces of same buckling load. Stocky braces have larger buckling stresses than slender braces, hence they require less cross-sectional area to achieve the same buckling load. As a result their axial stiffness is much lower than that of more slender braces. The smaller axial stiffness of stocky braces causes larger elastic drifts compared to slender braces of same buckling load.

5.7.4. Coupling of horizontal and vertical deformations:

A very interesting phenomenon observed in the dynamic response results is the sharp drop in story resistance upon brace buckling, followed by small amplitude high frequency fluctuations in resistance (e.g. Figure 5-18-a). This phenomenon can be related to two separate causes: a quasi-static and a dynamic influence of vertical and horizontal motions.

The quasi-static effect occurs when the unbalance force from the braces pulls down the beam and imposes on the frame a deformation pattern that bends the columns in single curvature. Therefore the frame's instantaneous contribution to story resistance is often reduced to zero, or even is made opposite to that of the bracing system (Figure 5-19-a). This effect is responsible for the sharp drop in story resistance right after brace buckling as observed in Figure 5-19-c. Similarly, Figure 5-19-d shows the instantaneous ratio of frame to bracing resistance which can take values far from the nominal values assumed in design. Since this effect is independent of the rate of deformation, it is called quasi-static.

The dynamic coupling of vertical and horizontal vibrations depends on the rate of application of the loads and cannot be observed for quasi-statically applied loads. It is responsible for the small amplitude high frequency variation in story resistance, particularly after first brace buckling. It is caused by the sudden application on the beam of the vertical unbalance force developed by the braces. The beam then starts to oscillate vertically. On its downward stroke, it increases the compressive deformation in the buckled brace and thereby reduces its resistance. At the same time, it reduces the elongation in the tension brace and hence its resistance as well. The net result is a sharp reduction in the story strength. On its upward stroke, the beam tends to reduce the compressive deformation in the buckled brace. However, an increase in the lateral story drift will tend to compensate partially or totally for that reduction in brace shortening. The buckled brace will then shorten or possibly elongate slightly; but in either case its resistance will decrease. The tension brace elongates sharply, and since it is still elastic its tension force also increases sharply. The net effect is a momentary but noticeable increase in story strength. This phenomenon is equally observed with stocky and regular slenderness braces. It is less noticeable in the case of strong stiff beams (KSBM).

In the absence of direct experimental data on such phenomenon, numerical simulations were performed to verify whether these phenomena are genuine, and not a result of numerical problems in the simulation scheme. Numerical problems were ruled out after carefully checking the program and testing it. The results of KREG were compared to those of a frame similar to KREG except that the inertial mass for the vertical DOF at the brace to beam junction was set to zero. This frame is designated KMSLS. Figure 5-18-a and 5-18-b show a typical story hysteresis loop in KREG and KMSLS, respectively. The effect of the vertical beam vibration on story resistance is clearly evident. Similarly, Figure 5-18-c and 5-18-d show the path of the brace junction with the beam for KREG and KMSLS, respectively. The extent

of vertical beam vibration in KREG is clearly evident. Finally, Figure 5-18-c and 5-18-f show the history of the sum of vertical forces in the first story of KREG and KMSLS for HE35EW. These figures show the importance of vertical forces induced by the vertical vibration of the beam.

5.7.5. Column compression:

The maximum column compression has four components:

(1)- A gravity load component that is static.

(2)- A component due to the overturning moment on the structure caused by the lateral loads. This component increases the axial compression in exterior columns as frame participation is increased.

(3)- A quasi-static component due to the vertical unbalance load applied on the beam of the chevron-braced bay, upon brace buckling.

(4)- A vertical inertial component due to the excitation of vertical oscillation modes. This component is particularly important in the braced bays.

For interior columns all four components are significant. For exterior columns, the first two are the most significant.

As seen in Chapter 3, the magnitude of the quasi-static component of axial force increases with beam stiffness and brace slenderness. The inertial component's dependence on section characteristics and story mass is more complicated to determine. The magnitude of that component depends on the rate of application of the unbalance load relative to the fundamental period of the beam-braces assembly for vibration in the vertical direction. The rate of application of the unbalance force is equal to $\dot{P}_{un} = [dP_{un}/du\ ][\ du/dt]$ where du/dt is the story lateral drift velocity and dP/du is the rate of quasi-static unbalance generation with increasing story drift. As seen in Chapter 3, dP/du depends on brace slenderness and the stiffness of the beam compared to that of the brace. The fundamental period of the beam-braces assembly depends on the stiffnesses of the beam and braces and the story mass associated with the vertical displacement degree of freedom at the beam to braces junction. This period can be estimated as:

$$T_{bm} = \frac{\sqrt{\dfrac{M_{bm}}{K_{bm}+K_{brt}+K_{brc}}}}{2\pi}$$

It is clear from this brief overview that determining the peak value of the dynamic unbalance force is a difficult undertaking. However, a approximate bound may be

taken as the maximum unbalance force P_{ud} generated at any given story (quasi-static plus dynamic component). The details for making this approximation are fully covered in Appendix B.

5.8. CONCLUSIONS

The study of the dynamic inelastic response of chevron-braced frames shows that the advantages of the various proportioning strategies are not as clear cut and decisive as suggested from the results of the previous chapters (i.e. from static analysis or dynamic analysis of one story systems). For example, the combination of stiff beams and slender braces produces desirable story hysteretic characteristics but leads to a rapid build-up of column compression forces and eventually to the formation of soft stories. Similarly, the use of stocky braces still appears desirable, but only if local buckling failure can be controlled.

Increasing the frame participation does not improve the hysteretic characteristics and does not reduce the variability of the response. The concept of statically adding the strength of the braced bay and of the moment resisting frame is clearly invalid. Important static and dynamic interactions occur between the two systems that reduce the advantages of increasing the participation of the moment resisting frame. These dynamic interactions need further study before they can be included in design guidelines. On the other hand, designing the frame for a maximum strength larger than that of the bracing system seems to have some advantages (KUNDER versus KOVER). The only economical way of achieving this situation is to deliberately under-design the bracing system. Unfortunately, the damageability limit state imposes lower limits on the strength of the bracing system that are incompatible with the proposed underdesign approach.

Similarly, the idea of using an "improved strength and stiffness distribution" did not have as beneficial effects as desired. Such strength distributions are the result of an averaging process over several different earthquakes. Any single earthquakes imposes a force pattern that is generally quite different from the average pattern, and with the tendency of chevron-braced frames to form soft stories, damage still tends to concentrate in one or two stories.

In all the simulations done, the energy dissipation demand is concentrated in the braces ($>=90\%$) followed by the beams and then the columns, yet no reliable model for the energy dissipation capacity of braces has been developed. There is a need for experimental investigations to develop damage laws and failure criteria for braces.

In general, the dynamic inelastic response of chevron-braced frames seems to be more sensitive to the characteristics of the ground motion (such as frequency and pulse content, intensity) than to member proportioning strategies (such as brace slenderness, beam stiffness, frame participation, selection and distribution of strength levels). Proportioning parameters interact in a complex manner and often affect the mean and COV of response quantities in opposing ways. Consequently, the following two chapters will explore two different approaches for improving braced frame behavior. One is the use of an optimization approach which implicitly handles all the interactions. The second is to investigate the merits of alternative concentric bracing systems that would be less sensitive to ground motion characteristics and would have better seismic behavior.

CHAPTER 6

OPTIMIZATION OF CHEVRON-BRACED STEEL FRAMES

6.1. INTRODUCTION

In this chapter the structural optimization program DELIGHT.STRUCT is used to investigate the possibility of proportioning chevron-braced frames in a way that improves their seismic response. Moreover, it is expected that additional insight into the seismic behavior of such frames will be gained in the process. Also, attempts will be made to evaluate the adequacy of the new recommendations for their design (such as those formulated by SEAONC [75]).

In this chapter, the background of DELIGHT.STRUCT is briefly outlined, emphasizing its capabilities and limitations, and the underlying design strategy. Then, the trial problem structure is described and the optimization results are discussed. Finally, the implications of these results are reviewed.

6.2. BACKGROUND OF DELIGHT.STRUCT

DELIGHT.STRUCT is a structural optimization program developed at the University of California at Berkeley. It consists of the union of three components:

(1) DELIGHT [58]: an interactive user environment (shell) that includes optimization algorithms and graphics capabilities. The optimization algorithm that drives DELIGHT.STRUCT is based on a variant of the feasible directions method of Zoutendijk [97]. In this method, the new search direction at any point in the design space is a linear combination of the gradients of the objective functions and of the active constraints. In particular, the modification to handle multiple objective functions is due to Nye and Tits [57]. Gradient evaluation is done by numerical differentiation. Once the search direction is defined, the Armijo step length method [16] is used to carry out a one dimensional minimization along that direction.

(2) ANSR [52]:a structural analysis program capable of handling inelastic dynamic analyses of three dimensional structures. It has a library of structural element models including in particular an inelastic beam-column element and Ikeda's brace element [35].

(3) STRUCT; an interface between the two previous modules to handle problem definition and data exchange. STRUCT handles interactively the definition of problem geometry, the assignment of design variables, and the definition

of design objectives and of design constraints.

In its current version, DELIGHT.STRUCT is geared toward the optimal seismic resistant design of steel structures including braced steel frames. Balling et al [13] used DELIGHT.STRUCT in the design of planar moment resisting frames to minimize story drift and energy dissipation for severe earthquake excitations. Austin [11] used DELIGHT.STRUCT to investigate the merits of friction damping in X-braced steel frames subjected to strong earthquakes, and to explore the implications of a reliability based optimization formulation for moment resisting steel frames [12].

6.3. DESIGN METHODOLOGY SUPPORTED BY DELIGHT.STRUCT

The design methodology supported by DELIGHT.STRUCT assumes three limit states which must be satisfied for every design to be acceptable. These limit states differ by the nature of the loads they include, their intensity, their frequency of occurrence and the acceptable performance under these conditions.

6.3.1. Limit states:

The first limit state is the serviceability limit state (limit state I). Here the structure must remain elastic and the deflections must remain within acceptable bounds for combined dead and live loads. This limit state is represented by inequality constraints on allowable member stresses and nodal deflections under gravity loading.

The second limit state considered is the damageability limit state (limit state II). Here the structure is subjected to a combination of dead loads, live loads and moderate earthquake excitations. Since moderate earthquakes may occur several times during the life of the building, the structure is required to remain elastic and deflections must be limited to avoid non-structural damage. This limit state is represented by functional inequality constraints where maximum member stresses and nodal displacements during an earthquake must remain within the allowable values.

The third limit state is the ultimate limit state (limit state III). Here the structure is subjected to dead loads, live loads and severe earthquake loads. Since such a severe earthquake is expected to occur at most once during the life of the building, and since its characteristics are not accurately predictable,
it is neither economical nor reasonable to expect the structure to resist such an earthquake elastically. Inelastic behavior and structural damage are expected, and large deformations are tolerated on the condition that no collapse occurs so that

occupants can evacuate the building safely. Typically, damage is measured by two parameters: the energy ductility demand of structural elements, and the maximum sway in the structure. The limits on ductility demand are to protect against the possibility of fracture and collapse, and the limits on sway should prevent geometric instability. Accordingly, inequality constraints are placed on the maximum element ductility demand, and on maximum lateral sway.

6.3.2. Constraints:

To account for the uncertainties in earthquake resistant design (earthquake occurrence and characteristics, inelastic dynamic behavior, strength and capacity of structural elements), the constraints are recast in terms of probability of exceeding acceptable response levels instead of in terms of the absolute difference between the maximum response demand and the allowable one. Instead of using the response for a single earthquake in computing the constraint violations, the responses for a set of "similar design earthquakes" are considered. The average structural response and its standard deviation are used in computing the probability of exceeding the acceptable response levels.

To normalize the constraint values, the designer is required to specify 'good' and 'bad' values for the deterministic variables and 'high' and 'low' probability of exceedance for the stochastic variables. For example, in case of a deterministic variable which must be kept below a certain 'good' value, the constraint violation value is set to zero if the mean response is less than the 'good' value. It is set to [Mean - Good]/[Bad - Good] otherwise. Similarly, in case of a stochastic variable which must be kept below a certain probability of exceedance, the constraint violation is set to zero if the mean response is below 'high-V' (the value which has a 'high' probability of being exceeded). It is set to [Mean - Good]/[Low_V - High_V + Bad - Good]. See Austin [12] for more details.

6.3.3. Objective functions:

Several objective functions are supported by DELIGHT.STRUCT. These can be used separately or simultaneously:

(1)- Minimum volume design. This is equivalent to minimum weight design since only one type of material is used (steel). The quest towards minimum weight design has its origin in the optimization of aerospace structures where weight minimization has compound benefits. For earthquake resistant design of building structures, the benefits of weight minimization are less evident. It can

be argued that minimizing structural weight reduces the magnitude of seismic induced inertial forces. However, the weight of the load resisting elements is often a minor fraction of the total weight of the structure. Nevertheless, it is generally accepted that weight minimization reflects an efficient use of materials. This is the only objective function used in this study.

(2)- Minimum story drift. This is a design objective that might be required in flexible building structures where nonstructural components might be damaged by excessive story drifts. This design objective is less applicable in case of braced steel frames where interstory stiffness is very high and story drifts small.

(3)- Minimum earthquake energy input. This is a design objective that is usually selected for base isolated structures. Base isolation for seismic purposes works by moving the resonant frequencies of the structure away from the region of peak power input. Such a design objective is not valid for this study.

(4)- Maximum energy dissipation in selected structural elements. This is the energy counterpart of fully stressed design. Such a design objective is justifiable when the structure incorporates special elements (structural fuses) whose energy dissipation capacity is very high (friction devices) or that is reliably predictable (shear links, lead cores, flexural plates, etc.). These considerations effectively rule out its application to braced frames where the braces are notorious for their limited energy dissipation capacity and for the absence of data to predict such a capacity accurately.

6.3.4. Design variables:

To keep the problem down to a manageable size only plane frames are considered as in the previous chapters. One design variable at most (the moment of inertia I) is allowed for each flexural member. Balling [13] derived empirical relations tying the remaining section properties to this primary design variable. At least two design variables are required for each brace section. These are the brace cross-sectional area (A) and the brace effective slenderness λ. The remaining brace section properties (elastic section modulus S, plastic section modulus Z) can be obtained from empirical relations similar to those of Balling (see Chapter 2).

6.4. CASES CONSIDERED

Ideally, one of the frame models of the previous chapter should be selected for optimization, but practical constraints related to storage and execution time prevented the realization of this goal. Accordingly, the problem chosen to optimize

using the capabilities of DELIGHT.STRUCT is a four story, one bay, chevron-braced frame reported in the SEAONC tentative recommendations for seismic design [75]. This model is small enough to be computationally practicable, yet large enough to exhibit characteristics of a multi-degree of freedom braced frame. Moreover, it indirectly serves as a test of the SEAONC recommendations for chevron-braced frames. Two sets of four ground motions each were considered in the design process (Table 6-1).

The frame shown in Figure 6-1 is assumed to have rigid in-plane floor and roof diaphragms. Uniformly distributed dead loads of 2.4 kip/ft (35.0kN/m) and live loads of 1.0 kip/ft (14.6kN/m) are assumed for the beams. Beams are connected to columns by moment resisting connections. Member section sizes are reported in Tables 6-2-a and 6-2-b. Notice that braces in the original design were selected to have a slenderness ratio of less than 80. The design as reported in Reference [75] is incomplete with brace sections only being determined. The initial beam and column sections are chosen herein according to the design recommendations prescribed in that reference.

The primary design variables considered in optimizing this frame are the moment of inertia for the columns in every story, the moment of inertia of the beams, and the cross-sectional area and slenderness of braces in every story. For reasons of practicability, the columns in the top two stories are constrained to have the same moment of inertia, and all the beams are assumed to have the same moment of inertia. As indicated in Figure 6-1 there are twelve design variables to be determined.

During the optimization process, the structure is subjected to four ground motions. Two sets of four accelerograms are considered for comparison. In the first set, ground motions are taken from a single site in El Centro. This case will be referred to as the El Centro set. In the second set, the ground motions selected are varied as in the previous chapter. Two of the earthquakes contain strong pulses (Helena, Parkfield) and two are characterized by many harmonics (El Centro, Olympia). This case will be referred to as the mixed set. Comparing results for these two cases should reveal which aspects of the optimization process depend on ground motion characteristics and which optimal proportioning trends are independent of the excitation characteristics. The ground motions are all scaled to the same Arias intensity and are used at two intensity levels; one where the El Centro record is scaled to 0.2g for limit state II (damageability during recurring moderate earthquakes), and another where the El Centro record is scaled to 0.5g for limit state III

(safety against collapse during the design severe earthquake, Table 6-1).

The objective function used is the minimization of total volume. The minimum volume design is not necessarily the most economical, but the process of reaching it while satisfying all the constraints is a useful exercise that indicates the desirable proportions for an efficient design. The constraints are on allowable member stresses for gravity load and during the moderate earthquakes, on allowable deformations (deflections for gravity load, story drift for the damageability limit state, and sway for the severe earthquake), and on allowable deformations (deflections for gravity load, story drift for the damageability limit state, and sway for the severe earthquake), and on allowable energy dissipation in each type of members during severe earthquakes. Given the uncertainty of the energy dissipating capacity of buckled braces and based on the results of Chapter 2 (Figure 2-11), the constraint on energy dissipation capacity of braces is set to an energy ductility of 1 for the good value and 2 for the bad value, irrespective of the brace slenderness. Otherwise, the same values as Austin's [12] are used for the allowable stresses in the flexural elements, and the same "good" and "bad" constraint values, "high" and "low" probabilities of exceedance of stresses, deflections and energy dissipation demands (see Tables 6-4 and 6-5). The "bad-volume" value is reset after the second (El Centro set) or third (mixed set) iteration to allow the algorithm to improve element responses after reducing the overall volume.

6.5. DESCRIPTION OF RESULTS

Applying DELIGHT.STRUCT to the original design leads to drastic changes in several structural parameters. The results are itemized in the following sections:

6.5.1. Volume of structure:

For both sets of earthquakes, the final structure volume is about two thirds of the original volume (67700 in^3 or 1.11 m^3). The largest reduction in volume occurs in the first iteration. The final volume for the case of El Centro excitations is noticeably smaller than for the case of mixed excitations (40990 in^3 or 0.67 m^3 against 47310 in^3 or 0.77 m^3).

6.5.2. Columns:

For both sets of earthquakes there is a considerable reduction in column sizes, the largest reduction being for the first story columns. The final distribution of column sizes is opposite to the original one, the stiffest columns being in the top two

stories, and the most flexible columns being in the first story. This pattern is observed for both sets of earthquakes but is more acute for the El Centro set (Figures 6-3-a and 6-3-b, and Tables 6-2-a and 6-2-b). A possible justification for this unexpected pattern will be discussed in a later section regarding frame participation.

Mean peak column moments are larger for the mixed earthquakes set than for the El Centro case. For both cases, the column moments in the optimal design and Limit State II are smaller than those in the original design, for all stories except the top two (Tables 6-2-a and 6-2-b). For Limit State III all columns remain elastic in the original design and for both sets of earthquakes. In the optimal design some columns are slightly damaged. For the mixed earthquake set, the columns in the first three stories have to dissipate moderate amounts of energy (Table 6-2-b). For the El Centro set, only the second story columns dissipate a small amount of energy (Table 6-2-a).

6.5.3. Beams:

For both sets of earthquakes the change in beam size is small. The final beam sections are comparable, the beam size for the El Centro set being slightly smaller than for the mixed set (582 in^4 or $2.42x10^{-4}m^4$ against 595 in^4 or $2.48x\ 10^{-4}m^4$).

For both sets of earthquakes, there is a reduction in beam end moments and an increase in midspan moments (Tables 6-2-a and 6-2-b). This trend can be traced to two factors:

(1)- The drastic reduction in column sizes changes the beam end conditions from practically fixed-ends conditions to almost hinged ends, especially in the lower stories.

(2)- The braces also decrease in cross-sectional area which decreases the effectiveness of the midspan support provided by the braces to the beam.

For the El Centro set, all beams in the original and optimal design remain elastic (Table 6-2-a). For the mixed earthquake set, the first and second story beams in both the original and final design have to dissipate a moderate amount of energy (Table 6-2-b).

6.5.4. Braces:

This is the area in which the largest differences appear between the El Centro and the mixed earthquake sets. For the El Centro set, the brace sizes in all stories are reduced, the final brace sections being about two thirds of the original ones. Brace slendernesses in all stories remain practically unchanged. As a result,

maximum story shear strength is reduced in all stories (Table 6-2-a).

For the mixed earthquake set, brace sizes in all stories are reduced except in the first story where the brace cross-sectional area increases by approximately 30% (9.32 in^2 or 60.13 cm^2 to 12.00 in^2 or 77.42 cm^2). The final brace sizes in the remaining stories are approximately 60% of their original values. Curiously, the smallest brace size is at the third story not at the fourth (top story) as is expected. Brace slendernesses do not change significantly in all stories except the first. In the first story, brace slenderness increases from 78 to 107 to offset the increase in story strength that would otherwise be expected based on the increase in brace cross sectional area alone. The actual increase in story strength is 5% only instead of 30% (Table 6-2-b).

For limit state II, maximum brace compression forces are larger in the case of mixed earthquakes than for the El Centro set. In both cases, maximum brace forces in the optimal design are smaller than those in the initial design (Tables 6-2-a and 6-2-b).

Similarly for limit state III, the energy dissipation demand in the braces of the optimal design is larger in case of mixed earthquakes than for the El Centro set. In both cases, the brace energy dissipation demand is distributed over the first two stories. Braces in the original design remain elastic for the El Centro set, while the first story braces dissipate a small amount of energy for the mixed earthquake set (Tables 6-2-a and 6-2-b).

6.5.5. Structural period:

For both sets of excitations the fundamental period of the optimal design is longer than that of the original design (Figures 6-5-a and 6-5-b, and Tables 6-2-a and 5-2-b). Refering to Figures 6-6-a and 6-6-b which show the average input power spectrum for the El Centro and the mixed sets, respectively, interesting trends can be observed. In the original design, the fundamental period of the structure is slightly below that of a peak in the input power spectrum. Occurrence of inelastic response typically elongates the instantaneous elastic period and places it right on a peak of the power spectrum. This is likely to increase the amount of damage due to resonance and amplification of the deformation demand. In the final design the fundamental period of the structure is slightly longer than that of the peak in the power spectrum. As inelastic activity occurs it shifts the fundamental period of the structure further away from the peak in power input, and hence limits the amount of additional damage suffered by the structure. The elongation in elastic fundamental

period of the optimal design is limited by minimum stiffness requirements for stability under gravity loads, by deflection limitations for the damageability limit state, and by strength requirements for the ultimate strength limit state.

In the case of mixed earthquakes, the average input power spectrum still contains large peaks at periods larger than the fundamental period of the optimal design, unlike the El Centro case. Thus, the beneficial effects of period shifting can not be as completely realized as for the El Centro records. That is probably why the optimal design for the mixed earthquakes case has a higher level of design dissatisfaction than that for the El Centro set.

6.5.6. Frame participation:

The frame participation ratio as defined in Chapter 3 is the ratio of moment resisting frame stiffness to bracing stiffness for interstory drift deformation $(K_{fr}/K_{br})_h$. In the original design, this ratio changes from one story to the next and is largest in the second story. Both sets of excitations lead to the same evolution in the distribution of frame participation ratios. The final distribution of frame participation ratios is almost opposite to the original one, the smallest ratio being in the first story, and the largest being at the top story (Figures 6-7-a and 6-7-b and Tables 6-2-a and 6-2-b). These results, disconcerting at first glance, are reasonable if one considers the different deformation patterns of braced bays and of moment resisting frames. The braced bay rate of deflection under distributed lateral load is large at the top and minimal at the bottom of the structure. Conversely, the moment resisting frame rate of deflection under distributed lateral loads is small at the top and large at the bottom of the structure. Therefore, in resisting lateral loads, the braced bay is more efficient than the moment resisting frame in the lower stories, and the opposite is true in the upper stories. Moreover, when the braced bay and the moment resisting frame are forced to undergo the same pattern of deformations in a dual system, the total strength is less than the sum of the individual strengths of each system considered separately. In the lower stories the frame imposes additional loads on the braced bay and the braced bay loads the moment resisting frame in the upper stories. It is then remarquable that the optimization algorithm manages to reduce this undesirable interaction by decreasing the frame participation in the lower stories and increasing it in the upper stories. It is therefore able to "squeeze out" the maximum possible story strength while reducing the overall volume of the structure. Paulay [29,61] describes similar interactions in reinforced concrete hybrid systems consisting of shear walls and moment resisting frames.

6.5.7. Beam to brace stiffness ratio:

For both sets of earthquakes the ratio of beam to brace stiffness for vertical displacements at the beam to brace connection $(K_{bm}/K_{br})_v$ increases slightly in all stories except the first (Figures 6-8-a and 6-8-b and Tables 6-2-a and 6-2-b). Since most of the brace inelastic activity occurs in the first story, one can conclude that increasing the beam to brace stiffness ratio is not essential for improving the response of this structure. In fact, it may be harmful in this case to the columns whose size is being tremendously reduced. Increasing the beam to brace stiffness ratio would throw additional compressive forces on the columns and increase the possibility of their failure. The observed increase in the ratio K_{bm}/K_{br} is only incidental and a side effect of the more rapid reduction in brace size than in the beam size.

6.5.8. Story strength and stiffness distribution:

In the original braced frame design, the story strength and stiffness distributions are proportional. This can be attributed to the overwhelming contribution of bracing to story stiffness, and the linear relation between bracing stiffness and bracing strength. In the original design, the story strength and stiffness distributions are almost parabolic with a peak at the second story. For the El Centro set, the story strength and stiffness distributions in the optimal design are also parabolic but with a less distinct peak at the third story (Figure 6-9-a and Table 6-2-a). Recalling that for that case inelastic activity in the optimal design is concentrated in the first story braces, it can be concluded that the distribution of story strength is of secondary importance. It is a by-product of other considerations like moving the fundamental period away from the peaks of the power input spectrum, and reducing the undesirable interactions between frame and bracing. These considerations would explain the unusual distribution of story stiffness.

For the mixed earthquake set, the story strength and stiffness distributions in the optimal design are practically linear with the maximum story strength in the first story (Figure 6-9-b and Table 6-2-b). The story strengths in this case are larger than their counterparts in the El Centro case. The occurrence of inelastic activity in the first two stories of the optimal design and the overall higher story strength indicate that in case of mixed earthquakes the distribution of story strengths plays a role as important as the other two factors previously mentioned.

6.5.9. Modal shapes and modal correlation:

For both sets of earthquakes it is noticed that the first mode shape of the optimal design has a kink at the first story level and a larger amplitude at the top story level than in the original design (Figures 6-10-a and 6-10-b). The second mode shape also has a larger amplitude in the top two stories than in the original design. No remarquable changes are observed in the remaining two mode shapes.

A random vibration analysis carried with the mean input power spectra for the two sets of earthquakes reveals that the modal correlations of the first mode with the other modes in the final designs are noticeably smaller than in the original design (Table 6-3). The trend is more evident for the El Centro set than for the mixed earthquakes set. No physical explanation for this trend can now be offered. However, this trend warrants further investigation, especially for three dimensional systems where translational and torsional modes are often highly correlated.

6.5.10. Set of active constraints:

The El Centro set of earthquakes leads to a lower number of active constraints in the optimization process than the mixed earthquake set. Moreover, the governing constraint dissatisfaction for the El Centro set is smaller than the corresponding one for the mixed set. It also keeps decreasing from one iteration to another, while for the mixed set the governing constraint value becomes practically fixed after the third iteration.

The active constraints for the El Centro set are limited to energy dissipation demands in the first two story braces. The active constraints for the mixed set include in addition to those of the El Centro set energy dissipation demand in the columns and beams of the first two stories.

6.6. CONCLUSIONS

This study implies that the two major factors in improving the inelastic behavior of chevron-braced frames are avoiding the peaks in the input power spectrum, and reducing any undesirable interaction between bracing and moment resisting frame.

Reduction of the undesirable interaction between bracing and moment resisting frame was achieved for the trial design by reducing the frame participation in the lower stories and increasing it in the upper stories. In the examples considered where all the beams are constrained to have the same size, this leads to an unusual distribution of column stiffnesses where the stiffest columns are at the top of the

structure. Allowing the beams in every story to have different stiffnesses would probably lead to the same distribution of frame participation, but with a more traditional distribution of column stiffnesses.

The distribution of story strength does not seem to be of primary importance for this structure, at least in the case of earthquakes lacking strong pulses. Other parameters such as brace slenderness and beam to brace stiffness ratio also seem to be of secondary importance. It should be recognized that these structures suffered only limited inelastic deformations.

The chevron-bracing scheme is once more proven to be very sensitive to the characteristics of earthquake excitations. Comparing the results of the El Centro set and those of the mixed earthquake set shows that to get the maximum benefit from the optimization procedure, the seismicity of the site must be well known. One must have several earthquake records representative of the site or must be able to generate them. For some areas where many earthquakes have been recorded applying the optimization procedure presents no major problems. In areas where earthquake records are scarce or inexistent, there is a need to develop better models for generation of earthquakes that are typical of the site on which a structure is to be erected.

The SEAONC recommendations tested in this chapter are clearly superior to those of the 1985 UBC tested in the previous chapter. However, the elastic response of the SEAONC design to the El Centro set and its slight damage when subjected to the mixed earthquake set might suggest that the SEAONC recommendations are possibly too conservative. The SEAONC recommendations therefore fulfill their mission of providing a minimum of safety with a simplified design approach, at the expense of economy. The optimization procedure shows that one can improve on the SEAONC design's economy without sacrificing the safety of the structure. However the procedure involved is complex and computationally expensive, and cannot be recommended as a standard design procedure, at least for the time being.

The reduced modal correlation in the optimal design deserves further investigation to determine whether it is only incidental or whether it represents a basic phenomenon. In the latter case it would be interesting to extend the study to three dimensional systems where torsional and translational modes may be highly correlated. Such an approach combined with the avoidance of the peaks in the input power spectrum might lead to a modal synthesis approach that would be attractive by its economy and simplicity compared to the currently used simulation approach.

The minimum weight optimization did not lead to a uniform distribution of energy dissipation demand over all braces as desired. One should probably activate

an additional objective functions aiming at maximizing the energy dissipation demand in the braces or minimizing the COV of this demand. Alternatively, different structural systems might be considered as will be done in the next chapter.

CHAPTER 7

ALTERNATIVE STRUCTURAL SYSTEMS

7.1. INTRODUCTION

The last two chapters have shown that complex interactions exist between design and response parameters in chevron-braced frames subjected to severe earthquake loading. The previous chapter demonstrated that an optimization approach can be used to help control these interactions and to substancially improve the performance of a chevron-braced frame. However, optimal proportions were found to be highly site specific i.e., they depend to a large extent on the characteristics of the earthquake motions expected at the building site. This chapter examines the performance of structural variants that might be used to reduce the sensitivity of braced frame response to earthquake characteristics. The variants considered have been intentionally restricted to those consisting of simple rearrangements of braces, including the addition of vertical tie-bars. They all have in common the objective of reducing the tendency of braced frames to form soft stories, mitigating any adverse effects of post-buckling force redistributions, and achieving a trilinear hysteresis loop without having to use overly stiff beams in the chevron-braced bay. Other variants such as eccentric bracing, base isolation, use of friction dampers, and allowing column uplift (rocking of the braced core) are not included in this study. Each constitutes a possible solution, but they are outside the scope of this investigation.

Accordingly, this chapter is divided into three main sections. The first section introduces several basic chevron-bracing variants and compares them to the original chevron-bracing scheme. The second section develops a new configuration and explains how it works. The third section compares simulation results for this configuration to those for the original chevron-bracing scheme and to the competing variants. The findings of this chapter and additional research needs are summarized in the conclusion.

7.2. BASIC STRUCTURAL VARIANTS

The first set of variants consists of various alternative arrangements of K and X braced systems. The same geometry and assumptions as used in Chapter 5 are used here to facilitate comparison with the earlier work. Except for the X-braced frame (XREG), they all use the same sections as the reference chevron-braced frame (KREG). The following configurations were used as schematically illustrated in

Figure 7-1.

(1)- XREG: is an X-braced frame designed for the same loads as KREG. Braces were assumed to be pinned at their ends and not to be connected at their midspans. Their slenderness ranges from 135 in the first two stories to 139 in the top two stories. Such frames are often used as alternatives to chevron-braced frames. They are almost universally used for fixed steel offshore platforms located in seismic regions.

(2)- INVK: is similar to KREG in all points except that the braces are arranged in a V shape instead of a chevron. This is often cited as having the advantage of preloading the braces into tension prior to the application of lateral loads. Thus, initial buckling would be delayed or smaller members might be used.

(3)- SPLIT-X: differs from KREG by having the braces of every two consecutive stories meeting at a single point. This gives a double story X braced frame arrangement. It is hoped that such a configuration would avoid the problems associated with vertical unbalance loads acting on the beams in chevron-braced frames.

(4)- TBTG: differs from KREG by having additional vertical struts (tie-bars) placed in all the braced bay stories. These tie bars are used to distribute the vertical unbalanced loads occurring in chevron-braced frames.

(5)- INVZIP: differs from INVK by the addition of vertical tie-bars in all stories except the top.

The comparison of the different variants uses the same protocol as in Chapter 5. This involves subjecting each frame model to the "worst ten seconds" of six earthquakes (Table 5-2). The earthquakes are normalized to have the same Arias intensity and are scaled so that the North-South component of the 1940 El Centro earthquake has a peak acceleration of 0.5g. In addition to the previously established comparison parameters (story shears, drift, energy dissipation demand and column compressions), the tie-bar forces are also monitored.

7.3. SIMULATION RESULTS

7.3.1. X-bracing (Figure 7-2 and Table 7-2):

Compared to KREG (Fig. 5-3), XREG has slightly larger story shears and smaller drifts thanks to its trilinear hysteresis characteristics. The trilinear characteristics are obtained because the tension brace resistance keeps increasing after the buckling of the compression brace until the tension yield stress is reached. The

energy dissipation demand is smaller in every story except the third, but it has a larger COV, except in the fourth and fifth stories. The total energy dissipation demand is less than that of KREG. However, the energy dissipation demand is still concentrated in the braces of a few stories.

Both interior and exterior columns compression forces are significantly larger than the corresponding ones in KREG and have larger COVs. The increase in exterior columns compression is compatible with the increased overturning moment associated with increased story shears. The large increase in interior column compressions results from the tension yielding of the braces. Every brace that yields in tension induces into the story column adjacent to it a compression force of $P_y \sin\Theta$. This force is usually larger than what a buckled brace in a chevron-braced frame can feed into the column ($1/2P_{ud}$).

Notice that an additional source of uncertainty, not considered in analyzing XREG, is the effective restraint at the brace intersection. Since this uncertainty affects the effective length of braces and hence their actual buckling load, it controls the value of maximum elastic story shear. Another issue that was not considered is the axial compression in the beam of the X-braced bay. The compressive force in the beam of an X-braced bay is significant and can lead to the collapse of the structure if it buckles that beam. This compression is more critical for the case of X-braced bays than for chevron-braced bays for several reasons: In X-braced bays the horizontal force applied by the braces must be totally resisted by compression in the beam, while in chevron-braced bays it is resisted partly in compression in one half of the beam, and partly in tension in the other half. In X-braced bays the whole length of the beam is in compression while in chevron-braced bays only half the beam span is in compression.

7.3.2. V Bracing (Figure 7-3, Table 7-3):

It has been shown (Chapter 3) that intermediate slenderness braces and flexible beams lead to reduced maximum story strength and early deterioration of the story resistance. The V bracing scheme proposes to mitigate these undesirable response aspects by delaying brace buckling through tensile preloading, and by improving the hysteretic characteristics through the use of gravity forces as a restoring stiffening force. The presumed advantages of preloading the braces in tension, and of using gravity load as a restoring force, were not observed in the simulations done (Figure 7-3). The maximum story shears in INVK are practically equal to those of KREG, but show considerably more variance. Story drifts and energy dissipation demands

are larger in all stories except the first one. It must be noticed that since the first story braces are connected at their intersection to the ground, they act as if they were part of an X-braced frame or a chevron-braced frame with an infinitely stiff beam. This is reflected in the first story's radically different behavior: trilinear hysteresis, large story shear, limited drift and reduced energy dissipation demand. The overly strong first story leads to a distribution of energy dissipation demand that is noticeably different from that of KREG, and in particular to a concentration of energy dissipation demand in the second story. Interior column compression forces in INVK are much larger (20% to 40%) than in KREG, since the vertical components of brace forces are applied to the columns at the top of the story rather than at the bottom. The application of the vertical unbalance force from the braces to the beam is so sudden that the impact sets up vertical vibrations in the beam. The inertia forces generated override the beneficial effects due to gravity loads.

Reducing section sizes in the first story to compensate for the strength provided by base fixity might increase lateral deflections sufficiently to create stability problems under gravity and lateral wind loadings.

7.3.3. Split-X (Figure 7-4, Table 7-4):

SPLIT-X (Figure 7-1) is used to designate a configuration where the braces form an X-pattern spanning over two successive stories. This arrangement is intended to relieve the problems associated with flexible beams and intermediate slenderness braces, to couple successive stories, and hence to reduce the occurrence of soft stories. It aims at obtaining the advantages of an X-braced system (trilinear hysteresis loops) without incurring the detailing problems associated with the intersection of braces in a conventional X-bracing scheme. Compared to KREG, this system increases story shears slightly (10% to 20%) and reduces story drifts and energy dissipation demands. However, it causes a sizable increase in interior column forces (30%), and a concentration of energy dissipation demand in the lower braces and columns of every two-story module. The two stories in every module have usually equal strengths, but the lower story is subjected to larger shears. Therefore it tends to be more heavily damaged than the upper story, and hence it must dissipate more energy.

7.3.4. Tie-Bars-To-Ground (TBTG) (Figure 7-5, Table 7-5):

In this variant, vertical tie bars are connected at each floor at the intersection of the braces with the beams (Fig. 7-1). The tie bars resist the vertical unbalance load caused by the buckling of compression braces. The tension braces are allowed to develop their yield strength, and the braced bay columns are protected from additional compression. It is hoped that this configuration may achieve the advantages of a stiff beam without incurring any of its disadvantages (increased column compression, plastic hinge formation in the columns). The analyses done have confirmed these advantages (Figure 7-5). Compared to KREG, TBTG shows larger story shears, trilinear hysteresis loops, and noticeably smaller story drifts and energy dissipation demand. The COVs of all these quantities are also smaller. The increase in interior columns compression is compatible with the increased story shear. The only disadvantage is that the mean peak compression forces in the tie bars are comparable to those in the interior columns, but have considerably larger COVs (Figure 7-15). If tie bars must remain elastic, they have to be designed for such large compression loads that they become another set of columns.

INVZIP (Figure 7-6, Table 7-6), a variant of TBTG, uses the same tie bar arrangement but within a V-braced frame. The performance of this variant is basically similar to that of TBTG in all points, except that the tie bars work mostly in tension (Figure 7-15), and that interior column compressions are increased as in INVK. However, the first story tie-bar develops a large tension force which must be resisted in some way by the foundation.

7.4. NEED FOR A NEW CONFIGURATION

The preceding analyses have shown that some of the proposed variants do not accomplish what they were intended to do (INVK), or only partially do so (SPLIT-X). Others (XREG, TBTG, INVZIP) achieve stable trilinear hysteresis loops, but at the cost of increased column compressions. Compared to the regular chevron-bracing, none of these variants exhibits a clearly reduced sensitivity to ground motion characteristics (intensity, frequency content, pulse sequencing). Similarly, none of them can have an optimal site independent strength and stiffness distribution for the same reasons as the regular chevron-bracing scheme (Chapter 5).

Hence there is a need for a structural configuration that achieves trilinear hysteresis loops without having to use stiff beams and slender braces, and without causing large increases in column axial forces. It must be less sensitive to earthquake characteristics. In other words, it must react in basically the same way no matter

how intense the earthquake is or varied its frequency content is. This implies that the structure must behave in the inelastic range more as a single degree of freedom system than as a multidegree of freedom system. It must provide a reliably predictable and more uniformly distributed energy dissipation demands.

To accomplish this in a chevron-braced frame, one must make sure that all compression braces buckle simultaneously or at least successively. Since the occurrence of such an inelastic deformation mechanism depends on the earthquake characteristics, it is highly unprobable. Therefore, one must find a way of "telling other braces that one of them has already buckled and that they must now buckle". The proposed configuration, called the "Zipper" configuration for reasons that will become clear, does exactly that.

7.5. MECHANISM OF THE ZIPPER EFFECT

The Zipper configuration (Figure 7-1) features the same tie-bar arrangement as the Tie-Bar-To-Ground configuration, except that the first story tie-bar is deleted. This seemingly minor modification causes major changes in the structure's behavior as follows.

Consider a Zipper-braced frame (Fig. 7-14) subjected to severe earthquake induced lateral loads. If the compression brace in the first story buckles while all other braces remain elastic, a vertical unbalance force is then applied at midspan of the first story beam. The vertical tie-bars mobilize the stiffnesses of all beams and remaining braces to resist this unbalance. One then has the effect of a very stiff beam without physically having one. The unbalance force transmitted through the tie-bars increases the compression of the second story compression brace, eventually causing it to buckle. At this stage, one has a larger total vertical unbalance for the same beam stiffness.

If the excitation is still forcing the structure in the same direction, then the large unbalance will buckle the third story compression brace. The brace buckling will propagate up in the structure such that all compression braces are buckled and beam plastic hinges are activated, hence the name: the zipper effect. The desired effect of distributing inelastic energy dissipation and obtaining a trilinear behavior is achieved. If the excitation reverses sign, then unloading will occur and one would have had the benefit of a trilinear force-deformation curve that limits drift to tolerable values.

Figure 7-14 compares the development of the zipper effect to what normally happens in a regular chevron-braced frame. In this figure Δ is the first story drift and V is the base shear. The thick lines indicate yielded or buckled members, and

the dark dots mark the plastic hinges.

7.6. COMPARISON OF THE ZIPPER CONFIGURATION WITH KREG AND TBTG

To verify the effectiveness of the zipper configuration, a frame model similar to KREG is fitted with tie-bars between the second and the sixth stories. This model will be referred to as ZIPPER (Figure 7-7, Table 7-7). For simplicity, the tie-bars used have the same cross-sectional area over the height of the structure and are assumed to remain elastic. Their cross-sectional area is of the same order as that of the first story braces ($10in^2$ or $64.52\ cm^2$). The dynamic inelastic performance of ZIPPER is compared to that of KREG and TBTG using the previously established comparison protocol.

In addition to the tests with the standard set of ground excitations, two more simulation sets were conducted to examine the sensitivity of tie-bar-to-ground and zipper configurations to the intensity of excitations. In the first set, the ground motion intensities are uniformly scaled down such that the peak ground acceleration in the EC40NS record is reduced to 0.3g. The simulation results for this case are referred to as TBTG30 (Figure 7-8, Table 7-8) and ZIPPER30 (Figure 7-9, Table 7-9) and are compared to those of KREG30 (Figure 5-10, Table 5-10). In the second set, the excitations are scaled up such that the peak acceleration in the EC40NS record rises to 0.7g. The simulation results for this case are referred to as TBTG70 (Figure 7-10, Table 7-10) and ZIPPER70 (Figure 7-11, Table 7-11) and are compared to those of KREG70 (Figure 5-11, Table 5-11).

Moreover, "proportional brace" variants of the tie-bar-to-ground and zipper systems are also designed and tested using the standard set of ground excitations. These are designed similarly to the KPRO configuration described in Chapter 5. These new configurations are referred to as TPRO (Figure 7-12, Table 7-12) and ZPRO (Figure 7-13, Table 7-13), respectively, and are compared to KPRO (Figure 5-17, Table 5-17). Their brace sections are the same as those of KPRO (Table B9), and their beam and column sections are the same as those of KREG and KPRO (Table 5-2).

7.6.1. Maximum story shears:

TBTG has larger mean maximum story shears than KREG, while mean maximum story shears in ZIPPER are slightly smaller than their counterparts in KREG. Similarly, KPRO has maximum story shears falling between those of TPRO and

those of ZPRO, with TPRO having the largest story shears. The COVs of story shears are larger in both TBTG and ZIPPER than in KREG. Using "proportional braces" reduces slightly the COVs of story shears in TPRO and ZPRO compared to KPRO.

The sensitivity of maximum story shear to earthquake intensity is approximately the same in TBTG and ZIPPER as in KREG. However, the story shear COVs in TBTG and ZIPPER are less sensitive to earthquake intensity than in KREG.

The larger maximum story shears in TBTG are due to the presence of tie-bars which allow the tension braces to develop their yield strength. The smaller maximum story shears in ZIPPER can be attributed to the Zipper action where the tie-bars "prematurely" induce brace buckling in adjacent stories, hence limiting their contribution to maximum elastic story shear. In both TBTG and ZIPPER, the tie-bars action is responsible for the increase in COVs of maximum story shear. Because of the tie-bars, maximum story shear is no more $2P_c\cos\Theta$; it now also depends on the instantaneous tie-bar forces. This is confirmed by the larger story shear COVs and their relative insensitivity to earthquake intensity. It should be noted, however that in all cases story shear COVs remain small compared to COVs of other quantities such as story drift and energy dissipation demand.

7.6.2. Maximum story drifts:

Story drifts in the lower stories of both TBTG and ZIPPER are smaller than their counterparts in KREG. Upper story drifts in TBTG and ZIPPER are larger than those in KREG. That is, both of these systems achieve a more uniform distribution of displacements than the original chevron-braced system. Compared to KREG, the COVs of story drifts in ZIPPER and in TBTG are also smaller, except in the top two stories. These two stories remained nearly elastic in KREG.

"Proportional braces" as used in TPRO and ZPRO reduce both story drifts and their COVs compared to KPRO. However, compared to the standard designs (TPRO versus TBTG, ZPRO versus ZIPPER and KPRO versus KREG) maximum story drifts increase in the upper stories of the "proportional brace" designs because braces of smaller areas are more flexible and cause larger elastic drifts.

The distributions of maximum story drifts in TBTG and ZIPPER change with earthquake intensity in a way different from that in KREG. Unlike KREG, which tends to concentrate damage in a few soft stories, these two alternatives tend to achieve more uniform story drifts distribution. Because of the dispersed inelastic action, the COVs of story drifts in both TBTG and ZIPPER are more sensitive to

earthquake intensity than in KREG.

7.6.3. Energy dissipation demand:

TBTG has the lowest total energy dissipation demand thanks to its trilinear hysteretic behavior and large maximum story shears. ZIPPER has the largest total energy dissipation demand despite its trilinear hysteretic behavior because of its lower effective maximum elastic story shears.

KREG has a concentration of energy dissipation demand in the first story (34% of total), while TBTG has its maximum demand at the second story (25% of total) and the maximum for ZIPPER is located in the first story (27% of total). The COVs of energy dissipation demand are largest in KREG, and smallest in ZIPPER (one quarter to one tenth the values for KREG).

Using proportional bracing makes the energy dissipation demand more evenly distributed in all three variants (KPRO, TPRO, ZPRO), and increases the COVs of energy dissipation demand in KPRO only. Compared to TBTG, the COVs of energy dissipation demand in TPRO decrease only slightly. The largest reduction in COVs of energy dissipation demand occurs in ZPRO (30% to 50% reduction compared to KREG and up to 90% reduction compared to KPRO).

Compared to KREG, TBTG seems to be more sensitive to a change in the magnitude of the excitation. The increase in total energy dissipation demand in going from TBTG to TBTG70 is greater than the increase in going from KREG to KREG70. Similarly, the reduction in total energy dissipation demand in going from TBTG to TBTG30 is larger than that observed between KREG and KREG30. The same trend is observed for the COVs of energy dissipation demand. On the other hand, ZIPPER seems to be less sensitive than KREG to changes in the intensity of the earthquake. The changes in energy dissipation demand in ZIPPER are proportional to those that occur in KREG, but the COV values change more slowly.

7.6.4. Maximum interior column compression loads:

Maximum interior column compression loads in both TBTG and ZIPPER are larger than those in KREG. Compared to KREG, the COVs of column compression loads are smaller in TBTG and larger in ZIPPER.

Using "proportional braces" reduces the column compression loads in all the variants (KPRO, TPRO, and ZPRO) to practically the same values. Compared to KPRO, the COVs of column compression in TPRO and ZPRO become much

smaller.

Interior column compression tends to be less sensitive to earthquake intensity in TBTG and ZIPPER than in KREG.

7.6.5. Maximum exterior column compression loads:

Maximum exterior column compression loads in both TBTG and ZIPPER are noticeably larger than their counterparts in KREG. This is associated in part with the larger lateral drifts in the upper stories for these systems. Their COVs are much larger than those in KREG.

Using "proportional braces" increases the exterior column compression loads to practically the same level in all three variants (KPRO, TPRO, and ZPRO). This reflects an increased frame participation. The COVs of exterior column compression load in TPRO and ZPRO are slightly reduced but are still larger than in KPRO.

Exterior column compression loads in TBTG and ZIPPER seem to be more sensitive to earthquake intensity than in KREG. The COV values of exterior column compression load show no definite trend in this respect.

7.6.6. Maximum tie-bar forces:

Among the variants examined, three (TBTG, INVZIP, and ZIPPER) use tie-bars to modify the response characteristics of chevron-braced frames. Yet, the tie-bars in each of these variants have a drastically different mission:

(1)- In TBTG, tie-bars are intended to transfer unbalance forces generated by brace buckling, and to carry them in compression to the ground.

(2)- In INVZIP, the tie-bars have the same function as in TBTG, except that they carry their loads in tension.

(3)- In ZIPPER, the tie-bars are intended to distribute over all stories the unbalance forces generated by brace buckling. They must do that either in tension or in compression.

In all these variants, the tie-bars should remain elastic to perform their function properly. For economy, tie-bar compressions must be limited, and the tension mode of action must be favored. Figures 7-15 shows for each of TBTG, TPRO, INVZIP, ZIPPER and ZPRO the mean maximum tie-bar compression, tension, and a plus and minus one standard deviation confidence interval. Figures 7-15-a compares tie-bar forces for different variants of chevron-bracing: TBTG, ZIPPER and INVZIP. Figures 7-15-b compares tie-bar forces for different tie-bar-to-ground cases:

TBTG30, TBTG70 and TPRO. Figures 7-15-c compares tie-bar forces for different zipper cases: ZIPPER30, ZIPPER70 and ZPRO.

Figures 7-15 shows how rapidly the tie-bar compression builds up in TBTG and TPRO, and how limited it is in INVZIP, ZIPPER and ZPRO. Conversely, tie-bar tension is limited in TBTG and TPRO, but more developed in INVZIP, ZIPPER and ZPRO. Notice that for Zipper configurations (ZIPPER and ZPRO), the maximum tie-bar tension occurs about midheight in the structure, while in INVZIP it occurs at the base level and must be resisted by the foundations.

Compared to ZIPPER, tie-bar compressions in ZPRO are larger and show more variance. That is because in ZPRO, brace buckling is more likely to initiate in upper stories than in ZIPPER, hence there is more unbalance forces to be carried in compression than in ZIPPER. Otherwise, the tie-bar compressive forces in ZIPPER, ZPRO and INVZIP, and the tensile tie-bar forces in TBTG and TPRO are evidence of the importance of the vertical vibration modes in chevron-braced structures, even when subjected to horizontal excitation
only.

Appendix C presents a method for estimating the maximum tie-bar forces for the TBTG and ZIPPER configurations. Such a method is essential for achieving the benefits of the ZIPPER and TBTG configurations which depend on elastic tie-bar response. To simplify the comparisons in the examples analyzed, all the tie-bars were chosen to have the same section and to remain elastic.

7.7. CONCLUSION

Several common alternatives to chevron-bracing have been reviewed in this chapter. It has been shown that while some of them fail to achieve their goals (INVK, SPLIT-X), others show definite improvement in inelastic performance at the cost of increased column compression. However, all these variants are as sensitive to earthquake characteristics as the original chevron-bracing scheme. Their relative merits can be summarized as follows:

The X-braced design has the advantages of achieving stable trilinear hysteresis loops, limited energy dissipation demand, and energy dissipation by tension yield in the braces. Among its disadvantages are the large compressive forces generated in the beams and columns of the braced bay.

The SPLIT-X design achieves the advantages of stable trilinear hysteresis loops, but it still suffers from a concentration of energy dissipation in the lower panel of

every two story module. Moreover, braced bay columns are subjected to large compression forces.

The V-bracing design tries to delay brace buckling by preloading them in tension, and to use gravity loads as restoring forces to improve the hysteretic characteristics. These modifications lead to increased column compression forces and to an inevitable overstrength in the first story. This leads to excessive ductility demands in the remaining stories.

The tie-bar-to-ground configuration achieves the advantages of stable hysteretic loops, and limited energy dissipation demand, without large increases in column compressions. The only problem is that the tie-bars in such a design are subjected to large compression forces.

The inverted tie-bar-to-ground (INVZIP) configuration has the advantages of TBTG and tie-bars that work mostly in tension. However, it is subject to increased column forces, and requires the foundations to resist the large pull-out forces applied by the first story tie-bar.

The Zipper configuration introduced herein seems to overcome several of the problems suffered by the other systems, namely it achieves:

(1)- A reduction in the response sensitivity to ground motion characteristics (amplitude, frequency content, number of pulses and their duration).

(2)- A more uniform damage distribution (maximum story drifts, and energy dissipation demand).

(3)- Trilinear, stable hysteresis loops.

(4)- Limited column compressions if "proportional braces" are used throughout.

(5)- It is ideally suited for cases with flexible beams and intermediate slenderness braces.

There are still several important questions to be resolved before the Zipper configuration can be safely recommended for practical use. What happens if the first brace to buckle is not in the first story? What if the structure is not in a first mode deflected shape when the zipper effect is activated? How to proportion the braces to maximize the effectiveness of the zipper effect? How to choose the relative stiffnesses of the tie-bars and beams? What are the expected axial forces in the tie-bars and in the columns? What would be the effect of simultaneous horizontal and vertical excitations?

Many of these questions require full analytical and experimental research to be answered. However, based on the numerical simulations completed, one can

already outline the answers to several of these questions:

The zipper effect is still effective when first brace buckling occurs at other than the first story, provided the tie-bars do not buckle. The effectiveness of the zipper effect is maximized when "proportional braces" are used (minimum COVs on energy dissipation and story drifts, minimum column compressions). However, first brace buckling in the first story may be the ideal case for the zipper effect since it forces the tie-bars to act mostly in tension, and it mobilizes the energy dissipation capacity of the largest number of braces.

The choice of the best design criteria for the braces is the subject of future research. The methodology developed and the results obtained by other researchers in the study of multiply supported secondary systems should be very useful in such an enterprise [9]. In the mean time, a design methodology for the tie bars is proposed in Appendix C.

In choosing the relative stiffness of tie-bars and beams, a variant of equation 3-19 can be used to determine the minimum tie-bar stiffness needed.

$$K_{bm}+K_{bt}\geq\frac{4K_{bb}K_{br}}{(K_{br}-K_{bb})}\sin^2\Theta$$

where $K_{bt} = (AE/L)_{tie-bar}$ is the effective axial stiffness of the tie-bar. In this respect, flexible beams and intermediate slenderness braces are ideal since intermediate slenderness braces induce the most rapid build-up of unbalance force, and flexible beams allow most of the unbalance to go to the tie-bars. The determination of maximum likely axial forces in tie-bars and consequently in the columns requires further studies.

Similarly, more studies are needed to clarify the effect of combined horizontal and vertical excitations. Additional work on the dynamic force redistributions must also be completed before final proportioning recommendations can be made. In the mean time, modal analysis procedures to compute the lateral design force distribution are suggested and a simplified capacity design approach is recommended to estimate column and beam forces (appendix B) and tie-bar forces (Appendix C) once the brace sizes have been selected.

CHAPTER 8

CONCLUSIONS AND RECOMMENDATIONS

8.1. SUMMARY

The objectives of this study included identifying the design parameters that control the inelastic behavior of chevron-braced frames, and tracing the effects of each parameter in order to formulate rational design recommendations. These objectives have been partially realized, the relationships obtained being less clear-cut than originally hoped. The governing design parameters and their effects have however, been identified and examined. These effects are complex and often conflicting; hence complicating the formulation of definitive design rules. However, the explicit identification of the governing design parameters, their effects and how they interact will help designers make more informed decisions.

In concluding this work, the complex aspects of the inelastic behavior of chevron-braced frames are reviewed. Research results are summarized under three categories: concepts that have been validated, concepts that have been invalidated, and new concepts. Finally, further research needs identified during this work are outlined.

8.2. INELASTIC BEHAVIOR OF CHEVRON-BRACED FRAMES

The complex inelastic behavior of chevron-braced frames requires a system approach. Different conclusions can be reached by looking at limited subsystems, or by adopting simplified analysis techniques. For example, a comparison of the behavior of different slenderness braces having the same yield force leads to conclusions quite different than if the braces have the same buckling force. The comparison should be based on equal buckling force (Chapter 2). In another example, the study of braces alone under monotonic compressive deformation (Chapter 2) led to the conclusion that intermediate slenderness braces should be avoided. Similarly, the analysis of a chevron-braced one bay two story structure under monotonically increasing lateral load favorized the use of stocky braces or of slender braces with stiff beams over intermediate slenderness braces with flexible beams. Yet, the optimization procedure (Chapter 6) lead in one case to a combination of intermediate slenderness braces and flexible beams for the optimal design. Moreover, a consideration of force redistributions (Chapter 3) and dynamic inelastic simulations (Chapter 5) discouraged the use of slender braces with stiff beams. Besides being

difficult to achieve for the usual frame geometries, such proportions lead to a rapid build up of column compressive forces which is to be avoided. Similarly, the use of stocky braces or of larger frame participation increases the dissipation capacity of the structure and reduces its energy dissipation demand, but also increases the variance of the response.

8.3. CONCEPTS VALIDATED

The results of this research have once more proven the extreme sensitivity of the inelastic response of chevron-braced frames to the characteristics of ground excitation, and their tendency to form soft stories (Chapters 5 and 6). Considerable force redistributions occur in chevron-braced frames and affect the overall performance to a large extent. Comparing the performance of a 1985 UBC designs (Chapter 5) to those of SEAONC designs (Chapter 6) shows that the SEAONC recommendations are superior to those of UBC in terms of safety, without being overly conservative. Comparing the optimization results of the El Centro set to those of the mixed earthquakes set (Chapter 6) clearly shows the need for a better knowledge of site seismicity to take full advantage of the optimization procedure.

8.4. CONCEPTS INVALIDATED

Several widely accepted concepts in the design of chevron-braced frames have been more or less invalidated by the results of this research. Chapter 5 showed that the use of stiff beams in a multistory chevron-braced frame can be counterproductive by generating large column compressive forces which may induce column yielding. Designing columns to resist the increased compression would require much larger column sizes. Similarly, the use of stocky braces did not significantly improve the response of chevron-braced frames (Chapter 5), except for a slight reduction in maximum compression in the braced bay columns. Until there is a reliable model for the energy dissipation capacity of braces (stocky ones in particular), stocky braces should be used with caution. The large b_f/t ratios needed to achieve small slenderness for a given strength favor the occurrence of local buckling which can prematurely terminate the useful life of braces.

The concept of statically adding the individual strengths of braced bays and moment resisting frames was shown to be invalid in Chapter 5 (directly, and indirectly in Chapter 6). The different individual deformation patterns of both systems under distributed lateral loads create additional interaction forces between the two systems when they are forced to undergo the same deformation in a dual

system. These internal forces can reduce the total strength available to resist external loads. Moreover, important force redistributions occur upon brace buckling, such that the instantaneous frame participation is quite greater than the original elastic one.

The idea of increasing the elastic design forces to improve the safety of the structure is valid to a certain extent. It assumes that the peak ground acceleration (or other measure of the earthquake damage potential) can be accurately predicted so the structure can be designed to remain elastic. It neglects the massive force redistributions that occur in chevron-braced frames after brace buckling (Chapter 3). Careful consideration of these force redistributions is essential to improve the ductility of chevron-braced structures in the inelastic range, when the actual earthquake intensity exceeds the predicted value. This point was most clearly illustrated in Chapter 6 for the mixed earthquake set, when the optimization algorithm increased not only the brace cross-sectional area in the first story but the brace slenderness also, to avoid increasing the story strength.

The concept of an optimal distribution of story strength heralded by many [49, 5] and adopted by the Japanese Earthquake Resistant Design Code, does not seem to be valid for chevron-braced steel structures. The optimal strength distribution (for elasto-plastic models of story hysteresis) is obtained by trial and error such that the average story ductility demand over several earthquakes is uniformly distributed. This concept does not seem to be valid for chevron-braced steel structures. Besides the fact that the hysteresis loop for chevron-braced stories is far from elasto-plastic, the distribution of ductility demand for any given earthquake is quite different from the average value. With the tendency of chevron-braced frames to form soft stories, this can still result in excessive local ductility demands. This was demonstrated in Chapter 5 where the proportional braces design (KPRO) had larger variances for story drift and energy dissipation demand than the UBC design (KREG).

8.5. NEW CONCEPTS

The dynamic simulations of Chapter 5 have revealed that brace buckling introduces a coupling between vertical and horizontal modes of vibrations. This coupling has quasistatic and dynamic components, and its effects are comparable in importance to other parameters such as brace slenderness, beam stiffness and frame participation. Moreover, it contributes to increasing the axial compressive forces in the braced bay columns.

The optimization study of Chapter 6 shows that the two main concepts in improving the behavior of chevron-braced frames are avoiding tuning to the peaks of the input power spectrum,
and reducing the detrimental interaction between braced bay and moment resisting frame. The idea of avoiding the peaks of the input power spectrum is already widely known and applied in the case of elastic systems (base isolation). For inelastic systems, the idea is to shift the fundamental elastic period to right above a peak in the input power spectrum,
such that occurrence of damage will elongate the instantaneous fundamental period enough to shift away from the peak of energy input, and hence limit further damage. This strategy requires knowledge about the characteristics of future earthquakes that is often not available. To reduce the detrimental interaction between braced bay and moment resisting frame it is necessary to reduce the frame participation at the base of the structure and to increase it at the top.

The optimization study showed that the optimal design depends to a large extent on knowing the seismicity of the site and on the earthquake motions used to simulate that seismicity. The optimal design of a standard chevron-braced frame is therefore more sensitive to the characteristics of the ground motions than the original design, and that in itself is undesirable. Chapter 7 considered several variants of chevron-bracing, two of which enjoy behavior characteristics clearly superior to those of the original chevron-bracing scheme. One of them (TBTG) achieves the advantages of trilinear hysteresis characteristics without increasing column compression or using stiff beams. However, it causes large compression forces in the tie-bars. The other (ZIPPER) adds to the advantages of TBTG the virtue of reduced sensitivity to ground motion characteristics, and a predictable collapse mode.

Chapters 5 and 7 have shown the importance and the complexity of predicting the maximum column compressions and the maximum forces in the tie-bars additions required by the TBTG and ZIPPER modifications. These forces cannot be adequately predicted from extrapolation of elastic analysis results. Simplified procedures were developed to estimate the mean peak column compression in the braced bay (Appendix B) and the mean peak tie-bar forces for the TBTG and ZIPPER variants (Appendix C).

8.6. FURTHER RESEARCH NEEDS

In the course of this investigation several research areas that need to be explored had to be left unexplored. These can be classified under one of three categories: analytical, experimental and numerical.

8.6.1. Analytical:

(1)- The important coupling between vertical and horizontal vibration modes requires investigating the behavior of chevron-braced frames and of their variants (ZIPPER and TBTG) when subjected to combined horizontal and vertical excitations.

(2)- The bounds developed in Appendices B and C for maximum column compression loads and for maximum tie-bar forces need to be refined. One approach would involve representing the tie-bars and masses at beam to brace connections as a secondary system subjected to multiple support inputs [22,43,9].

(3)- The optimization study revealed the sensitivity of the optimum design to the characteristics of ground motions. The relationship between parameters characterizing the earthquake and the response parameters of the structure need to be studied in more detail. The damage potential of an earthquake or given site for a proposed structural system could then be easily estimated at the preliminary design stage. That would speed up the design process and make it less expensive by avoiding costly revisions and extended comparative studies between alternative structural systems.

(4)- The optimization results indicating a reduction in modal correlation in the optimal design warrant a careful investigation and an evaluation of the consequences for three dimensional systems where torsional and translational deformation modes are often highly correlated.

(5)- The reliability formulation currently implemented in DELIGHT.STRUCT is based on a component reliability approach. While this formulation is acceptable in many cases for simple structures made of only one type of elements (flexural members in moment resisting frames), it is deficient for hybrid structures that involve different types of elements interacting in several ways (braced frames comprising braces and flexural members). A system reliability formulation is more desirable. There is evidence that the design space for hybrid systems such as chevron-braced steel frames is not convex. The optimization algorithm may thus converge to a local minimum. Hence there is a need for an

optimization algorithm that can handle such problems; the "simulated annealing" algorithm [71,72,73] is claimed to have such a capacity.

8.6.2. Experimental:

The lack of a reliable and general model for the energy dissipation capacity of braces under cyclic loading was sorely missed in this study. Such a model would be based at least on the brace geometric and material properties, and possibly would consider the deformation history in deciding whether a brace is still serviceable or not. Until recently, most of the experimental work on brace buckling concentrated on understanding the behavior of these elements and on improving the models of such behavior to include the effects of brace slenderness, imperfections and end conditions.

Computer simulations have led to two alternative bracing schemes (TBTG and ZIPPER) that seem to perform better than the original chevron-bracing system. The feasibility and superiority of these variants remain to be proven experimentally in a shaking table or pseudo-dynamics tests.

8.6.3. Numerical:

DELIGHT.STRUCT was originally developed to provide the user with an extensive environment with many facilities that were not available in existing operating systems at the time. As a result it consumes big amounts of memory, is slow in execution (interpreted code) and is somewhat difficult to maintain. A modern version would be more streamlined and modular and would make maximum use of facilities now provided by existing operating systems (like UNIX) and libraries (like LINPACK, MATLAB) and graphic interfaces (X, GKS etc...). A vectorized version of the ANSR structural simulation program would be installed on a CRAY with facilities to run it remotely under the control of the optimization program which would be on a personal workstation. Such a version would increase the size and realism of problems that can be tackled since the structural simulation presently constitutes a time bottleneck, and the limited memory capacity of the personal workstation a space bottleneck.

APPENDIX A

MISCELLANEOUS ANALYTICAL DETAILS

A.1 INTRODUCTION

This appendix contains the details of some of the derivations whose results are discussed in Chapters 2 and 3. It is divided into two main sections the first of which describes in detail the development of a dimensionless model of post buckling brace behavior. The second main section is concerned with the tangent stiffness of a chevron-braced panel after buckling of a compression brace.

A.2 POST BUCKLING BEHAVIOR OF BRACE

Referring to figure 2-1, the deflection of the buckled brace is

$$y(x) = A\cos\left(\frac{\pi}{2}\sqrt{\frac{P}{P_c}}x\right) + B\sin\left(\frac{\pi}{2}\sqrt{\frac{P}{P_c}}x\right) \qquad A1$$

The boundary conditions being

$$y(0) = 0 \rightarrow A = 0 \qquad A2\text{-}1$$

$$y\left(\frac{L}{2}\right) = \frac{M_p(P)}{P} \rightarrow B = \frac{M_p(P)}{P\sin\left(\frac{\pi}{2}\sqrt{\frac{P}{P_c}}\right)} \qquad A2\text{-}2$$

The plastic rotation θ_p at the plastic hinge is given by

$$\theta_p = 2y'\left(\frac{L}{2}\right) = 2\frac{M_p}{P\sin\left(\frac{\pi}{2}\sqrt{\frac{P}{P_c}}\right)}\frac{\pi}{L}\sqrt{\frac{P}{P_c}}\cos\frac{\pi}{2}\sqrt{\frac{P}{P_c}} \qquad A3$$

The axial deformation of the brace Δ has three components; elastic Δ_e , geometric Δ_g and plastic Δ_p :

$$\Delta = \Delta_e + \Delta_g + \Delta_p \qquad A4$$

where the elastic deformation is

$$\Delta_e = \frac{PL}{AE} \qquad A5$$

and the geometric deformation:

$$\Delta_g = 2\int_0^{\frac{L}{2}} \frac{1}{2} y'^2 dx \qquad \text{A6}$$

and the plastic deformation

$$\Delta_p = -\frac{dM_p(P)}{dP}\theta_p\Big|_{P_.}^{P} + \int_{P_.}^{P} \frac{d^2M_p(P)}{dP^2}\theta_p(P)dP \qquad \text{A7}$$

Let $M_p(P) = M_p(1 - \frac{P^2}{P_y^2})$

Then

$$\frac{M_p}{P_y} = 2\nu r\frac{r}{d} = 2\gamma r \qquad \text{A8}$$

where $\gamma = \nu r/d$ is a section property. For wide flange sections bent about their minor axis, γ has a narrow range of values (between 0.3 and 0.4; see Table 2-1). For simplicity, let us define the following dimensionless parameters:

$$u = \frac{P}{P_y} \qquad \text{A9-1}$$

$$a = \frac{P_c}{P_y} = \begin{cases} 1 - \frac{1}{2}\frac{\lambda^2}{\lambda_c^2} & \lambda \le \lambda_c \\ \frac{1}{2}\frac{\lambda_c^2}{\lambda^2} & \lambda > \lambda_c \end{cases} \qquad \text{A9-2}$$

where $\lambda_c = \sqrt{2\pi^2/\epsilon_y}$

$$z = \pi\sqrt{\frac{P}{P_c}} = \pi\sqrt{\frac{u}{a}} \qquad \text{A9-3}$$

$$\eta = \frac{z}{2} \qquad \text{A9-4}$$

$$\lambda = \frac{kL}{r} \qquad \text{A9-5}$$

Notice that $\eta = \pi/2\sqrt{u/a}$ $-u = 4a\eta^2/\pi^2 = b\eta^2$ where $b = 4a/\pi^2$. We then have in dimensionless terms

$$\Delta_e = \epsilon_y Lu = \epsilon_y b\eta^2 L \qquad \text{A10-1}$$

$$\Delta_g = \pi^2\gamma^2(\frac{r}{L})^2\frac{(1-u^2)^2}{au}\frac{1+\frac{\sin z}{z}}{\sin^2\frac{z}{2}}L \qquad \text{A10-2}$$

$$\Delta_p = 32\frac{\gamma^2}{\lambda^2}\eta\cot\eta(1 - b^2\eta^4) - \ln\sin\eta + b^2\int_{\frac{\pi}{2}}^{\eta}\eta^4\cot\eta d\eta L \qquad \text{A10-3}$$

Using series expansions from Abramowitcz [1] for some terms

$$\cot\eta = \frac{1}{\eta} - \frac{\eta}{3} - \frac{\eta^3}{45} - \frac{2\eta^5}{945} \cdots = \frac{1}{\eta} + \sum_{i=1}^{\infty} C_{2i-1}\eta^{2i-1} \qquad \text{A11-1}$$

$$\eta\cot\eta = 1 + \sum_{i=1}^{\infty} C_{2i-1}\eta^{2i} \qquad \text{A11-2}$$

$$\frac{\cot\eta}{\eta} = \frac{1}{\eta^2} + \sum_{i=1}^{\infty} C_{2i-1}\eta^{2i-2} \qquad \text{A11-3}$$

$$\frac{1}{\sin^2\eta} = \frac{1}{\eta^2} - \sum_{i=1}^{\infty}(2i-1)C_{2i-1}\eta^{2i-2} \qquad \text{A11-4}$$

$$\ln\sin\eta = \ln\eta + \sum_{i=1}^{\infty}\frac{C_{2i-1}}{2i}\eta^{2i} \qquad \text{A11-5}$$

it is possible to express the term $\Delta_{gp} = \Delta_g + \Delta_p$ as

$$\Delta_{gp} = 8\frac{\gamma^2}{\lambda^2}[\frac{1}{b^2}Q_1 + 2Q_2 - b^2Q_3]L \qquad \text{A12}$$

where

$$Q_1 = \frac{1}{\eta^4} - \sum_{i=1}^{\infty}(i-1)C_{2i-1}\eta^{2i-4} \qquad \text{A13-1}$$

$$Q_2 = 1 - 2\ln\eta + \sum_{i=1}^{\infty}\frac{(i^2+i-1)}{i}C_{2i-1}\eta^{2i} \qquad \text{A13-2}$$

$$Q_3 = 4D + 2\eta^4 + \sum_{i=1}^{\infty}\frac{(i+1)(i+4)}{(i+2)}C_{2i-1}\eta^{2i+4} \qquad \text{A13-3}$$

Notice that the expressions for Q_1 , Q_2 , and Q_3 are independent of brace properties like slenderness λ and section shape factor γ. Therefore they can be economically and accurately (see figure 2-2a,b,c) replaced by a least square approximation:

$$Q_1 - P_1 = \frac{1}{\eta^4} + 2.16941e^{-2} + 6.112386e^{-3}\eta^2 \qquad \text{A14-1}$$

$$Q_2 - P_2 = -2\ln\eta + 0.99524 - 0.29613\eta^2 - 9.50725e^{-2}\eta^4 \qquad \text{A14-2}$$

$$Q_3 - P_3 = 2.18817 + 2.59573\eta^4 - 1.68026\eta^6 \qquad \text{A14-3}$$

The term $-2\ln\eta$ in Q_2 can be approximated for $0.005\pi \le \eta \le 0.5\pi$ by

$$-2\ln\eta = 14.96810 - 22.432173\eta^{0.25} + 7.43265\eta^{0.50} \qquad \text{A15}$$

P_2 then becomes

$$P_2 = 15.96334 - 22.432173\eta^{0.25} + 7.43265\eta^{0.5} - 0.29613\eta^2 - 9.50723e^{-2}\eta^4 \qquad \text{A16}$$

Finally, the total deformation is

$$\frac{\Delta}{L} = \epsilon_y b\eta^2 + 8\frac{\gamma^2}{\lambda^2}\frac{1}{b^2}\left[\left(\frac{1}{\eta^4} + 2.16941e^{-2} + 6.112386e^{-3}\eta^2\right)\right. \qquad \text{A17}$$

$$+2(15.96334 - 22.432173\eta^{0.25} + 7.43265\eta^{0.50} - 0.29613\eta^2 - 9.50725e^{-2}\eta^4)$$

$$\left.-b^2(2.18817 + 2.59573\eta^4 - 1.68026\eta^6)\right]$$

Using this polynomial expression, it is relatively easy to track the effect of brace slenderness λ and section shape factor γ on such quantities as post buckling tangent stiffness K_{bt} and inelastic energy dissipation E_{in}

A.3 POST BUCKLING TANGENT STIFFNESS:

Since Equation A17 expresses the deformation in terms of the force, it is easier to obtain the flexibility in terms of the force level and then invert it to obtain the instantaneous stiffness in terms of the force level.

$$\frac{1}{K_{bt}} = \frac{\partial\Delta}{\partial\eta}\cdot\frac{\partial\eta}{\partial P} = \frac{\pi}{2}\frac{1}{\sqrt{PP_c}}\frac{\partial\Delta}{\partial\eta} \qquad \text{A18}$$

but

$$\frac{\frac{\partial\Delta}{\partial\eta}}{L} = 2\epsilon_y b\eta + 8\frac{\gamma^2}{\lambda^2}\frac{1}{b^2}\left[\left(\frac{-4}{\eta^5} + 2x6.112386e^{-3}\eta\right)\right. \qquad \text{A19}$$

$$-2\left(\frac{2x2.432173}{4}\eta^{\frac{-3}{4}} - \frac{7.43265}{2}\eta^{\frac{-1}{2}} + 2x0.29613\eta + 4x9.50725e^{-2}\eta^3\right)$$

$$\left.-b^2(4x2.59573\eta^3 - 6x1.68026\eta^5)\right]$$

and

$$\frac{\pi}{2}\frac{1}{\sqrt{PP_c}} = \frac{\pi}{2}\frac{1}{\eta\epsilon_y}\frac{1}{\sqrt{ab}} \qquad \text{A20}$$

which implies

$$\frac{K_0}{K_{bt}} = \frac{\pi^2}{2\epsilon_y a}\epsilon_y b + 8\frac{\gamma^2}{\lambda^2}\left[\frac{1}{b^2}\left(\frac{-2}{\eta^6} + 6.112386c^{-3}\right)\right. \quad \text{A21}$$

$$-(5.60804\eta^{\frac{-7}{4}} - 3.71633\eta^{\frac{-3}{2}} + 0.59226 + 0.38029\eta^2)$$

$$\left.-b^2\eta^2(5.19146 - 5.04028\eta^2)\right]$$

Evaluating Equation A21 at $\eta = \frac{\pi}{2}$

$$\frac{K_{bt}(\frac{\pi}{2})}{K_0} = \frac{1}{2}\frac{1}{1 + 2\pi^2\frac{\gamma^2}{\epsilon_y\lambda^2 a^3}(2.93676a^4 - 2.18737a^2 - 0.7137)} \quad \text{A22}$$

A.4 DERIVATION OF CHEVRON BRACED STORY POST BUCKLING STIFFNESS

The derivation of the post-buckling stiffness of a chevron-braced bay may be simply obtained from first principles. Refer to Figures 3-2 and 3-3 for the geometry and kinematics of the problem.

A.4.1 Geometry

$$\Delta_{brc} = \Delta_t\cos\Theta + \Delta_{bm}\sin\Theta \quad \text{A23}$$

$$\Delta_{brt} = \Delta_t\cos\Theta - \Delta_{bm}\sin\Theta \quad \text{A24}$$

A.4.2 Material Properties

$$\Delta T = K_{br}\Delta_{brt} \quad \text{A25}$$

$$\Delta C = -K_{bb}\Delta_{brc} \quad \text{A26}$$

$$\Delta P_{un} = K_{bm}\Delta_{bm} \quad \text{A27}$$

A.4.3 Equilibrium

$$\Delta F = (\Delta T + \Delta C)\cos\Theta \quad \text{A28}$$

$$\Delta P_{un} = (\Delta T - \Delta C)\sin\Theta \quad \text{A29}$$

Get effective stiffness $K_e = \Delta F/\Delta t$

$$\Delta T - \Delta C = K_{br}\Delta_{brt} + K_{bb}\Delta_{brc} \quad \text{A30}$$

$$= K_{br}\Delta_t\cos\Theta - K_{br}\Delta_{bm}\sin\Theta + K_{bb}\Delta t\cos\Theta + K_{bb}\Delta_{bm}\sin\Theta \quad \text{A31}$$

$$\Delta P_{un} = (K_{br} + K_{bb})\cos\Theta\sin\Theta\Delta t - (K_{br} - K_{bb})\sin^2\Theta\Delta_{bm} = K_{bm}\Delta_{bm} \quad \text{A32}$$

$$-\Delta_{bm} = \Delta_t\sin\Theta\cos\Theta\frac{K_{br} + K_{bb}}{K_{bm} + (K_{br} - K_{bb})\sin^2\Theta} \quad \text{A33}$$

$$\Delta T + \Delta C = K_{br}\Delta_{brt} - K_{bb}\Delta_{brc} \quad \text{A34}$$

$$= K_{br}\Delta_t\cos\Theta - K_{br}\Delta_{bm}\sin\Theta - K_{bb}\Delta_t\cos\Theta - K_{bb}\Delta_{bm}\sin\Theta \quad \text{A35}$$

$$= (K_{br} - K_{bb})\Delta_t\cos\Theta - (K_{br} + K_{bb})\sin\Theta\Delta_{bm} \quad \text{A36}$$

$$= [(K_{br} - K_{bb})\cos\Theta - \frac{(K_{br} + K_{bb})^2\sin^2\Theta\cos\Theta}{K_{bm} + (K_{br} - K_{bb})\sin^2\Theta}]\Delta_t \quad \text{A37}$$

$$\Delta F = (\Delta T + \Delta C)\cos\Theta \quad \text{A38}$$

$$= \Delta_t\cos^2\Theta[(K_{br} - K_{bb}) - \frac{(K_{br} + K_{bb})^2\sin^2\Theta}{K_{bm} + (K_{br} - K_{bb})\sin^2\Theta}] \quad \text{A39}$$

$$K_e = \cos^2\Theta[(K_{br} - K_{bb}) - \frac{(K_{br} + K_{bb})^2\sin^2\Theta}{K_{bm} + (K_{br} - K_{bb})\sin^2\Theta}] \quad \text{A40}$$

If $K_{bm} = \infty$, then $K_e = K_{br}\cos^2\Theta$.

If $K_{bb} = 0$, then $K_e = \dfrac{K_{br}\cos^2\Theta}{1 + \dfrac{K_{br}}{K_{bm}}\sin^2\Theta}$

In order to have $K_e > 0$ (assuming $K_{bb} < K_{br}$), the following relation must be satisfied:

$$K_{br} - K_{bb} \geq \frac{(K_{br} + K_{bb})^2\sin^2\Theta}{K_{bm} + (K_{br} - K_{bb})\sin^2\Theta} \quad \text{A41}$$

or

$$K_{bm} + (K_{br} - K_{bb})\sin^2\Theta \geq \frac{(K_{br} + K_{bb})^2\sin^2\Theta}{(K_{br} - K_{bb})} \quad \text{A42}$$

or

$$K_{bm} \geq [(K_{br}+K_{bb})^2-(K_{br}-K_{bb})^2]\sin^2\frac{\Theta}{(K_{br}-K_{bb})} \qquad A43$$

Hence

$$K_{bm} \geq 4\frac{K_{br}K_{bb}\sin^2\Theta}{(K_{br}-K_{bb})} \qquad A44$$

Given that the original braces stiffness is $K_0 = 2K_{br}\cos^2\Theta$, then the ratio K_e/K_0 equals

$$\frac{K_e}{K_0} = \frac{1}{2}[(1-\frac{K_{bb}}{K_{br}}) - \frac{(1+\frac{K_{bb}}{K_{br}})^2\sin^2\Theta}{\frac{K_{bm}}{K_{br}}+(1-\frac{K_{bb}}{K_{br}})\sin^2\Theta}] \qquad A45$$

Let $C_1 \leq \frac{K_e}{K_0} \leq C_2$, $C_1 \geq 0, C_2 \geq 0$, then

$$2C_1 \leq (1-\frac{K_{bb}}{K_{br}}) - \frac{(1+\frac{K_{bb}}{K_{br}})^2\sin^2\Theta}{\frac{K_{bm}}{K_{br}}+(1-\frac{K_{bb}}{K_{br}})\sin^2\Theta} \leq 2C_2 \qquad A46$$

or

$$0 \leq \frac{\frac{(1+K_{bb})^2\sin^2\Theta}{K_{br}}}{\frac{K_{bm}}{K_{br}}+(1-\frac{K_{bb}}{K_{br}})\sin^2\Theta} \leq (1-\frac{K_{bb}}{K_{br}}) - 2C_1 \qquad A47$$

and

$$0 \leq (1-\frac{K_{bb}}{K_{br}}) - 2C_2 \leq \frac{(1+\frac{K_{bb}}{K_{br}})^2\sin^2\Theta}{\frac{K_{bm}}{K_{br}}+(1-\frac{K_{bb}}{K_{br}})\sin^2\Theta} \qquad A48$$

Taking the inverses

$$\frac{1}{(1-\frac{K_{bb}}{K_{br}})-2C_1} \leq \frac{\frac{K_{bm}}{K_{br}}+(1-\frac{K_{bb}}{K_{br}})\sin^2\Theta}{(1+\frac{K_{bb}}{K_{br}})^2\sin^2\Theta} \leq \frac{1}{(1-\frac{K_{bb}}{K_{br}})-2C_2} \qquad A49$$

or

$$\frac{(1+\frac{K_{bb}}{K_{br}})^2\sin^2\Theta}{1-\frac{K_{bb}}{K_{br}}-2C_1} - (1-\frac{K_{bb}}{K_{br}})\sin^2\Theta \le \frac{K_{bm}}{K_{br}} \le \frac{(1+\frac{K_{bb}}{K_{br}})^2\sin^2\Theta}{1-\frac{K_{bb}}{K_{br}}-2C_2} - (1-\frac{K_{bb}}{K_{br}})\sin^2\Theta \qquad \text{A50}$$

This complicated expression simplifies considerably if $K_{bb} = 0$;

$$\frac{2C_1\sin^2\Theta}{1-2C_1} \le \frac{K_{bm}}{K_{br}} \le \frac{2C_2\sin^2\Theta}{1-2C_2} \qquad \text{A51}$$

Given Equation A44 and the beam stiffness

$$K_{bm} = 48\,\alpha\,(\frac{EI}{L^3})_{bm} \qquad \text{A52}$$

where $1 \le \alpha \le 4$, $\alpha = 1$ for simply supported beams and $\alpha = 4$ for fixed ends beams.

Recalling that the brace stiffness for lateral load is

$$K_{br} = (A\frac{E}{L})_{br}\cos^2\Theta \qquad \text{A53}$$

and $L_{br} = L_{bm}/2\cos\Theta$, Equation A53 becomes

$$K_{br} = 2\frac{A_{br}E}{L_{bm}}\cos^3\Theta \qquad \text{A54}$$

Then Equation A44 implies

$$I_{bm} \ge \frac{1}{6\alpha}\frac{A_{br}L_{bm}^2\cos^3\Theta}{(\frac{K_{br}}{K_{bb}}-1)} \qquad \text{A55}$$

A flexible beam then has $\alpha = 4$ and satisfies

$$I_{bm} \le \frac{1}{24}\frac{A_{br}L_{bm}^2\cos^3\Theta}{(\frac{K_{br}}{K_{bb}}-1)} \qquad \text{A56}$$

A stiff beam has $\alpha = 1$ and

$$I_{bm} \ge \frac{1}{6}\frac{A_{br}L_{bm}^2\cos^3\Theta}{(\frac{K_{br}}{K_{bb}}-1)} \qquad \text{A57}$$

While a beam of intermediate stiffness has

$$\frac{1}{24}\frac{A_{br}L_{bm}^2\cos^3\Theta}{(\frac{K_{br}}{K_{bb}}-1)} \le I_{bm} \le \frac{1}{6}\frac{A_{br}L_{bm}^2\cos^3\Theta}{(\frac{K_{br}}{K_{bb}}-1)} \qquad \text{A58}$$

The increment in vertical unbalance force at the beam midspan ΔP_{un} as expressed in Equation A32 becomes

$$\Delta P_{un} = K_{bm}\Delta_{bm} = \frac{K_{bm}\sin\Theta\cos\Theta(K_{br}+K_{bb})}{K_{bm}+(K_{br}-K_{bb})\sin^2\Theta}\Delta T \qquad \text{A59}$$

which can be rearranged as

$$\Delta P_{un} = \frac{\sin\Theta\cos\Theta K_{bm}}{\frac{K_{bm}}{K_{br}+K_{bb}}+\frac{K_{br}-K_{bb}}{K_{br}+K_{bb}}\sin^2\Theta}\Delta T \qquad \text{A60}$$

or

$$\Delta P_{un} = \frac{(K_{br}+K_{bb})\sin\Theta\cos\Theta}{1+\frac{K_{br}-K_{bb}}{K_{bm}}\sin^2\Theta}\Delta T \qquad \text{A61}$$

APPENDIX B

BOUNDS ON MAXIMUM COLUMN COMPRESSION LOADS

B.1 INTRODUCTION

This research has shown the importance of the post-buckling force redistributions in chevron-braced frames, the difficulty of predicting the magnitude of the redistributed forces, and hence the need for a capacity design approach. In particular, the determination of maximum column compression and tension is essential to insure the safety of the structure. A direct application of capacity design concepts is simple, but leads to overly conservative column force estimates. This section describes a proposed design procedure for chevron-braced frames in general, and emphasizes the steps to follow in determining the maximum credible column forces. The central idea is that in a dynamic loading case, not all elements reach their capacity at the same time. In the absense of an adequate random vibration theory for inelastic systems, it is assumed that the events of elements reaching their capacity are uncorrelated. Hence, a Square Root of Sum of Squares (SRSS) approach is justified.

A comprehensive approach to the seismic design of chevron-braced frames would involve the following steps:

(1)- Obtain averaged nonlinear design strength spectra for a set of earthquakes typical of the site on which the proposed structure is to be erected. For this purpose, programs such as NOSPEC can be used in conjunction with an adequate hysteresis model: deteriorating strength models for regular chevron-bracing, trilinear models for ZIPPER or TBTG variants.

(2)- Select the maximum design strength level corresponding to the estimated fundamental period of the structure and to acceptable displacement ductility and energy ductility demands. The acceptable ductility levels would have been established based on a study of the seismicity of the area and a determination of the ductility capacity of the structural system chosen as well as the allowable probability of exceedance of the specified ductility level (seismic risk study).

(3)- Select a lateral load distribution based on the vertical mass distribution and an assumed story displacement distribution (e.g. linear or quadratic). This distribution may be later refined by modal analysis if necessary.

(4)- Compute the base shear using a first mode mass, the design pseudo-spectral acceleration for the site, and the design strength level chosen in Step 2. Compute the equivalent lateral forces based on the base shear obtained and the

lateral load distribution obtained in Step 3.

(5)- Select beam and brace sizes for the specified gravity service loads and equivalent lateral loads. The selection may be based on the yield stresses for flexural members and on buckling stresses for bracing members. In designing the beams, the support provided by the braces at midspan will be neglected. The results of Chapter 3 (Eq. 3-28) may be used in proportioning the beams and braces for the desired type of post-buckling behavior.

(6)- Compute the maximum story shear capacity using a simplified plastic analysis approach as detailed below.

(7)- Compute the maximum possible overturning moment using an SRSS approach as detailed below.

(8)- Compute the quasi static maximum vertical unbalances P_{ud} at every story as detailed below.

(9)- Compute the maximum column compression (using capacity approach) as detailed below. As discussed in Chapter 5, column compression has four components: a gravity load component, an overturning moment component, a quasi-static brace component, and a dynamic unbalance force component.

(10)- Compute the maximum column moments. The sum of column plastic moments at a joint should be superior to the sum of beam plastic moments and $P\Delta$ moment.

(11)- Select column sections. Proceed from the top of the structure to the bottom, selecting column sections such that the maximum column compression (from Step 9) and the maximum column moment (from Step 10) remain within the section yield surface.

(12)- Evaluate the design for stability, serviceability, strength and constructibility. It may be necessary to go back to previous steps (as far as step 1) to correct any deficiencies in the design.

(13)- In the final design, proportion connections to develop the strength of connecting elements.

In the following, we will illustrate the application of Steps 6 to 9 in the determination of column compression for three examples: KREG, KSTO and KPRO.

B.2 COLUMN FORCES IN KREG

B.2.1 Maximum interior column compression loads for KREG:

Determine the maximum story shear capacity. For the frames discussed herein, one might use for story i:

$$V_i = 2P_{ci}\cos\Theta \qquad \text{B1}$$

This formula assumes a weak girder design and neglects the frame contribution to maximum story strength. The values of V_i are listed in Column 6 of Table B-1.

TABLE B-1 Miscellaneous Brace Data for KREG

Story	Brace Section	Brace Area (in^2)	P_y (k)	P_c (k)	V_i (k)	P_{ud1} (k)	P_{ud2} (k)	P_{ud} (k)
6	W8x28	8.25	297	177	226	116	70	35
5	W8x28	8.25	297	177	226	116	70	35
4	W8x31	9.13	329	243	311	178	70	35
3	W8x31	9.13	329	243	311	178	70	35
2	W8x35	10.3	371	275	352	200	70	35
1	W8x35	10.3	371	275	352	200	70	35

The dynamic vertical unbalance force in any story applied to that story's braced bay column is bounded by

$$P_{ud} = \frac{1}{2}\min\begin{bmatrix} 2P_{un} = P_{ud1} \\ (KM_{pb}/L_{bm} - P_g) = P_{ud2} \end{bmatrix} \qquad \text{B2}$$

where P_{un} is computed from Equation 3-29. The factor of 2 in P_{ud1} is an upper bound for dynamic magnification due to impact loading. The K factor assumes a value of 4 or 8 depending on whether the beam has hinged connections to the columns or fixed connections. M_{pb} is the plastic moment of the beam and L_{bm} is the span of the beam in the chevron-braced bay. $P_g = w_g L_{bm}/4$ is the equivalent gravity load at beam midspan. The second bound $K\frac{M_{pb}}{L_{bm}} - P_g$ is an approximation to the maximum point load increment that can be applied to the beam at midspan before it forms a collapse mechanism. Each column of the braced bay would have to be designed for one half of P_{ud}, hence the 1/2 factor. For this case K=8, $P_g = w_g L/4$, and w_g=1.9k/ft (27.74 kN/m) is the total gravity service load. For the

beam section used (W18x35), the moment of inertia I equals 510 in^4 ($2.12x10^{-4}m^4$), and the plastic section modulus Z equals 66.5 in^3 ($1.09x10^{-3}m^3$). For A36 steel, the beam plastic moment is M_{pb} = 200k−ft (271 kNm), and a P_{ud2} = 70k (299kN). For the configuration used; a braced bay between two unbraced bays of equal spans and no frame contribution, the quasistatic brace contribution to column compression is the same as the overturning component. The frame contribution ($2M_{pbl}/L_l - M_{pbr}/L_r$) cancels out. The vertical unbalance force is shown in Column 9 of Table B-1. The SRSS overturning moment at any story is obtained from the following equation:

$$M_{oi}^{OV} = [\sum_{j=i}^{N}[V_j(H_j - H_i)]^2]^{1/2} \qquad B3$$

The column axial force due to overturning is computed using the "cantilever" method of preliminary analysis for lateral loads. In this case, the overturning component of compression in the braced bay columns reduces to:

$$P_{oi} = M_{oi}/L_{bm} = M_{oi}/20 \text{ (ft)} \qquad B4$$

Table B-2 shows the application of this formula in computing the overturning moments that are used in obtaining maximum column axial forces in the braced bay. For comparison, the overturning moments and axial force obtained from a straight addition of overturning moment components (SAV) are also shown in the table.

$$M_{oi}\ (SAV) = \sum_{j=i}^{N}[V_j(H_j - H_i)] \qquad B5$$

TABLE B-2 Computation of M_o for KREG

Story	1	2	3	4	5	6	M_o	$M_o/20$	M_o	$M_o/20$
Shear (k)	352	352	311	311	226	226	SRSS (k-ft)	SRSS (k)	SAV (k-ft)	SAV (k)
6	0	0	0	0	0	0	0	0	0	0
5	0	0	0	0	0	2712	2712	136	2712	136
4	0	0	0	0	2712	5424	6064	303	8136	407
3	0	0	0	3732	5424	8136	10466	523	17292	865
2	0	0	3732	7464	8136	10843	15922	796	30175	1509
1	0	4224	7464	11196	10848	13560	22370	1118	47292	2364

The gravity component of column axial force at any story level is equal to the sum

of gravity loads for the stories above (P_g in Table B-3). The effective axial component due to the vertical unbalance forces is obtained using an SRSS approach (P_d in Table B-3).

$$P_{di} = [\sum_{j=i}^{N} P_{udj}^2]^{1/2} \qquad B6$$

Finally, the maximum column force at any story level (P_T in Table B-3) is estimated by applying an SRSS sum to the components of overturning moment and dynamic unbalance, and then adding the gravity component.

$$P_{Ti} = P_{gi} + [P_{di}^2 + P_{oi}^2]^{1/2} \qquad B7$$

For comparison, $\bar{P} + 3\sigma$ in Table B-3 shows the mean peak column compression plus three standard deviations recorded during numerical simulations. Assuming a normal distribution for maximum column compressions, the probability of exceeding this value is 0.3 %. P_{UBC} shows the UBC design elastic forces. P_{SEAOC} show the 1985 SEAOC [75] estimate of column compression, assuming an R_w of 8. P_{CAP} shows the yield strength of the column section.

TABLE B-3 Maximum Interior Column Forces for KREG

Story	P_g (k)	P_d (k)	P_o (k)	P_T (k)	$\bar{P}+3\sigma$ (k)	P_{UBC} (k)	P_{SEAOC} (k)	P_{CAP} (k)
6	38	35	0	73	100	38	38	454
5	76	49	136	220	270	107	169	454
4	114	61	303	423	367	203	381	785
3	152	70	523	679	575	319	653	785
2	190	78	796	990	831	451	973	1271
1	228	85	1118	1349	862	594	1326	1271

Figure B-1 compares the estimated peak interior column forces (solid line) to the mean peak forces obtained in the analysis (long dashed line), the UBC design forces (short dashed line), and the column yield forces (dotted line).

B.2.2 Maximum exterior column compression loads in KREG:

There is no dynamic vertical unbalance force applied to the exterior columns. The gravity load component at any story level (P_g of Table B-4) is equal to the linear sum of the gravity forces of the floors above. The axial force component due to over-turning moment is limited by the amount of force that the beam can transmit

to the column. This component is accumulated using the SRSS technique (P_{OV} of Table B-4) on the dynamic components. Assuming plastic hinges occur at the end of the beam:

$$P_{oi} = [\sum_{j=i}^{N} 2M_{pbj}/L_{bm}^2]^{1/2} \qquad \text{B8}$$

The estimate for maximum exterior column compression P_T has only two components; a gravity load component and the overturning component defined hereabove. $P_{T_{SRSS}}$ of Table B-4 shows the exterior column compression computed by the SRSS capacity technique $P_{T_{SRSS}} = \sqrt{P_g^2 + P_o^2}$, and $P_{T_{SAV}}$ shows the straight addition of the two components P_g and P_o. $\bar{P}$ shows the mean peak column compression obtained during the simulations, P_{UBC} shows the UBC elastic design force, and P_{CAP} shows the column section yield force.

TABLE B-4 Maximum Exterior Column Compression for KREG

Story	P_g (k)	P_o (k)	$P_{T_{SRSS}}$ (k)	$P_{T_{SAV}}$ (k)	$\bar{P}+3\sigma$ (k)	P_{UBC} (k)	P_{SEAOC} (k)	P_{CAP} (k)
6	19	20	28	39	29	19	19	454
5	38	28	47	78	61	38	38	454
4	57	35	67	117	94	57	57	454
3	76	40	86	156	111	76	76	454
2	95	45	105	195	167	95	95	454
1	114	49	124	234	173	114	114	454

The SRSS approach underestimates maximum exterior column compression while the SAV approach is on the conservative side. The unconservative results for SRSS may be mitigated by including frame contribution to story capacity.

B.3 COLUMN FORCES IN KSTO

B.3.1 Maximum interior column compression loads for KSTO:

The same procedures used for KREG are also used here, so only the relevant tables are listed. Figure B-2 has the same function for KSTO as Figure B-1 for KREG.

TABLE B-5 Miscellaneous Brace Data for KSTO

Story	Brace Section	Brace Area (in^2)	P_y (k)	P_c (k)	V_i (k)	P_{ud1} (k)	P_{ud2} (k)	P_{ud} (k)
6	$\lambda=55$	5.25	189	177	226	83	70	35
5	$\lambda=55$	5.25	189	177	226	83	70	35
4	$\lambda=46$	7.21	260	243	311	85	70	35
3	$\lambda=46$	7.21	260	243	311	85	70	35
2	$\lambda=46$	8.13	293	275	352	96	70	35
1	$\lambda=46$	8.13	293	275	352	96	70	35

Notice that the maximum unbalance force is still governed by the beam strength rather than by the brace unbalance force. The maximum column forces will therefore be the same as for KREG.

TABLE B-6 Computation of M_o for KSTO

Story	1	2	3	4	5	6	M_o	$M_o/20$	M_o	$M_o/20$
Shear (k)	352	352	311	311	226	226	SRSS (k-ft)	SRSS (k)	SAV (k-ft)	SAV (k)
6	0	0	0	0	0	0	0	0	0	0
5	0	0	0	0	0	2712	2712	136	2712	136
4	0	0	0	0	2712	5424	6064	303	8136	407
3	0	0	0	3732	5424	8136	10466	523	17292	865
2	0	0	3732	7464	8136	10843	15922	796	30175	1509
1	0	4224	7464	11196	10848	13560	22370	1118	47292	2364

and the maximum column forces are put in Table B-7:

TABLE B-7 Maximum Interior Column Forces for KSTO

Story	P_g (k)	P_d (k)	P_o (k)	P_T (k)	$\bar{P}+3\sigma$ (k)	P_{UBC} (k)	P_{SEAOC} (k)	P_{CAP} (k)
6	38	35	0	73	78	38	38	454
5	76	49	136	220	216	107	169	454
4	114	61	303	423	280	203	381	785
3	152	70	523	679	449	319	653	785
2	190	78	796	990	602	451	973	1271
1	228	85	1118	1349	787	594	1326	1271

B.3.2 Maximum exterior column compression loads for KSTO:

There are no changes in the assumptions or in the original numbers so the values obtained are the same as for KREG.

TABLE B-8 Maximum Exterior Column Compression for KSTO

Story	P_g (k)	P_o (k)	$P_{T_{STRESS}}$ (k)	$P_{T_{SAV}}$ (k)	$\bar{P}+3\sigma$ (k)	P_{UBC} (k)	P_{SEAOC} (k)	P_{CAP} (k)
6	19	20	28	39	28	19	19	454
5	38	28	47	78	60	38	38	454
4	57	35	67	117	92	57	57	454
3	76	40	86	156	137	76	76	454
2	95	45	105	195	181	95	95	454
1	114	49	124	234	229	114	114	454

B.4 COLUMN FORCES IN KPRO

B.4.1 Maximum interior column compression loads for KPRO:

The same procedure as for the previous two frames is applied to KPRO. The results of the calculations are shown in Tables b-9 to B-11.

TABLE B-9 Miscellaneous Brace Data for KPRO

Story	Brace Section	Brace Area (in^2)	P_y (k)	P_c (k)	V_i (k)	P_{ud1} (k)	P_{ud2} (k)	P_{ud} (k)
6	$\lambda=92$	2.71	98	73	93	63	70	31
5	$\lambda=92$	5.74	207	153	196	118	70	35
4	$\lambda=92$	6.86	247	183	234	139	70	35
3	$\lambda=92$	8.71	314	232	297	172	70	35
2	$\lambda=92$	10.2	367	272	348	198	70	35
1	$\lambda=92$	10.3	371	275	352	200	70	35

Even in this case, the maximum unbalance force is limited by what the beam can transmit to the columns, except at the top story.

TABLE B-10 Computation of M_o for KPRO

Story	1	2	3	4	5	6	M_o	$M_o/20$	M_o	$M_o/20$
Shear (k)	352	348	297	234	196	93	SRSS (k-ft)	SRSS (k)	SAV (k-ft)	SAV (k)
6	0	0	0	0	0	0	0	0	0	0
5	0	0	0	0	0	1116	1116	56	1116	56
4	0	0	0	0	2352	2232	3242	162	4584	229
3	0	0	0	2808	4704	3348	6420	321	10860	543
2	0	0	3564	5616	7056	4464	10675	534	20700	1035
1	0	4176	7128	8424	9408	5580	16089	804	34716	1736

It can be noticed that the column axial forces due to overturning are noticeably reduced.

TABLE B-11 Maximum Interior Column Forces for KPRO

Story	P_g (k)	P_d (k)	P_o (k)	P_T (k)	$\bar{P}+3\sigma$ (k)	P_{UBC} (k)	P_{SEAOC} (k)	P_{CAP} (k)
6	38	31	0	69	159	38	38	454
5	76	46	56	148	188	107	169	454
4	114	58	162	286	306	203	381	785
3	152	68	321	480	449	319	653	785
2	190	76	534	729	670	451	973	1271
1	228	84	804	1036	938	594	1326	1271

The SRSS capacity approach underestimates column forces badly for KPRO, especially in the upper stories where frame contribution to story shear is less negligeable than in other cases (because of the smaller braces). The force estimate may be improved by adding the frame strength contribution to story shear capacity. To do this, multiply the story capacity based on the strength of braces by the following correction factor

$$F_i = (K_{bri} + K_{fri})/K_{bri} \qquad B9$$

where K_{bri} is the braces contribution to story drift stiffness, and K_{fri} is the frame contribution to story drift stiffness. This correction was deliberately left out in this demonstration to simplify the presentation.

B.4.2 Maximum exterior column compression loads for KPRO:

The estimates of peak exterior column compressions are unchanged. The actual peak column compressions obtained from the simulations are actually higher than for two other frames.

TABLE B-12 Maximum Exterior Column Compression for KPRO

Story	P_g (k)	P_o (k)	$P_{T_{SRSS}}$ (k)	$P_{T_{SAV}}$ (k)	$\bar{P}+3\sigma$ (k)	P_{UBC} (k)	P_{SEAOC} (k)	P_{CAP} (k)
6	19	20	28	39	30	19	19	454
5	38	28	47	78	67	38	38	454
4	57	35	67	117	108	57	57	454
3	76	40	86	156	155	76	76	454
2	95	45	105	195	203	95	95	454
1	114	49	124	234	240	114	114	454

In this case also, the SRSS approach underestimates the mean peak column compressions. Here, the SAV approach is more adequate.

B.5 CONCLUSION

When using a capacity design approach, a straight addition of the capacities of the members feeding forces in a column adjacent to a braced bent is conservative since the maximum member forces do not occur simultaneously. The UBC estimate for column forces is consistently low, however the code has several factors of safety built in. The SEAOC estimate for column forces is conservative at the lower stories and unconservative at the upper stories. In both codes, the estimated column forces do not vary over the building height in the same way as the simulated forces. Both code estimates can therefore be unconservative in some sections of the building (e.g. top), or too conservative at others (e.g. base).

An SRSS summation of the dynamic and redistributed force components seems to be very adequate in bounding column forces. The resulting mean value P_{dc} would be added in absolute value to the static gravity component P_g to obtain the final estimate of column compression. Subtracting P_{dc} from P_g would give an estimate of the maximum column tension. Such an estimate is very useful in the design of column base plates and of column splices. For exterior columns, a better bound of maximum column compression is obtained by directly adding the absolute values of the gravity component and of the overturning component (SAV).

The SRSS (Square Root of Sum of Squares) approach for the dynamic terms seems to be adequate for bounding the column forces in the lower stories in the braced bay. This approach tends to under-estimate column forces in the upper stories in the braced bay, and in all stories of the exterior unbraced bays. One

possible reason is that frame contribution has not been included in the calculations. It is also consistent with the theory that for the small set of members feeding forces into the columns in the upper stories, the assumption of uncorrelated inelastic action is not adequate. These member forces tend to be highly correlated and tend to occur simultaneously. For the lower stories, the set of elements contributing forces to the columns is larger and the assumption of uncorrelation may be more acceptable. This indicates the need for an analysis technique that takes into account the correlation between member forces in the inelastic range, as did Der Kiureghian et al. [22] for the analysis of elastic structures.

The SRSS approach is suggested in three separate instances:

(1)- To compute the overturning moment component of column compression for columns at any story and bay.

(2)- To compute the effective dynamic vertical unbalance component of column compression in the braced bay columns.

(3)- To compute the total estimate of dynamic components of column compression in any braced bay column.

APPENDIX C

BOUNDS OF MAXIMUM TIE-BAR FORCES IN TBTG AND ZIPPER CONFIGURATIONS

C.1 INTRODUCTION

It has been mentioned that an accurate prediction of maximum tie-bar forces would involve a random vibration theory for inelastic systems with multiple support inputs; a theory that has not yet been developed. On the other hand, simple SRSS capacity bounds can be easily developed. In the following sections, bounds are proposed for the maximum tie-bar compression in the TBTG and ZIPPER configurations, and for the maximum tie-bar tension in the ZIPPER configuration only. Maximum tie-bar tension in the TBTG system is negligible compared to the tie-bar compression load which governs the design.

C.2 MAXIMUM TIE-BAR COMPRESSION IN TBTG

The maximum tie-bar compression C_i at story level i is estimated by:

$$C_i = [\sum_{j=i}^{N} P_{unj}^2]^{1/2} \qquad \text{C-1}$$

It is assumed that the presence of tie-bars stiffens the system enough to eliminate the need for dynamic amplification; P_{un} is equal to the value computed from Equation 3-29. However, in using Equation 3-29, the contribution of the tie-bars to the effective beam stiffness must be included, or alternatively an infinitely stiff beam may be assumed. In the following, C_{iold} is the estimate obtained using the bare beam stiffness in Equation 3-29 (not including the tie-bar stiffness), and C_i is calculated assuming a rigid beam. In Table C-1 $\bar{C}$ is the mean peak tie-bar compression in TBTG.

TABLE C-1 Tie-bar compression in TBTG				
Story	P_{un} (k)	C_i (k)	C_{iold} (k)	$\bar{C}$ (k)
6	192	192	116	42
5	192	272	164	120
4	187	330	242	174
3	187	379	300	275
2	212	434	361	352
1	212	483	413	472

C.3 MAXIMUM TIE-BAR COMPRESSION IN ZIPPER

In the ZIPPER configuration where the beam forms plastic hinges, the maximum unbalance force that can be applied to the brace at any story is twice the value obtained from Equation 3-29. The 1/2 factor in Equation 3-29 for equal distribution to the two columns of the braced bay is not needed here. Therefore, the maximum tie-bar compression C_i at story i is:

$$C_i = 2[\sum_{j=i}^{N} P_{usj}^2]^{1/2} \qquad \text{C-2}$$

In a ZIPPER system P_{us} would most often be equal to P_{us2}, because of the formation of plastic hinges, and because the presence of tie-bars increases P_{us1} tremendously.

TABLE C-2 Tie-bar compression in ZIPPER			
Story	$2P_{us}$ (k)	C_i (k)	$\bar{C}$ (k)
6	70	70	39
5	70	99	83
4	70	121	97
3	70	140	97
2	70	156	74
1	70	-	-

C.4 MAXIMUM TIE-BAR TENSION IN ZIPPER

The bound for maximum tie-bar tension load in the ZIPPER configuration is slightly more complicated than the compression bounds.

$$T_i = \min \begin{cases} [\sum_{j=1}^{i-1} P_{unj}^2]^{1/2} \\ [\sum_{j=i}^{N} P_{unj}^2]^{1/2} \end{cases} \qquad \text{C-3}$$

The first bound is an SRSS approximation of the maximum tie-bar tension that can be transmitted from the stories below. The second bound is an estimate of the maximum tie-bar tension that can be transmitted to the stories above the tie-bar in consideration.

TABLE C-3 Tie-bar tension in ZIPPER

Story	P_{un} (k)	$[\sum_{j=1}^{i-1} P_{un}^2]^{1/2}$ (k)	$[\sum_{j=1}^{i-1} P_{un}^2]^{1/2}$ (k)	T_i (k)	$\bar{T}$ (k)
6	192	443	192	192	154
5	192	400	271	271	180
4	187	353	329	329	223
3	187	300	379	300	200
2	212	212	434	212	117
1	212	-	-	-	-

C.5 TIE-BAR STIFFNESS IN THE ZIPPER CONFIGURATION

The requirement of resisting elastically the maximum probable compression is sufficient to determine the tie-bar section size in the tie-bar-to-ground configuration. For the zipper configuration, the tie-bars must satisfy an additional minimum stiffness requirements so that they can transmit a larger portion of the unbalance forces to adjacent stories. In choosing the relative stiffness of tie-bars and beams, a variant of Equation 3-19 can be used to determine the minimum tie-bar stiffness needed.

$$K_{bm} + K_{bt} \geq \frac{4K_{bb}K_{br}}{(K_{br} - K_{bb})} \sin^2\Theta$$

where $K_{bt} = (AE/L)_{tie-bar}$ is the effective axial stiffness of the tie-bar. In this respect, flexible beams and intermediate slenderness braces are ideal since

intermediate slenderness braces induce the most rapid build-up of unbalance force, and flexible beams allow most of the unbalance to go to the tie-bars.

C.6 CONCLUSION

The bounds developed could be refined by more carefully including the frame contribution, but the method would lose its attractive simplicity. However, this might be necessary in cases where the frame stiffness is not negligible compared to that of the braced system. Moreover, the bounds obtained are quite close to the mean peak tie-bar forces, but given the considerable scatter in peak tie-bar forces (COV~0.5-0.6) and the approximations involved in the analysis. The design tie-bar forces should be scaled up accordingly. Assuming a probability distribution for the mean peak tie-bar forces with a mean computed as above, and an estimated COV, it is possible to compute factors of safety necessary to achieve a given probability of exceedance of design forces.

REFERENCES:

1. M. ABRAMOWITCZ and I. A. STEGUN, Handbook of mathematical functions, Dover.
2. AISC, Manual of steel construction, AISC, 1980.
3. J. C. ANDERSON, "Seismic behavior of K-braced frames", ASCE Strct. Div. Vol. 101 no. 10, 1975.
4. A. H. ANG and W. H. TANG, Probability concepts in engineering planning and design, Vol. II, Wiley and sons, 1984.
5. H. AOYAMA, "Outline of earthquake provisions in the recently revised japanese building code", Bulletin New Zealand National Society for Earthquake Engineering Vol. 14 no. 2, 1981.
6. API, API recommended practice for planning, designing and constructing fixed offshore platforms, API, 9th edition.
7. A. ARIAS, A measure of earthquake intensity, MIT Press, 1970.
8. ASCE, The Mexico earthquake 1985: factors involved and lessons learned, ASCE Proceedings, 1986.
9. A. ASFURA and A. DER KIUREGHIAN, A new floor response spectrum method for seismic analysis of multiply supported secondary systems, University of California at Berkeley EERC 84/04, 1984.
10. A. ASTANEH-ASL, Cyclic behavior of double angle bracing members with end gusset plate, University of Michigan at Ann Arbor UMEE 82R7, 1982.
11. M. A. AUSTIN and K. S. PISTER, Optimal design of friction braced frames under seismic loading, University of California at Berkeley EERC 83/10, 1983.
12. M. A. AUSTIN, K. S. PISTER and S. A. MAHIN, A methodology for computer aided design of earthquake resistant steel structures, University of California at Berkeley EERC 85/13, 1985.
13. R. J. BALLING, V. CIAMPI, K. S. PISTER and E. POLACK, Optimal design of seismic resistant planar steel frames, University of California at Berkeley EERC 81/20, 1981.
14. V. V. BERTERO, Identification of research needs for improving aseismic design of building structures, University of California at Berkeley EERC 75/27, 1973.
15. V. V. BERTERO, J. HERRERA and S. A. MAHIN, Establishment of design earthquakes; evaluation of present methods, Proceedings of International Symposium on Earthquake Engineering, 1976.
16. M. A. BHATTI, Optimal design of localized nonlinear systems with dual performance criteria under earthquake excitations, University of California at Berkeley EERC 79/15, 1979.
17. J. M. BIGGS, Introduction to structural dynamics, Mc Graw-Hill.
18. G. R. BLACK, W. A. WENGER and E. P. POPOV, Inelastic buckling of steel struts under cyclic load reversals, University of California at Berkeley EERC 80/40, 1980.
19. P. F. CHEN and G. H. POWELL, Generalized plastic hinge concepts for 3D beam-column elements, University of California at Berkeley EERC 82/20, 1982.
20. F. CHENG and D. S. JUANG, Optimum design of braced and unbraced frames for static, seismic and wind forces with UBC, ATC-3 and TJ-11, University of Missouri-Rolla, 1985.
21. R. W. CLOUGH and S. B. JOHNSTON, Effect of stiffness degradation on

earthquake ductility requirements, Proceedings of Japanese Earthquake Symposium, 1966.
22. A. DER KIUREGHIAN, J. L. SACKMAN and B. NOUR-OMID, Dynamic response of light equipment in structures, University of California at Berkeley EERC 81/05, 1981.
23. M. FUJIMOTO, A. WADA, K. SHIBATA and R. KOSUGI, "Nonlinear analysis of K-type braced steel frames", Trans. AIJ no. 209, 1973.
24. T. FUJIWARA, "Inelastic earthquake response and optimum distribution of dynamic characteristics of bending type structures", Trans. AIJ no. 255, 1977.
25. T. FUKUTA, H. YAMANOUCHI, I. NISHIYAMA, H. ENDOH and T. WATANABE, "Hysteresis behavior of 3 story concentric K-braced frames", Proceedings 8th WCEE, 1984.
26. Y. GHANAAT and R. W. CLOUGH, Study of X-braced steel structures under earthquake simulation, University of California at Berkeley EERC 80/08, 1980.
27. Y. GHANAAT, Shaking table test of a tubular steel frame model, University of California at Berkeley EERC 82/02, 1982.
28. S. G. GOEL, Seismic behavior of multistory K-braced frames under combined horizontal and vertical ground motion, 6th WCEE, 1977.
29. W. J. GOODSIR, T. PAULEY and A. J. CARR, "A study of the inelastic seismic response of reinforced concrete coupled frame shear-wall structures", Bulletin New Zealand National Society for Earthquake Engineering, Vol. 16 no. 3, 1983.
30. H GUGERLI, Inelastic cyclic behavior of steel bracing members, University of Michigan at Ann Arbor UMEE 82R1, 1982.
31. A. B. HIGGINBOTHAM, The inelastic cyclic behavior of axially loaded steel members, University of Michigan at Ann Arbor UMEE 73R9, 1973.
32. ICBO, Uniform building code, ICBO, 1982.
33. S. IGARASHI, I. INOUE, K. OGAWA and M. ASANO, "Hysteretic characteristics of steel braced frames. Part I; the behavior of bracing members under cyclic axial forces", Trans. AIJ no. 196, 1972.
34. S. IGARASHI, I. INOUE and K. OGAWA, "A study on the plastic design of braced multistory steel frames", Trans. AIJ no. 263, 1978.
35. K. IKEDA, Analysis of the cyclic inelastic response of braced steel structures, University of California at Berkeley EERC 84/12, 1984.
36. A. K. JAIN, S. C. GOEL and R. D. HANSON, "Inelastic response of restrained steel tubes", ASCE Stret. Div. Vol. 104 no. 6, 1978.
37. A. K. JAIN, S. C. GOEL and R. D. HANSON, Static and dynamic hysteresis behavior of steel tubular members with welded gusset plates, University of Michigan at Ann Arbor UMEE 77R3, 1977.
38. A. K. JAIN, S. C. GOEL and R. D. HANSON, Hysteresis behavior of bracing members and seismic response of braced frames with different proportions, University of Michigan at Ann Arbor UMEE 78R3, 1978.
39. A. K. JAIN and S. C. GOEL, Seismic response of eccentric and concentric braced steel frames with different proportions, University of Michigan at Ann Arbor UMEE 79R1, 1979.
40. L. KAHN and R. D. HANSON, "Inelastic cycles of axially loaded steel members", ASCE Stret. Div. Vol. 102 no. 5, 1976.
41. B. KATO and H. AKIYAMA, "Seismic design of steel buildings", ASCE Stret. Div. Vol. 108 no. 8, 1982.

42. B. KATO, H. AKIYAMA and Y. OBI, "Deformation characteristics of H shaped steel members influenced by local buckling", Trans. AIJ no. 257, 1977.
43. J. M. KELLY and A. D. COWELL, Experimental studies of multisupport seismic loading on piping systems, University of California at Berkeley EERC 82/19, 1982.
44. H. KRAWINKLER and B. LASHKARI-IRVANI, Damage parameters for bilinear SDOF systems, 7th WCEE, 1982.
45. S. A. MAHIN and V. V. BERTERO, "An evaluation of inelastic seismic design spectra", ASCE Strct. Div. Vol. 107. no. 9, 1981.
46. B. MAISON and E. P. POPOV, "Cyclic response prediction for braced steel frames", ASCE Strct. Div. Vol. 106 no. 7, 1980.
47. M. MAKINO, C. MATSUI and I. MITANI, "Post local buckling behavior of steel beam-columns, part 1-4", Trans. AIJ no. 281, 286, 288, 290, 1979.
48. S. S. MANSON, "Fatigue: a complex subject, some simple approximations", Experimental Mechanics Vol. 5 no. 7, 1965.
49. Y. MATSUSHIMA, Optimum distribution of shear coefficients for MDOF systems subjected to white excitations, 8th WCEE, 1984.
50. I. MITANI, M. MAKINO and C. MATSUI, Influence of local buckling on cyclic behavior of steel beam-column, 6th WCEE, 1977.
51. I. MITANI and M. MAKINO, Post local buckling behavior and plastic rotation capacity of steel beam-columns, 7th WCEE, 1980.
52. D. P. MONDKAR and G. H. POWELL, ANSR-1; general purpose program for analysis of nonlinear structural response, University of California at Berkeley EERC 75/37, 1975.
53. P. MUELLER, Towards rational inelastic aseismic design procedures, Lehigh University Fritz Eng'g Laboratory, 1984.
54. N. M. NEWMARK and E. ROSENBLUETH, Fundamentals of earthquake engineering, Prentice Hall Inc., 1971.
55. R. NILFOROUSHAN, Seismic behavior of multistory K-braced frame structures, University of Michigan at Ann Arbor UMEE 73R9, 1973.
56. G. J. NORDENSON, Notes on the seismic design of concentrically braced frames, 8th WCEE, 1984.
57. W. T. NYE and A. L. TITS, DELIGHT for beginners, University of California at Berkeley UCB/ERL M82/55, 1982.
58. W. T. NYE and D. WANG, DELIGHT for intermediates, University of California at Berkeley UCB/ERL M85/32, 1985.
59. S. P. TIMOSHENKO and J. M. GERE, Theory of elastic stability, Mc Graw-Hill.
60. S. P. TIMOSHENKO and S. WOINOWSKY-KRIEGER, Theory of plates and shells, Mc Graw-Hill.
61. T. PAULAY and W. J. GOODSIR, "The capacity design of reinforced concrete hybrid structures for multistory buildings", Bulletin New Zealand National Society for Earthquake Engineering Vol. 19 no. 1, 1986.
62. E. P. POPOV and R. M. STEPHEN, Cyclic loading of full size steel connections, University of California at Berkeley EERC 70/03, 1970.
63. E. P. POPOV, V. V. BERTERO and H. KRAWINKLER, Inelastic behavior of steel beam to column subassemblages, University of California at Berkeley, EERC 71/07, 1971.

64. E. P. POPOV, V. V. BERTERO and H. KRAWINKLER, Further studies on seismic behavior of steel beam column subassemblages, University of California at Berkeley EERC 73/27, 1973.
65. E. P. POPOV, V. V. BERTERO and S. CHANDRANOULI, Hysteretic behavior of steel columns, University of California at Berkeley EERC 75/11, 1975.
66. E. P. POPOV, Inelastic behavior of steel braces under cyclic loading, Proc. 2nd US National Conf. on Earthquake Engineering, 1979.
67. D. PRAGTHUANGSIT, S. C. GOEL and R. D. HANSON, "Axial hysteresis behavior with end restraints", ASCE Strct. Div. Vol. 104 no. 6, 1978.
68. G. REGA and F. VESTRONI, "Statistical analysis of the inelastic response of shear structures subjected to earthquakes", EESD Vol. 12, 1984.
69. C. W. ROEDER and E. P. POPOV, "Eccentrically braced steel frames for earthquakes", ASCE Strct. Div. Vol. 104 no. 3, 1978.
70. J. SAKAMOTO, Y. KOHAMA and T. YAMAZAKI, "on the dynamic behavior of braced steel frames", Trans. AIJ no. 270, 1978.
71. A. SANGIOVANNI-VINCENTELLI, W. NYE and A. TITS, 'Enhanced methods of feasible directions for engineering design problems", Journal of optimization theory and applications.
72. A. SANGIOVANNI-VINCENTELLI, F. ROMEO and C. SECHEN, Research on simulated annealing at Berkeley, Proceedings of the 1984 International Conference on Computer Design, 1984.
73. A. SANGIOVANNI-VINCENTELLI, D. MITRA and F. ROMEO, Convergence and finite time behavior of simulated annealing, Proceedings of IEEE Conference on Decision and Control, 1985.
74. SEAONC, Earthquake resistant design of concentric and K-braced frames, SEAONC, 1982.
75. SEAONC, Tentative lateral force requirements and commentary, Seismology Committee Structural Engineers Association of California, 1985.
76. R. SHEPHERD, "Multiphase cross bracing in earthquake resistant structures", EESD Vol. 1, 1973.
77. SINGH, Seismic behavior of braces and braced steel frames, University of Michigan at Ann Arbor UMEE 77R1, 1977.
78. R. SRINIVASAN and W. H. MUNSE, Fatigue damage in steel members, ASCE-IABSE Proceedings of International Conference on Planning and Design of Tall Buildings, 1972.
79. K. STEINBRUGGE, A progress report: engineering aspects of the Alaskan earthquake of March 27 1964, 3d WCEE, 1965.
80. G. SUBIMANI and J. ROESSETT, "Design spectra for degrading systems", ASCE Strct. Div. Vol. 111 no. 12, 1985.
81. H. SUGIMOTO and W. F. CHEN, "Inelastic post buckling behavior of tubular members", ASCE Strct. Div. Vol. 111 no. 9, 1985.
82. H. T. SUIDAN and R. A. EUBANKS, "Cumulative fatigue damage", ASCE Strct. Div. Vol. 99 no. 5, 1973.
83. K. TAKANASHI and K. OHI, Shaking table tests on 3 story braced and unbraced steel frames, 8th WCEE, 1984.
84. H. TAKANE and K. TOKYAMA, A study on the earthquake resistant behavior of steel braced frames, part 2, Proceedings of Annual Convention AIJ no. 4, 1981.

85. A. TANAKA, K. MORITA and H. YAMANOUCHI, Damage of braced steel frames due to the 1978 Myagiken Oki earthquake, 7th WCEE, 1980.
86. X. TANG and S. C. GOEL, Seismic analysis and design considerations of braced steel structures, University of Michigan at Ann Arbor, 1987.
87. T. TSUGAWA, Y. GOTOH, H. MORIKAWA and Y. TAKENADA, A study on the earthquake resistant behavior of steel frames, Proceedings of Annual Convention AIJ no. 6, 1983.
88. M. WAKABAYASHI and M. SHIBATA, "Ultimate strength of K-type braced frames", Trans. AIJ no. 326, 1983.
89. M. WAKABAYASHI, C. MATSUI, K. MINAMI and I. MITANI, Inelastic behavior of steel frames subjected to constant vertical and alternating horizontal loads, Annual Conference Preprints AIJ, 1970.
90. M. WAkABAYASHI, Experiments on the elastic plastic behavior of bars subjected to cyclic axial loads, Annual Conference Preprints AIJ, 1972.
91. M. WAKABAYASHI, T. NONAKA, T. NAKAMURA, S. MORINO and N. YOSHIDA, Experimental studies on the behavior of steel bars under repeated axial loading, Bulletin Disaster Prevention Research Institute Kyoto University no. 16B, 1973.
92. M. WAKABAYASHI and M. SHIBATA, "Experimental study on the hysteretic behavior of K-type braced frames subjected to repeated load", Trans. AIJ no. 326, 1983.
93. W. R. WALPOLE, "Concentrically braced frames", Bulletin New Zealand National Society for Earthquake Engineering Vol. 18 no. 4, 1985.
94. G. WORKMAN, The inelastic behavior of multistory braced frame structures subjected to earthquake excitation, University of Michigan at Ann Arbor UMEE 69R1, 1969.
95. V. ZAYAS, S. A. MAHIN and E. P. POPOV, Cyclic inelastic behavior of steel offshore structures, University of California at Berkeley EERC 80/27, 1980.
96. V. ZAYAS, P. B. SHING, S. A. MAHIN and E. P. POPOV, Inelastic structural modeling of braced offshore platforms for seismic loading, University of California at Berkeley, EERC 81/04, 1981.
97. G. ZOUTENDIJK, Methods of feasible directions, Elsevier Amsterdam, 1960.

Table 2-1: Typical γ values for selected steel cross-sections

Section	γ
W14x730	0.40
W14x145	0.39
W14x22	0.33
W12x336	0.40
W12x65	0.38
W12x14	0.30
W10x112	0.39
W10x45	0.38
W10x12	0.31
Standard Pipe 1/2"	0.28
Standard Pipe 12"	0.31
Extra Strong Pipe 1/2"	0.27
Extra Strong Pipe 12"	0.31
Double Extra Strong Pipe 2"	0.26
Double Extra Strong Pipe 8"	0.29

Table 3-1: Member sizes for the various cases in the numerical simulations

Constant P_c						
Case of	Flexible Beam			Stiff Beam		
Brace Slenderness	$\lambda = 20$	$\lambda = 100$	$\lambda = 200$	$\lambda = 20$	$\lambda = 100$	$\lambda = 200$
Beam I in^4	41	58	204	410	580	2040
Brace A in^2	0.33	0.47	1.64	0.33	0.47	1.64
K_{bm}/K_{br}	0.1	0.1	0.1	1.0	1.0	1.0
Constant P_y						
Case of	Flexible Beam			Stiff Beam		
Brace Slenderness	$\lambda = 20$	$\lambda = 100$	$\lambda = 200$	$\lambda = 20$	$\lambda = 100$	$\lambda = 200$
Beam I in^4	41	41	41	410	410	410
Brace A in^2	0.33	0.33	0.33	0.33	0.33	0.33
K_{bm}/K_{br}	0.1	0.1	0.1	1.0	1.0	1.0

Table 4-1 Ductility ratio for pulse loading

Ductility Ratio for Pulse Loading						
Case	Displacement Ductility			Energy Ductility		
	P_{max}/F_y	t_r/T	Ratio	P_{max}/F_y	t_r/T	Ratio
1	0.6	1.0	2.830	0.5	0.1	14.50
2	0.6	1.0	3.114	0.5	0.9	171.00
3	0.5	0.3	1.500	0.5	0.3	8.00
4	0.6	1.0	2.260	0.5	0.1	14.00
5	0.6	1.0	1.714	0.5	0.9	29.00
6	0.5	0.3	1.429	0.5	0.4	1.78

Table 4-2 Ductility ratio for harmonic loading

Ductility Ratio for Harmonic Loading						
Case	Displacement Ductility			Energy Ductility		
	P_{max}/F_y	t_f/T	Ratio	P_{max}/F_y	t_f/T	Ratio
1	1.0	1.0	1.596	0.4	1.0	1.382
2	0.5	1.0	1.339	0.4	1.0	2.308
3	0.2	1.0	1.286	0.4	1.0	1.409
4	1.0	1.0	1.502	0.8	0.2	1.040
5	0.4	1.0	1.156	0.4	1.0	1.120
6	0.2	1.0	1.286	0.4	0.8	0.648

Table 4-3 Earthquake records used

EARTHQUAKE RECORDS USED			
EARTHQUAKE	ABBREVIATION	RMSA (cm/s^2)	Max Acc (g)
ELCENTRO 1940 NS	EC40N	69.31	0.348
HELENA 1935 EW	HE35EW	18.96	0.145
OLYMPIA 1949 N86W	OL4986	56.37	0.280
TAFT 1952 S69E	TA5269	39.98	0.179
PACOIMA 1971 N34E	PA7134	154.69	1.076
PARKFIELD N65E	PAN65E	50.89	0.489

Table 4-4 Design strength ratio of K-braced systems

Ratio of design design strength level of K-braced system to elasto-plastic system				
	SNAP40 to LEPP		SNAP70 to LEPP	
T	$\eta_{db}/\eta_{df}=0.75$	$\eta_{eb}/\eta_{ef}=0.75$	$\eta_{db}/\eta_{df}=0.75$	$\eta_{eb}/\eta_{ef}=0.75$
0.200	1.706	1.342	1.467	1.340
0.300	1.693	1.335	1.498	1.329
0.400	1.964	1.306	1.466	1.303
0.500	1.653	1.354	1.370	1.339
0.600	1.613	1.378	1.328	1.375
0.700	1.635	1.335	1.335	1.325
0.800	1.711	1.331	1.328	1.324
0.900	1.802	1.294	1.466	1.287
1.000	1.643	1.341	1.386	1.331
1.100	1.517	1.346	1.355	1.335
1.200	1.533	1.315	1.322	1.317
1.300	1.548	1.316	1.402	1.314
1.400	1.704	1.216	1.522	1.227
1.500	1.601	1.195	1.464	1.212
1.600	1.540	1.160	1.227	1.178
1.700	1.359	1.219	1.331	1.222
1.800	1.714	1.154	1.492	1.180
1.900	1.868	1.145	1.726	1.153
2.000	*****	1.221	*****	1.221

Table 5-1 BRACED FRAMES SECTION SIZES

BRACED FRAMES SECTION SIZES										
CASE	BEAM	IC1	IC2	IC3	EC1	EC2	EC3	BR1	BR2	BR3
KREG	W18x35	W14x120	W14x74	W14x43	W14x43	W14x43	W14x43	W8x35	W8x31	W8x28
KSTO	W18x35	W14x120	W14x74	W14x43	W14x43	W14x43	W14x43	8.13 in^2	7.21 in^2	5.25 in^2
KD00	W18x35	W14x109	W14x68	W14x43	W14x43	W14x43	W14x43	6x6x5/16	6x6x1/4	5x5x1/4
KD25	W18x35	W14x109	W14x68	W14x43	W14x68	W14x48	W14x43	W8x31	W8x31	W8x24
KS25	W18x35	W14x109	W14x68	W14x43	W14x68	W14x48	W14x43	7.21 in^2	7.21 in^2	4.64 in^2
KD50	W18x35	W14x109	W14x74	W14x48	W14x90	W14x74	W14x48	W8x31	W8x31	W8x24
KS50	W18x35	W14x109	W14x74	W14x48	W14x90	W14x74	W14x48	7.21 in^2	7.21 in^2	4.64 in^2

Table 5-2 EARTHQUAKE RECORDS USED

EARTHQUAKE RECORDS USED					
EARTHQUAKE	ABBREVIATION	Tstart	Tend	RMSA	Max Acc
ELCENTRO 1940 NS	EC40N	0.92	10.92	87.49	0.50
HELENA 1935 EW	HE35EW	0.24	10.24	49.52	0.68
OLYMPIA 1949 N86W	OL4986	9.84	19.84	68.85	0.56
TAFT 1952 S69E	TA5269	3.48	13.48	84.60	0.44
PACOIMA 1971 N34E	PA7134	0.96	10.96	19.95	0.62
PARKFIELD N65E	PAN65E	1.66	11.66	41.64	0.59

Table 5-3 STATISTICS FOR KREG

STATISTICS FOR KREG						
Story Number	1	2	3	4	5	6
Story Shear Mean (k)	392.067	357.350	323.150	321.467	253.650	210.350
Story Shear COV	0.015	0.024	0.052	0.041	0.023	0.084
Story Drift Mean (in)	1.465	1.747	1.428	0.712	1.137	0.503
Story Drift COV	0.619	0.653	0.596	0.473	0.392	0.050
Story Energy Mean (k-in)	820.258	634.212	344.207	86.732	289.700	0.000
Story Energy COV	0.727	0.750	0.762	1.850	0.935	0.000
Brace Energy Mean (k-in)	553.030	562.073	322.308	85.752	268.447	0.000
Brace Energy COV	0.552	0.709	0.769	1.848	0.913	0.000
Column Energy Mean (k-in)	178.997	9.030	1.347	0.000	10.615	0.000
Column Energy COV	1.278	1.394	1.484	0.000	1.748	0.000
Beam Energy Mean (k-in)	88.230	63.112	20.550	0.978	10.643	0.000
Beam Energy COV	1.297	1.292	0.962	1.999	1.108	0.000
Interior Column Compression Mean (k)	751.707	685.767	505.853	312.832	197.013	68.518
Interior Column Compression COV	0.049	0.071	0.046	0.058	0.125	0.157
Exterior Column Compression Mean (k)	151.115	147.467	96.840	87.633	57.415	26.993
Exterior Column Compression COV	0.049	0.045	0.049	0.024	0.020	0.022

Table 5-4 STATISTICS FOR KPIN

STATISTICS FOR KPIN						
Story Number	1	2	3	4	5	6
Story Shear Mean (k)	378.683	330.783	304.800	294.050	224.167	191.050
Story Shear COV	0.033	0.048	0.019	0.061	0.006	0.150
Story Drift Mean (in)	1.190	1.900	2.082	1.242	1.343	0.605
Story Drift COV	0.799	0.715	0.589	0.937	0.279	0.097
Story Energy Mean (k-in)	362.757	572.602	459.568	122.503	383.635	7.580
Story Energy COV	0.741	0.577	0.476	1.610	0.799	2.047
Brace Energy Mean (k-in)	284.912	516.275	427.258	115.608	358.642	6.482
Brace Energy COV	0.552	0.555	0.466	1.632	0.786	2.442
Column Energy Mean (k-in)	57.842	1.765	0.947	0.000	10.292	1.098
Column Energy COV	1.521	1.554	1.365	0.000	1.631	2.449
Beam Energy Mean (k-in)	20.005	54.563	31.362	6.895	14.702	0.000
Beam Energy COV	1.451	1.068	0.855	1.764	0.833	0.000
Interior Column Compression Mean (k)	952.150	748.743	556.302	365.167	236.027	68.972
Interior Column Compression COV	0.046	0.058	0.031	0.069	0.146	0.190
Exterior Column Compression Mean (k)	114.040	95.022	76.020	57.010	38.000	19.000
Exterior Column Compression COV	0.000	0.000	0.000	0.000	0.000	0.000

Table 5-5 STATISTICS FOR KELAS

STATISTICS FOR KELAS						
Story Number	1	2	3	4	5	6
Story Shear Mean (k)	1054.483	980.383	883.017	773.167	633.400	398.567
Story Shear COV	0.303	0.351	0.401	0.402	0.334	0.284
Story Drift Mean (in)	0.705	0.967	1.173	1.292	1.325	1.190
Story Drift COV	0.307	0.385	0.413	0.405	0.369	0.386
Story Energy Mean (k-in)	0.000	0.000	0.000	0.000	0.000	0.000
Story Energy COV	0.000	0.000	0.000	0.000	0.000	0.000
Brace Energy Mean (k-in)	0.000	0.000	0.000	0.000	0.000	0.000
Brace Energy COV	0.000	0.000	0.000	0.000	0.000	0.000
Column Energy Mean (k-in)	0.000	0.000	0.000	0.000	0.000	0.000
Column Energy COV	0.000	0.000	0.000	0.000	0.000	0.000
Beam Energy Mean (k-in)	0.000	0.000	0.000	0.000	0.000	0.000
Beam Energy COV	0.000	0.000	0.000	0.000	0.000	0.000
Interior Column Compression Mean (k)	1730.318	1276.262	853.533	486.593	221.875	48.135
Interior Column Compression COV	0.694	0.657	0.613	0.561	0.100	0.526
Exterior Column Compression Mean (k)	212.578	183.373	149.895	111.698	84.338	37.998
Exterior Column Compression COV	0.570	0.566	0.561	0.554	0.214	0.194

Table 5-6 STATISTICS FOR KSBM

STATISTICS FOR KSBM						
Story Number	1	2	3	4	5	6
Story Shear Mean (k)	505.983	533.350	448.500	428.950	355.283	342.767
Story Shear COV	0.030	0.056	0.025	0.023	0.009	0.127
Story Drift Mean (in)	22.585	0.483	0.900	0.650	2.938	2.573
Story Drift COV	0.666	0.104	0.218	0.200	0.387	0.453
Story Energy Mean (k-in)	5089.740	105.157	459.588	119.533	4760.144	1825.325
Story Energy COV	0.675	0.396	0.533	0.482	0.530	0.602
Brace Energy Mean (k-in)	2117.975	103.532	431.668	116.233	3057.122	1423.505
Brace Energy COV	0.367	0.392	0.509	0.474	0.533	0.602
Column Energy Mean (k-in)	2971.768	1.623	27.922	3.298	1703.027	401.820
Column Energy COV	0.950	0.856	0.910	1.299	0.538	0.634
Beam Energy Mean (k-in)	0.000	0.000	0.000	0.000	0.000	0.000
Beam Energy COV	0.000	0.000	0.000	0.000	0.000	0.000
Interior Column Compression Mean (k)	794.897	533.702	410.647	295.475	256.327	171.517
Interior Column Compression COV	0.038	0.024	0.075	0.096	0.140	0.325
Exterior Column Compression Mean (k)	346.455	313.420	227.617	213.210	143.748	69.467
Exterior Column Compression COV	0.061	0.053	0.493	0.091	0.119	0.141

Table 5-7 STATISTICS FOR KSTO

STATISTICS FOR KSTO						
Story Number	1	2	3	4	5	6
Story Shear Mean (k)	326.117	292.583	261.200	258.450	190.900	152.983
Story Shear COV	0.034	0.039	0.048	0.064	0.041	0.088
Story Drift Mean (in)	1.463	1.905	1.653	0.742	1.162	0.422
Story Drift COV	0.659	0.663	0.662	0.633	0.142	0.083
Story Energy Mean (k-in)	658.718	638.993	388.643	98.372	341.112	2.348
Story Energy COV	0.476	0.584	0.776	1.531	0.537	2.449
Brace Energy Mean (k-in)	456.665	518.423	353.492	96.257	317.955	2.348
Brace Energy COV	0.240	0.534	0.758	1.530	0.537	2.449
Column Energy Mean (k-in)	120.307	6.557	0.532	0.000	11.212	0.000
Column Energy COV	1.375	1.215	2.449	0.000	1.150	0.000
Beam Energy Mean (k-in)	81.747	114.015	34.622	2.115	11.943	0.000
Beam Energy COV	1.044	1.010	1.078	1.555	0.964	0.000
Interior Column Compression Mean (k)	728.058	548.137	393.395	243.917	177.517	96.152
Interior Column Compression COV	0.027	0.033	0.047	0.050	0.073	0.133
Exterior Column Compression Mean (k)	178.017	143.312	111.810	82.687	53.070	25.047
Exterior Column Compression COV	0.096	0.088	0.076	0.038	0.043	0.039

Table 5-8 STATISTICS FOR KOVER

STATISTICS FOR KOVER						
Story Number	1	2	3	4	5	6
Story Shear Mean (k)	500.200	459.700	418.483	412.483	366.083	285.650
Story Shear COV	0.023	0.013	0.022	0.064	0.072	0.155
Story Drift Mean (in)	1.515	1.193	1.547	0.675	0.918	0.697
Story Drift COV	1.193	0.835	0.496	0.098	0.415	0.105
Story Energy Mean (k-in)	807.202	404.418	915.430	23.038	105.477	13.977
Story Energy COV	1.011	1.115	0.918	1.587	1.510	1.044
Brace Energy Mean (k-in)	598.547	376.070	850.382	15.413	89.947	0.000
Brace Energy COV	0.816	1.060	0.872	2.449	1.676	0.000
Column Energy Mean (k-in)	173.223	2.082	60.478	0.000	2.722	0.000
Column Energy COV	1.640	2.449	1.758	0.000	2.281	0.000
Beam Energy Mean (k-in)	35.435	26.267	4.567	7.625	12.808	13.977
Beam Energy COV	1.551	2.012	1.617	1.822	1.122	1.044
Interior Column Compression Mean (k)	1089.097	819.178	514.525	399.668	215.498	54.273
Interior Column Compression COV	0.057	0.078	0.493	0.068	0.185	0.174
Exterior Column Compression Mean (k)	184.752	157.888	106.370	98.755	65.067	30.335
Exterior Column Compression COV	0.059	0.041	0.491	0.045	0.043	0.047

Table 5-9 STATISTICS FOR KUNDER

STATISTICS FOR KUNDER						
Story Number	1	2	3	4	5	6
Story Shear Mean (k)	238.167	202.383	184.567	166.300	155.967	122.667
Story Shear COV	0.067	0.049	0.082	0.054	0.130	0.077
Story Drift Mean (in)	1.717	2.438	2.480	1.690	1.418	0.738
Story Drift COV	0.927	0.623	0.541	0.334	0.234	0.153
Story Energy Mean (k-in)	350.682	390.297	351.050	229.983	157.993	71.573
Story Energy COV	0.702	0.239	0.207	0.212	0.355	0.320
Brace Energy Mean (k-in)	159.025	272.187	248.600	197.057	107.850	47.408
Brace Energy COV	0.267	0.301	0.283	0.290	0.473	0.551
Column Energy Mean (k-in)	105.312	11.017	3.820	2.638	4.933	0.000
Column Energy COV	1.994	0.768	1.689	2.449	1.789	0.000
Beam Energy Mean (k-in)	86.345	107.092	98.630	30.285	45.213	24.167
Beam Energy COV	0.543	0.732	0.457	0.408	0.401	0.562
Interior Column Compression Mean (k)	460.078	378.482	300.593	217.485	149.017	84.693
Interior Column Compression COV	0.026	0.037	0.048	0.020	0.035	0.101
Exterior Column Compression Mean (k)	198.660	163.325	126.072	89.237	54.830	24.182
Exterior Column Compression COV	0.060	0.055	0.057	0.047	0.038	0.020

Table 5-10 STATISTICS FOR KREG30

STATISTICS FOR KREG30						
Story Number	1	2	3	4	5	6
Story Shear Mean (k)	390.033	365.317	328.050	303.000	251.467	202.933
Story Shear COV	0.033	0.014	0.021	0.083	0.048	0.074
Story Drift Mean (in)	0.973	0.807	0.430	0.518	0.808	0.482
Story Drift COV	0.783	0.780	0.042	0.235	0.387	0.066
Story Energy Mean (k-in)	308.220	329.292	11.962	23.390	120.638	0.000
Story Energy COV	1.058	1.139	1.276	1.617	0.917	0.000
Brace Energy Mean (k-in)	241.765	314.427	1.448	16.395	119.815	0.000
Brace Energy COV	1.067	1.146	1.589	2.449	0.915	0.000
Column Energy Mean (k-in)	44.807	6.550	0.000	0.000	0.822	0.000
Column Energy COV	1.553	2.449	0.000	0.000	1.585	0.000
Beam Energy Mean (k-in)	21.652	8.318	10.515	6.995	0.000	0.000
Beam Energy COV	1.254	1.111	1.314	1.382	0.000	0.000
Interior Column Compression Mean (k)	834.752	645.988	470.018	313.050	180.695	61.142
Interior Column Compression COV	0.048	0.028	0.066	0.051	0.112	0.214
Exterior Column Compression Mean (k)	165.690	138.165	112.267	85.288	56.627	27.108
Exterior Column Compression COV	0.046	0.025	0.022	0.022	0.021	0.032

Table 5-11 STATISTICS FOR KREG70

STATISTICS FOR KREG70						
Story Number	1	2	3	4	5	6
Story Shear Mean (k)	399.933	355.367	333.217	323.050	256.700	209.017
Story Shear COV	0.034	0.023	0.036	0.059	0.023	0.108
Story Drift Mean (in)	2.347	2.847	2.093	0.640	1.177	0.520
Story Drift COV	0.640	0.680	0.806	0.323	0.201	0.053
Story Energy Mean (k-in)	1355.280	1079.713	741.205	167.330	352.130	33.818
Story Energy COV	0.617	0.446	0.540	1.306	0.689	1.261
Brace Energy Mean (k-in)	741.725	910.625	649.900	123.630	309.902	0.000
Brace Energy COV	0.381	0.391	0.588	1.914	0.776	0.000
Column Energy Mean (k-in)	396.920	31.535	19.412	0.000	15.020	0.000
Column Energy COV	1.102	1.101	0.950	0.000	1.124	0.000
Beam Energy Mean (k-in)	216.637	137.555	71.893	43.702	27.208	33.818
Beam Energy COV	0.851	1.032	0.475	0.733	0.684	1.261
Interior Column Compression Mean (k)	899.488	567.192	516.495	308.197	204.872	67.757
Interior Column Compression COV	0.055	0.494	0.054	0.045	0.078	0.097
Exterior Column Compression Mean (k)	180.328	124.232	116.838	87.965	57.580	27.163
Exterior Column Compression COV	0.048	0.486	0.011	0.021	0.019	0.021

Table 5-12 STATISTICS FOR KD00

STATISTICS FOR KD00						
Story Number	1	2	3	4	5	6
Story Shear Mean (k)	318.833	270.583	239.083	239.717	192.700	166.983
Story Shear COV	0.025	0.033	0.028	0.033	0.061	0.129
Story Drift Mean (in)	1.258	1.832	1.662	0.838	0.928	0.475
Story Drift COV	0.748	0.594	0.541	0.560	0.179	0.099
Story Energy Mean (k-in)	470.173	760.825	614.018	160.873	143.812	2.588
Story Energy COV	0.875	0.440	0.320	1.454	0.499	2.086
Brace Energy Mean (k-in)	305.788	622.185	563.012	154.030	139.035	2.588
Brace Energy COV	0.579	0.358	0.301	1.437	0.491	2.086
Column Energy Mean (k-in)	90.538	6.803	1.192	0.000	0.322	0.000
Column Energy COV	1.664	1.422	1.575	0.000	2.229	0.000
Beam Energy Mean (k-in)	73.845	131.835	49.815	6.840	4.455	0.000
Beam Energy COV	1.289	0.997	0.627	1.877	0.894	0.000
Interior Column Compression Mean (k)	696.538	549.583	410.738	261.648	171.145	56.098
Interior Column Compression COV	0.044	0.028	0.018	0.064	0.089	0.104
Exterior Column Compression Mean (k)	179.463	146.195	113.058	83.583	54.220	23.017
Exterior Column Compression COV	0.077	0.068	0.063	0.032	0.033	0.283

Table 5-13 STATISTICS FOR KD25

STATISTICS FOR KD25						
Story Number	1	2	3	4	5	6
Story Shear Mean (k)	356.350	328.083	313.700	303.667	221.217	186.300
Story Shear COV	0.057	0.026	0.053	0.088	0.022	0.123
Story Drift Mean (in)	1.513	1.933	1.103	0.505	1.250	0.505
Story Drift COV	0.533	0.553	0.769	0.067	0.167	0.072
Story Energy Mean (k-in)	916.402	709.848	272.175	0.515	289.655	0.000
Story Energy COV	0.640	0.531	1.189	2.449	0.528	0.000
Brace Energy Mean (k-in)	570.803	620.608	256.132	0.515	268.357	0.000
Brace Energy COV	0.273	0.489	1.196	2.449	0.548	0.000
Column Energy Mean (k-in)	205.497	3.105	0.000	0.000	12.068	0.000
Column Energy COV	1.435	2.077	0.000	0.000	1.161	0.000
Beam Energy Mean (k-in)	140.100	86.135	16.042	0.000	9.230	0.000
Beam Energy COV	1.187	1.034	1.208	0.000	0.683	0.000
Interior Column Compression Mean (k)	825.292	634.988	451.170	272.965	183.550	59.757
Interior Column Compression COV	0.060	0.046	0.036	0.032	0.124	0.064
Exterior Column Compression Mean (k)	178.952	145.410	117.565	89.138	57.818	27.325
Exterior Column Compression COV	0.047	0.037	0.021	0.027	0.025	0.026

Table 5-14 STATISTICS FOR KS25

STATISTICS FOR KS25						
Story Number	1	2	3	4	5	6
Story Shear Mean (k)	301.867	274.517	251.083	235.067	186.500	135.550
Story Shear COV	0.051	0.043	0.059	0.106	0.055	0.110
Story Drift Mean (in)	1.375	1.950	1.667	0.673	1.128	0.417
Story Drift COV	0.623	0.564	0.696	0.645	0.155	0.078
Story Energy Mean (k-in)	610.935	724.607	367.643	78.382	269.413	2.777
Story Energy COV	0.420	0.249	0.898	1.579	0.399	2.066
Brace Energy Mean (k-in)	429.552	603.638	331.288	76.835	252.530	2.777
Brace Energy COV	0.152	0.188	0.891	1.577	0.412	2.066
Column Energy Mean (k-in)	95.822	0.032	1.980	0.000	8.413	0.000
Column Energy COV	1.644	2.449	1.388	0.000	1.191	0.000
Beam Energy Mean (k-in)	85.560	120.937	34.373	1.547	8.468	0.000
Beam Energy COV	0.892	0.906	1.122	1.771	0.833	0.000
Interior Column Compression Mean (k)	673.452	531.357	379.770	228.915	172.263	59.160
Interior Column Compression COV	0.035	0.049	0.070	0.042	0.039	0.098
Exterior Column Compression Mean (k)	182.170	145.822	111.650	83.523	53.460	25.168
Exterior Column Compression COV	0.090	0.088	0.071	0.037	0.032	0.027

Table 5-15 STATISTICS FOR KD50

STATISTICS FOR KD50						
Story Number	1	2	3	4	5	6
Story Shear Mean (k)	362.833	323.033	310.633	318.067	229.367	185.883
Story Shear COV	0.026	0.041	0.073	0.086	0.054	0.129
Story Drift Mean (in)	1.318	1.850	1.420	0.673	1.270	0.488
Story Drift COV	0.591	0.543	0.499	0.416	0.184	0.075
Story Energy Mean (k-in)	736.198	724.198	390.802	87.970	290.075	0.113
Story Energy COV	0.712	0.584	0.774	1.599	0.545	2.449
Brace Energy Mean (k-in)	480.262	620.028	365.650	85.027	266.052	0.113
Brace Energy COV	0.416	0.510	0.766	1.615	0.563	2.449
Column Energy Mean (k-in)	140.460	2.095	0.000	0.000	11.610	0.000
Column Energy COV	1.597	1.755	0.000	0.000	1.586	0.000
Beam Energy Mean (k-in)	115.477	102.073	25.153	2.943	12.417	0.000
Beam Energy COV	1.285	1.254	0.996	2.066	0.789	0.000
Interior Column Compression Mean (k)	829.278	644.832	464.260	274.330	183.890	68.100
Interior Column Compression COV	0.044	0.042	0.049	0.040	0.078	0.129
Exterior Column Compression Mean (k)	185.362	150.478	120.665	90.710	58.840	27.517
Exterior Column Compression COV	0.052	0.041	0.023	0.028	0.028	0.026

Table 5-16 STATISTICS FOR KS50

STATISTICS FOR KS50						
Story Number	1	2	3	4	5	6
Story Shear Mean (k)	309.150	278.533	254.333	236.783	191.250	140.050
Story Shear COV	0.058	0.062	0.051	0.093	0.060	0.110
Story Drift Mean (in)	1.232	1.830	1.598	0.923	1.035	0.397
Story Drift COV	0.648	0.619	0.719	0.621	0.128	0.063
Story Energy Mean (k-in)	553.908	745.598	389.192	167.635	256.153	0.618
Story Energy COV	0.502	0.283	0.840	1.175	0.436	1.815
Brace Energy Mean (k-in)	394.885	613.228	343.995	159.182	246.613	0.618
Brace Energy COV	0.240	0.197	0.818	1.174	0.437	1.815
Column Energy Mean (k-in)	75.927	0.000	0.000	0.000	0.640	0.000
Column Energy COV	1.912	0.000	0.000	0.000	2.070	0.000
Beam Energy Mean (k-in)	83.095	132.370	45.198	8.453	8.898	0.000
Beam Energy COV	1.042	1.030	1.188	1.245	0.871	0.000
Interior Column Compression Mean (k)	665.612	530.492	384.417	232.592	170.722	61.465
Interior Column Compression COV	0.049	0.052	0.046	0.076	0.053	0.175
Exterior Column Compression Mean (k)	187.733	152.822	117.282	85.605	54.158	25.368
Exterior Column Compression COV	0.074	0.085	0.073	0.034	0.029	0.029

Table 5-17 STATISTICS FOR KPRO

STATISTICS FOR KPRO						
Story Number	1	2	3	4	5	6
Story Shear Mean (k)	389.900	344.800	303.600	260.617	214.833	145.917
Story Shear COV	0.032	0.063	0.050	0.029	0.024	0.134
Story Drift Mean (in)	1.453	1.485	1.383	1.325	1.393	0.923
Story Drift COV	0.977	1.052	0.912	0.400	0.311	0.277
Story Energy Mean (k-in)	493.018	442.255	362.562	488.540	470.292	192.705
Story Energy COV	0.994	1.022	1.276	0.624	0.788	1.187
Brace Energy Mean (k-in)	346.057	385.218	316.042	454.575	421.620	184.827
Brace Energy COV	0.685	0.892	1.261	0.615	0.764	1.150
Column Energy Mean (k-in)	104.945	4.387	8.865	1.385	23.113	0.468
Column Energy COV	1.933	2.153	1.550	1.572	1.623	2.449
Beam Energy Mean (k-in)	42.020	52.650	37.655	32.578	25.557	7.412
Beam Energy COV	2.042	2.169	1.363	0.767	1.057	2.147
Interior Column Compression Mean (k)	784.925	578.150	411.722	262.752	155.093	90.493
Interior Column Compression COV	0.065	0.053	0.030	0.055	0.070	0.253
Exterior Column Compression Mean (k)	187.337	157.153	126.940	94.282	60.375	27.862
Exterior Column Compression COV	0.095	0.098	0.074	0.050	0.034	0.032

Table 5-18 Total Energy Dissipation Statistics

Total Energy Dissipation Statistics									
	Columns		Beams		Frame		Braces		Total
CASE	Total (in-k)	Ratio	Total (in-k)	Ratio	Total (in-k)	Ratio	Total (in-k)	Ratio	Total (in-k)
KREG	199.988	0.078	183.511	0.072	383.498	0.150	1791.609	0.850	2175.107
KPIN	71.942	0.032	127.525	0.060	199.468	0.092	1709.178	0.908	1908.646
KELAS	0.000	0.000	0.000	0.000	0.000	0.000	0.000	0.000	0.000
KSBM	5109.459	0.339	0.000	0.000	5109.459	0.339	7250.032	0.661	12359.491
KSTO	138.606	0.055	244.441	0.100	383.048	0.154	1745.142	0.846	2128.189
KOVER	238.504	0.084	100.682	0.037	339.186	0.121	1930.358	0.879	2269.544
KUNDER	127.721	0.068	391.732	0.248	519.452	0.316	1032.128	0.684	1551.580
KREG30	52.180	0.056	47.478	0.042	99.657	0.098	693.844	0.902	793.501
KREG70	462.885	0.109	530.814	0.128	993.698	0.237	2735.779	0.763	3729.478
KD00	98.854	0.033	266.795	0.106	365.649	0.139	1786.641	0.861	2152.290
KD25	220.670	0.078	251.504	0.092	472.174	0.169	1716.414	0.831	2188.588
KS25	106.246	0.040	250.887	0.108	357.133	0.148	1696.620	0.853	2053.753
KD50	154.164	0.051	258.061	0.095	412.225	0.146	1817.130	0.854	2229.355
KS50	76.567	0.025	278.013	0.115	354.580	0.140	1758.525	0.860	2113.105
KPRO	143.164	0.073	197.872	0.065	341.036	0.139	2108.340	0.861	2449.376

Table 6-1 Earthquake records used

Table 6-1; Earthquake records			
Record	Abbreviation	$(\ddot{v}_g)_{max}$ II	$(\ddot{v}_g)_{max}$ I.I
El Centro 1940 NS	EC40NS	0.145	0.579
El Centro 1940 EW	EC40EW	0.117	0.446
El Centro 1934 NS	EC34NS	0.197	0.449
El Centro 1934 EW	EC34EW	0.288	0.551
El Centro 1940 NS	EC40NS	0.145	0.579
Helena 1935 EW	HE35EW	0.197	0.787
Olympia 1949 N86E	OL4986	0.162	0.647
Parkfield 1940 N65E	PAN65E	0.171	0.683

Table 6-2-a: Summary of results for the El Centro set

Table 6-2-a Summary of results for the El Centro set								
Case	Original				Optimal			
Story	1	2	3	4	1	2	3	4
Column I (in^4)	1530	796	723	723	104	352	480	480
Beam I (in^4)	612	612	612	612	582	582	582	582
Brace A (in^2)	9.36	9.36	9.36	9.36	6.33	5.00	4.97	4.96
Brace λ	78	72	72	72	79	72	72	72
Story Strength (k)	387	517	509	431	232	263	275	242
Story Stiffness (k/in)	963	1170	1150	975	584	590	622	547
Period (s)	0.254	0.0949	0.0551	0.0321	0.366	0.122	0.0691	0.0584
$(K_{fr}/K_{br})_h$	0.141	0.365	0.342	0.138	0.023	0.288	0.367	0.205
$(K_{bm}/K_{br})_v$	0.090	0.402	0.401	0.232	0.095	0.503	0.544	0.402
Limit State II Mean Peak values and corresponding yield values								
Column M_{max}(k–in)	472	249	248	398	427	208	279	409
Column M_y(k–in)	8241	4335	4029	4029	547	1770	2644	2686
Beam M_{max}(k–in)	581/560	495/575	533/528	400/548	241/844	479/587	479/522	409/495
Beam M_y(k–in)	2923	2923	2923	2923	2816	2816	2816	2816
Brace P_{max}(k)	82	77	64	50	82	69	58	48
Brace P_c(k)	275	284	284	284	184	152	151	151
Story Δ_{max}(in)	0.080	0.075	0.073	0.059	0.111	0.155	0.160	0.138
Story Δ_{all}(in)	0.864	0.756	0.756	0.756	0.864	0.756	0.756	0.756
Limit state III mean peak energy dissipation demand and allowable values								
Column E_{max}(k–in)	0	0	0	0	0	0	0	0
Column E_{all}(k–in)	152	68	68	68	8	28	44	44
Beam E_{max}(k–in)	0	0	0	0	0	0	0	0
Beam E_{all}(k–in)	44	44	44	44	30	30	30	30
Brace E_{max}(k–in)	0	0	0	0	52	23	0	0
Brace E_{all}(k–in)	157	145	145	145	106	77	77	77

Table 6-2-b: Summary of results for the mixed set

Table 6-2-b Summary of results for the mixed set								
Case	Original				Optimal			
Story	1	2	3	4	1	2	3	4
Column I (in^4)	1530	796	723	723	153	356	566	566
Beam I (in^4)	612	612	612	612	595	595	595	595
Brace A (in^2)	9.36	9.36	9.36	9.36	12.05	6.59	5.57	6.26
Brace λ	78	72	72	72	107	73	72	72
Story Strength (k)	387	517	509	431	361	328	311	293
Story Stiffness (k/in)	963	1170	1150	975	1101	742	705	664
Period (s)	0.254	0.0949	0.0551	0.0321	0.324	0.101	0.0591	0.0490
$(K_{fr}/K_{br})_h$	0.141	0.365	0.342	0.138	0.017	0.232	0.382	0.159
$(K_{brn}/K_{br})_v$	0.090	0.402	0.401	0.232	0.054	0.437	0.576	0.516
Limit State II Mean Peak values and corresponding yield values								
Column $\bar{M}_{max}$(k–in)	666	281	286	433	495	201	323	447
Column M_y(k–in)	8241	4335	4029	4029	767	1786	3185	3185
Beam $\bar{M}_{max}$(k–in)	657/560	533/576	577/528	433/548	209/900	451/634	479/622	447/516
Beam M_y(k–in)	2923	2923	2923	2923	2864	2864	2864	2864
Brace P_{max}(k)	110	100	86	70	100	80	68	66
Brace P_c(k)	275	284	284	284	285	199	169	150
Story Δ_{max}(in)	0.121	0.111	0.133	0.128	0.081	0.134	0.193	0.203
Story Δ_{all}(in)	0.864	0.756	0.756	0.756	0.864	0.756	0.756	0.756
Limit state III mean peak energy dissipation demand and allowable values								
Column E_{max}(k–in)	12.7	0	0	0	9.0	27.1	8.9	0
Column E_{all}(k–in)	152	68	68	68	13	26	54	54
Beam E_{max}(k–in)	34.3	9.8	0	0	49.7	30.4	0	0
Beam E_{all}(k–in)	44	44	44	44	42	42	42	42
Brace E_{max}(k–in)	221	0	0	0	178	98	0	0
Brace E_{all}(k–in)	157	145	145	145	202	102	86	97

Table 6-3-a: Initial and final modal correlations for the El Centro set

Table 6-3-a; Initial and final modal correlations for the El Centro set								
	Original				Final			
RHO0	1	2	3	4	1	2	3	4
1	1.000	0.147	0.170	0.153	1.000	0.047	0.073	0.077
2		1.000	0.489	0.431		1.000	0.442	0.449
3			1.000	0.574			1.000	0.658
4				1.000				1.000
RHO1	1	2	3	4	1	2	3	4
1	1.000	0.034	0.035	0.032	1.000	-0.044	-0.028	-0.025
2		1.000	0.170	0.137		1.000	0.216	0.200
3			1.000	0.279			1.000	0.332
4				1.000				1.000
RHO2	1	2	3	4	1	2	3	4
1	1.000	-0.011	-0.008	-0.007	1.000	-0.074	-0.047	-0.040
2		1.000	0.047	0.021		1.000	0.095	0.080
3			1.000	0.158			1.000	0.196
4				1.000				1.000

Table 6-3-b: Initial and final modal correlations for the mixed set

Table 6-3-b; Initial and final modal correlations for the mixed set								
	Original				Final			
RHO0	1	2	3	4	1	2	3	4
1	1.000	0.007	0.002	0.001	1.000	0.005	0.002	0.001
2		1.000	0.028	0.013		1.000	0.031	0.016
3			1.000	0.133			1.000	0.218
4				1.000				1.000
RHO1	1	2	3	4	1	2	3	4
1	1.000	-0.019	-0.019	-0.017	1.000	-0.020	-0.018	-0.017
2		1.000	-0.001	-0.016		1.000	0.002	-0.012
3			1.000	0.106			1.000	0.195
4				1.000				1.000
RHO2	1	2	3	4	1	2	3	4
1	1.000	0.006	0.001	0.001	1.000	0.004	0.001	0.001
2		1.000	0.027	0.012		1.000	0.031	0.016
3			1.000	0.136			1.000	0.224
4				1.000				1.000

Table 6-4: Deterministic optimization parameters

Deterministic optimization parameters		
Symbol	Value	Description
Good_Costvol	25000	Good volume (in^3)
Bad_Costvol	85000	Bad volume (in^3)
Limit State I constraint parameters		
Symbol	Value	Description
Good_Colax	0.500	Good gravity column axial force factor
Bad_Colax	0.600	Bad gravity column axial force factor
Good_Colgra	0.600	Good gravity column moment factor
Bad_Colgra	0.800	Bad gravity column moment factor
Good_Girgra	0.600	Good gravity girder moment factor
Bad_Girgra	0.800	Bad gravity girder moment factor
Good_Bragra	0.950	Good gravity brace axial force factor
Bad_Bragra	1.000	Bad gravity brace axial force factor
Good_Girdef	1/240	Good girder midspan deflection ratio
Bad_Girdef	1/220	Bad girder midspan deflection ratio
Limit State II constraint parameters		
Symbol	Value	Description
Good_Colyld	0.850	Good moderate column yield factor
Bad_Colyld	1.100	Bad moderate column yield factor
Good_Giryld	0.900	Good moderate girder yield factor
Bad_Giryld	1.100	Bad moderate girder yield factor
Good_Drift	4.50e-3	Good moderate maximum story drift
Bad_Drift	8.00e-3	Bad moderate maximum story drift
Limit State III constraint parameters		
Symbol	Value	Description
Good_Colduc	3.000	Good column energy ductility
Bad_Colduc	4.000	Bad column energy ductility
Good_Girduc	4.000	Good girder energy ductility
Bad_Girduc	6.000	Bad girder energy ductility
Good_Braduc	1.000	Good brace energy ductility
Bad_Braduc	2.000	Bad brace energy ductility
Good_Sway	1.4e-2	Good maximum sway
Bad_Sway	2.0e-2	Bad maximum sway

Table 6-5: Probabilistic optimization parameters

Probabilistic optimization parameters		
Symbol	Value	Description
High_Colax_prob	0.200	High column axial force factor
Low_Colax_prob	0.100	Low column axial force factor
High_Colgra_prob	0.200	High column moment factor
Low_Colgra_prob	0.100	Low column moment factor
High_Girgra_prob	0.200	High girder moment factor
Low_Girgra_prob	0.100	Low girder moment factor
High_Bragra_prob	0.200	High brace axial force factor
Low_Bragra_prob	0.100	Low brace axial force factor
High_Girdef_prob	0.200	High girder midspan deflection ratio
Low_Girdef_prob	0.100	Low girder midspan deflection ratio
High_Colyld_prob	0.200	High moderate column yield factor
Low_Colyld_prob	0.100	Low moderate column yield factor
High_Giryld_prob	0.200	High moderate girder yield factor
Low_Giryld_prob	0.100	Low moderate girder yield factor
High_Drift_prob	0.200	High moderate maximum story drift
Low_Drift_prob	0.100	Low moderate maximum story drift
High_Colduc_prob	0.200	High column energy ductility
Low_Colduc_prob	0.100	Low column energy ductility
High_Girduc_prob	0.200	High girder energy ductility
Low_Girduc_prob	0.100	Low girder energy ductility
High_Braduc_prob	0.200	High brace energy ductility
Low_Braduc_prob	0.100	Low brace energy ductility
High_Sway_prob	0.200	High maximum sway
Low_Sway_prob	0.100	Low maximum sway

Table 7-1: Distribution of Energy Dissipation demand for all variants

Total Energy Dissipation Statistics									
	Columns		Beams		Frame		Braces		Total
CASE	Total (in-k)	Ratio	Total (in-k)	Ratio	Total (in-k)	Ratio	Total (in-k)	Ratio	Total (in-k)
XREG	152.423	0.066	59.406	0.019	211.829	0.085	1415.288	0.915	1627.116
SPLIT-X	171.185	0.063	46.540	0.017	217.725	0.080	1543.224	0.921	1760.949
INVK	77.361	0.027	372.861	0.129	450.222	0.155	1498.265	0.845	1948.487
INVZIP	113.050	0.043	70.612	0.028	183.662	0.071	1710.228	0.929	1893.890
TBTG30	0.193	0.000	4.998	0.003	5.191	0.003	613.652	0.997	618.843
TBTG	33.633	0.015	55.723	0.019	89.355	0.034	2045.636	0.966	2134.991
TPRO	7.396	0.003	74.701	0.026	82.097	0.029	2015.336	0.971	2097.433
TBTG70	203.372	0.042	187.615	0.035	390.986	0.077	3791.594	0.923	4182.580
ZIPPER30	6.708	0.006	14.626	0.014	21.334	0.020	701.587	0.980	722.921
ZIPPER	74.863	0.023	144.648	0.044	219.511	0.067	2148.211	0.934	2367.722
ZPRO	64.605	0.020	172.799	0.054	237.404	0.074	2059.175	0.926	2296.579
ZIPPER70	193.272	0.039	318.451	0.067	511.723	0.106	3694.484	0.894	4206.207

Table 7-2: STATISTICS FOR XREG

STATISTICS FOR XREG						
Story Number	1	2	3	4	5	6
Story Shear Mean (k)	455.633	411.917	367.767	353.000	311.783	232.767
Story Shear COV	0.057	0.032	0.024	0.035	0.050	0.135
Story Drift Mean (in)	1.130	1.208	1.372	0.865	0.980	0.707
Story Drift COV	0.830	0.691	0.485	0.215	0.219	0.103
Story Energy Mean (k-in)	464.477	559.072	476.767	72.942	53.283	0.580
Story Energy COV	1.234	1.043	0.984	1.185	0.726	2.449
Brace Energy Mean (k-in)	295.692	527.712	465.790	72.870	52.650	0.580
Brace Energy COV	1.037	1.027	0.983	1.186	0.708	2.449
Column Energy Mean (k-in)	137.757	6.050	8.108	0.000	0.510	0.000
Column Energy COV	1.581	2.252	1.029	0.000	2.449	0.000
Beam Energy Mean (k-in)	31.028	25.312	2.870	0.072	0.123	0.000
Beam Energy COV	1.843	2.122	1.564	2.449	2.449	0.000
Interior Column Compression Mean (k)	1079.810	856.667	656.332	434.257	262.637	86.247
Interior Column Compression COV	0.041	0.049	0.051	0.086	0.117	0.104
Exterior Column Compression Mean (k)	196.198	167.088	134.405	100.708	65.752	29.990
Exterior Column Compression COV	0.069	0.056	0.049	0.050	0.048	0.041

Table 7-3: STATISTICS FOR INVK

STATISTICS FOR INVK						
Story Number	1	2	3	4	5	6
Story Shear Mean (k)	430.450	384.000	351.033	331.100	276.050	231.633
Story Shear COV	0.055	0.010	0.025	0.077	0.030	0.198
Story Drift Mean (in)	0.642	2.247	2.248	0.718	0.955	0.663
Story Drift COV	0.325	0.714	0.666	0.184	0.304	0.083
Story Energy Mean (k-in)	294.050	981.642	542.410	38.395	91.425	0.562
Story Energy COV	1.308	0.660	0.656	2.248	1.128	2.449
Brace Energy Mean (k-in)	144.608	707.232	526.818	33.158	85.885	0.562
Brace Energy COV	0.990	0.471	0.651	2.445	1.120	2.449
Column Energy Mean (k-in)	5.767	53.898	12.158	0.000	5.540	0.000
Column Energy COV	1.146	1.771	1.231	0.000	1.470	0.000
Beam Energy Mean (k-in)	143.677	220.510	3.433	5.238	0.000	0.000
Beam Energy COV	1.666	1.306	2.440	1.276	0.000	0.000
Interior Column Compression Mean (k)	1096.777	833.623	627.368	465.262	282.185	148.808
Interior Column Compression COV	0.059	0.034	0.070	0.075	0.079	0.203
Exterior Column Compression Mean (k)	192.002	160.933	127.617	96.385	63.532	29.488
Exterior Column Compression COV	0.066	0.057	0.031	0.031	0.031	0.028

Table 7-4: STATISTICS FOR SPLIT-X

STATISTICS FOR SPLIT-X						
Story Number	1	2	3	4	5	6
Story Shear Mean (k)	452.450	409.367	366.383	352.100	311.317	255.300
Story Shear COV	0.072	0.040	0.040	0.042	0.058	0.104
Story Drift Mean (in)	1.180	1.192	1.260	0.785	1.023	0.697
Story Drift COV	0.798	0.690	0.324	0.242	0.168	0.065
Story Energy Mean (k-in)	754.818	236.462	606.347	14.652	148.675	0.000
Story Energy COV	0.912	1.107	0.800	2.457	0.249	0.000
Brace Energy Mean (k-in)	581.005	214.752	586.538	13.333	147.595	0.000
Brace Energy COV	0.774	1.059	0.770	2.457	0.249	0.000
Column Energy Mean (k-in)	146.203	5.355	17.228	1.318	1.080	0.000
Column Energy COV	1.615	2.136	1.820	2.449	1.255	0.000
Beam Energy Mean (k-in)	27.608	16.352	2.580	0.000	0.000	0.000
Beam Energy COV	1.693	1.880	1.712	0.000	0.000	0.000
Interior Column Compression Mean (k)	1011.582	957.528	610.242	569.227	260.995	221.133
Interior Column Compression COV	0.074	0.074	0.046	0.046	0.083	0.092
Exterior Column Compression Mean (k)	192.357	163.158	131.918	101.170	66.250	30.872
Exterior Column Compression COV	0.056	0.036	0.044	0.041	0.034	0.027

Table 7-5: STATISTICS FOR TBTG

STATISTICS FOR TBTG						
Story Number	1	2	3	4	5	6
Story Shear Mean (k)	443.500	399.950	345.117	333.650	277.883	219.533
Story Shear COV	0.070	0.066	0.038	0.036	0.049	0.075
Story Drift Mean (in)	0.807	1.100	1.135	1.048	0.992	0.782
Story Drift COV	0.650	0.518	0.463	0.228	0.207	0.176
Story Energy Mean (k-in)	413.542	580.232	513.398	319.697	225.378	82.745
Story Energy COV	0.705	0.712	0.652	0.667	0.511	0.581
Brace Energy Mean (k-in)	364.593	558.033	504.678	313.600	222.407	82.333
Brace Energy COV	0.664	0.688	0.650	0.658	0.496	0.577
Column Energy Mean (k-in)	31.863	1.452	0.000	0.000	0.318	0.000
Column Energy COV	1.672	2.449	0.000	0.000	1.624	0.000
Beam Energy Mean (k-in)	17.088	20.748	8.722	6.095	2.655	0.410
Beam Energy COV	1.556	1.866	1.405	1.183	1.811	1.915
Interior Column Compression Mean (k)	885.805	676.410	529.132	345.377	230.470	104.258
Interior Column Compression COV	0.038	0.022	0.042	0.038	0.083	0.222
Exterior Column Compression Mean (k)	190.735	162.017	130.303	95.867	61.708	27.925
Exterior Column Compression COV	0.096	0.091	0.094	0.085	0.051	0.027

Table 7-6: STATISTICS FOR INVZIP

STATISTICS FOR INVZIP						
Story Number	1	2	3	4	5	6
Story Shear Mean (k)	446.633	394.767	348.633	328.633	266.067	212.733
Story Shear COV	0.062	0.034	0.027	0.041	0.047	0.101
Story Drift Mean (in)	0.990	1.123	1.267	1.143	1.115	0.993
Story Drift COV	0.785	0.430	0.487	0.250	0.263	0.262
Story Energy Mean (k-in)	357.913	449.595	477.700	302.365	220.400	85.918
Story Energy COV	1.246	0.801	0.774	0.960	1.104	0.779
Brace Energy Mean (k-in)	245.322	423.137	452.630	291.030	212.365	85.747
Brace Energy COV	1.145	0.760	0.773	0.983	1.113	0.778
Column Energy Mean (k-in)	98.548	6.992	4.977	0.723	1.643	0.172
Column Energy COV	1.504	2.173	1.928	2.449	1.629	1.936
Beam Energy Mean (k-in)	14.045	19.465	20.097	10.612	6.390	0.000
Beam Energy COV	1.618	1.670	1.423	1.156	1.594	0.000
Interior Column Compression Mean (k)	1188.157	917.203	667.793	456.497	281.627	124.965
Interior Column Compression COV	0.101	0.099	0.107	0.154	0.128	0.085
Exterior Column Compression Mean (k)	210.822	180.345	145.438	107.412	70.047	31.735
Exterior Column Compression COV	0.084	0.084	0.083	0.082	0.083	0.085

Table 7-7: STATISTICS FOR ZIPPER

STATISTICS FOR ZIPPER						
Story Number	1	2	3	4	5	6
Story Shear Mean (k)	380.600	348.717	315.633	305.583	260.767	210.167
Story Shear COV	0.105	0.037	0.036	0.062	0.117	0.150
Story Drift Mean (in)	1.068	1.208	1.210	1.098	1.097	0.915
Story Drift COV	0.563	0.437	0.382	0.439	0.444	0.528
Story Energy Mean (k-in)	625.900	612.313	454.847	340.283	218.915	115.465
Story Energy COV	0.469	0.582	0.618	0.614	0.600	0.875
Brace Energy Mean (k-in)	506.405	576.632	429.513	321.210	207.235	107.222
Brace Energy COV	0.351	0.553	0.587	0.584	0.583	0.842
Column Energy Mean (k-in)	73.837	0.323	0.000	0.000	0.000	0.700
Column Energy COV	1.407	2.449	0.000	0.000	0.000	2.449
Beam Energy Mean (k-in)	45.655	35.358	25.335	19.075	11.680	7.543
Beam Energy COV	1.257	1.383	1.412	1.393	1.457	1.508
Interior Column Compression Mean (k)	861.925	690.460	525.570	352.205	225.320	101.913
Interior Column Compression COV	0.054	0.046	0.055	0.125	0.109	0.265
Exterior Column Compression Mean (k)	187.130	134.758	108.790	96.942	62.202	28.103
Exterior Column Compression COV	0.119	0.478	0.504	0.097	0.088	0.064

Table 7-8: STATISTICS FOR TBTG30

STATISTICS FOR TBTG30						
Story Number	1	2	3	4	5	6
Story Shear Mean (k)	405.333	373.633	335.433	316.767	265.550	199.867
Story Shear COV	0.031	0.034	0.015	0.052	0.062	0.111
Story Drift Mean (in)	0.420	0.642	0.742	0.707	0.687	0.533
Story Drift COV	0.342	0.391	0.376	0.323	0.149	0.098
Story Energy Mean (k-in)	103.298	169.648	166.962	93.002	65.760	20.173
Story Energy COV	0.797	1.063	1.126	1.235	1.057	1.671
Brace Energy Mean (k-in)	102.320	169.202	165.370	93.002	63.588	20.173
Brace Energy COV	0.782	1.059	1.117	1.235	1.039	1.671
Column Energy Mean (k-in)	0.193	0.000	0.000	0.000	0.000	0.000
Column Energy COV	2.449	0.000	0.000	0.000	0.000	0.000
Beam Energy Mean (k-in)	0.787	0.447	1.593	0.000	2.172	0.000
Beam Energy COV	2.449	2.449	2.221	0.000	1.629	0.000
Interior Column Compression Mean (k)	847.433	669.595	498.113	317.062	175.532	64.518
Interior Column Compression COV	0.035	0.020	0.014	0.062	0.197	0.312
Exterior Column Compression Mean (k)	170.815	145.242	117.277	87.655	57.757	26.842
Exterior Column Compression COV	0.071	0.060	0.033	0.010	0.021	0.026

Table 7-9: STATISTICS FOR ZIPPER30

STATISTICS FOR ZIPPER30						
Story Number	1	2	3	4	5	6
Story Shear Mean (k)	368.567	346.933	320.900	296.667	246.683	194.067
Story Shear COV	0.012	0.036	0.022	0.085	0.073	0.147
Story Drift Mean (in)	0.628	0.698	0.683	0.637	0.582	0.497
Story Drift COV	0.480	0.405	0.305	0.329	0.164	0.152
Story Energy Mean (k-in)	250.147	216.122	143.830	67.605	37.838	7.380
Story Energy COV	0.579	0.770	0.804	1.110	1.089	2.449
Brace Energy Mean (k-in)	235.545	215.970	139.157	67.408	36.130	7.377
Brace Energy COV	0.543	0.769	0.799	1.107	1.098	2.449
Column Energy Mean (k-in)	6.708	0.000	0.000	0.000	0.000	0.000
Column Energy COV	1.691	0.000	0.000	0.000	0.000	0.000
Beam Energy Mean (k-in)	7.893	0.152	4.673	0.195	1.708	0.003
Beam Energy COV	1.227	2.449	1.238	2.449	1.335	2.449
Interior Column Compression Mean (k)	865.257	670.000	498.060	323.433	178.023	63.202
Interior Column Compression COV	0.048	0.040	0.055	0.104	0.247	0.172
Exterior Column Compression Mean (k)	168.363	140.655	113.535	85.635	56.970	26.897
Exterior Column Compression COV	0.067	0.053	0.031	0.027	0.038	0.040

Table 7-10: STATISTICS FOR TBTG70

STATISTICS FOR TBTG70						
Story Number	1	2	3	4	5	6
Story Shear Mean (k)	457.033	392.717	362.883	346.833	293.950	221.567
Story Shear COV	0.027	0.037	0.023	0.050	0.049	0.107
Story Drift Mean (in)	1.473	1.702	1.740	1.350	1.155	0.918
Story Drift COV	0.747	0.645	0.500	0.255	0.247	0.265
Story Energy Mean (k-in)	957.012	1050.132	997.877	646.662	379.128	151.770
Story Energy COV	0.674	0.515	0.385	0.341	0.278	0.269
Brace Energy Mean (k-in)	699.307	998.187	939.137	639.963	363.398	151.607
Brace Energy COV	0.527	0.496	0.363	0.336	0.274	0.268
Column Energy Mean (k-in)	185.635	4.113	11.763	0.412	1.452	0.000
Column Energy COV	1.424	1.648	1.041	2.449	1.949	0.000
Beam Energy Mean (k-in)	72.070	47.835	46.980	6.285	14.282	0.163
Beam Energy COV	1.612	1.625	1.634	1.892	1.085	2.449
Interior Column Compression Mean (k)	864.425	711.165	524.945	342.922	231.537	104.927
Interior Column Compression COV	0.048	0.048	0.021	0.040	0.065	0.143
Exterior Column Compression Mean (k)	198.797	168.457	112.365	97.538	62.192	28.212
Exterior Column Compression COV	0.107	0.094	0.492	0.082	0.061	0.041

Table 7-11: STATISTICS FOR ZIPPER70

STATISTICS FOR ZIPPER70						
Story Number	1	2	3	4	5	6
Story Shear Mean (k)	392.650	340.633	321.217	306.933	251.033	206.067
Story Shear COV	0.094	0.021	0.055	0.088	0.141	0.103
Story Drift Mean (in)	1.607	1.795	1.823	1.702	1.720	1.460
Story Drift COV	0.624	0.599	0.602	0.649	0.651	0.592
Story Energy Mean (k-in)	1073.767	1046.677	850.568	615.365	432.922	186.900
Story Energy COV	0.316	0.265	0.304	0.304	0.163	0.563
Brace Energy Mean (k-in)	792.042	983.530	779.632	577.505	392.050	169.730
Brace Energy COV	0.156	0.241	0.278	0.276	0.164	0.541
Column Energy Mean (k-in)	186.763	2.528	0.507	0.000	2.275	1.200
Column Energy COV	1.290	2.092	1.571	0.000	2.004	2.271
Beam Energy Mean (k-in)	94.967	60.622	70.430	37.860	38.598	15.972
Beam Energy COV	0.976	1.274	1.143	1.330	1.010	1.082
Interior Column Compression Mean (k)	884.373	742.218	558.708	312.327	214.892	122.638
Interior Column Compression COV	0.038	0.037	0.046	0.500	0.502	0.159
Exterior Column Compression Mean (k)	207.162	173.388	138.842	103.428	65.982	28.777
Exterior Column Compression COV	0.119	0.097	0.082	0.071	0.070	0.054

Table 7-12: STATISTICS FOR TPRO

STATISTICS FOR TPRO						
Story Number	1	2	3	4	5	6
Story Shear Mean (k)	412.000	381.600	319.900	283.483	232.533	156.183
Story Shear COV	0.061	0.058	0.041	0.056	0.040	0.037
Story Drift Mean (in)	0.602	0.903	1.115	1.287	1.222	1.038
Story Drift COV	0.528	0.592	0.530	0.451	0.199	0.152
Story Energy Mean (k-in)	213.528	384.605	470.728	474.943	383.183	170.445
Story Energy COV	0.667	0.684	0.728	0.809	0.832	0.288
Brace Energy Mean (k-in)	201.937	367.220	445.322	455.797	376.235	168.828
Brace Energy COV	0.627	0.653	0.695	0.815	0.835	0.280
Column Energy Mean (k-in)	5.250	0.880	0.910	0.000	0.355	0.000
Column Energy COV	2.264	2.449	2.449	0.000	1.983	0.000
Beam Energy Mean (k-in)	6.343	16.505	24.497	19.148	6.595	1.617
Beam Energy COV	1.753	1.524	1.903	1.646	1.204	2.327
Interior Column Compression Mean (k)	798.688	595.033	418.630	267.702	155.678	98.093
Interior Column Compression COV	0.018	0.020	0.047	0.046	0.049	0.109
Exterior Column Compression Mean (k)	193.020	165.158	134.368	100.197	63.780	28.132
Exterior Column Compression COV	0.113	0.098	0.073	0.062	0.055	0.025

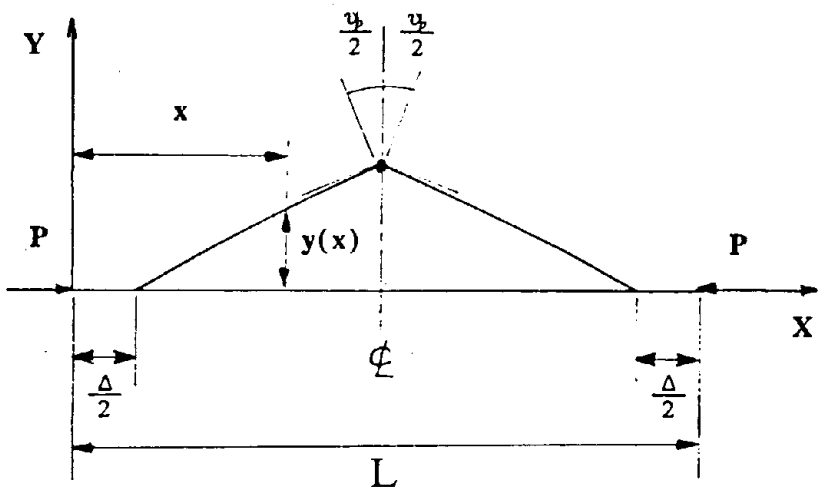

Figure 2-1 Brace deformation

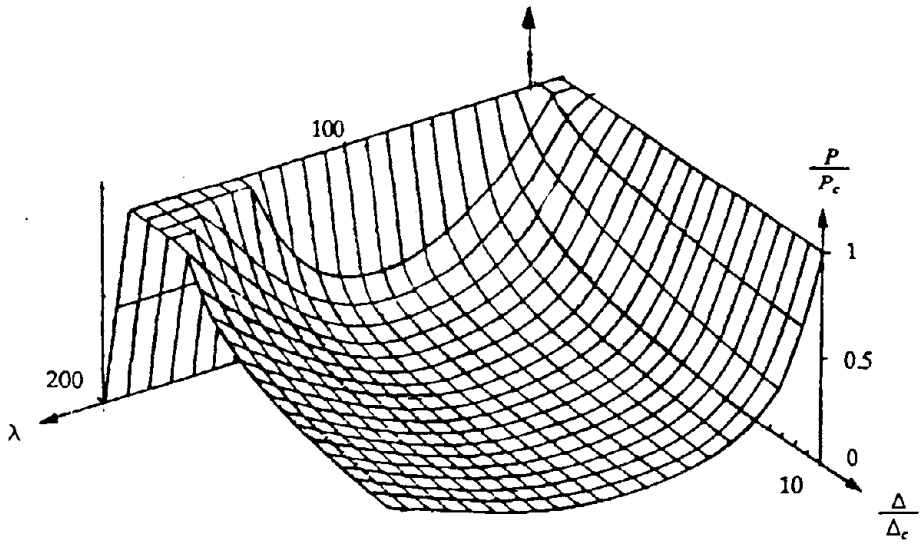

Figure 2-2 Variation of brace resistance with slenderness and deformation

$\varepsilon_y = 0.0012$ $\gamma = 0.3$

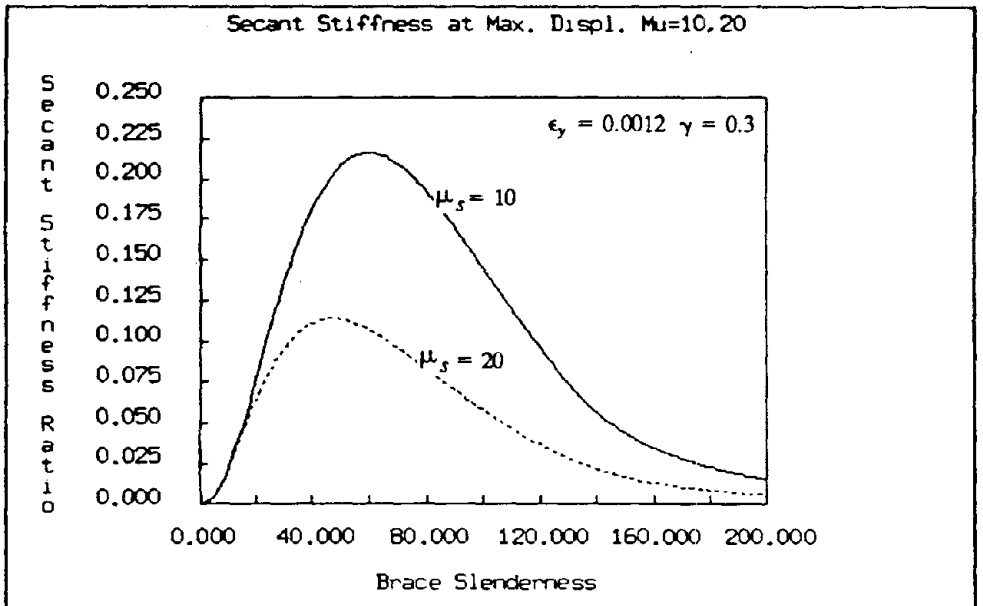

Figure 2-3 Variation of secant stiffness with slenderness and deformation

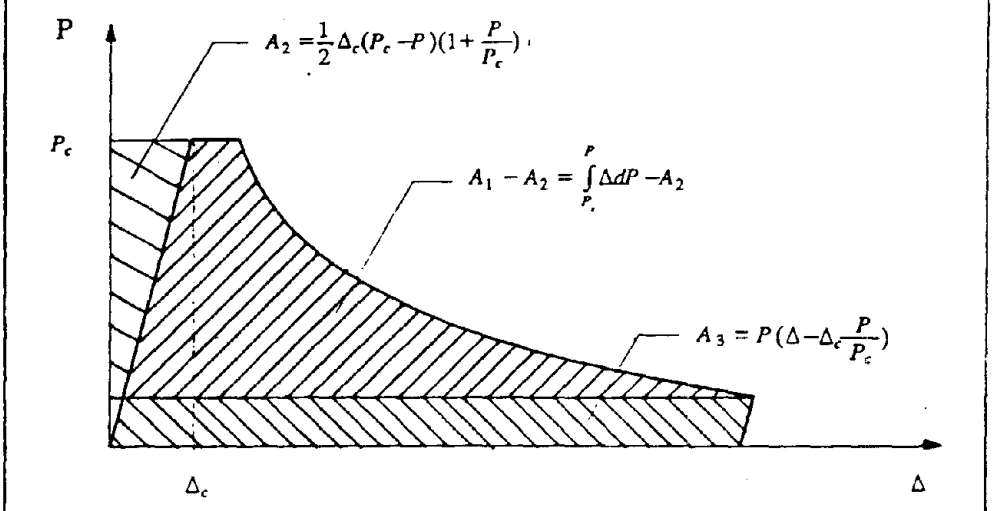

Figure 2-4 Energy dissipation demand

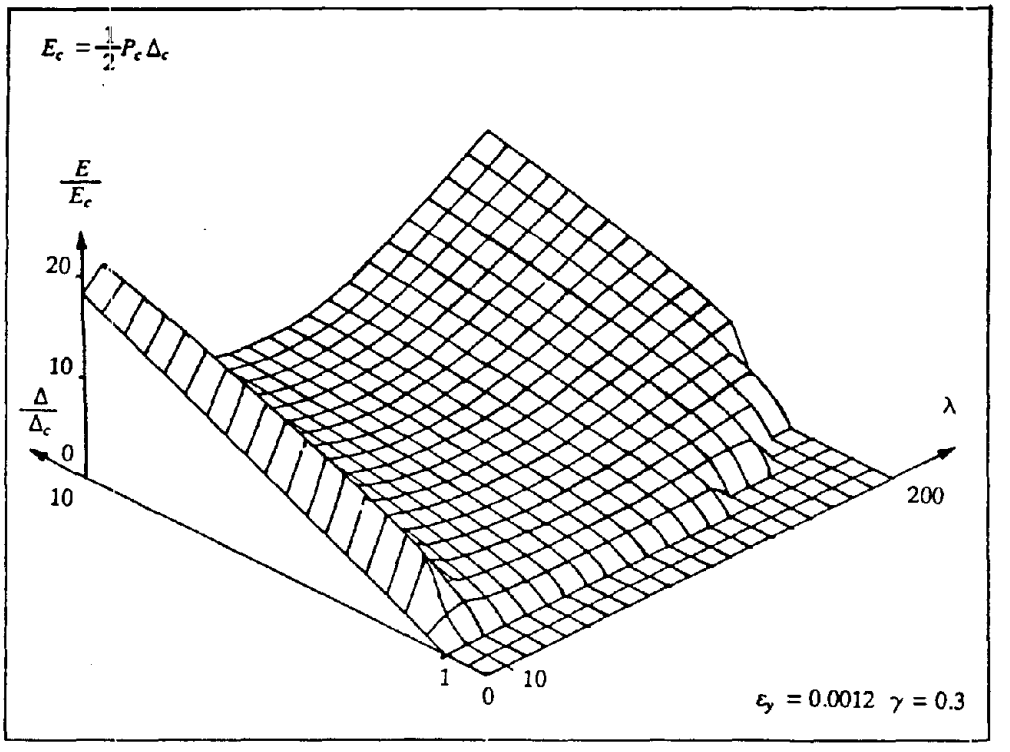

Figure 2-5 Variation of energy ductility with slenderness and deformation

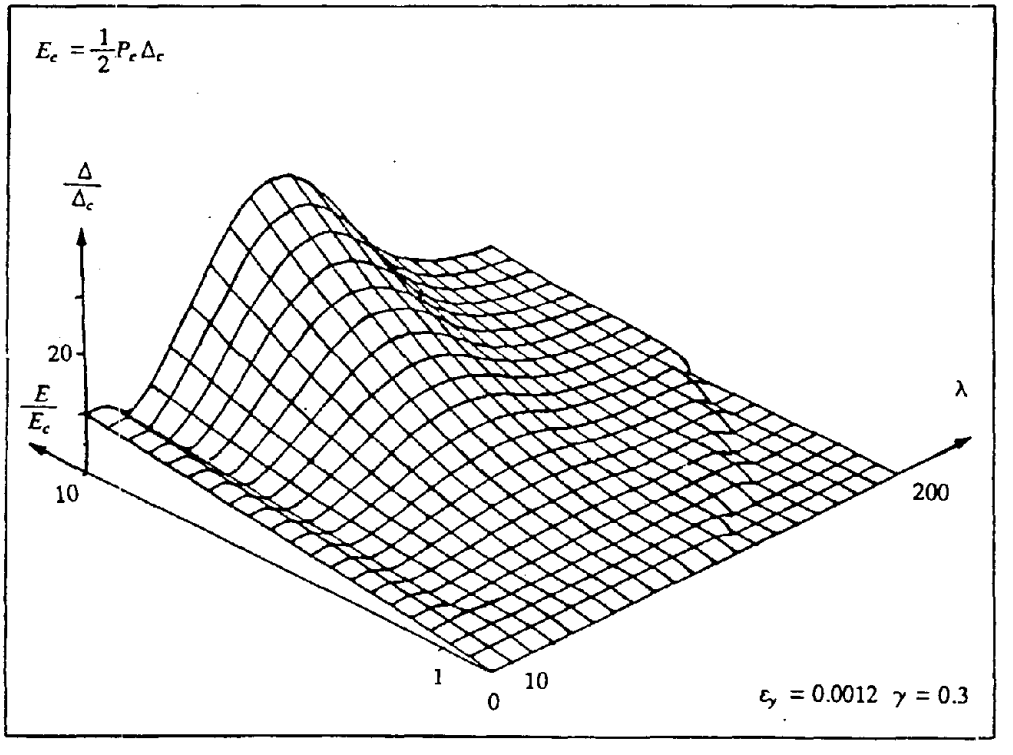

Figure 2-6 Variation of displacement ductility with slenderness and energy ductility

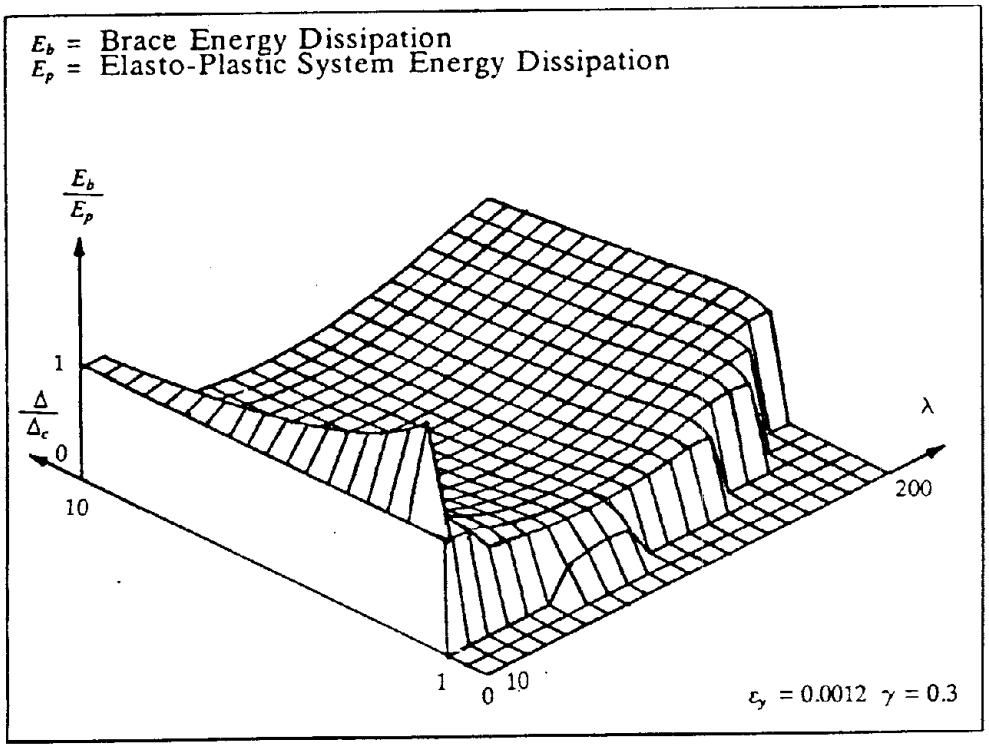

Figure 2-7-a Ratio of energy dissipations of brace to elasto-plastic system

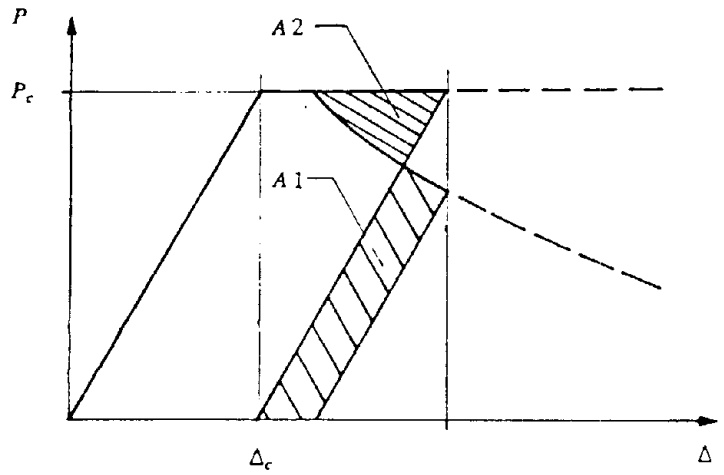

Figure 2-7-b Relative energy dissipation demand

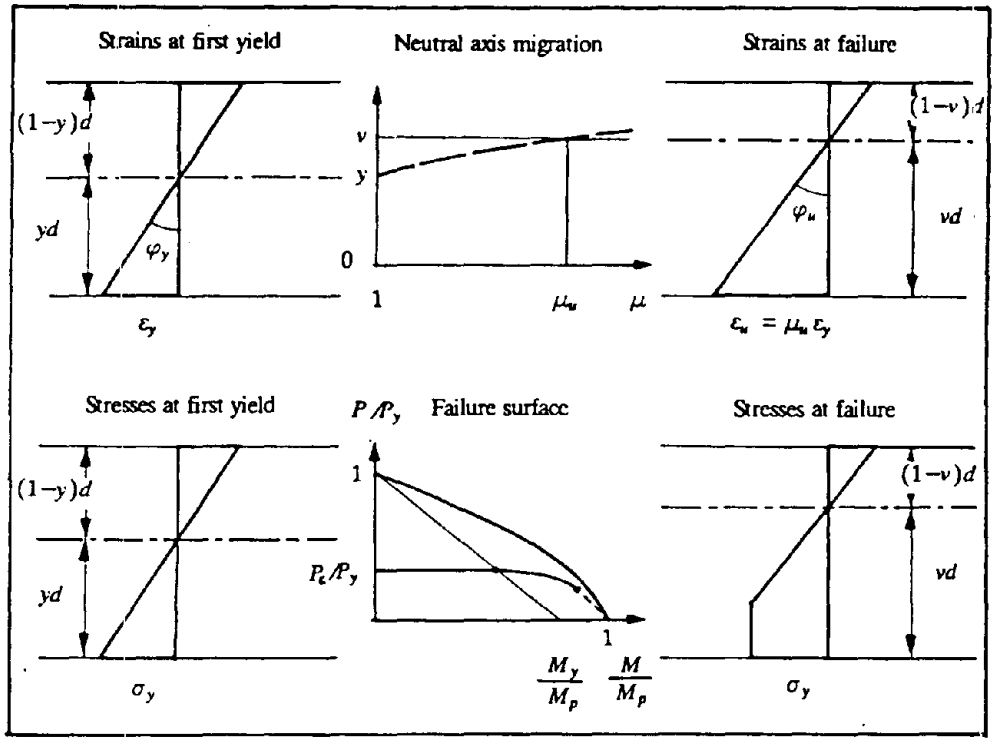

Figure 2-8 Neutral axis migration

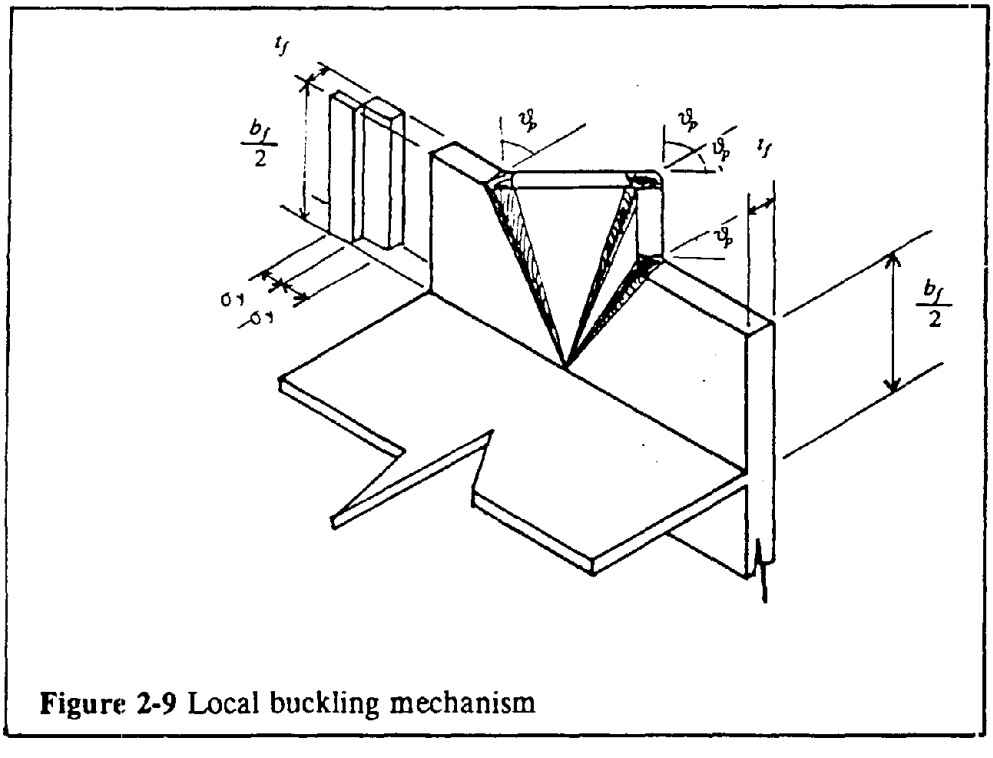

Figure 2-9 Local buckling mechanism

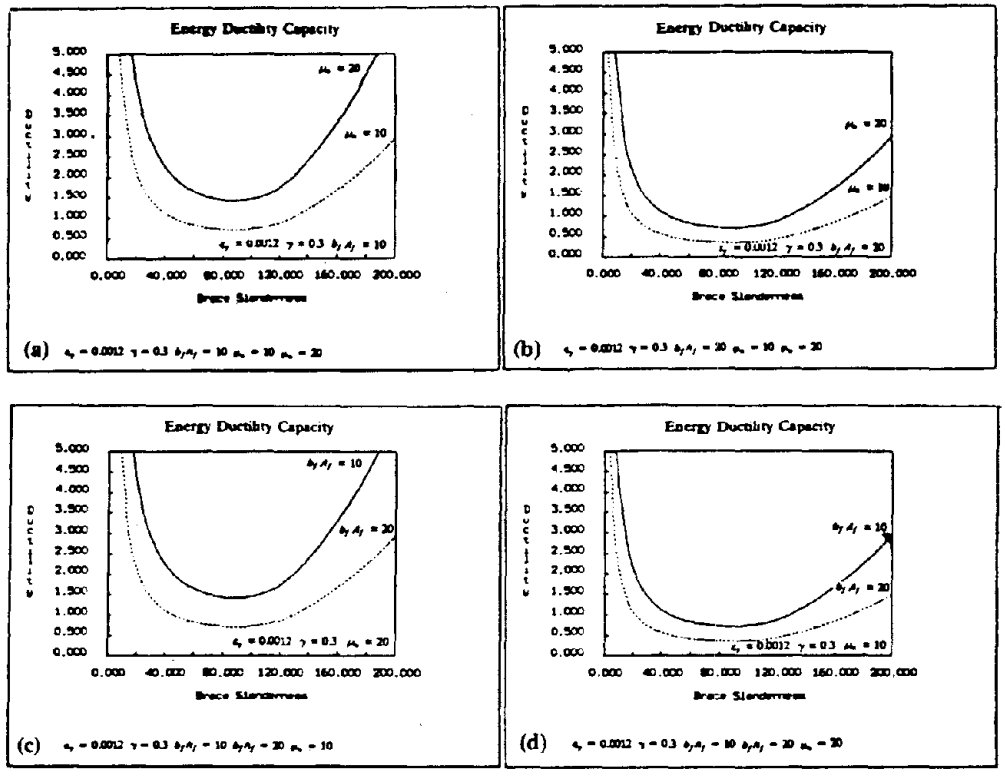

Figure 2-10 Energy Ductility Capacity

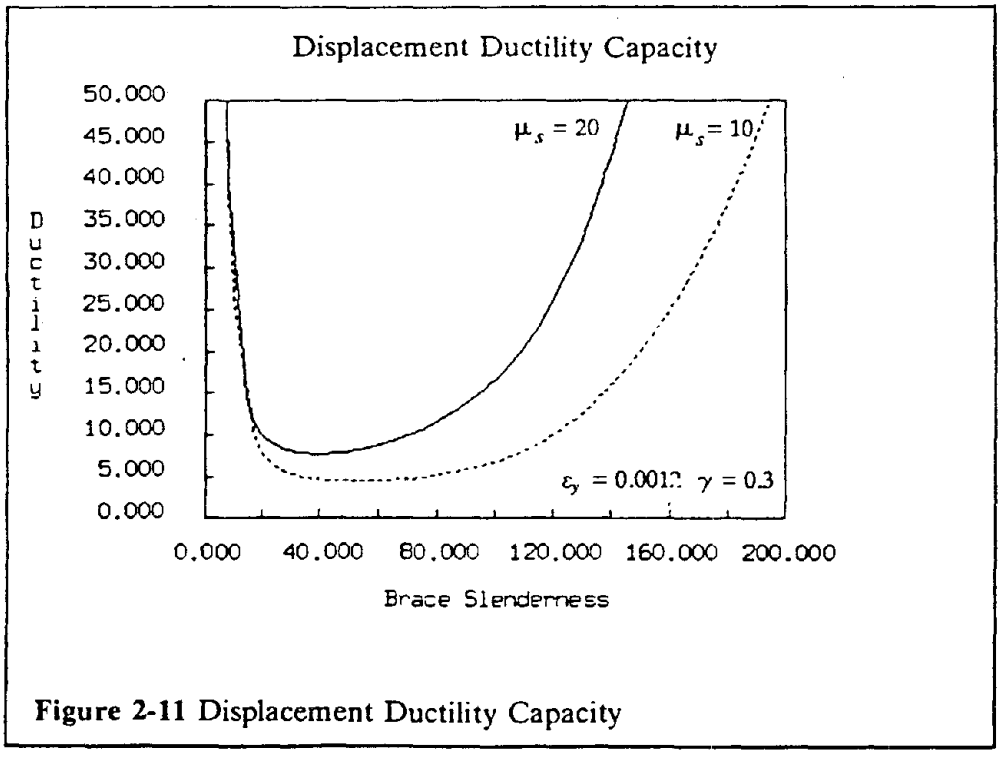

Figure 2-11 Displacement Ductility Capacity

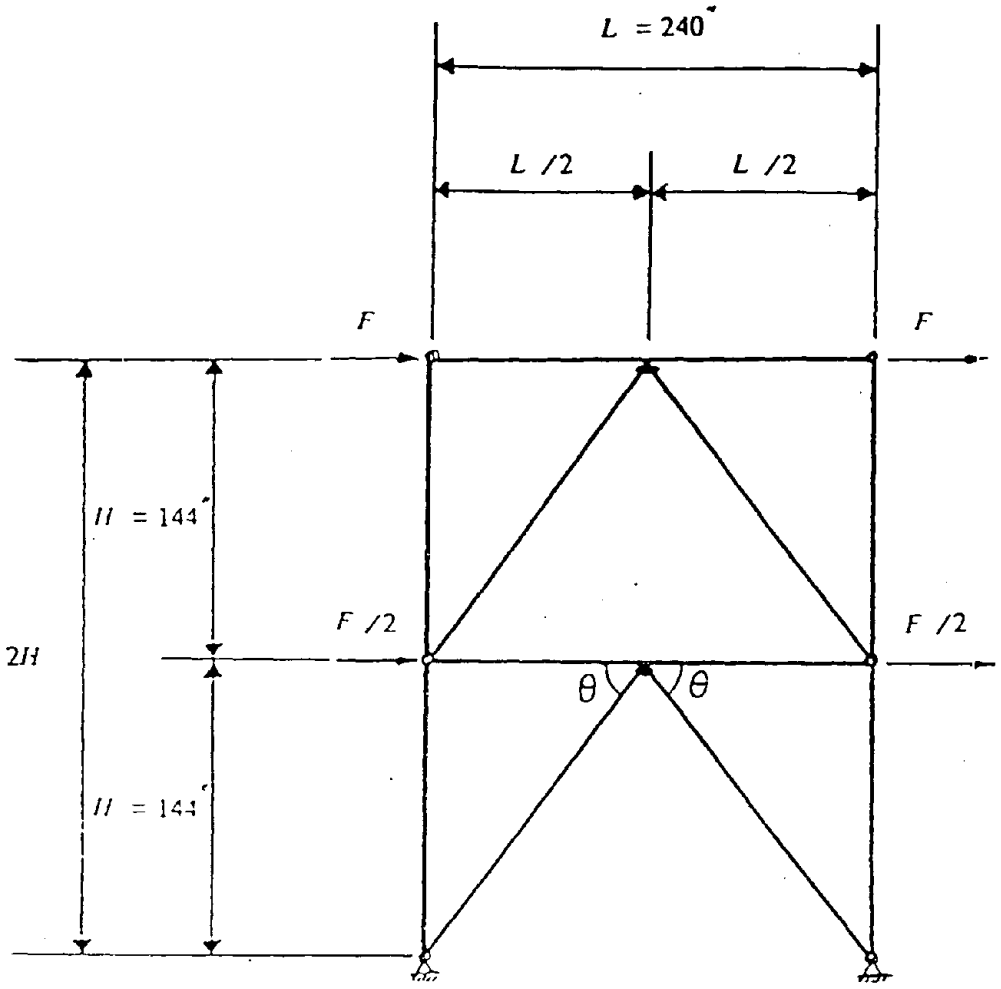

Figure 3-1 Typical K-braced frame

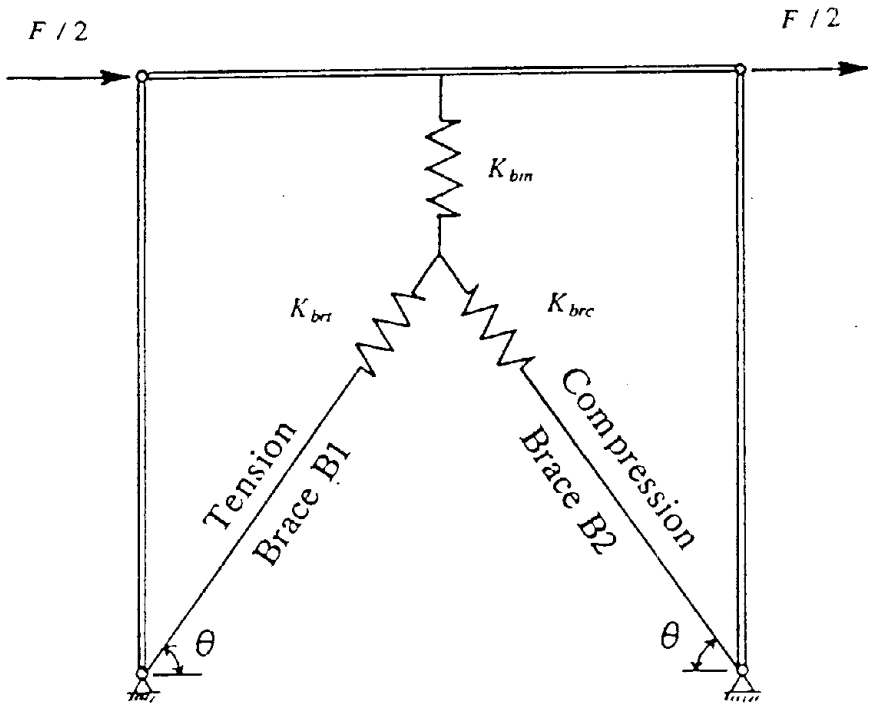

Figure 3-2 Equivalent spring model.

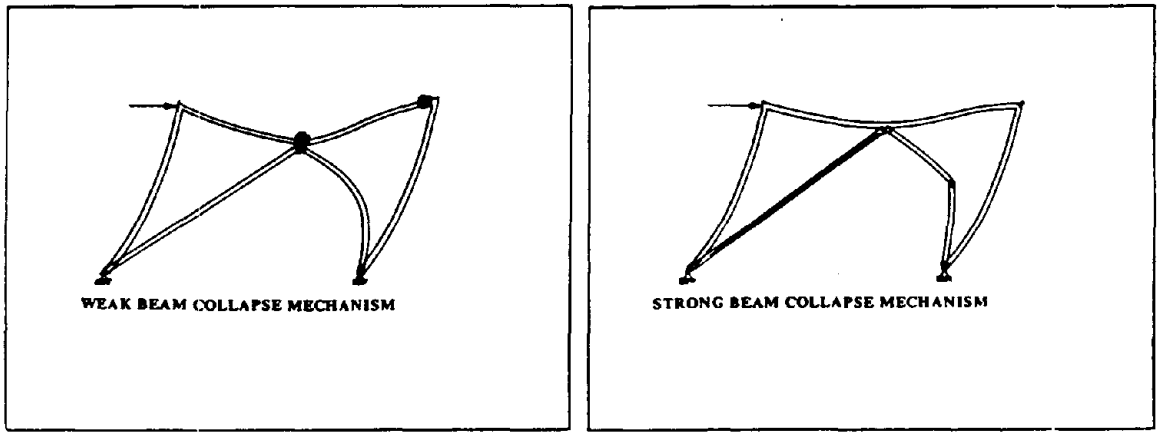

Figure 3-3-a Lateral deformation of a K-braced panel

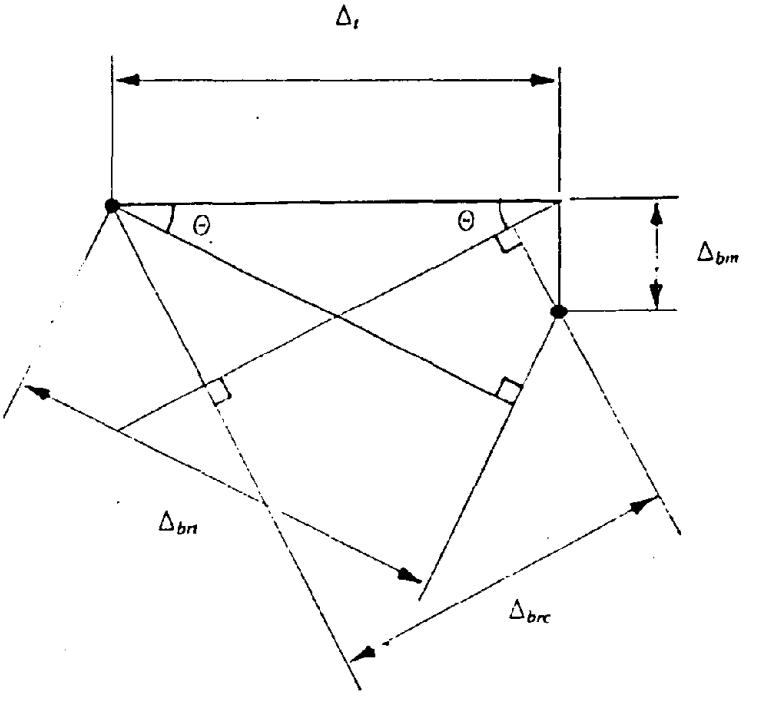

Figure 3-3-b Kinematics of deformations at braces-to-beam junction

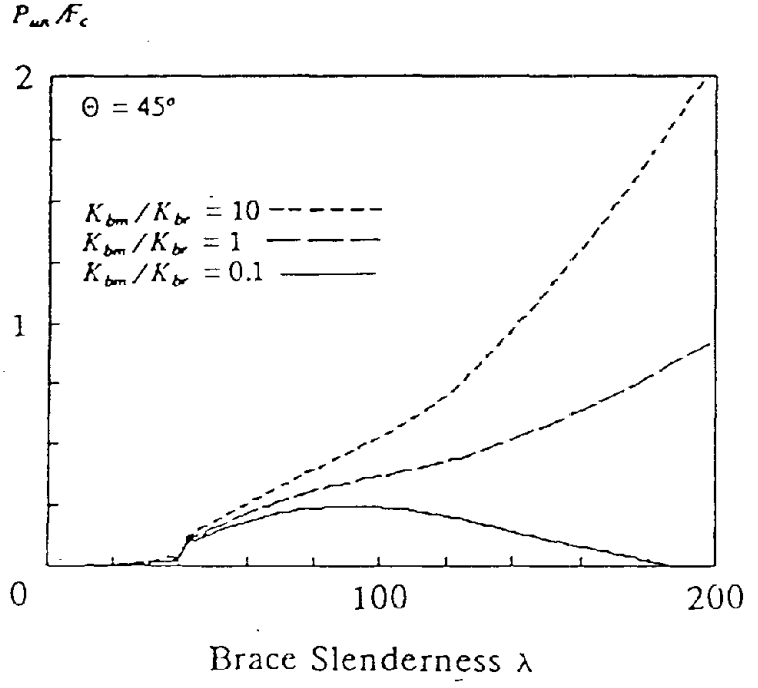

Figure 3-3-c Normalized unbalance force on beam.

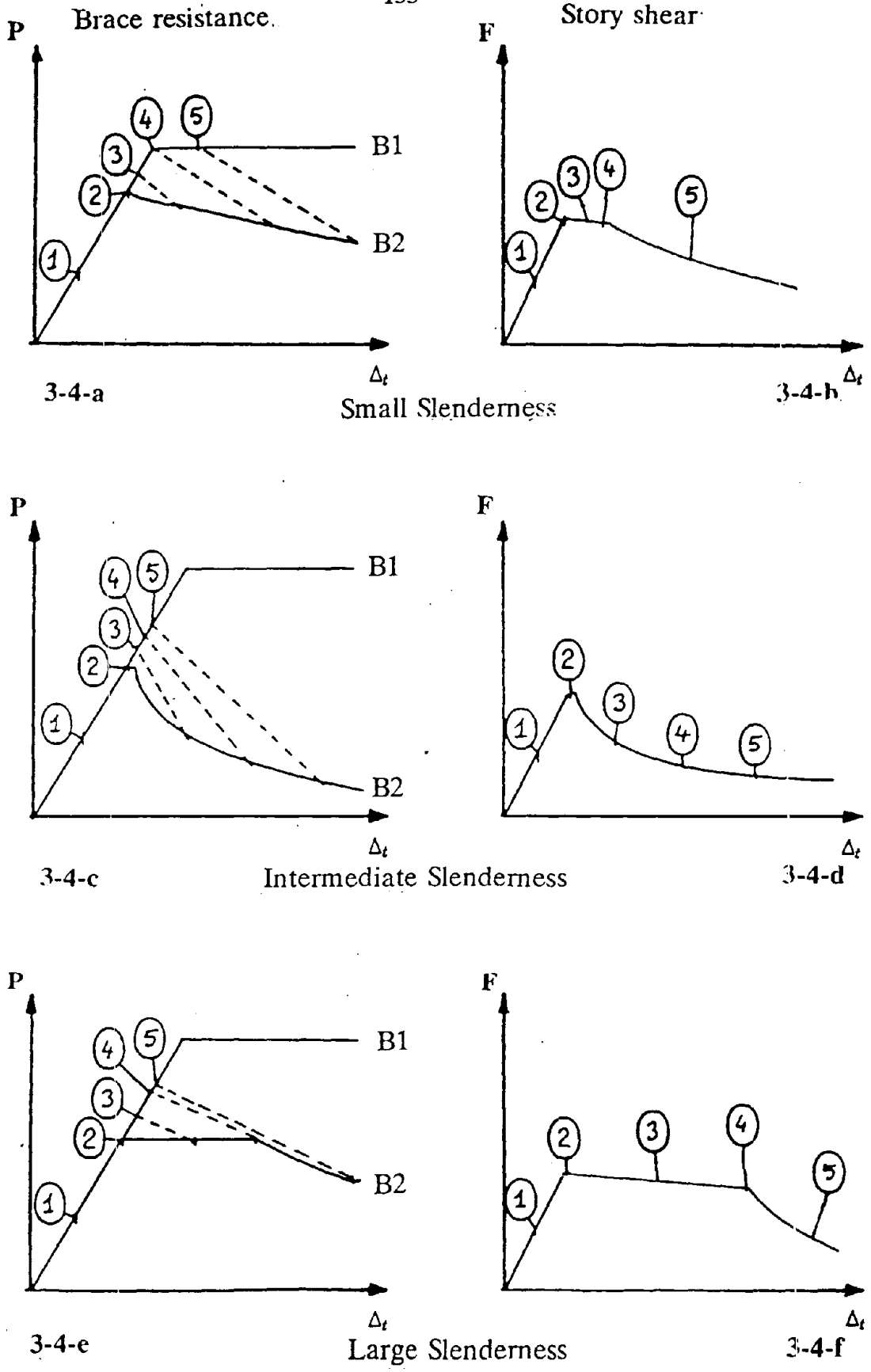

Figure 3-4 Story force-deformation characteristics for different brace slendernesses and flexible beams.

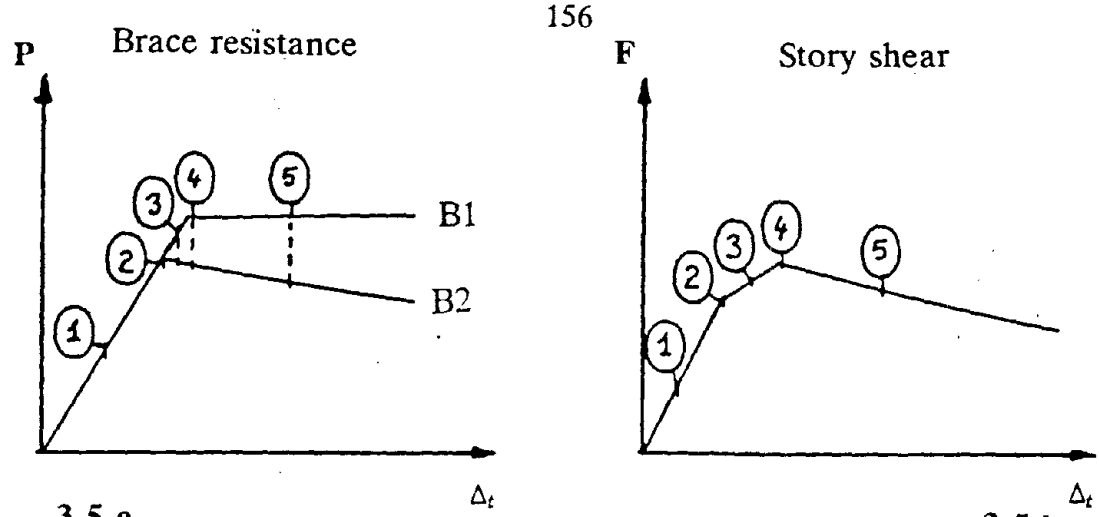

3-5-a

3-5-b

Small Slenderness

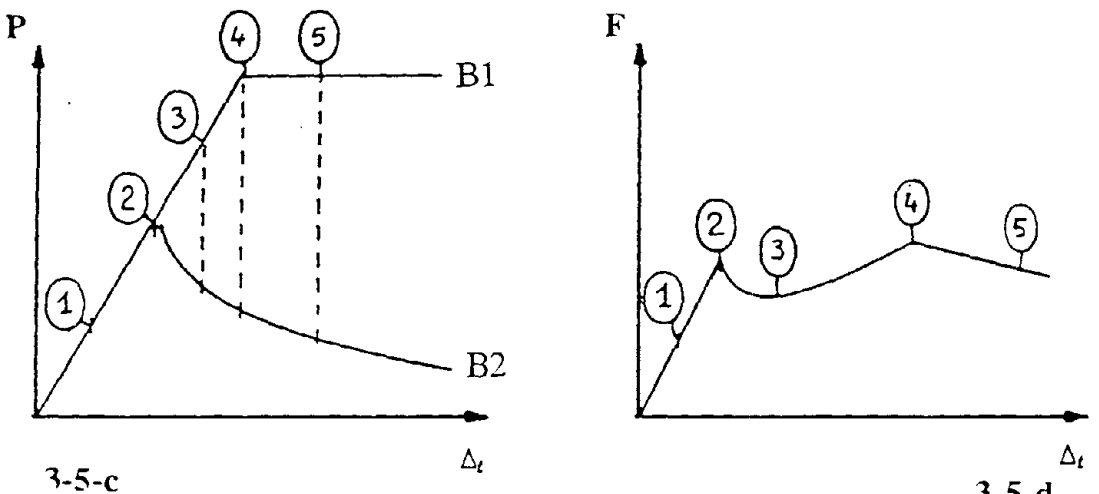

3-5-c

3-5-d

Intermediate Slenderness

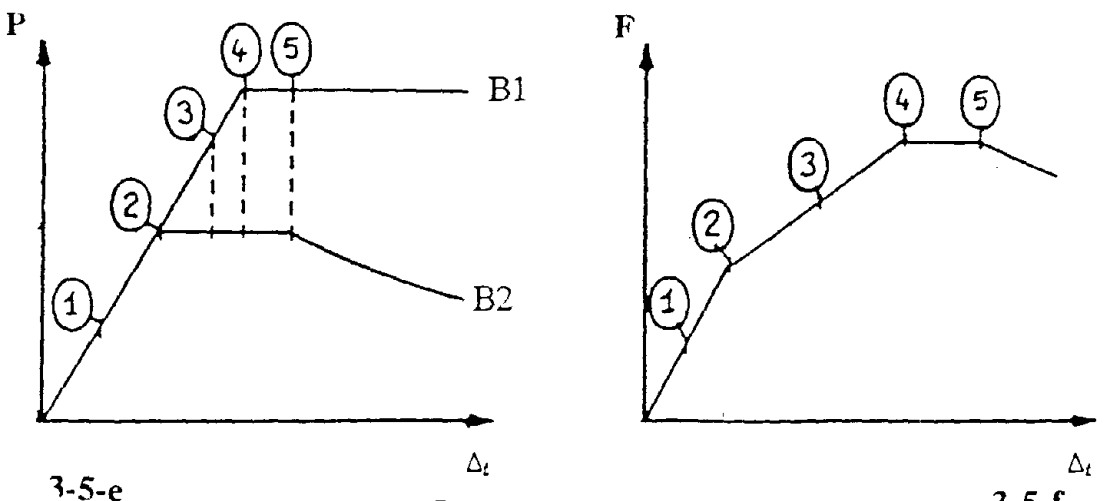

3-5-e

3-5-f

Large Slenderness

Figure 3-5 Story force-deformation characteristics for different brace slendernesses and stiff beams.

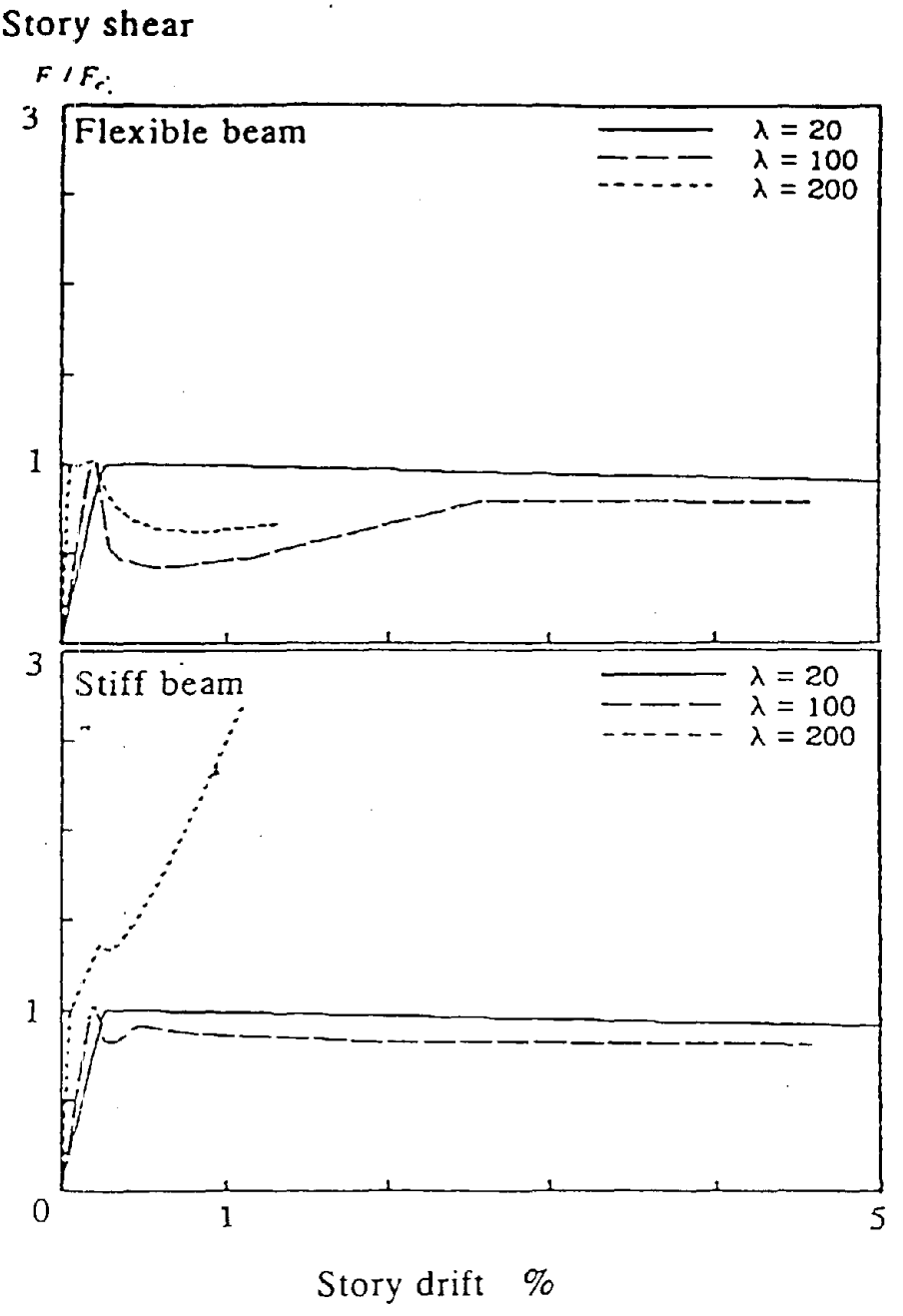

Figure 3-6 Quasi-static force-deformation characteristics for various beam stiffnesses and brace slendernesses. (2^{nd} story)

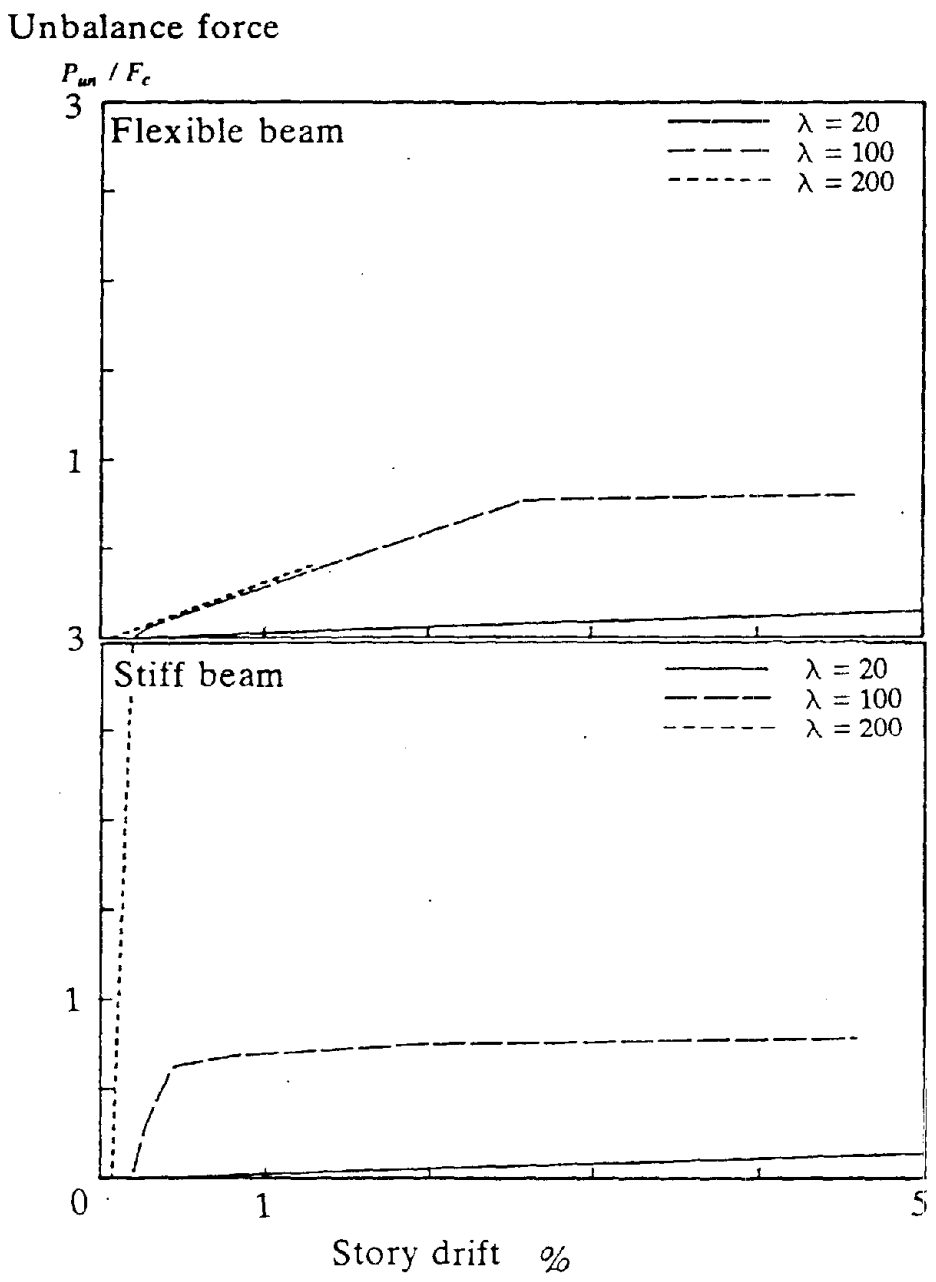

Figure 3-7 Unbalance force on beam versus story drift.

Column compression

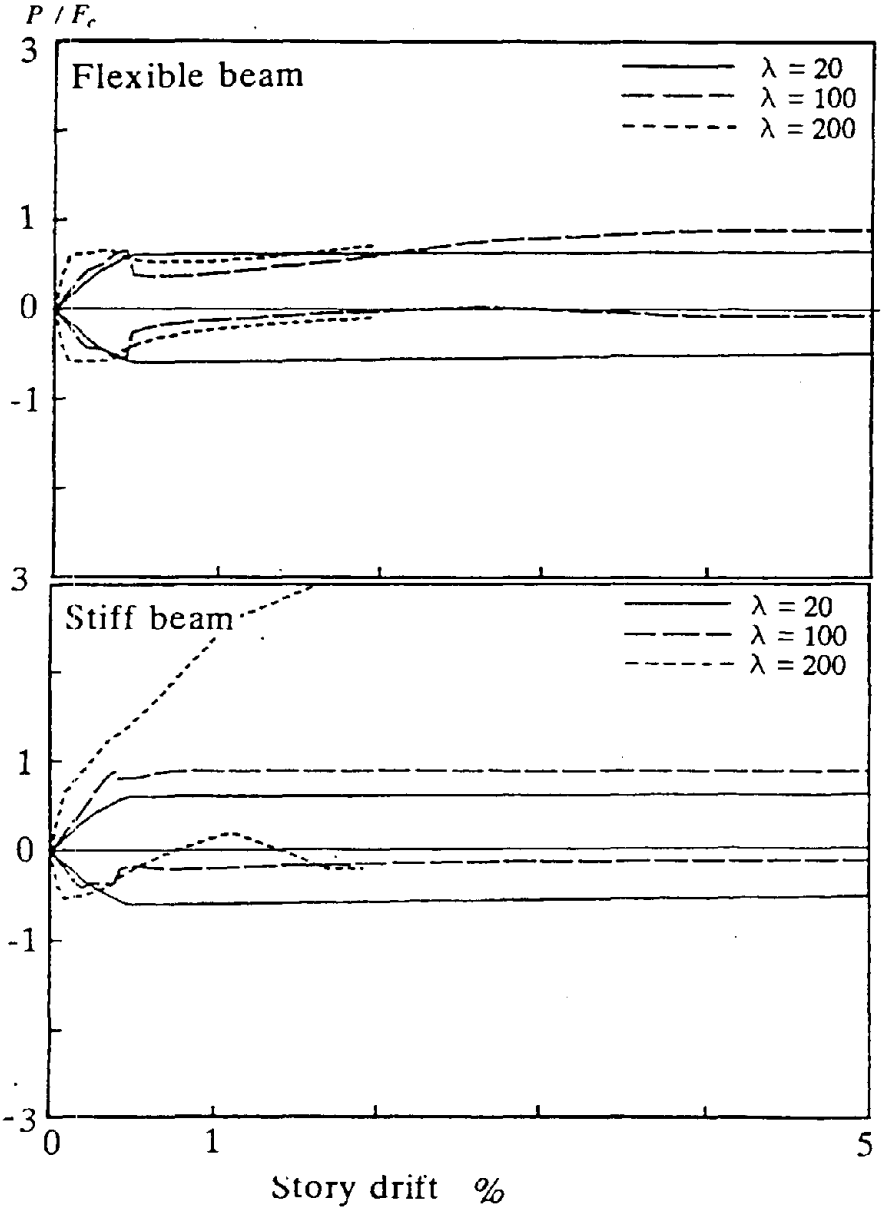

Figure 3-8-a First story columns compression versus story drift.

Column compression

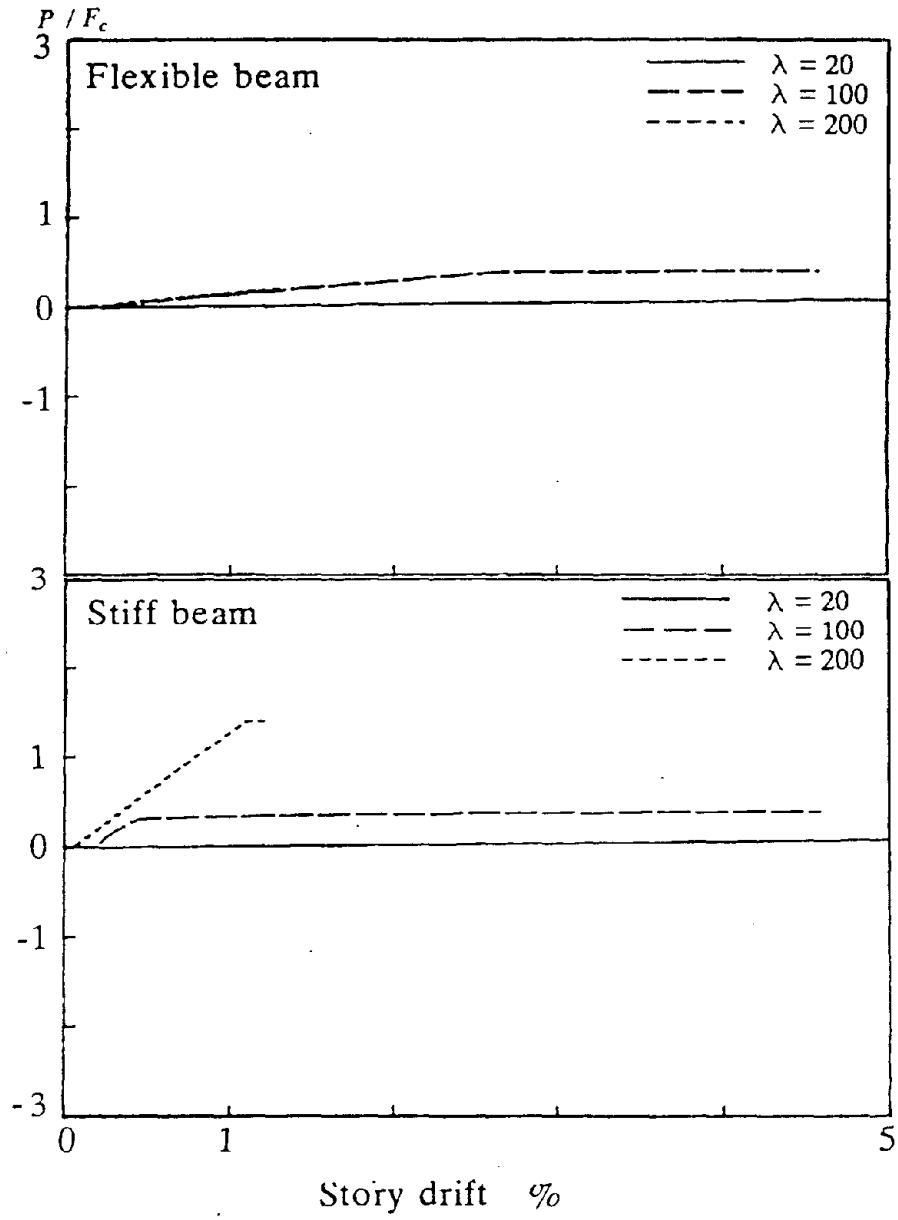

Figure 3-8-b Second story columns compression versus story drift.

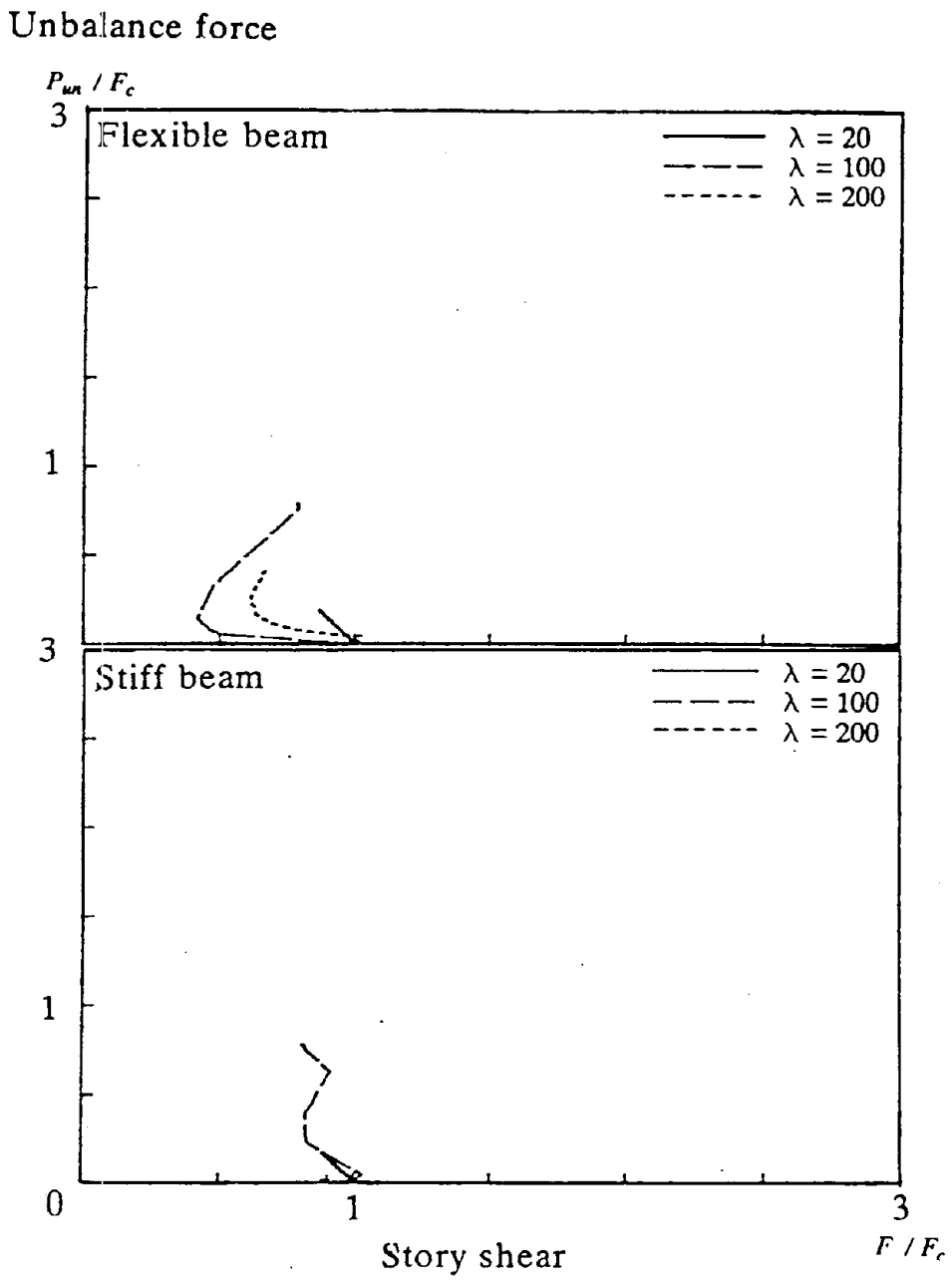

Figure 3-9 Unbalance force on beam versus story shear.

Column compression

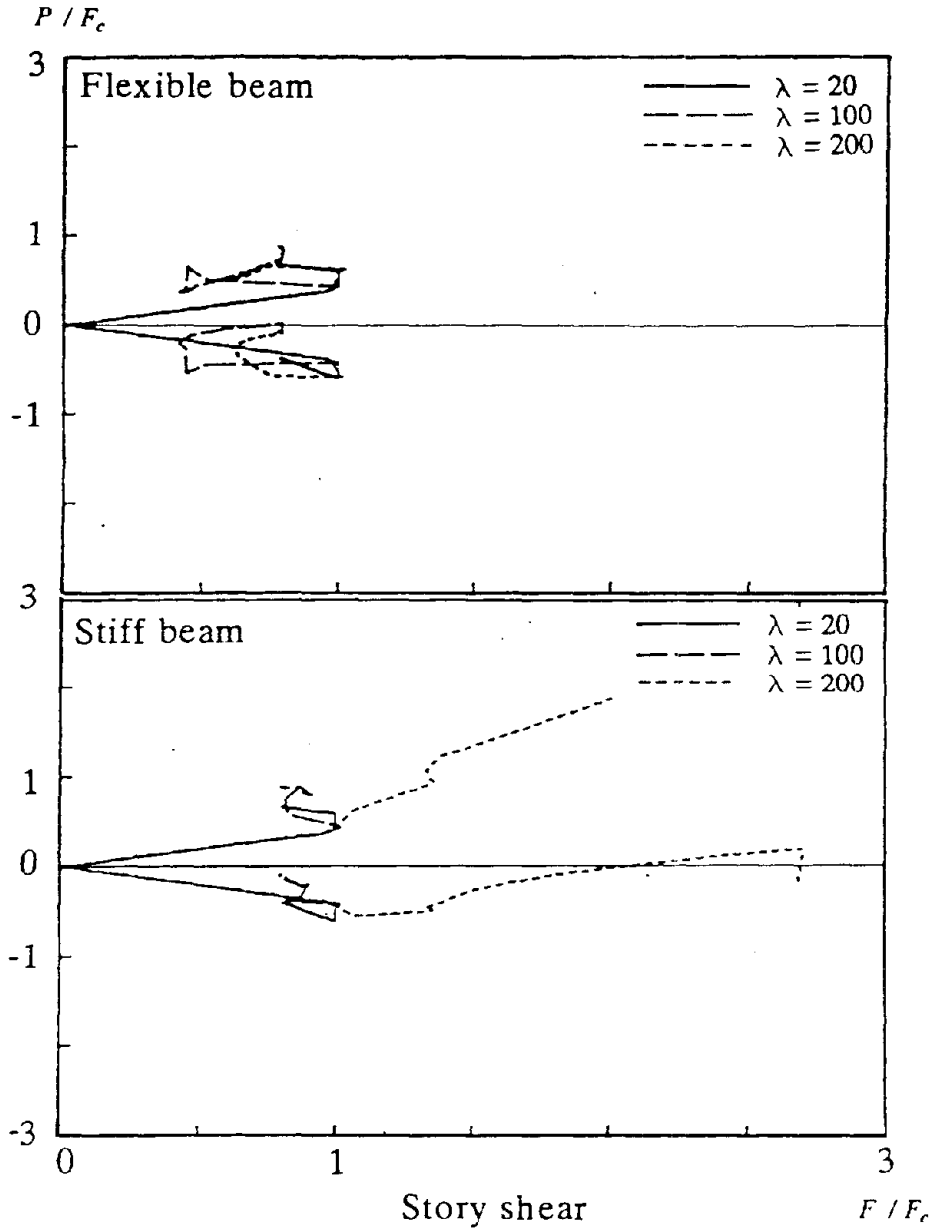

Figure 3-10-a First story columns compression versus story shear.

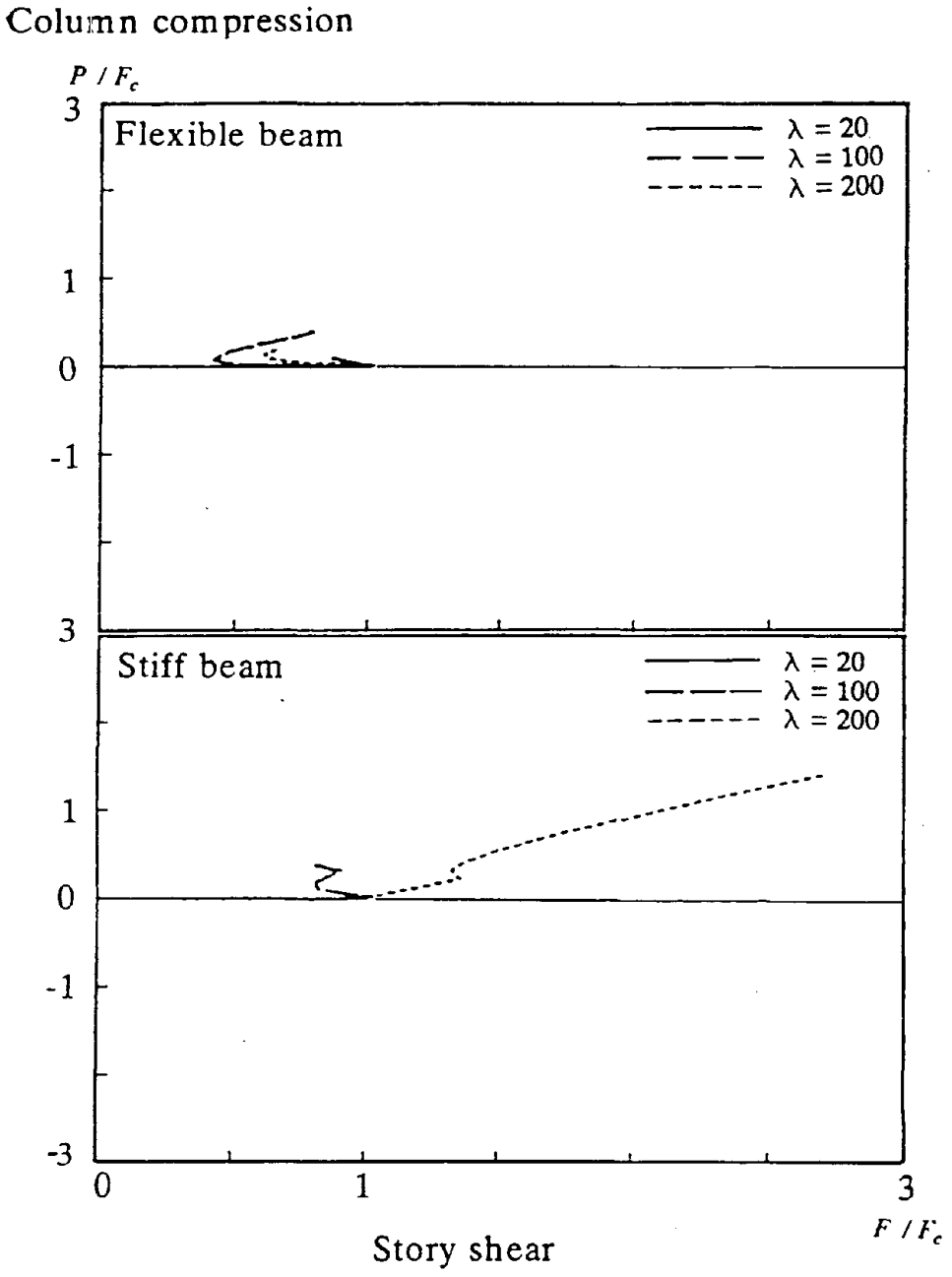

Figure 3-10-b Second story columns compression versus story shear.

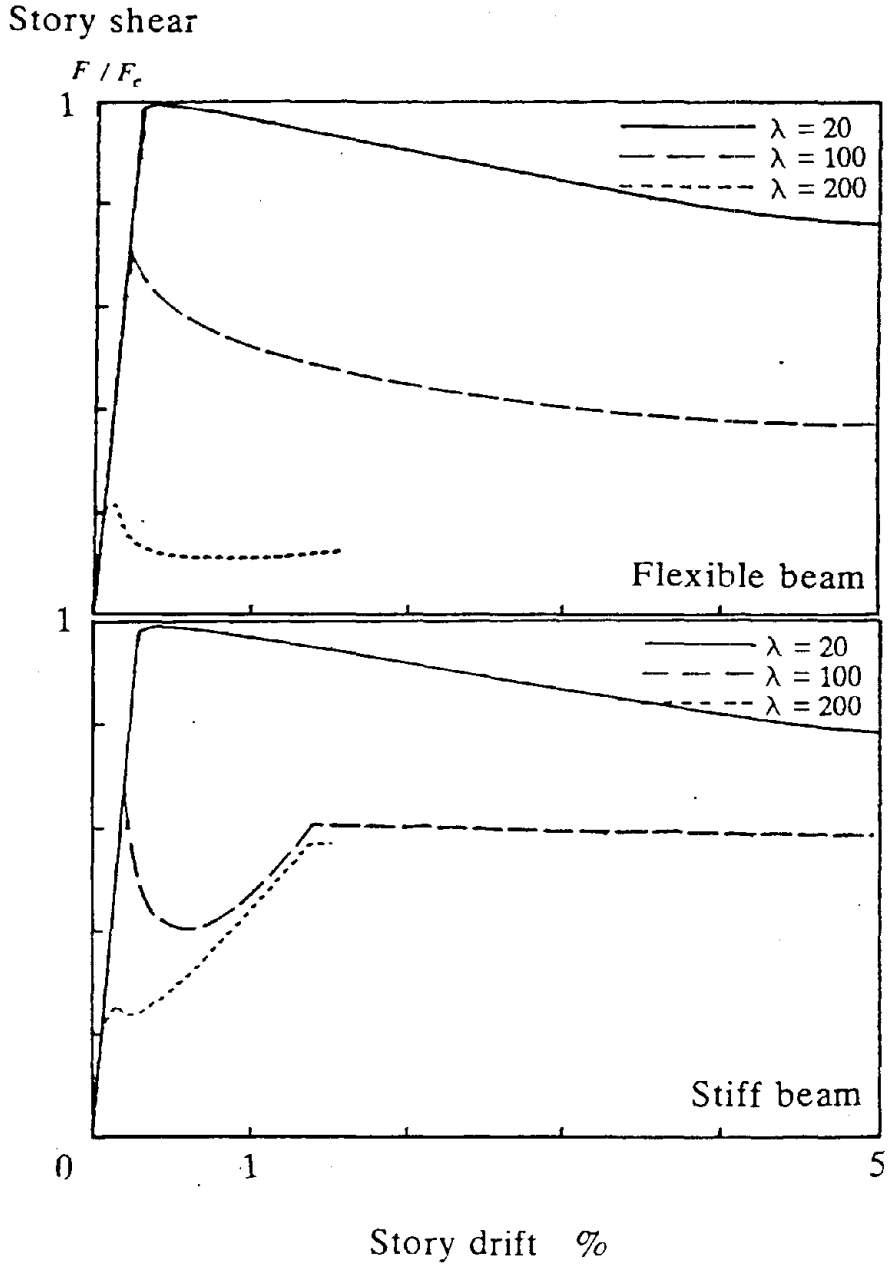

Figure 3-11 Quasi-static force-deformation characteristics for various beam stiffnesses and brace slendernesses.

Unbalance force

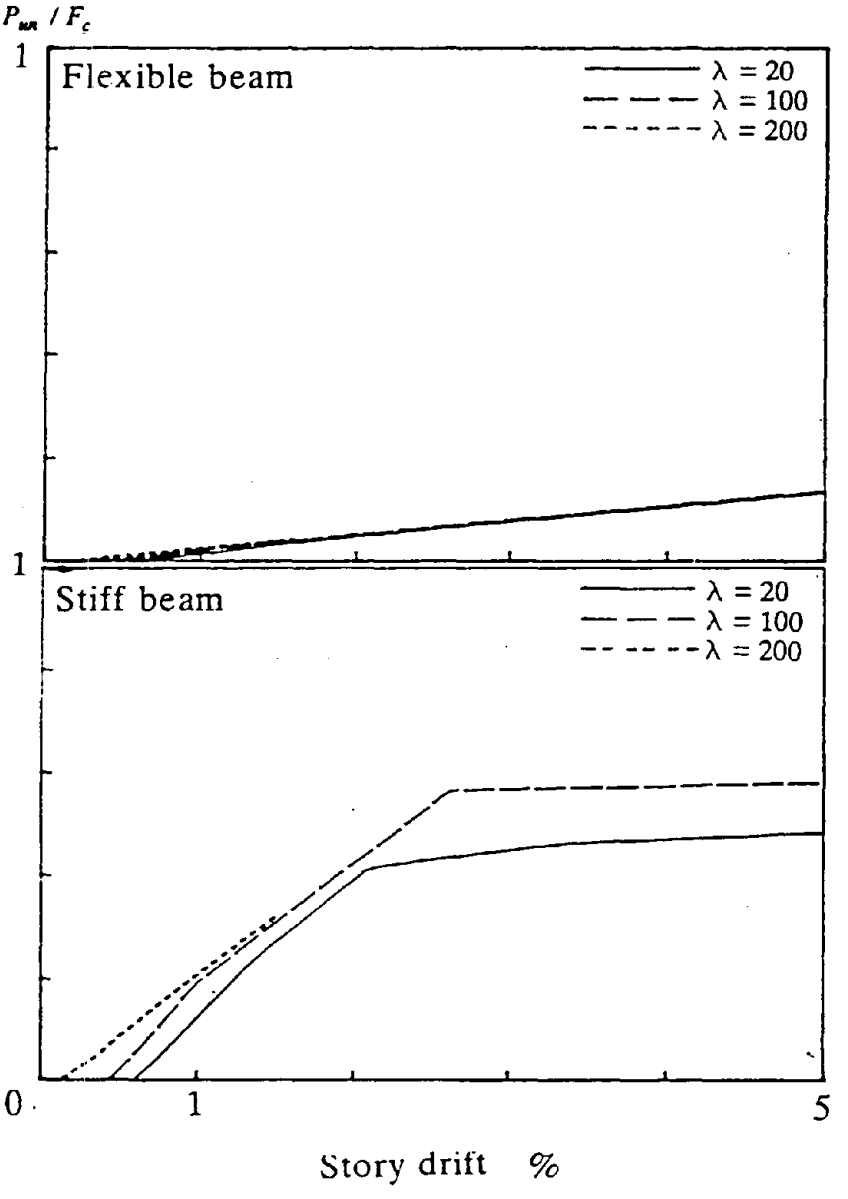

Figure 3-12 Unbalance force on beam versus story drift.

Column compression

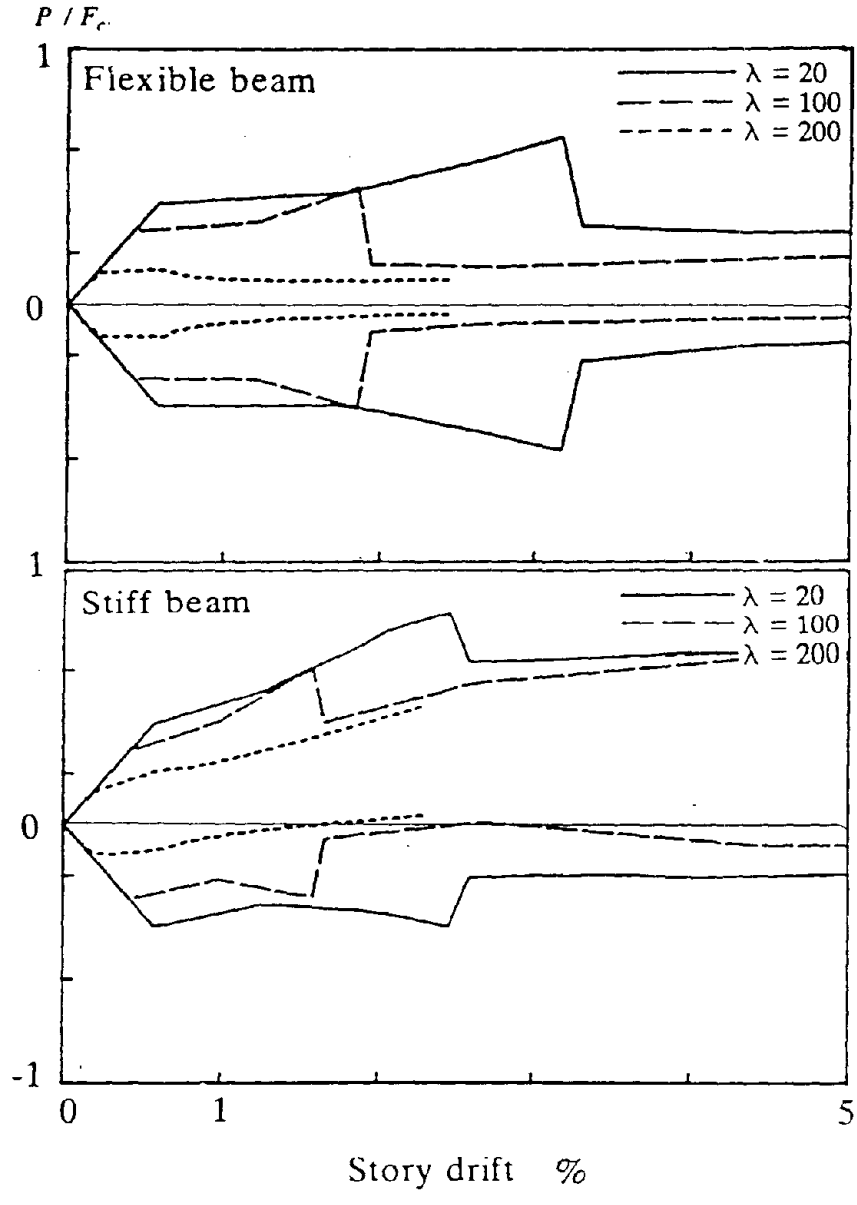

Figure 3-13-a First story columns compression versus story drift.

Column compression

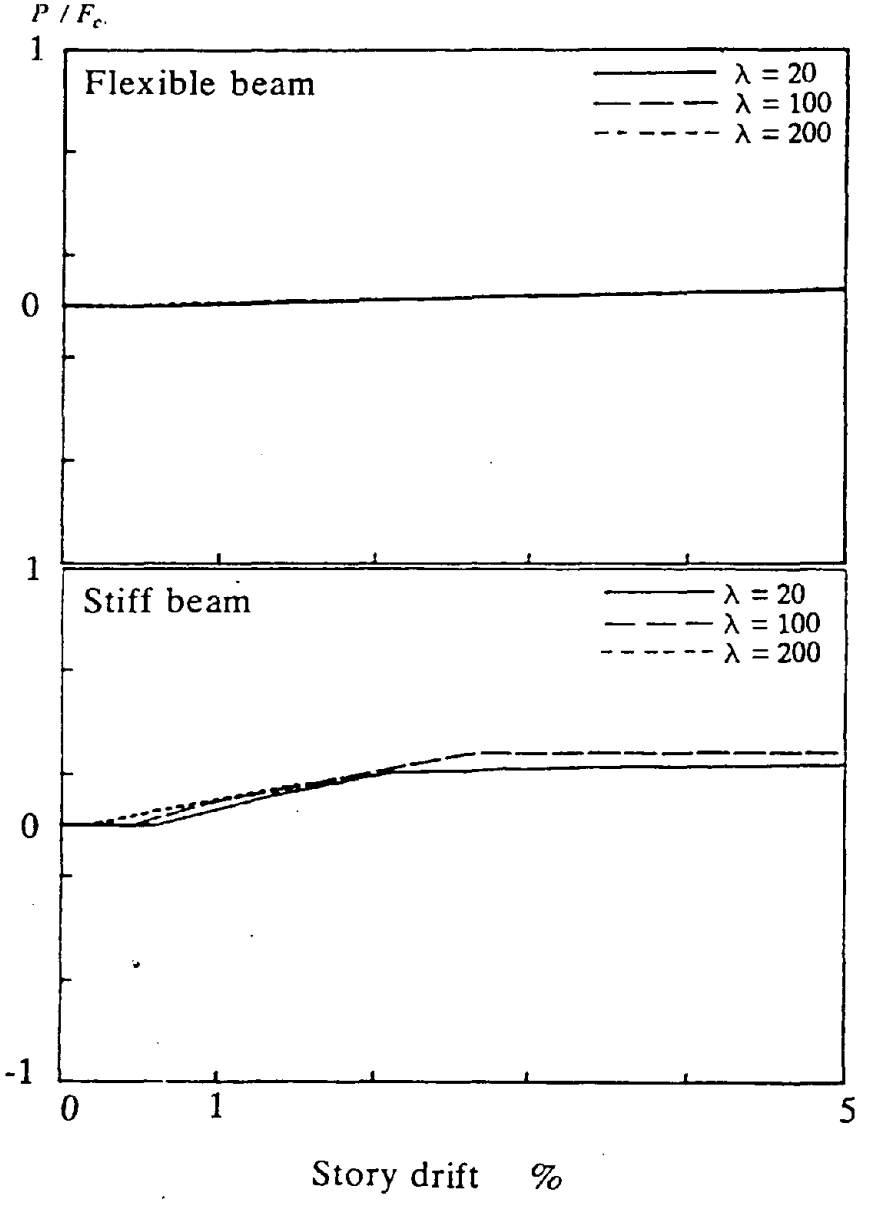

Figure 3-13-b First story columns compression versus story drift.

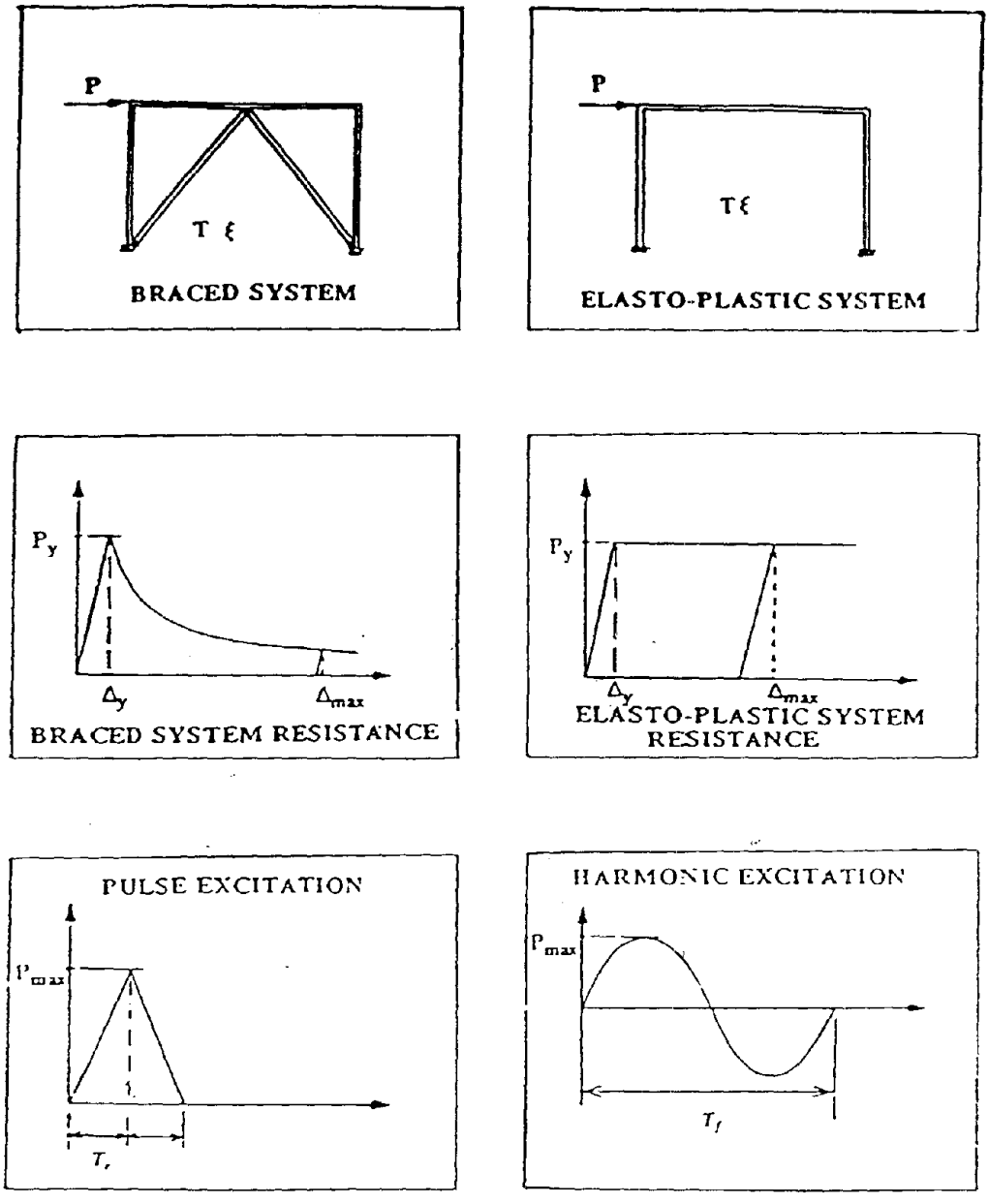

Figure 4.0 Idealized systems considered

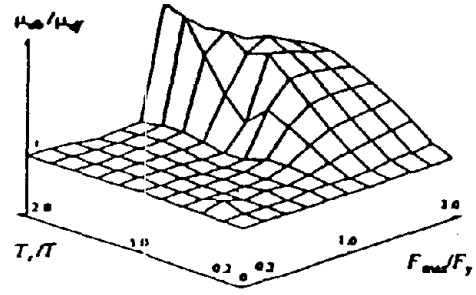

4-1-a Flexible Beam, λ=20

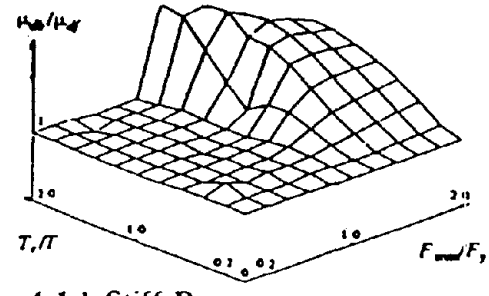

4-1-b Stiff Beam, λ=20

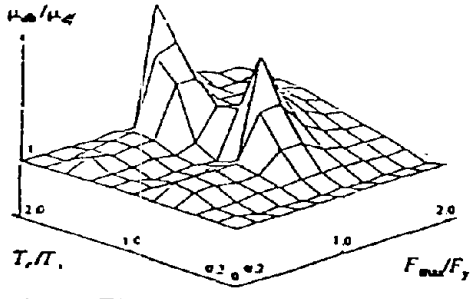

4-1-c Flexible Beam, λ=100

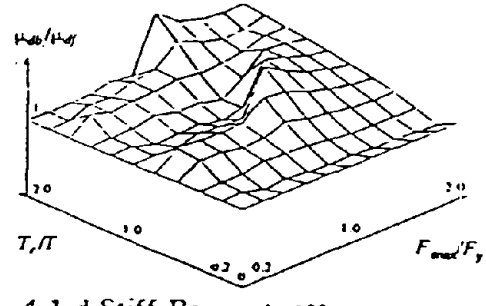

4-1-d Stiff Beam, λ=100

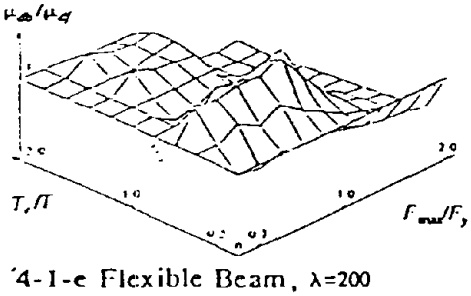

4-1-e Flexible Beam, λ=200

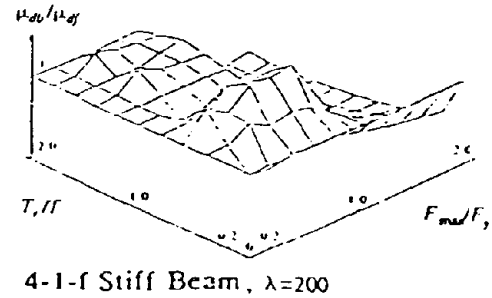

4-1-f Stiff Beam, λ=200

Figure 4-1 Ratio of displacement ductility of braced system to framed system for pulse loading

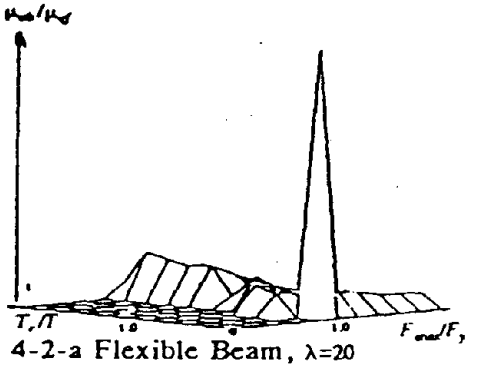

4-2-a Flexible Beam, λ=20

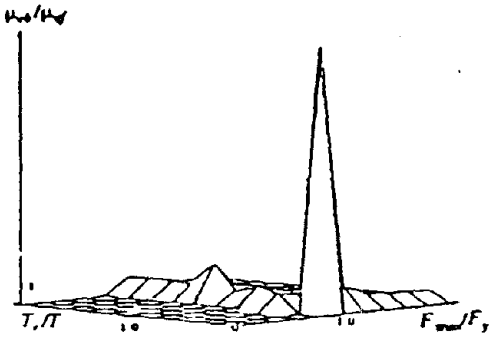

4-2-b Stiff Beam, λ=20

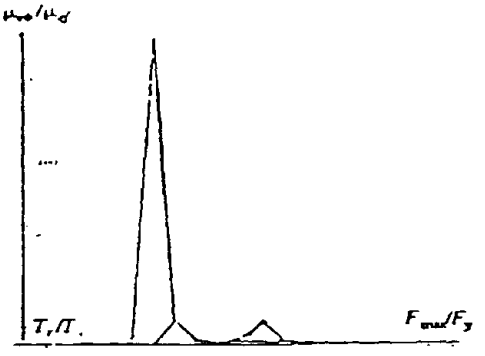

4-2-c Flexible Beam, λ=100

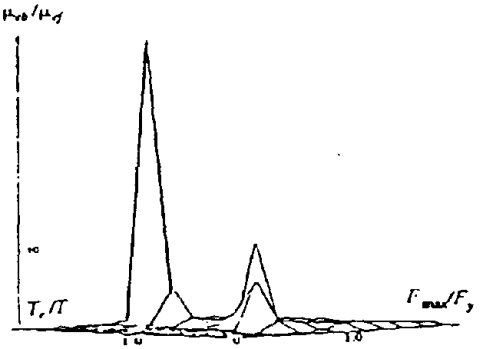

4-2-d Stiff Beam, λ=100

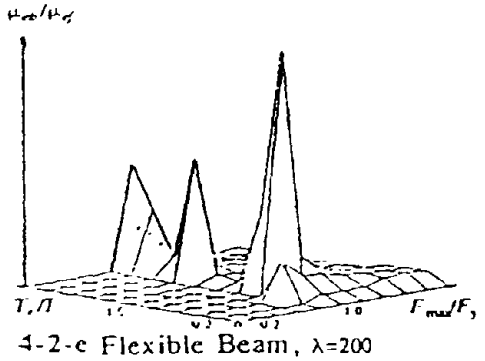

4-2-e Flexible Beam, λ=200

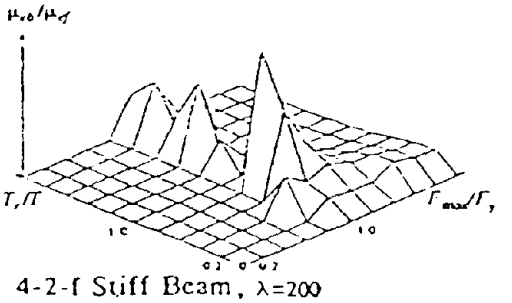

4-2-f Stiff Beam, λ=200

Figure 4-2 Ratio of energy ductility of braced system to framed system for pulse loading

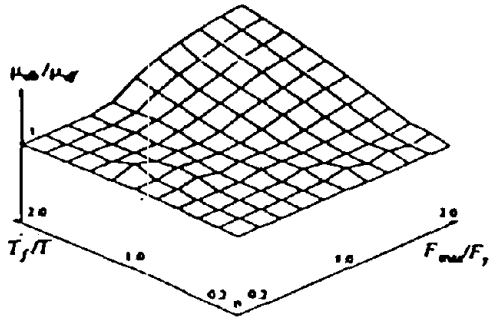

4-3-a Flexible Beam, λ=20

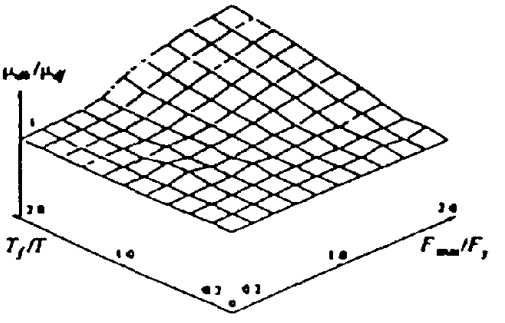

4-3-b Stiff Beam, λ=20

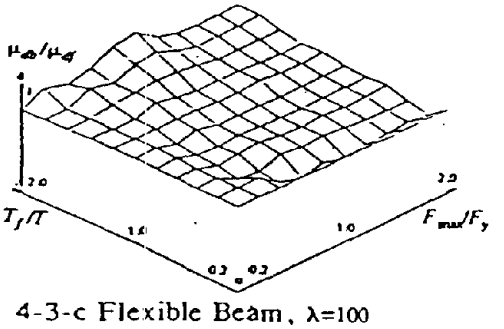

4-3-c Flexible Beam, λ=100

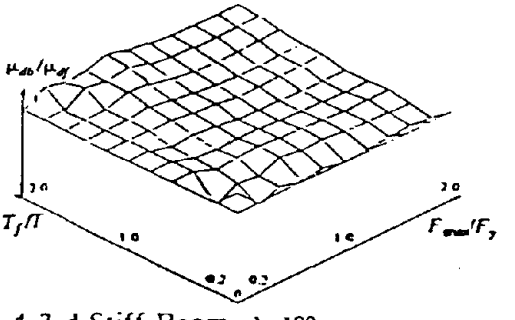

4-3-d Stiff Beam, λ=100

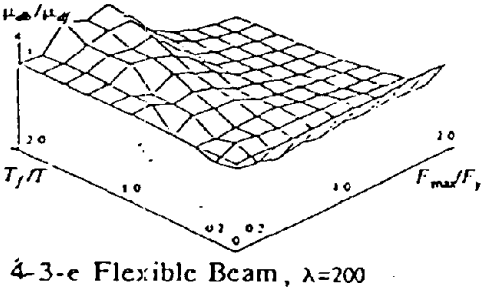

4-3-e Flexible Beam, λ=200

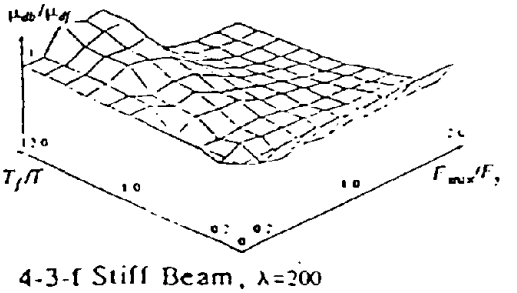

4-3-f Stiff Beam, λ=200

Figure 4-3 Ratio of displacement ductility of braced system to framed system for harmonic loading (sine wave)

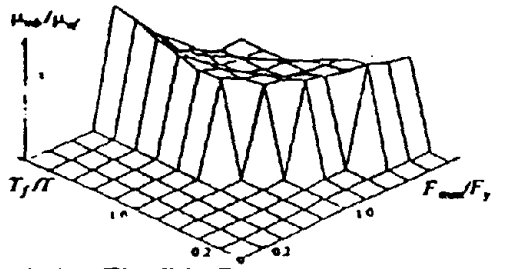

4-4-a Flexible Beam, λ=20

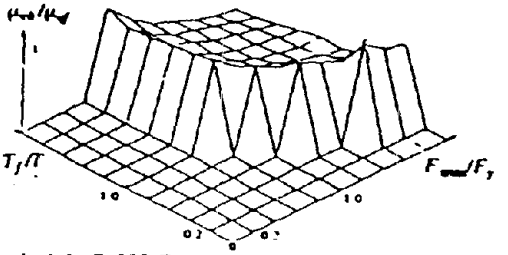

4-4-b Stiff Beam, λ=20

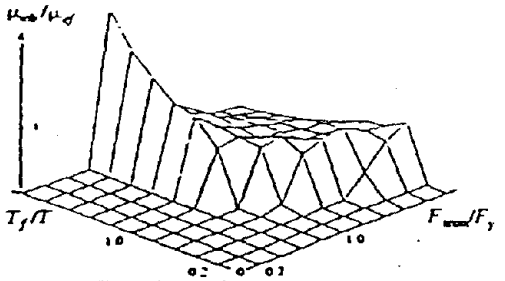

4-4-c Flexible Beam, λ=100

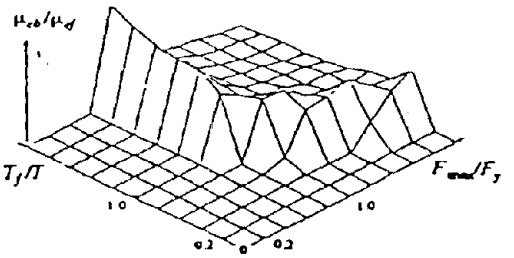

4-4-d Stiff Beam, λ=100

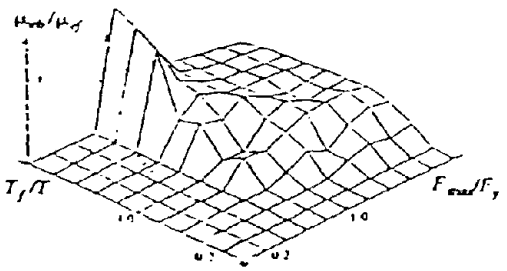

4-4-e Flexible Beam, λ=200

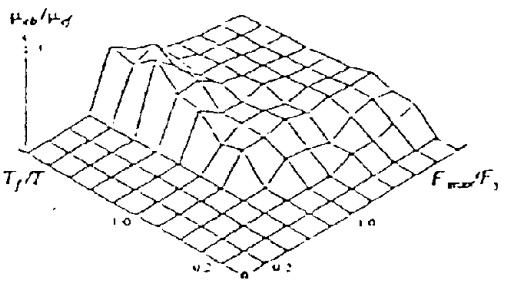

4-4-f Stiff Beam, λ=200

Figure 4-4 Ratio of energy ductility of braced system to framed system for harmonic loading (sine wave)

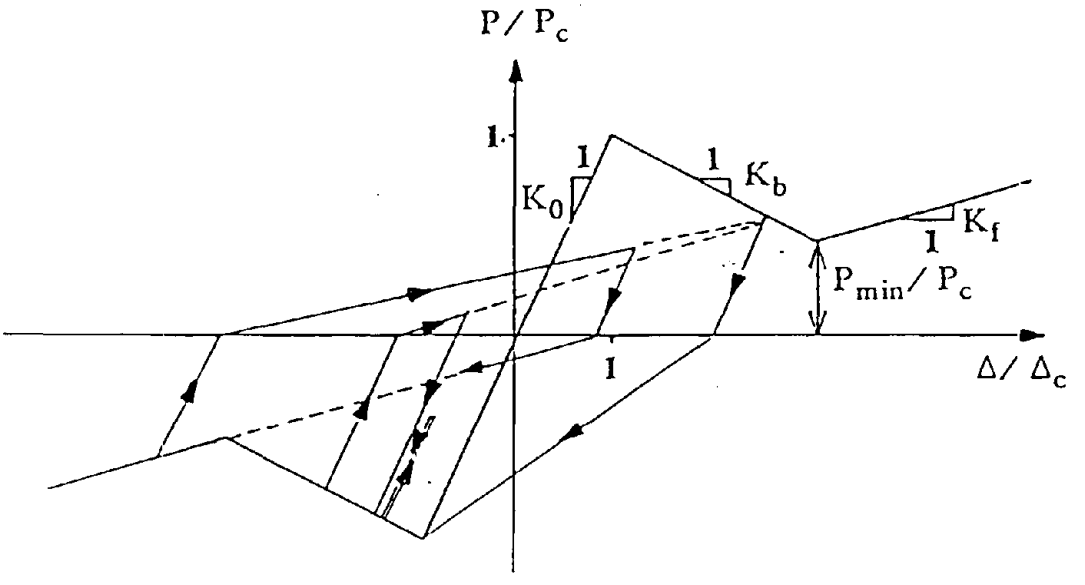

Figure 4-5 Idealized hysteresis model of K-braced systems

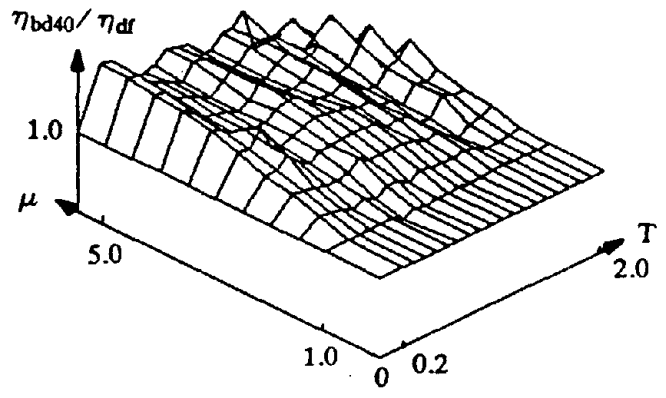

Figure 4-6-a Ratio of design strength of SNAP40 to LEPP for equal displacement ductility demand

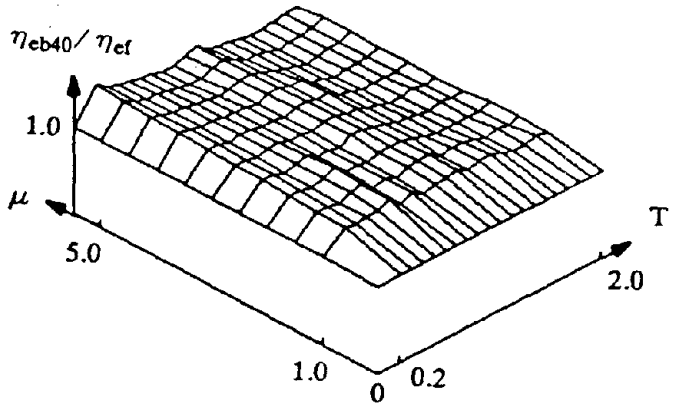

Figure 4-6-b Ratio of design strength of SNAP40 to LEPP for equal energy dissipation demand

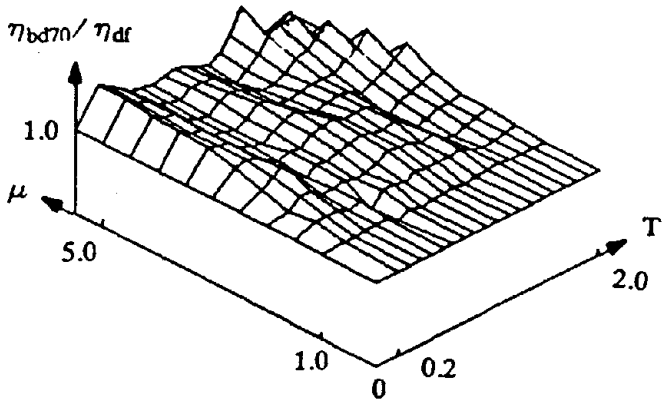

Figure 4-6-c Ratio of design strength of SNAP70 to LEPP for equal displacement ductility demand

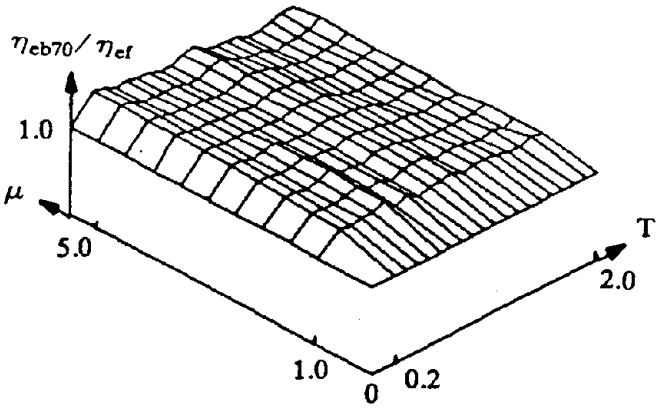

Figure 4-6-d Ratio of design strength of SNAP70 to LEPP for equal energy dissipation demand

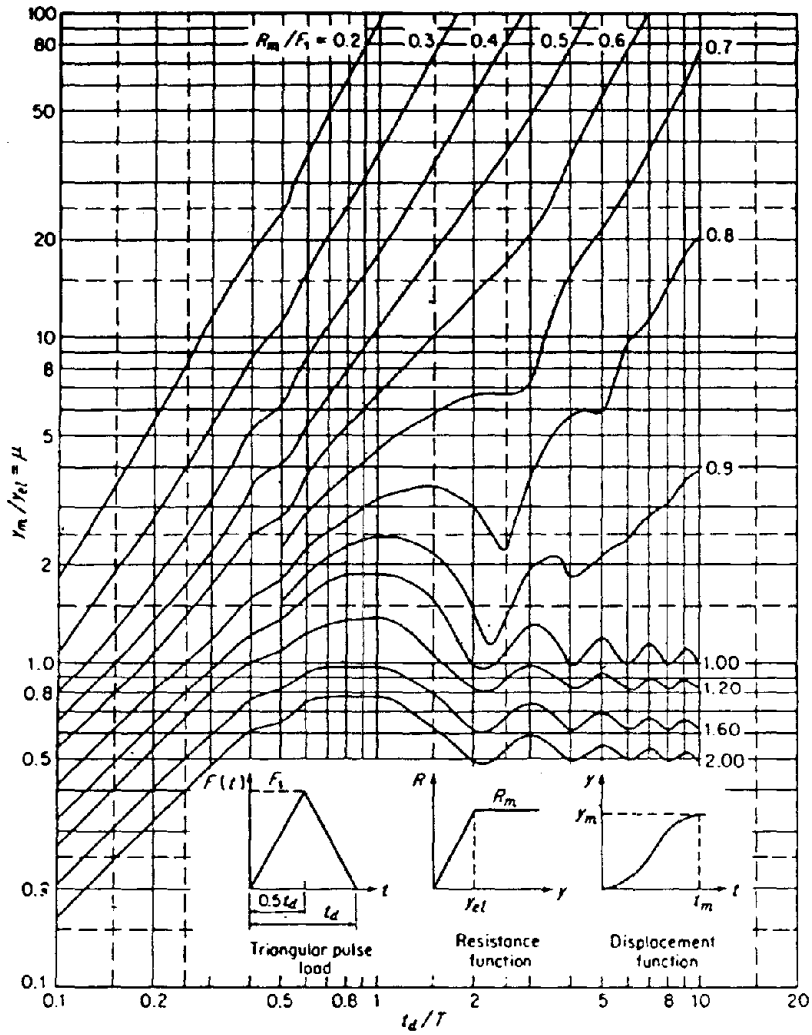

Figure 4-7: Maximum response of elasto-plastic systems (undamped) due to equilateral triangular load pulses (from "Introduction to structural dynamics" J. M. BIGGS, McGraw Hill ed.)

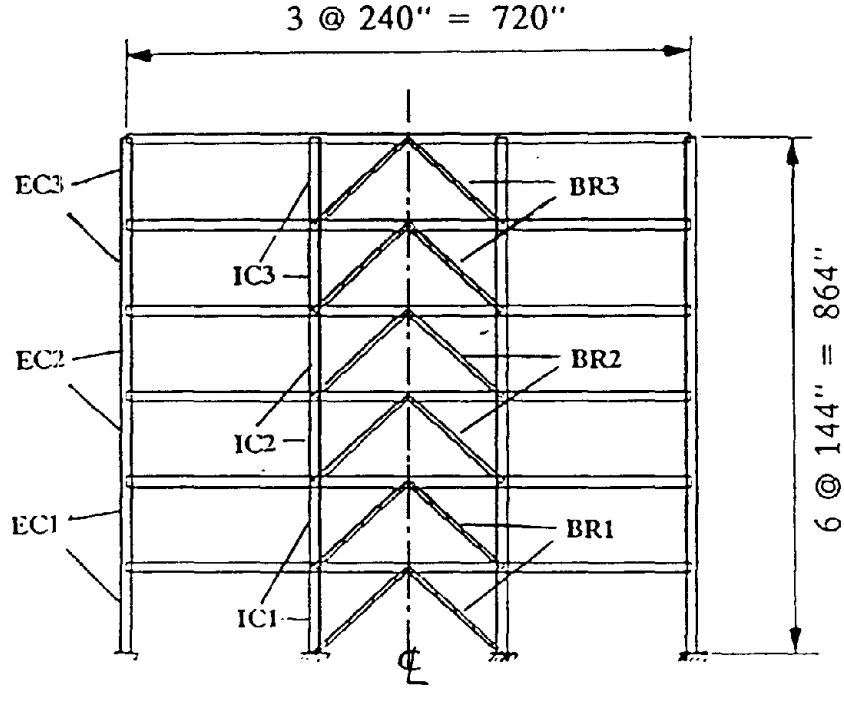

Figure 5-1 Elevation of a typical K-braced frame

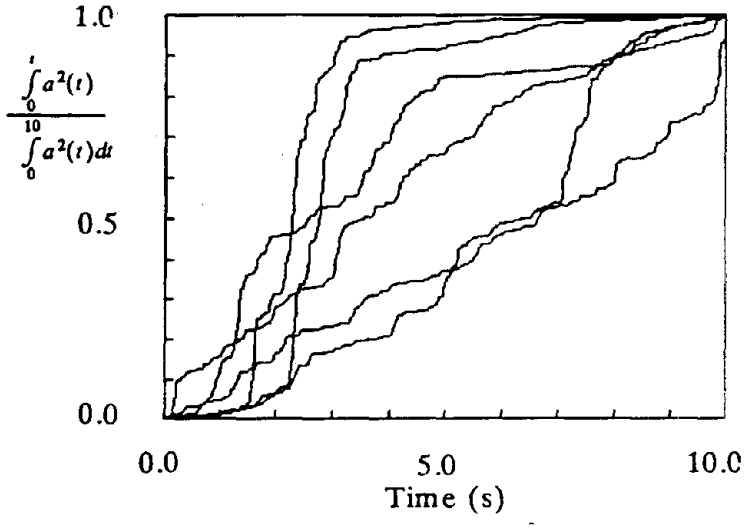

Figure 5-2-a Normalized cumulative Arias intensity for the ground motions used

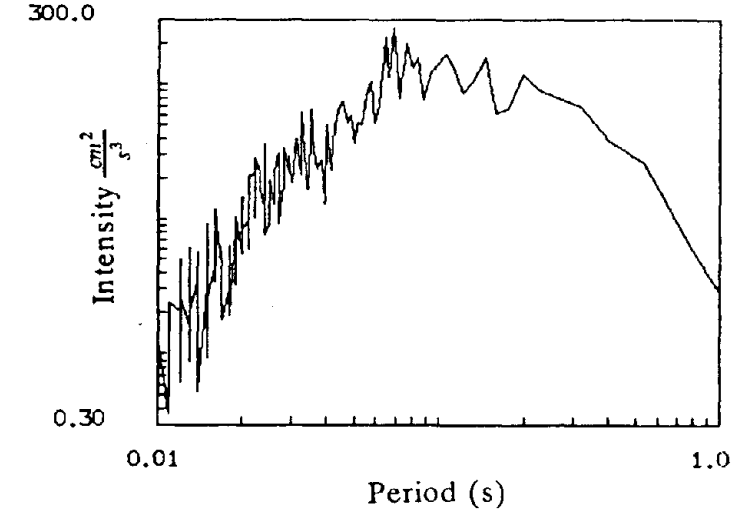

Figure 5-2-b Average power spectrum for the ground motions used

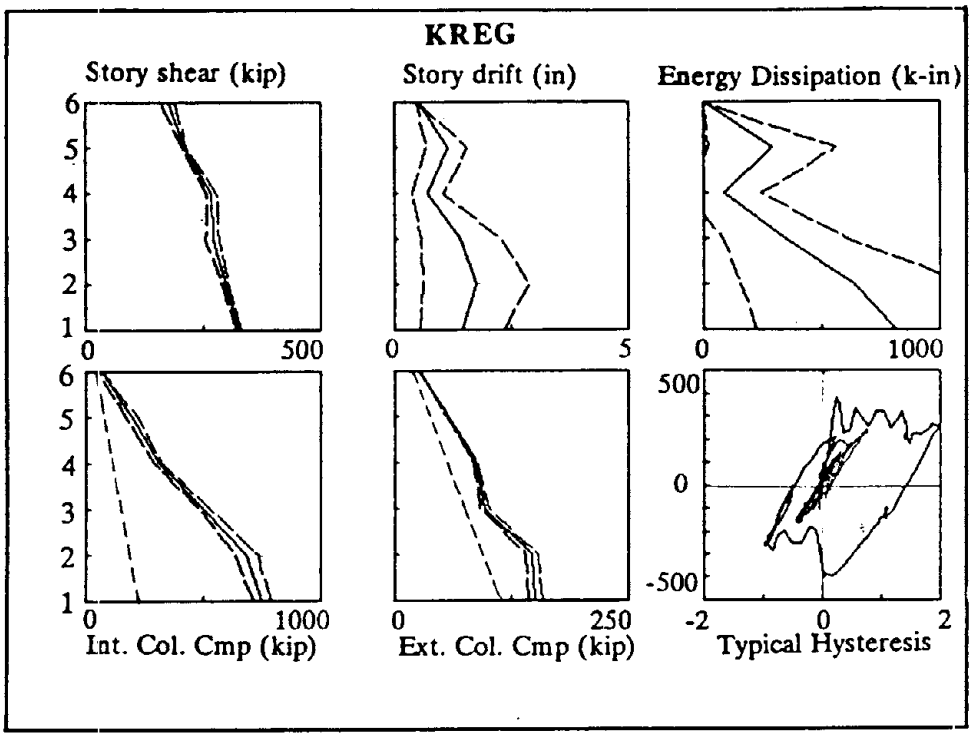

Figure 5-3 Summary of results for KREG (Regular K-braced frame)

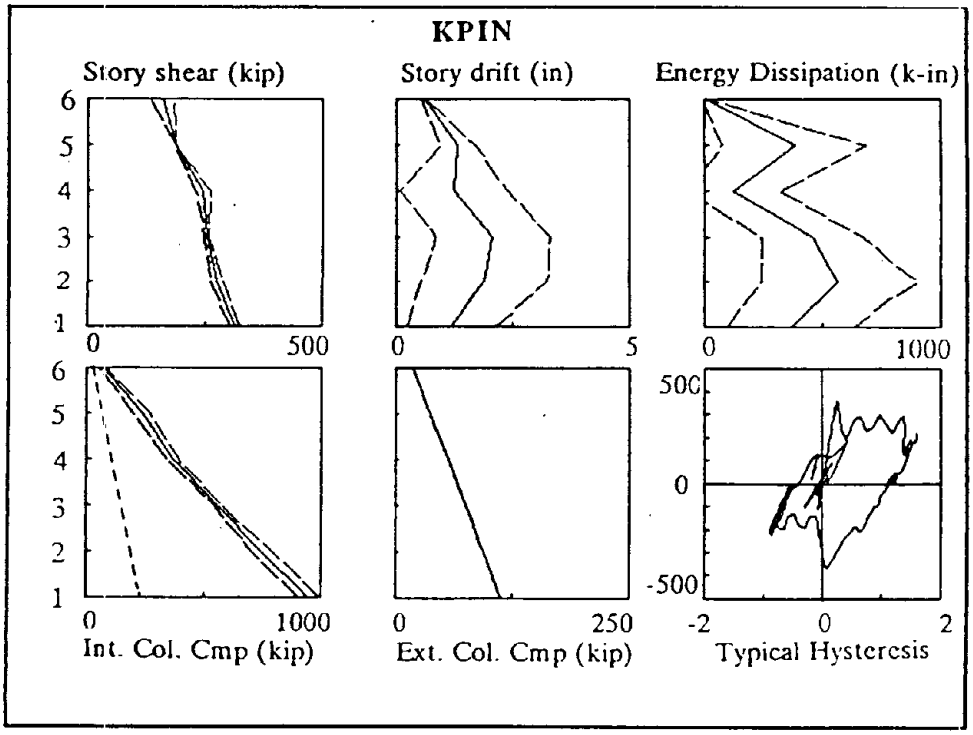

Figure 5-4 Summary of results for KPIN (K-braced frame with pinned beam connections)

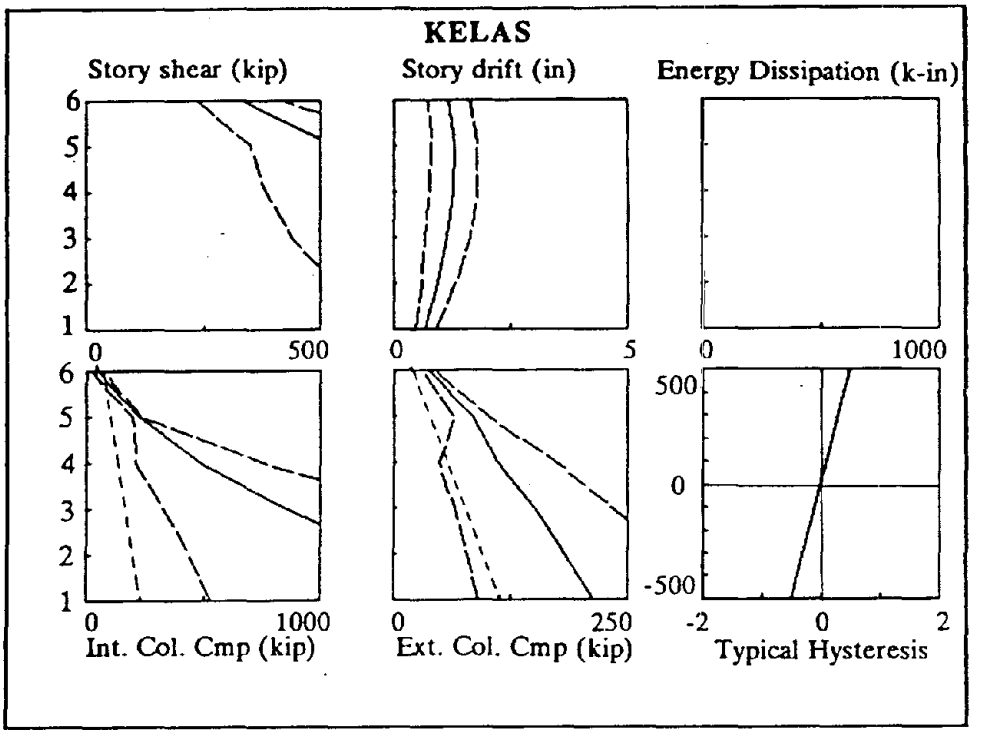

Figure 5-5 Summary of results for KELAS (Elastic K-braced frame)

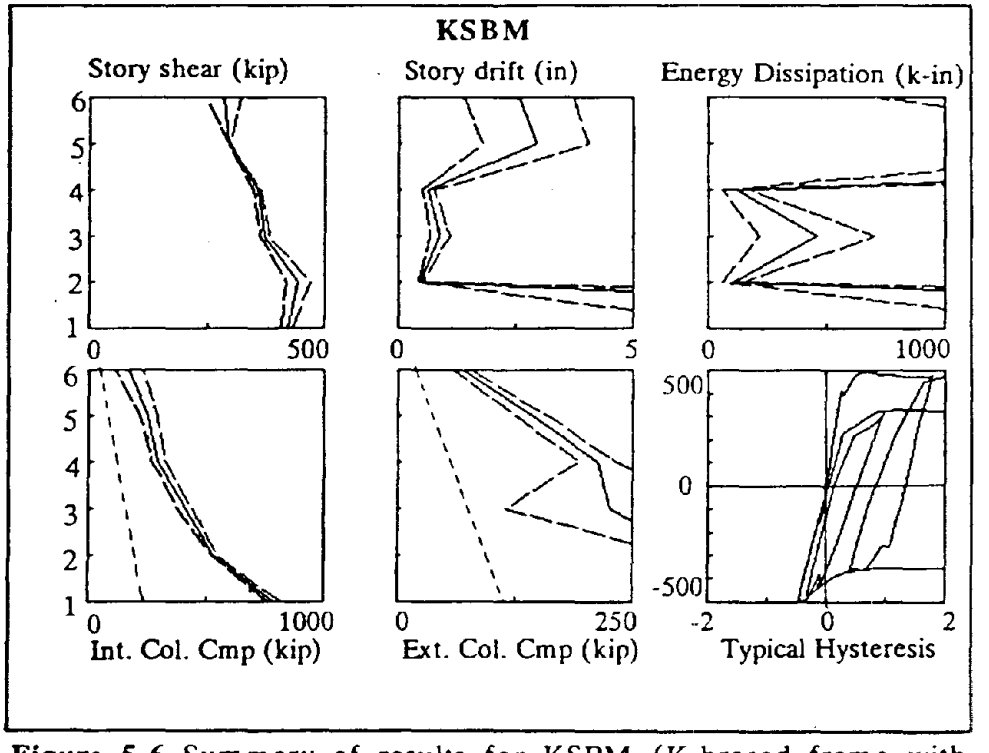

Figure 5-6 Summary of results for KSBM (K-braced frame with strong stiff beams)

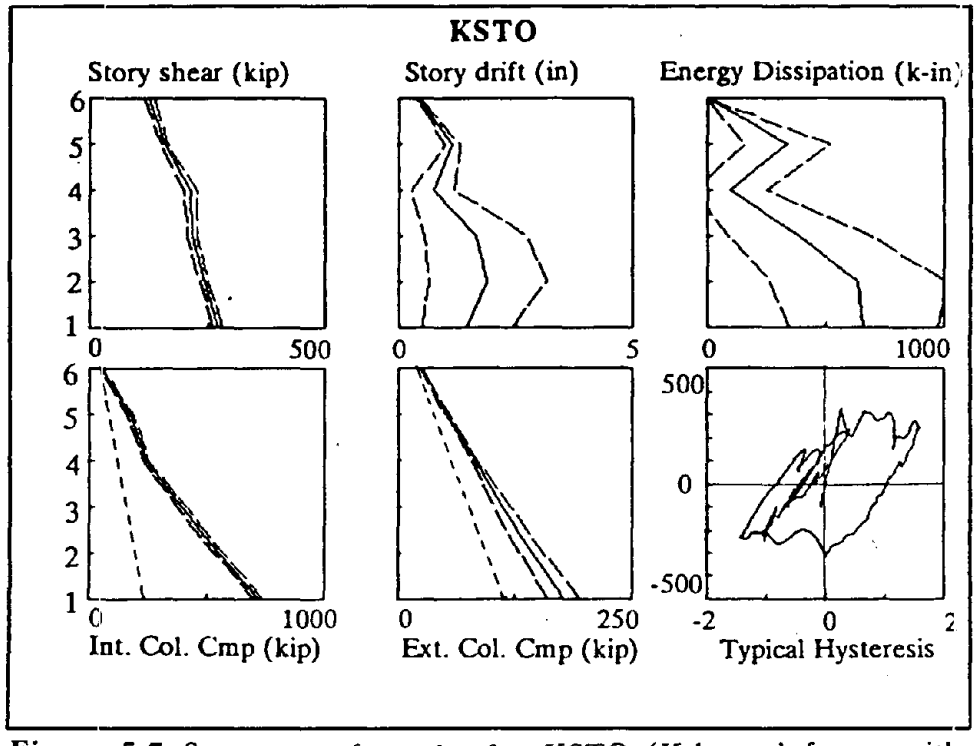

Figure 5-7 Summary of results for KSTO (K-braced frame with stocky braces)

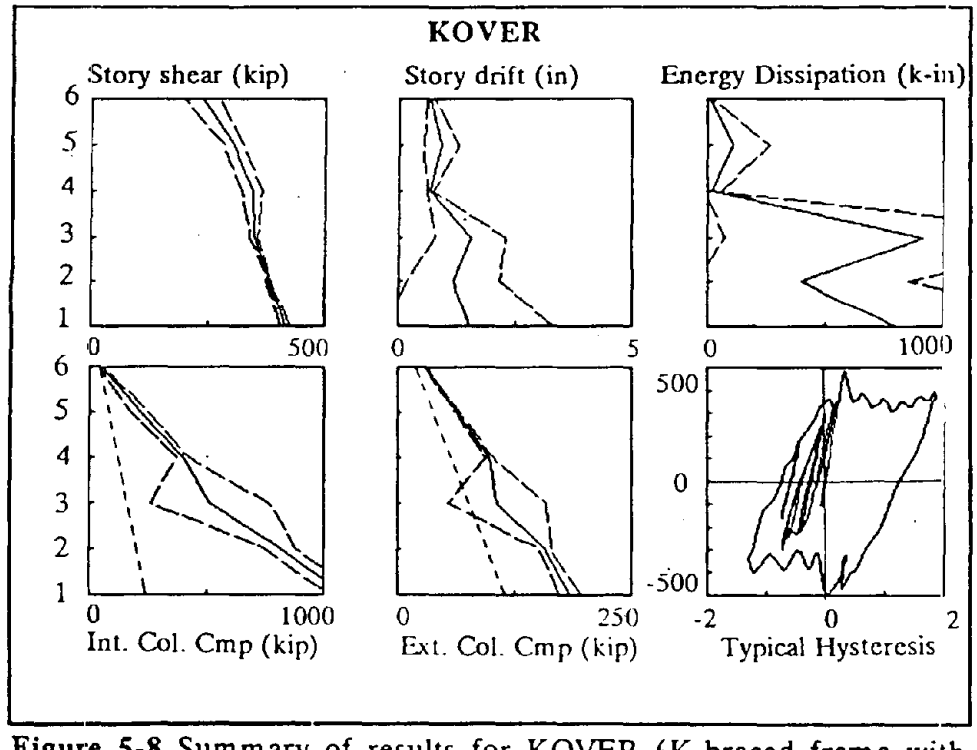

Figure 5-8 Summary of results for KOVER (K-braced frame with overstrong braces)

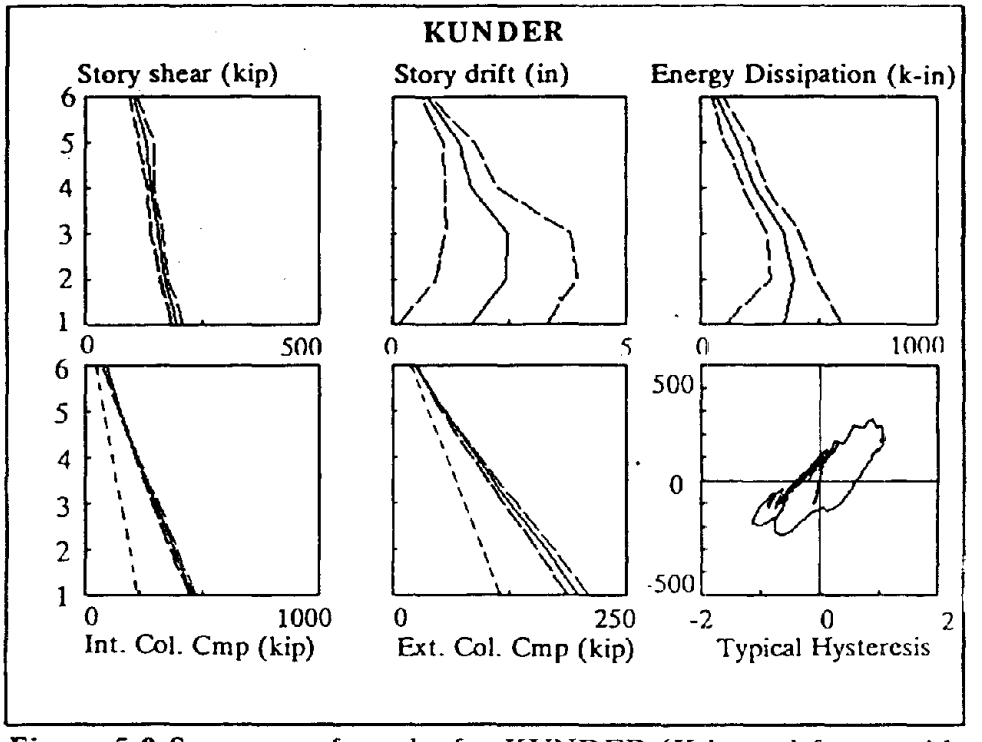

Figure 5-9 Summary of results for KUNDER (K-braced frame with understrong braces)

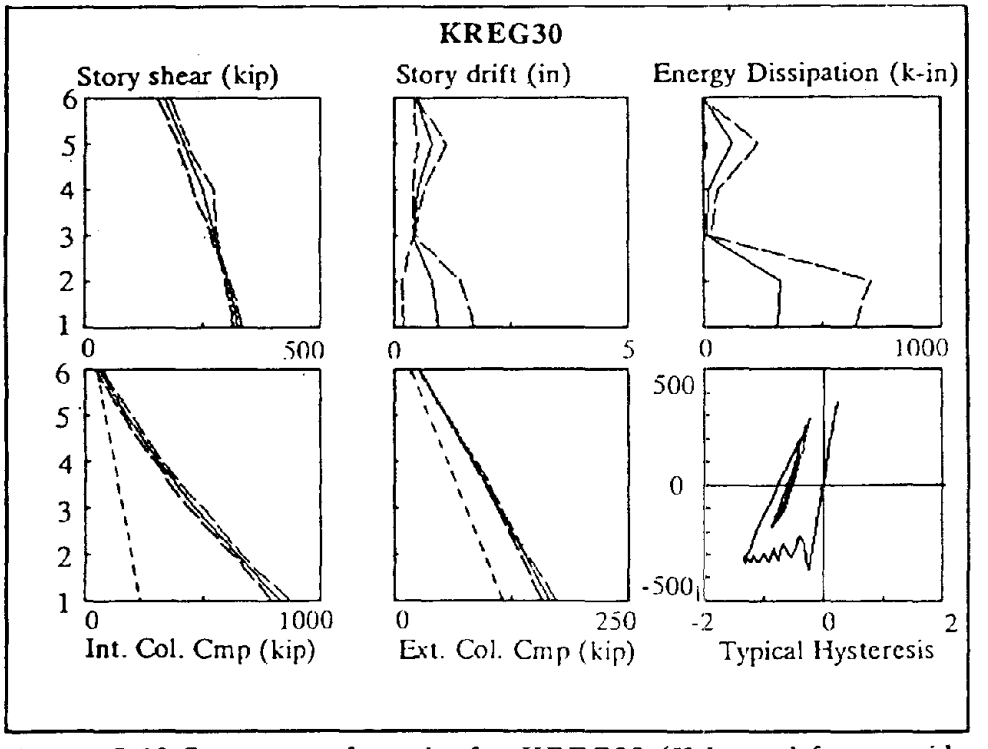

Figure 5-10 Summary of results for KREG30 (K-braced frame with 0.30g earthquakes)

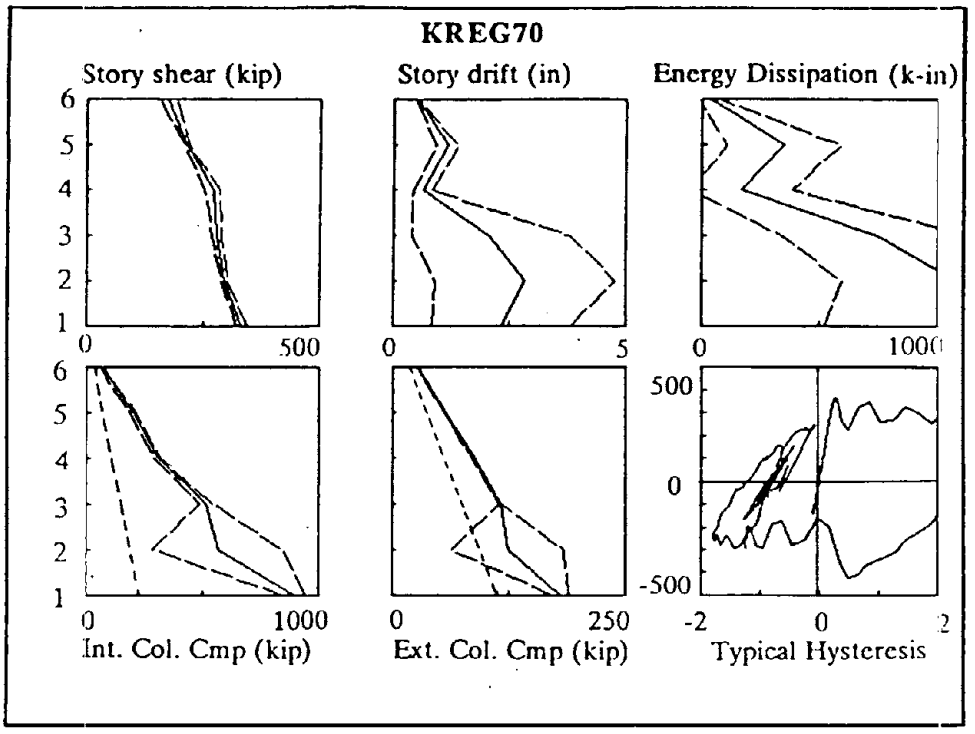

Figure 5-11 Summary of results for KREG70 (K-braced frame with 0.70g earthquakes)

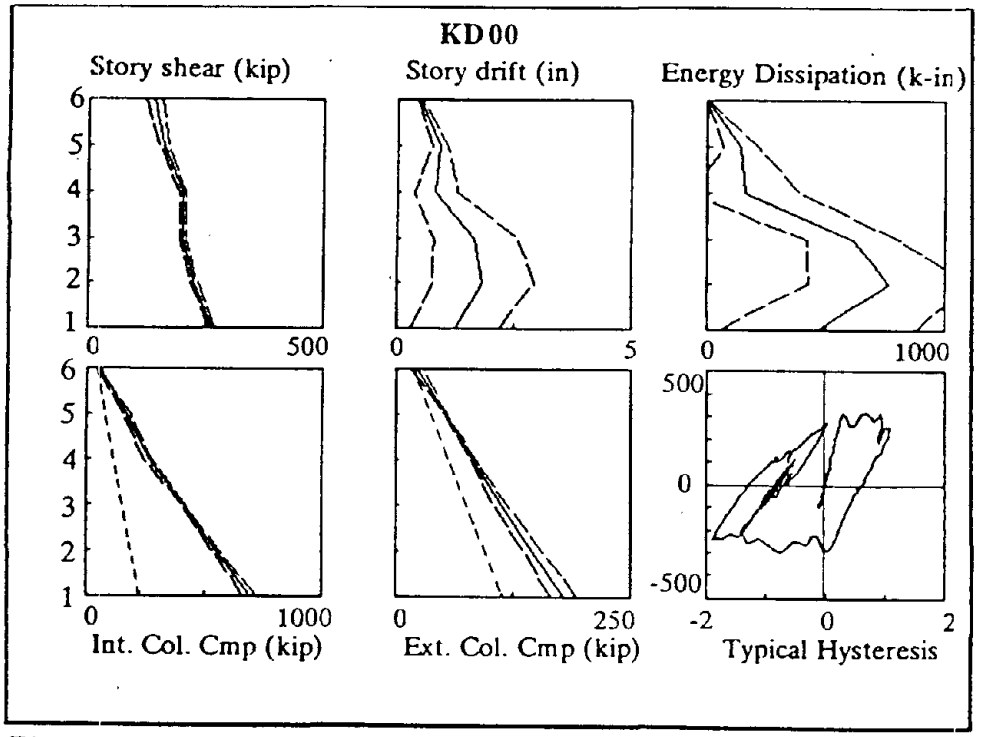

Figure 5-12 Summary of results for KD00 (Dual K-braced frame with 0% frame participation)

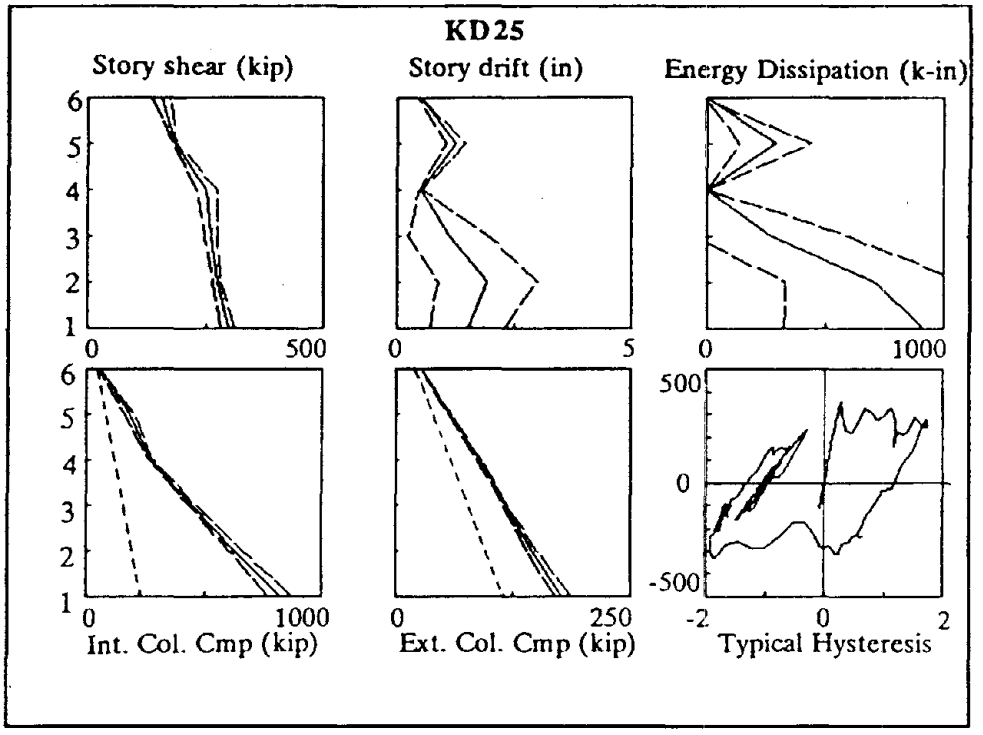

Figure 5-13 Summary of results for KD25 (Dual K-braced frame with 25% frame participation)

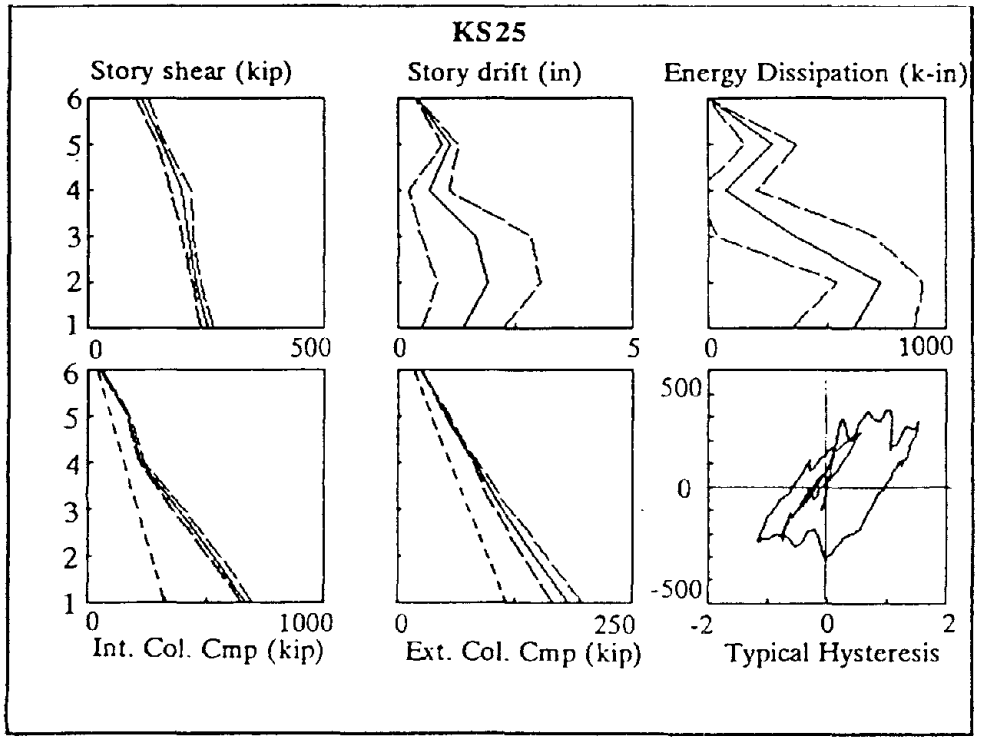

Figure 5-14 Summary of results for KS25 (Dual K-braced frame with 25% frame and stocky braces)

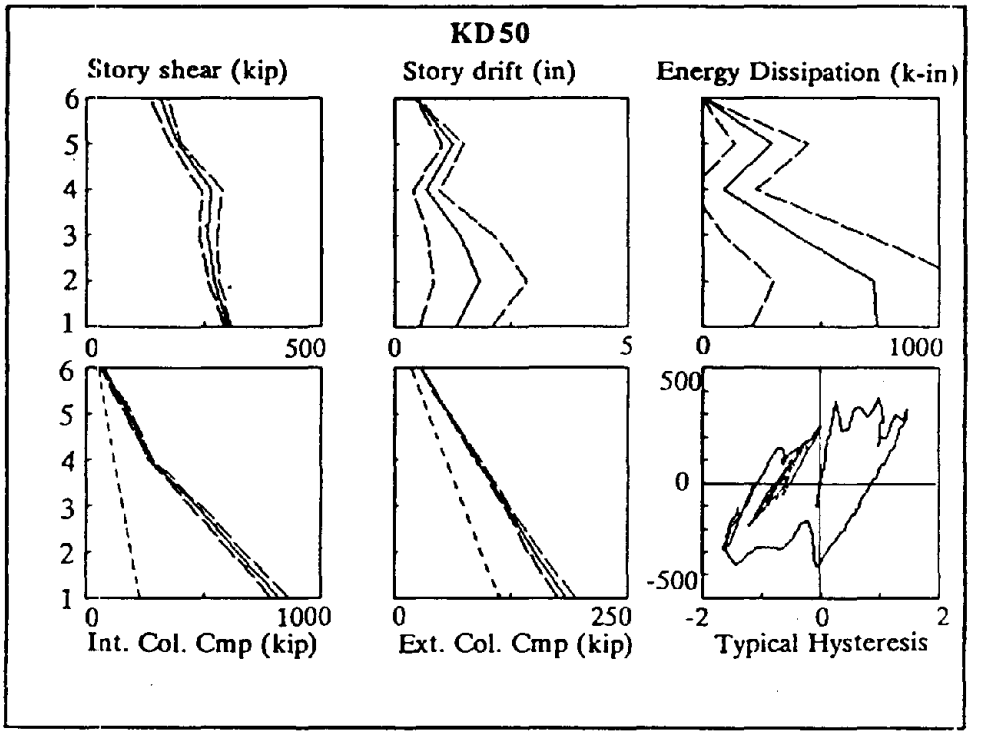

Figure 5-15 Summary of results for KD50 (Dual K-braced frame with 50% frame participation)

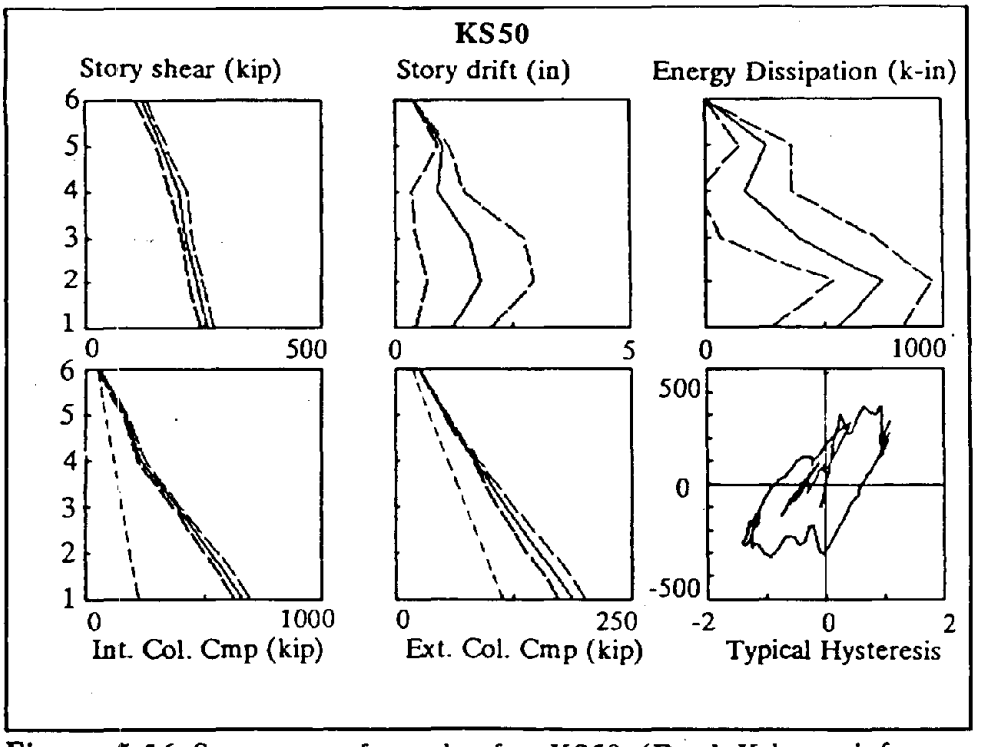

Figure 5-16 Summary of results for KS50 (Dual K-braced frame with 50% frame and stocky braces)

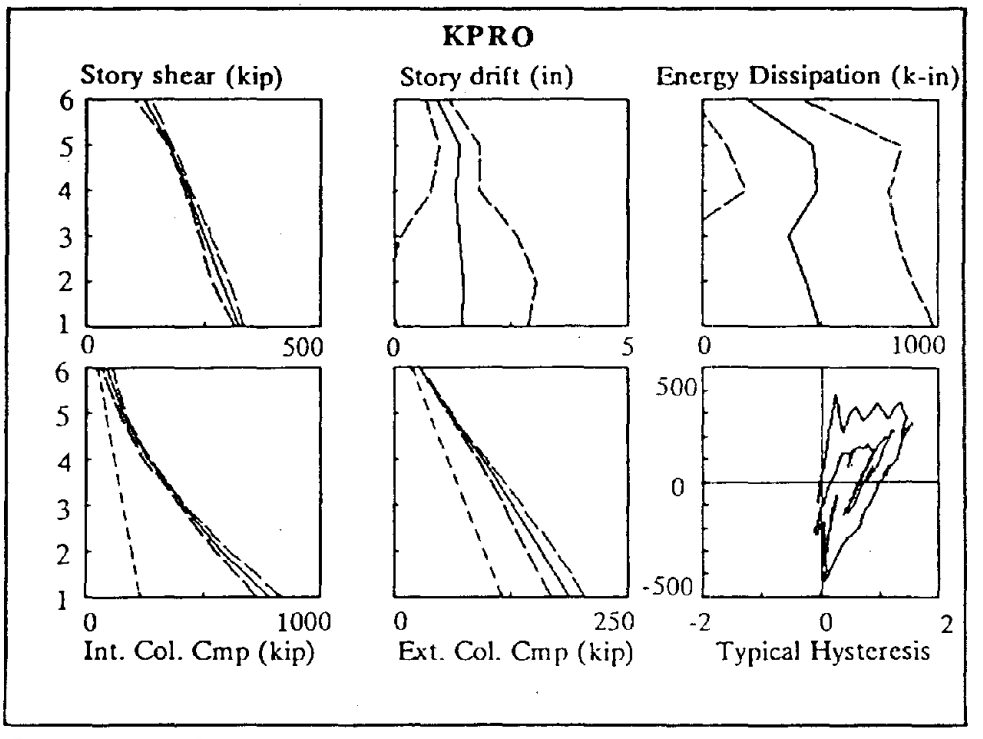

Figure 5-17 Summary of results for KPRO (K-braced frame with "proportional braces")

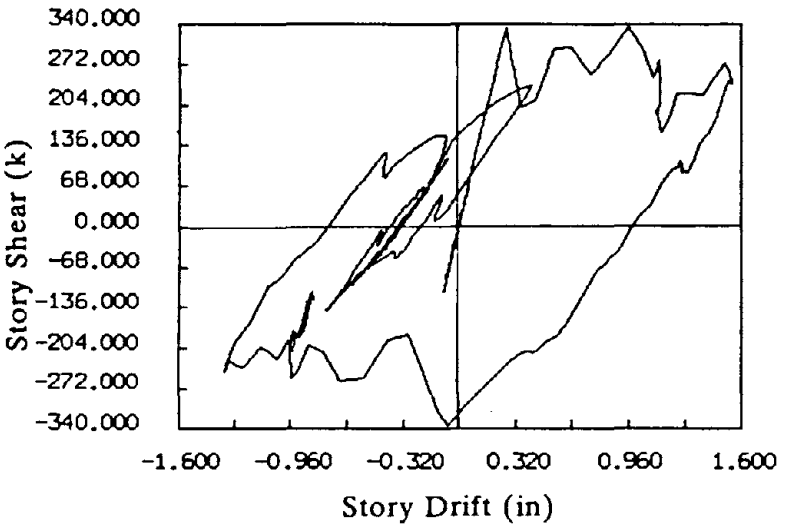

Figure 5-18-a First story hysteretic loop of KREG for HE35EW

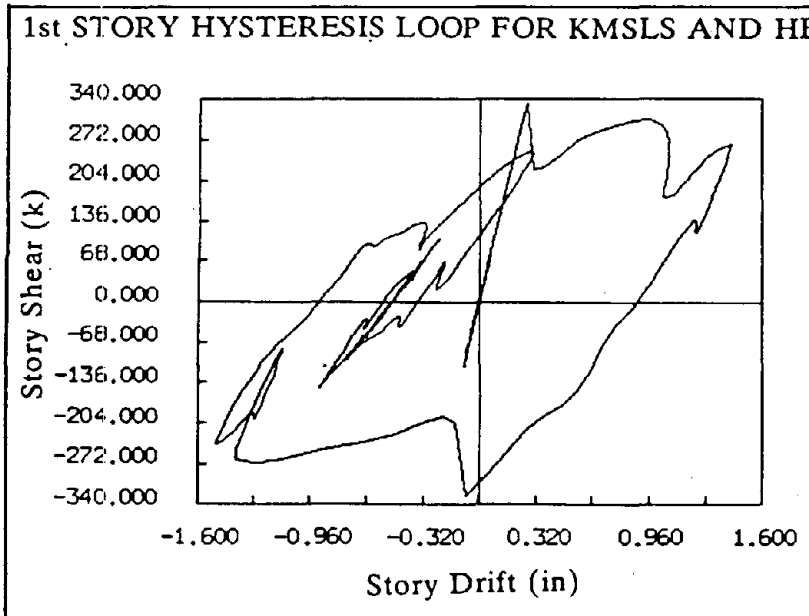

Figure 5-18-b First story hysteretic loop of KMSLS for HE35EW

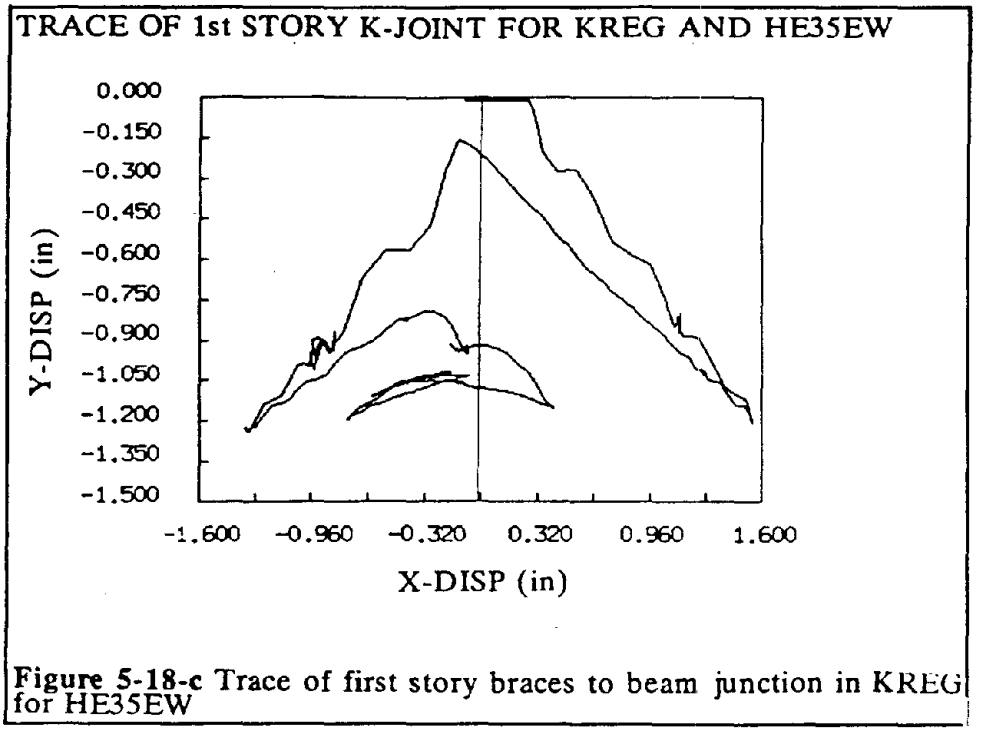

Figure 5-18-c Trace of first story braces to beam junction in KREG for HE35EW

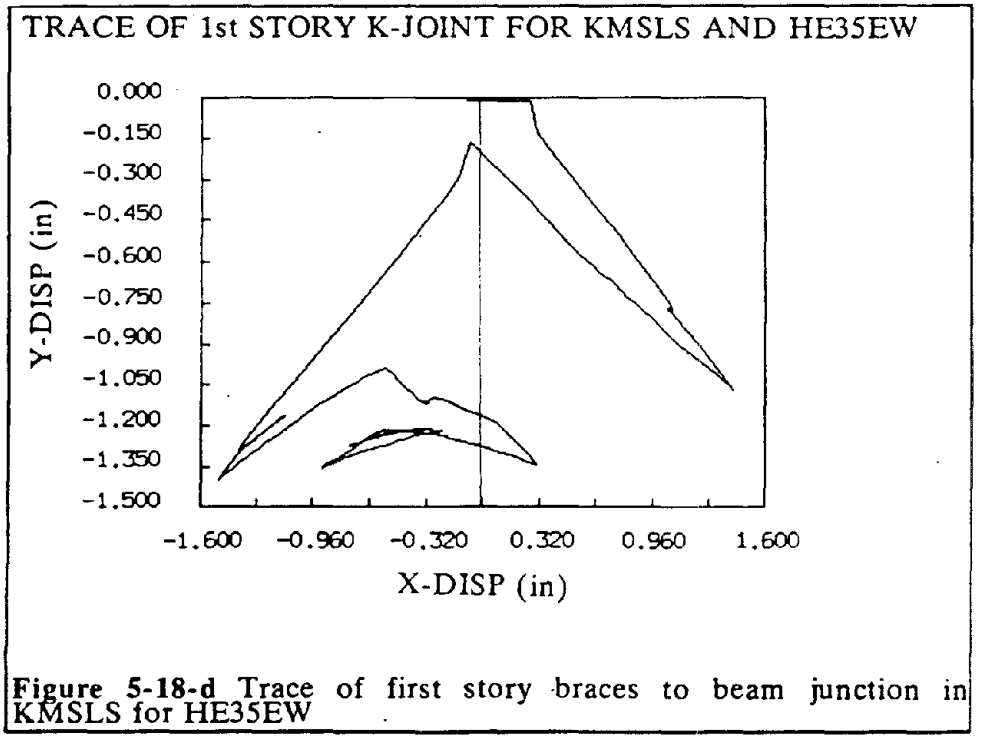

Figure 5-18-d Trace of first story braces to beam junction in KMSLS for HE35EW

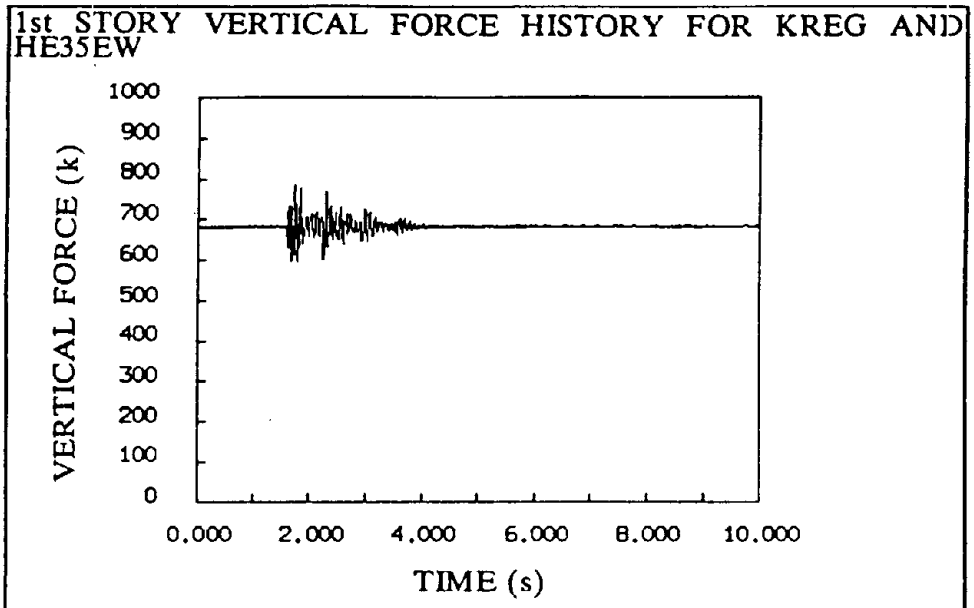

Figure 5-18-e First story vertical forces in KREG for HE35EW

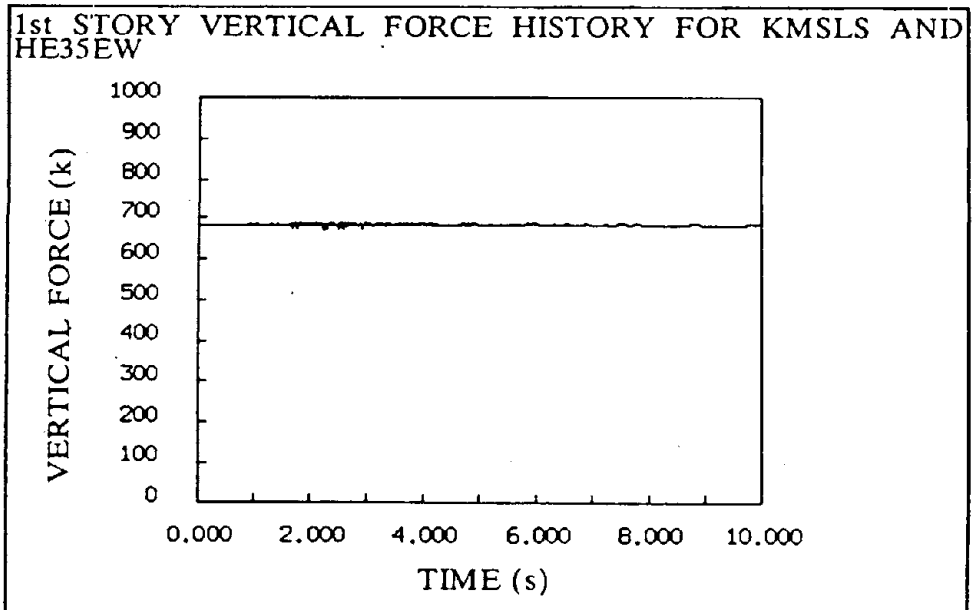

Figure 5-18-f First story vertical forces in KMSLS for HE35EW

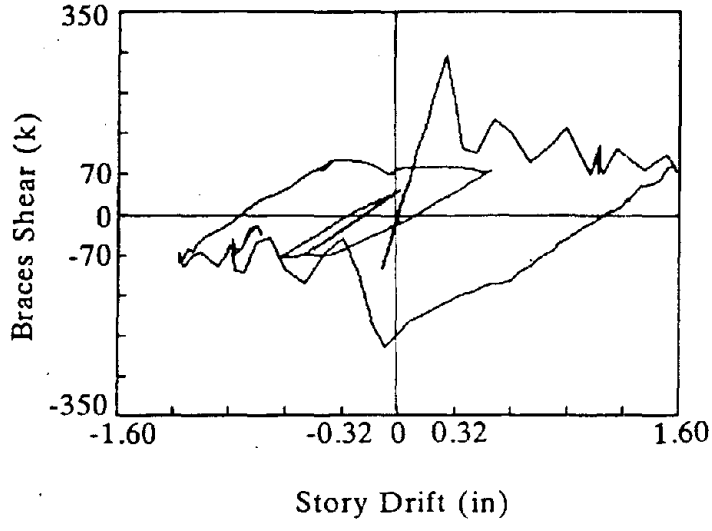

Figure 5-19-a Braces contribution to first story resistance in KREG for HE35EW

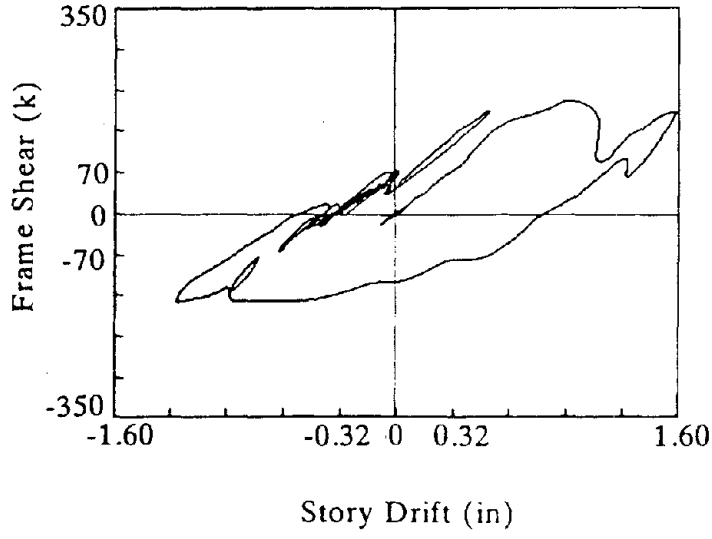

Figure 5-19-b Frame contribution to first story resistance in KREG for HE35EW

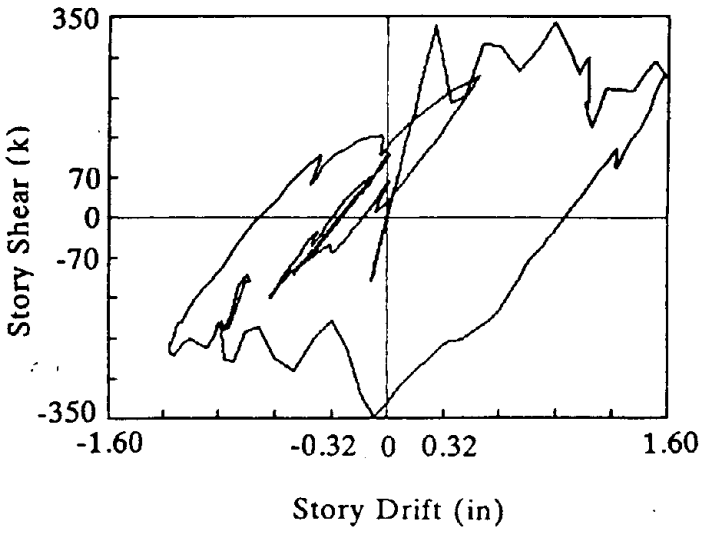

Figure 5-19-c Total story in shear in KREG for HE35EW

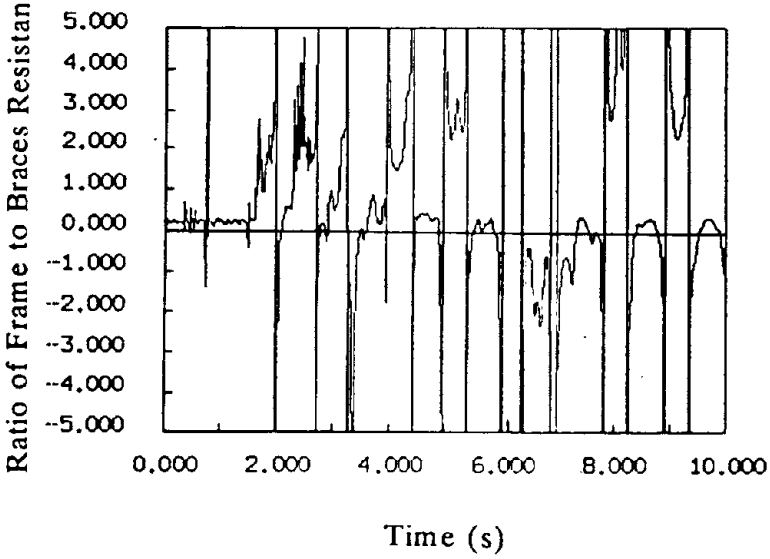

Figure 5-19-d Ratio of frame to braces resistance in first story of KREG for HE35EW

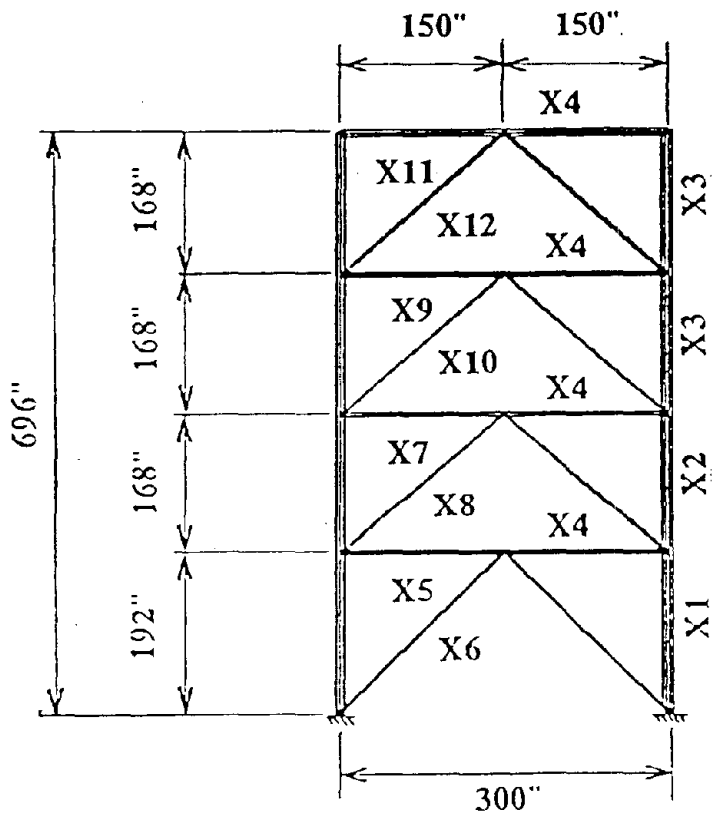

Figure 6-1 Elevation of the SEAONC K-braced frame

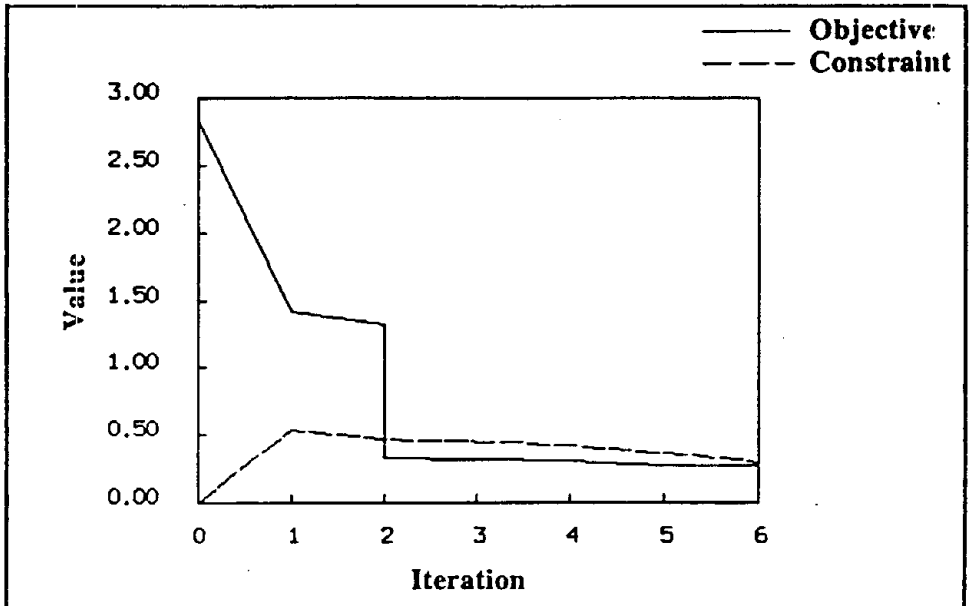

Figure 6-2-a Evolution of normalized objective function (volume) and of constraint value for the El Centro set

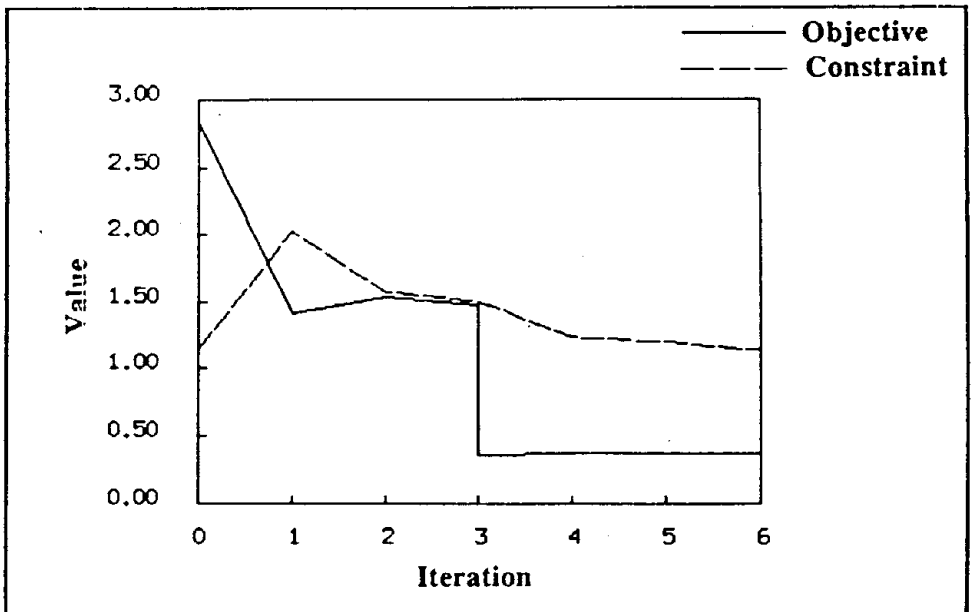

Figure 6-2-b Evolution of normalized objective function (volume) and of constraint value for the mixed set

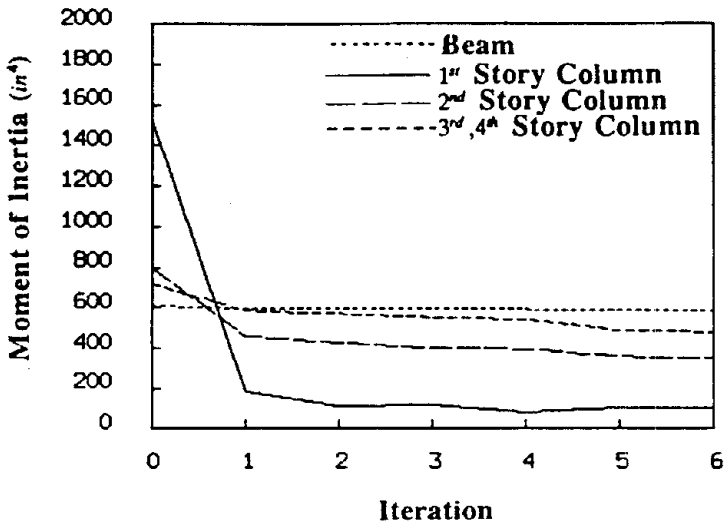

Figure 6-3-a Evolution of flexural member sizes for the El Centro set

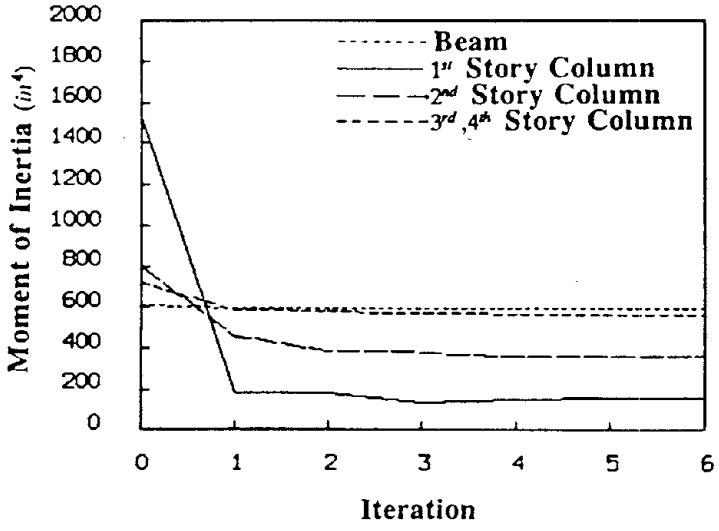

Figure 6-3-b Evolution of flexural member sizes for the mixed set

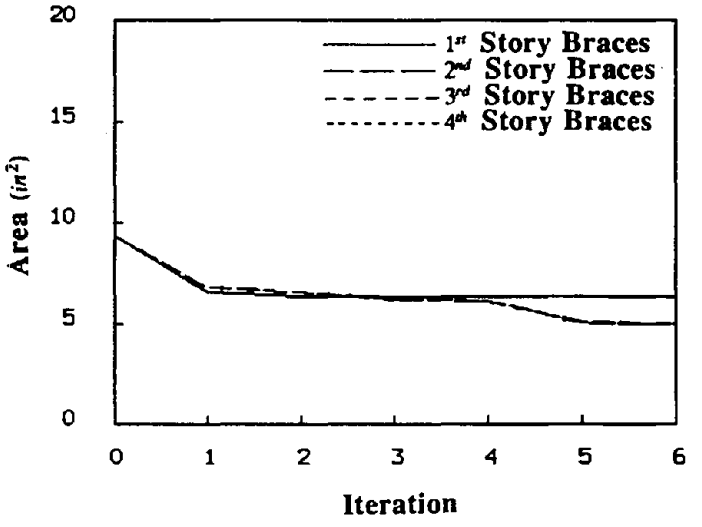

Figure 6-4-a Evolution of cross-section area of braces for the El Centro set

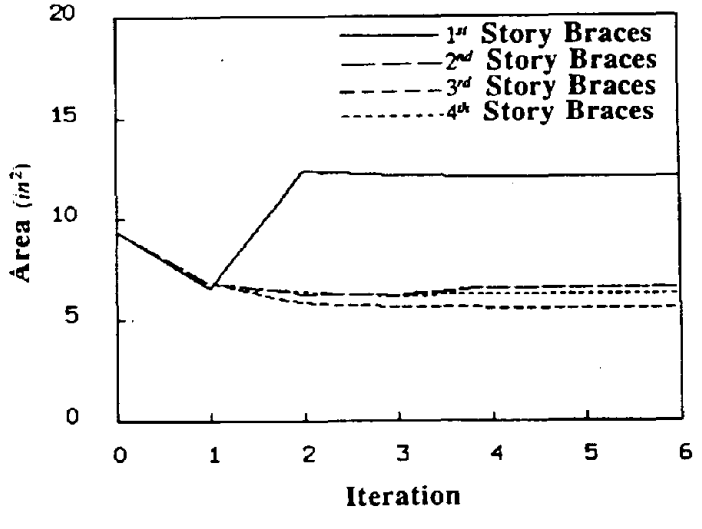

Figure 6-4-b Evolution of cross-section area of braces for the mixed set

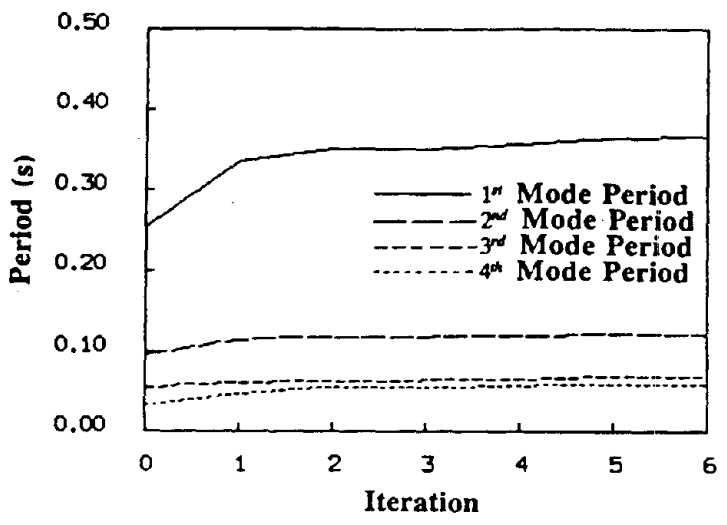

Figure 6-5-a Evolution of modal periods for the El Centro set

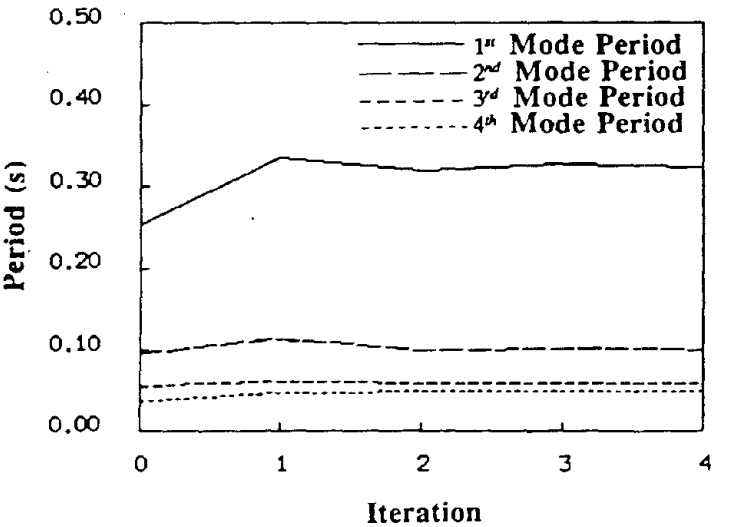

Figure 6-5-b Evolution of modal periods for the mixed set

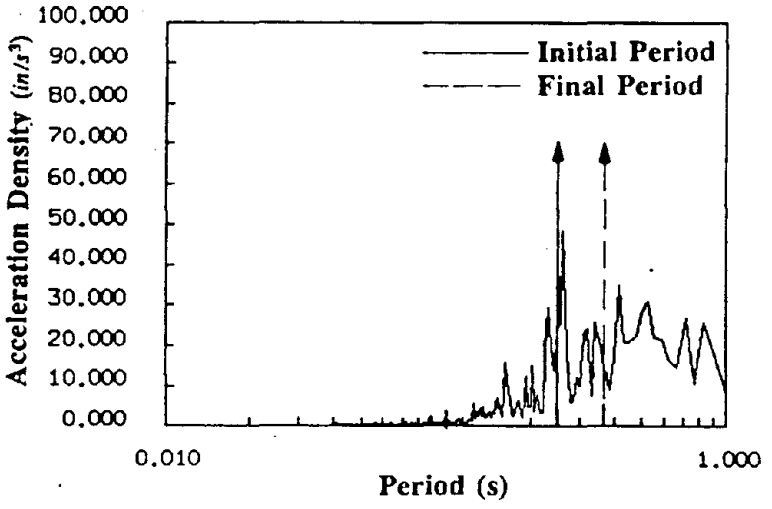

Figure 6-6-a Mean input power spectrum for the El Centro set

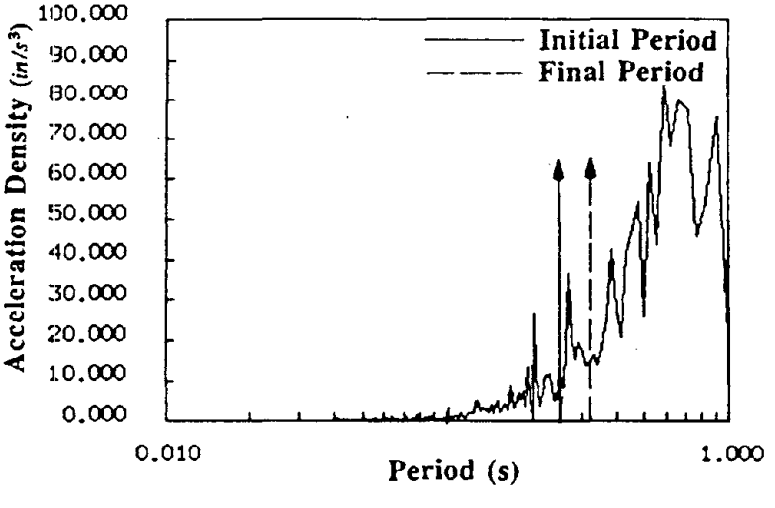

Figure 6-6-b Mean input power spectrum for the mixed set

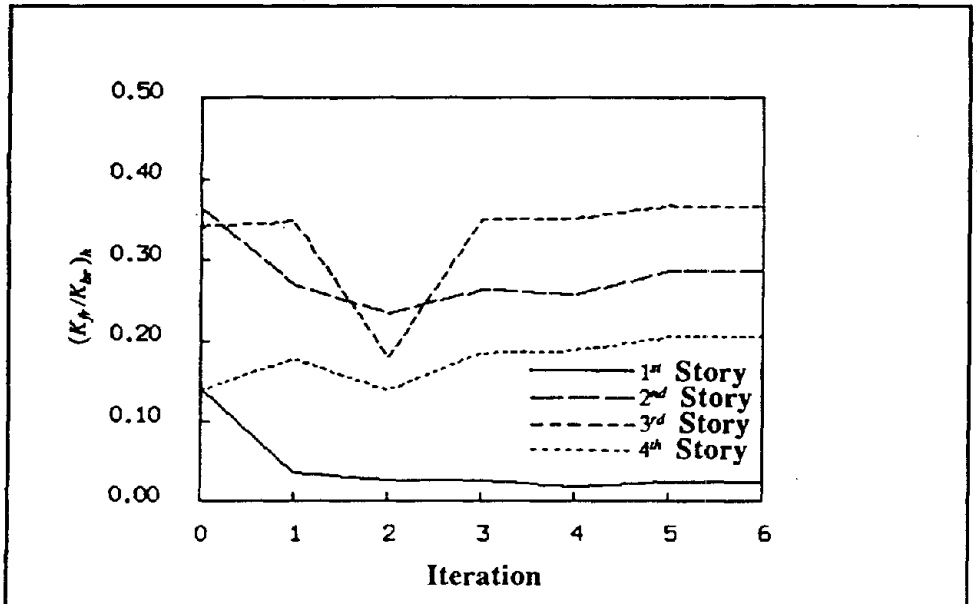

Figure 6-7-a Evolution of the frame participation ratio for the El Centro set

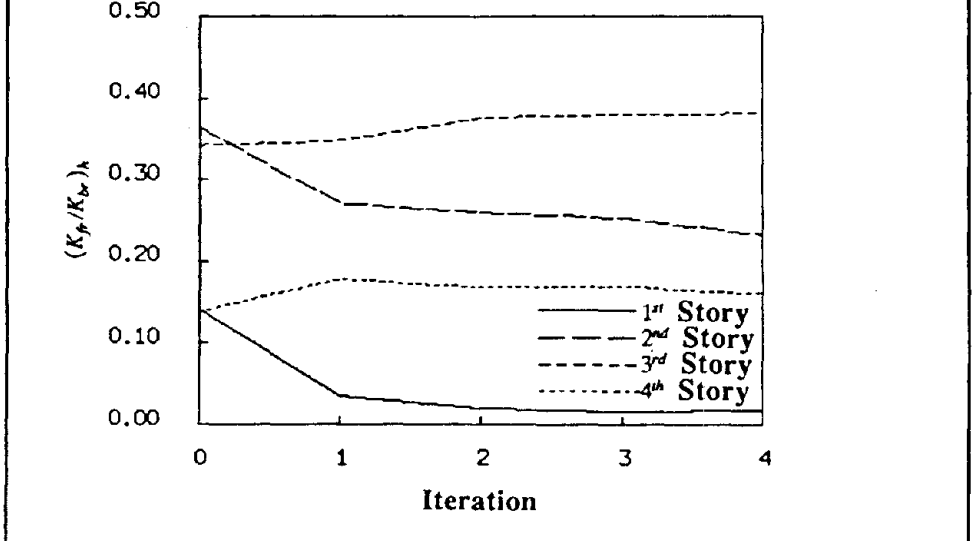

Figure 6-7-b Evolution of the frame participation ratio for the mixed set

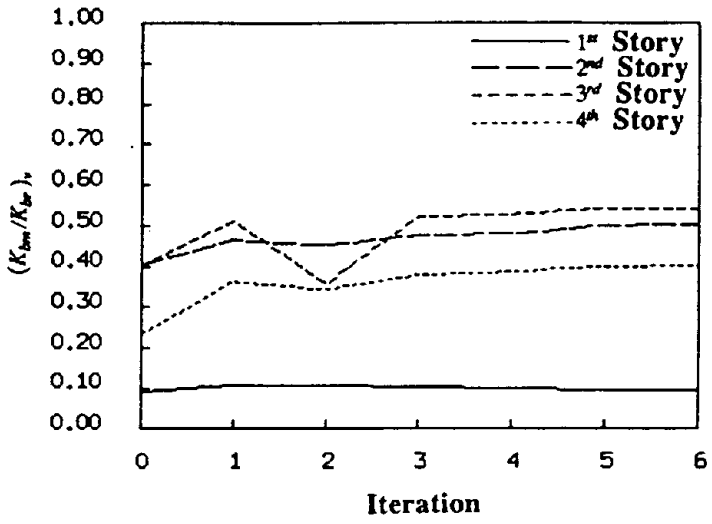

Figure 6-8-a Evolution of the beam to brace stiffness ratio for the El Centro set

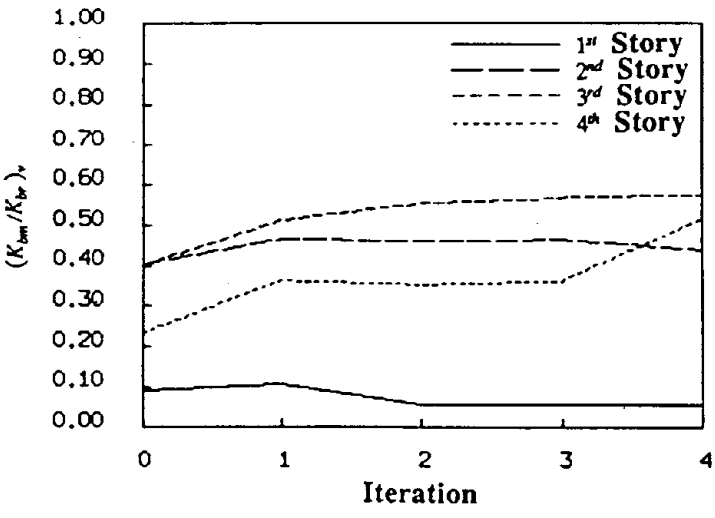

Figure 6-8-b Evolution of the beam to brace stiffness ratio for the mixed set

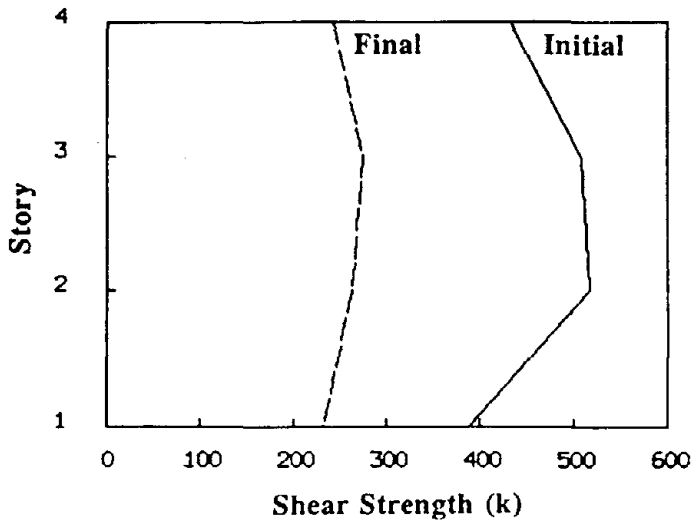

Figure 6-9-a Original and final story strength distribution for the El Centro set

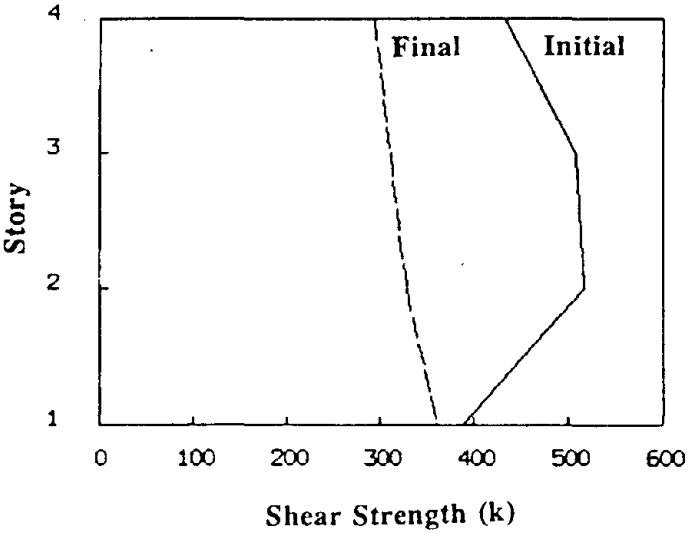

Figure 6-9-b Original and final story strength distribution for the mixed set

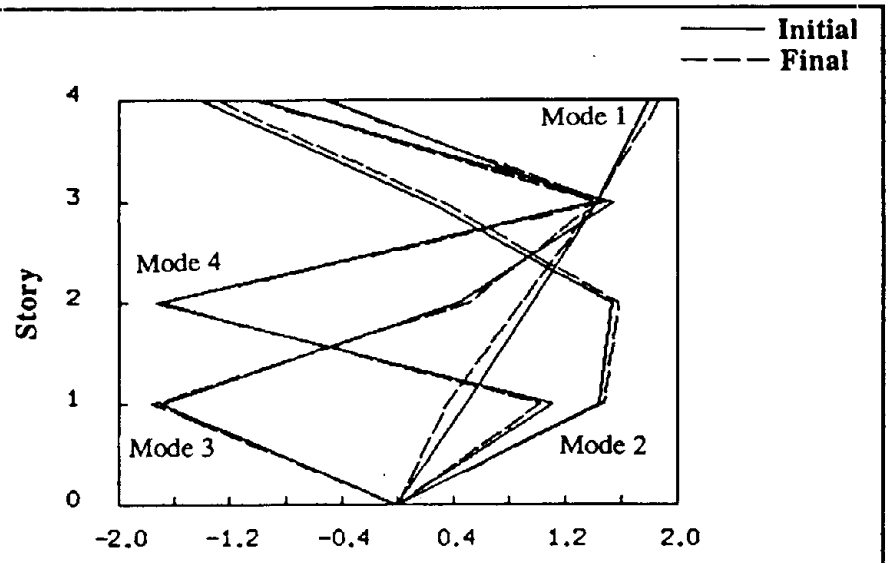

Figure 6-10-a Original and final mode shapes for the El Centro set

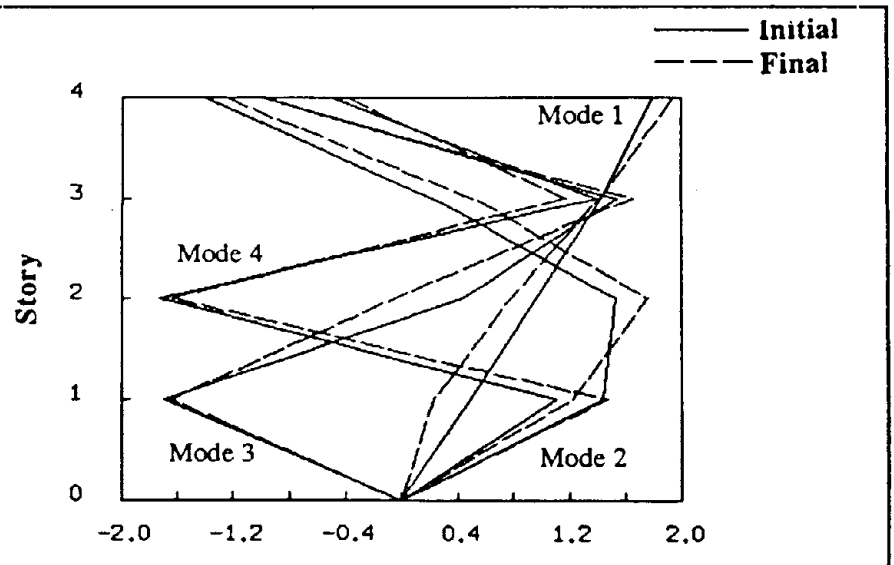

Figure 6-10-b Original and final mode shapes for the mixed set

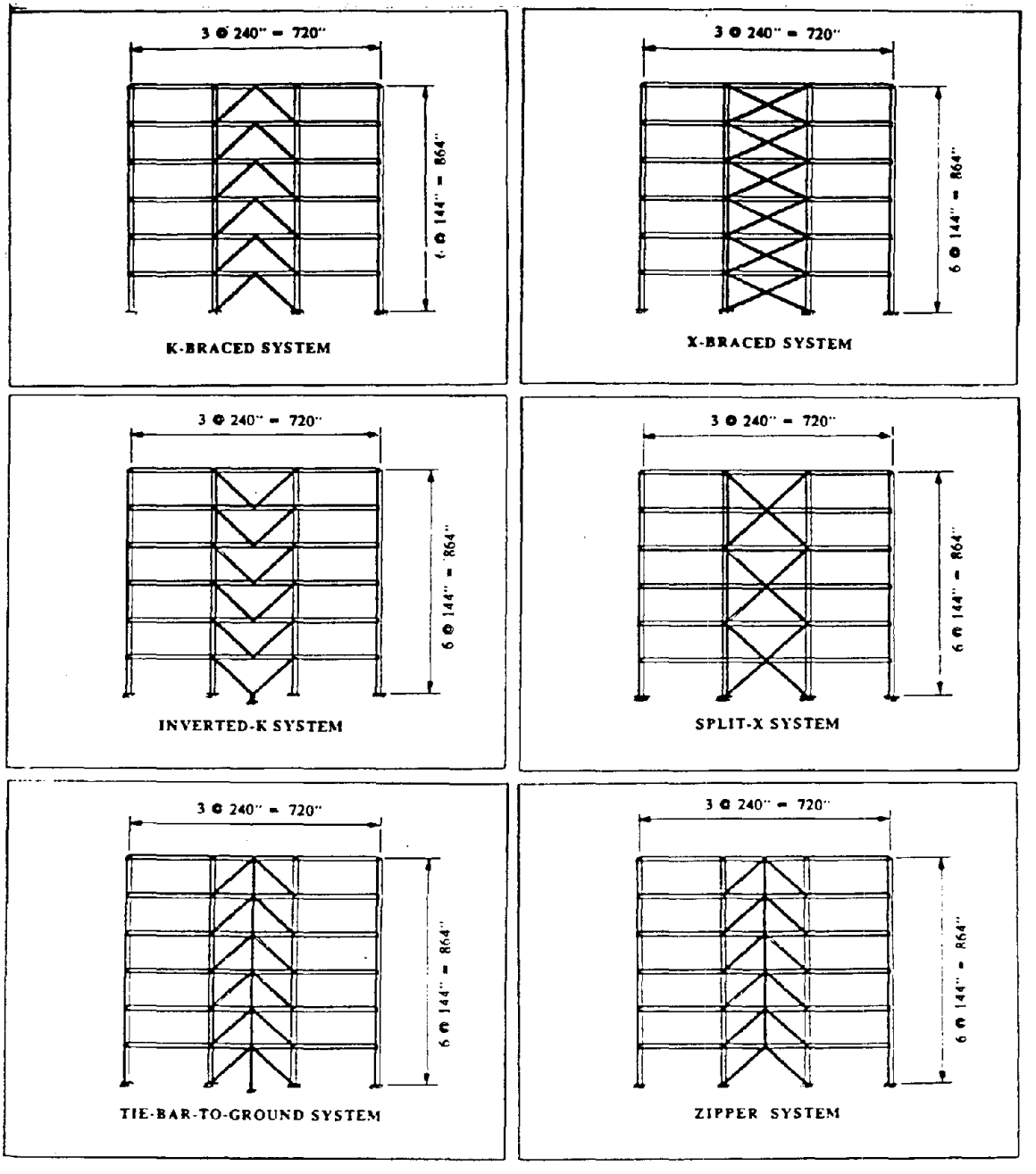

Figure 7-1 Alternative concentric bracing schemes

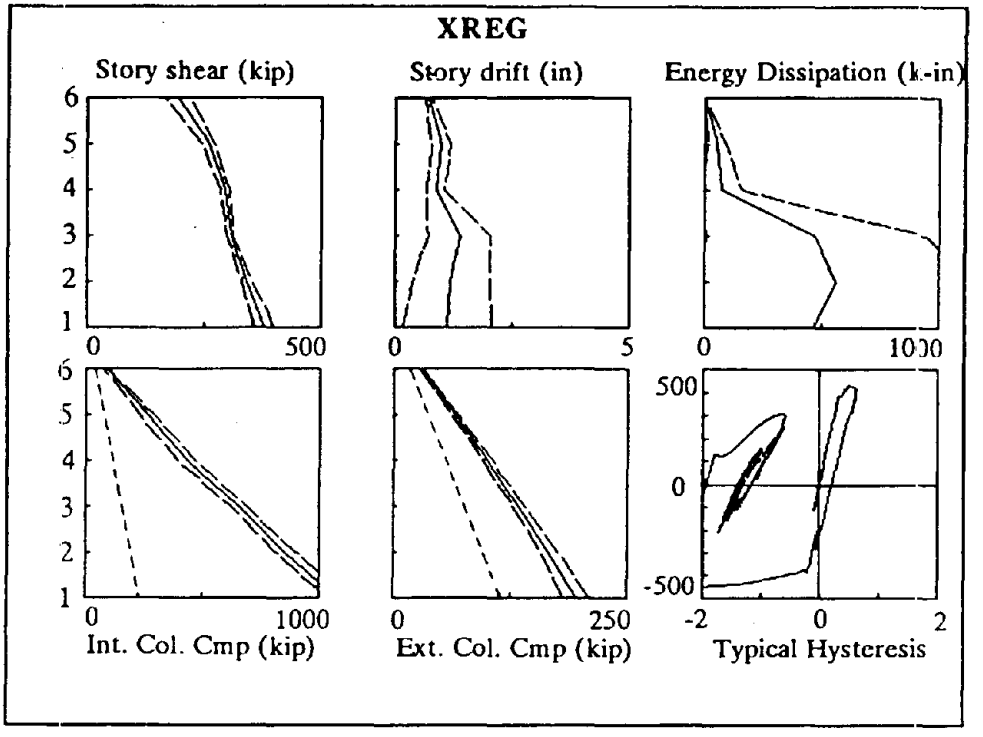

Figure 7-2: Summary of results for X-bracing

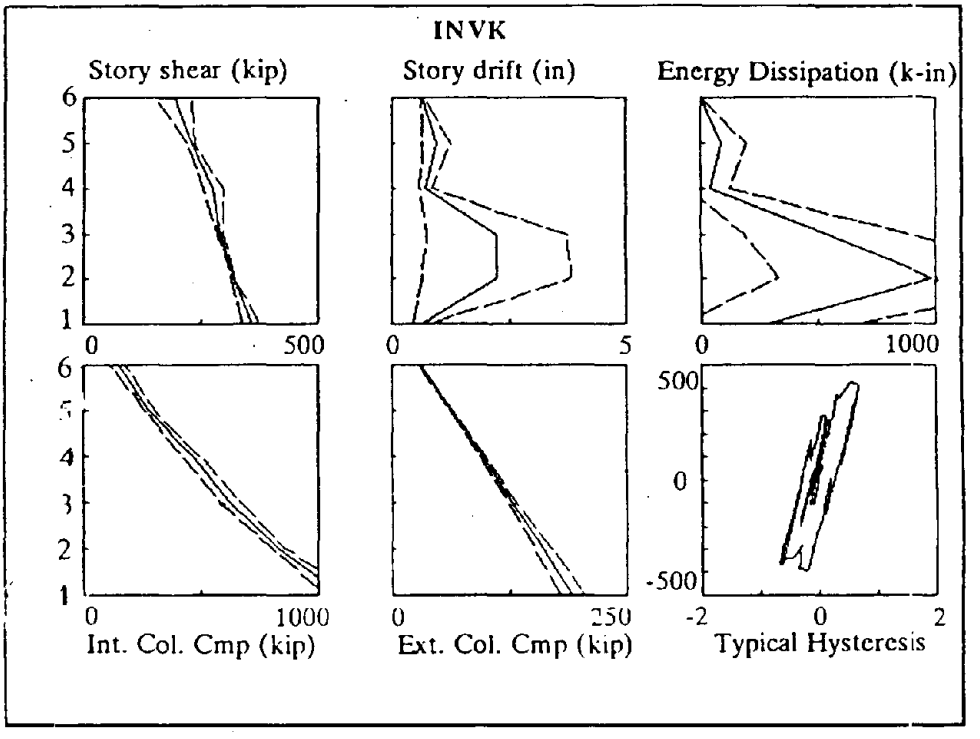

Figure 7-3: Summary of results for inverted K-bracing

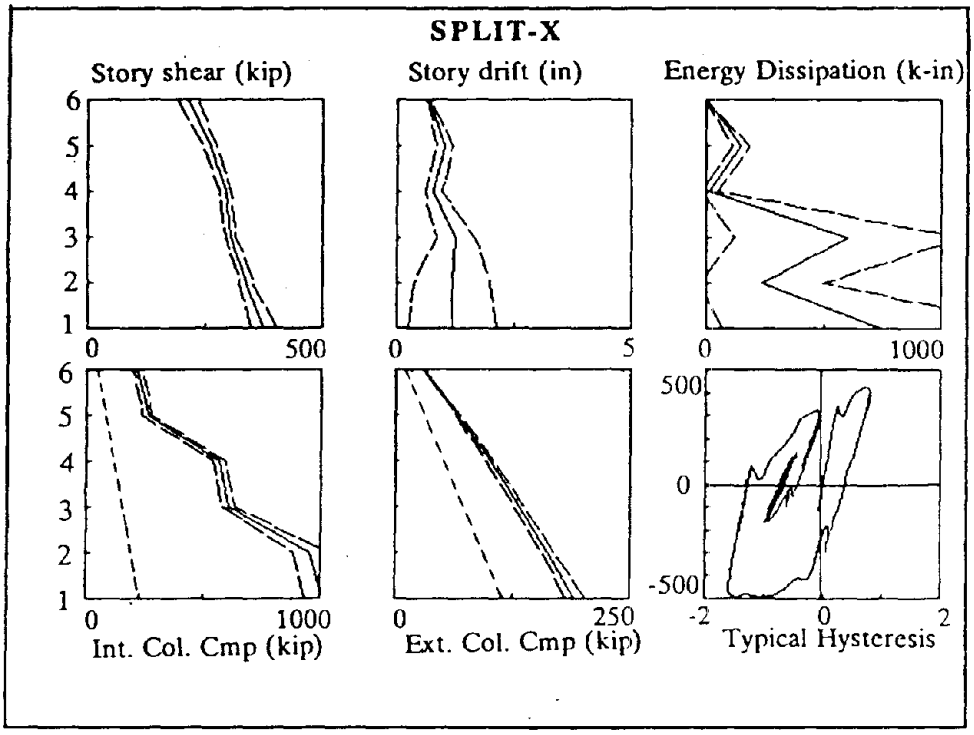

Figure 7-4: Summary of results for "split-X-bracing"

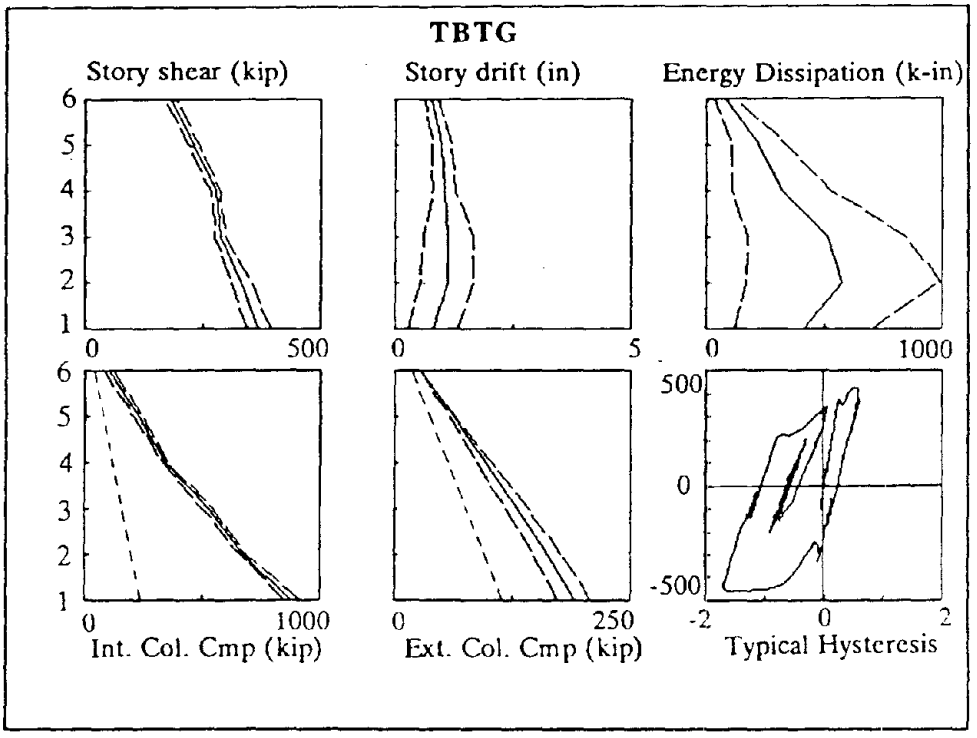

Figure 7-5: Summary of results for "Tie-Bars-To-Ground" bracing

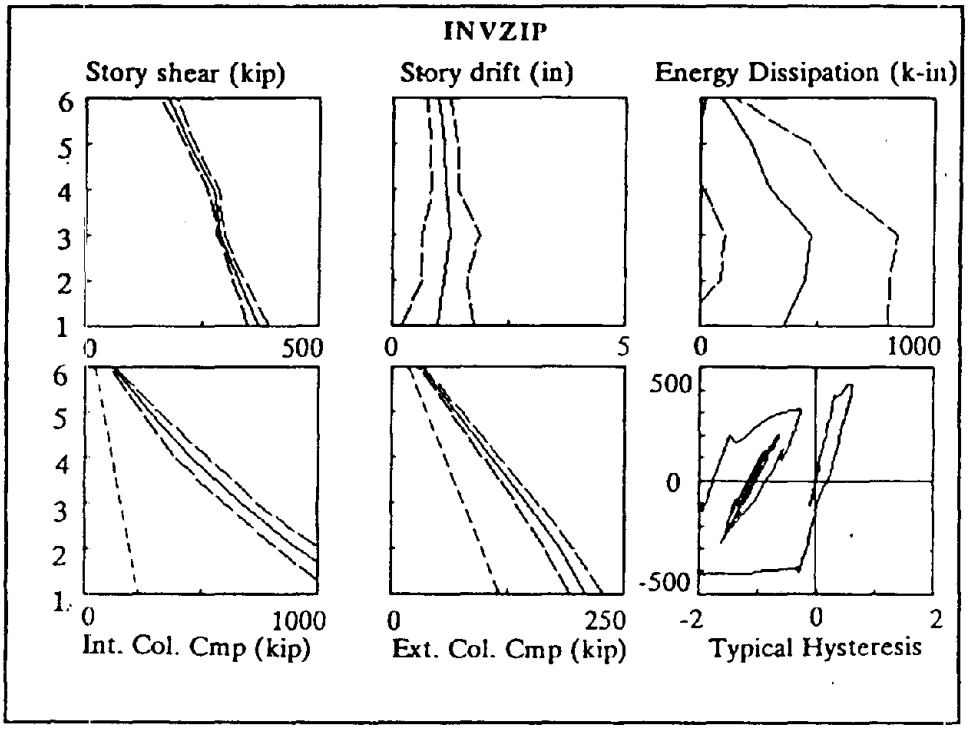

Figure 7-6: Summary of results for INVZIP bracing

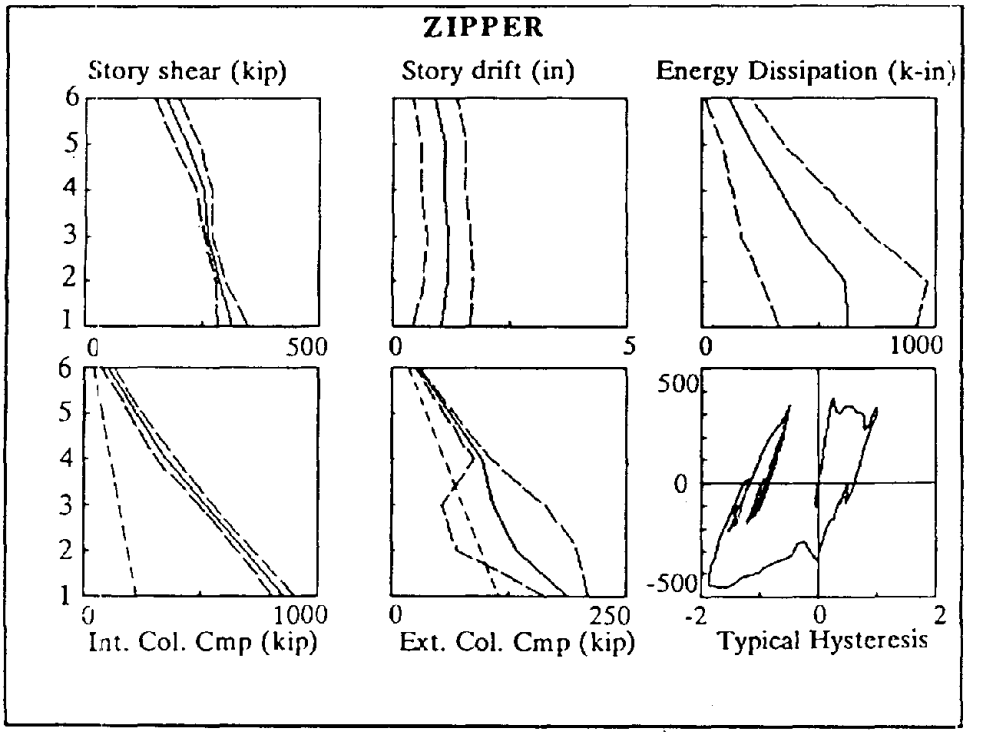

Figure 7-7: Summary of results for ZIPPER

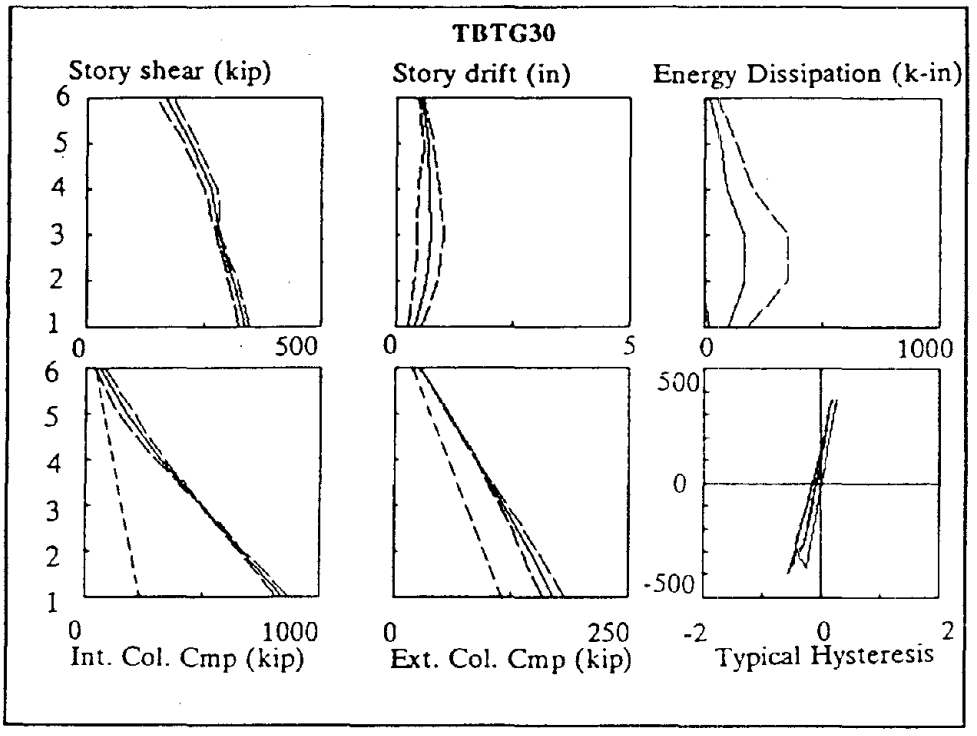

Figure 7-8: Summary of results for TBTG30 (TBTG at 0.3g)

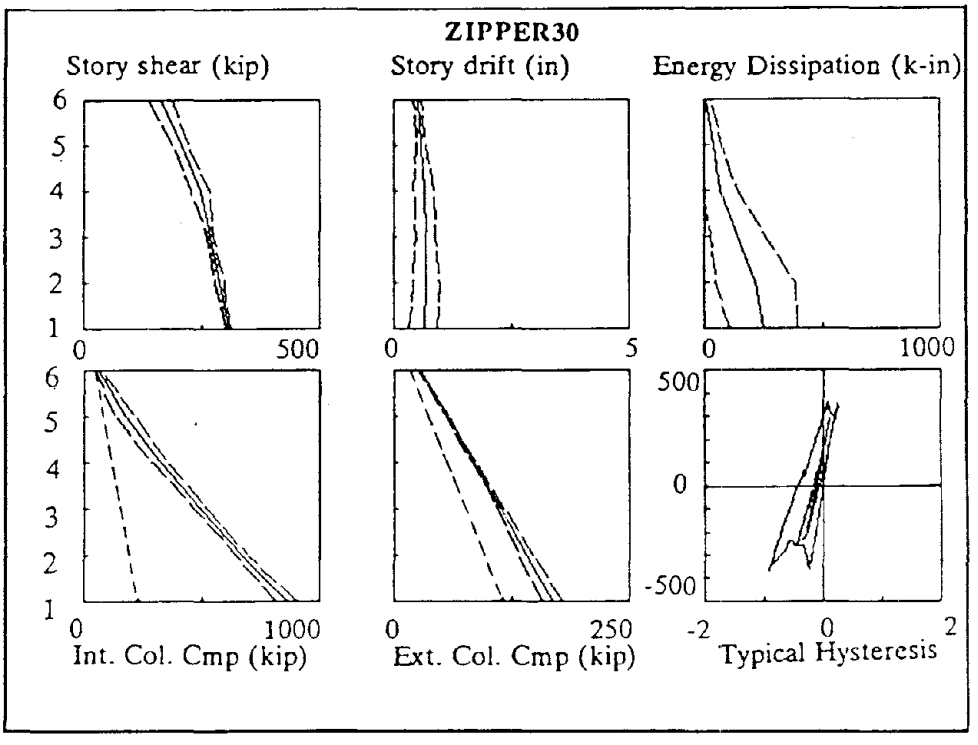

Figure 7-9: Summary of results for ZIPPER30 (ZIPPER at 0.3g)

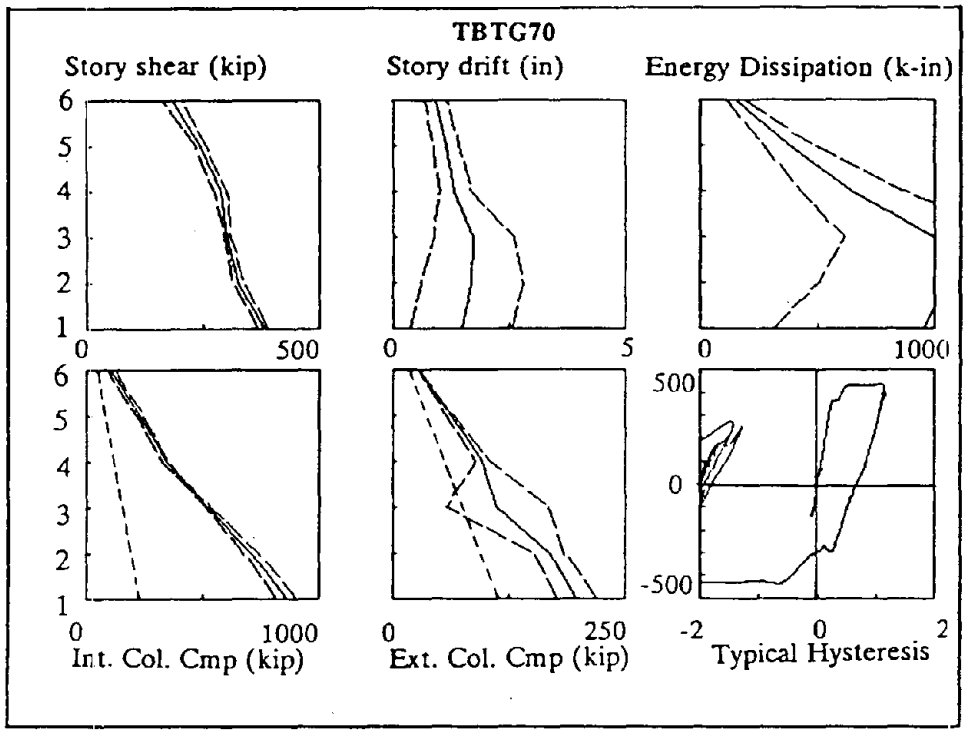

Figure 7-10: Summary of results for TBTG70 (TBTG at 0.7g)

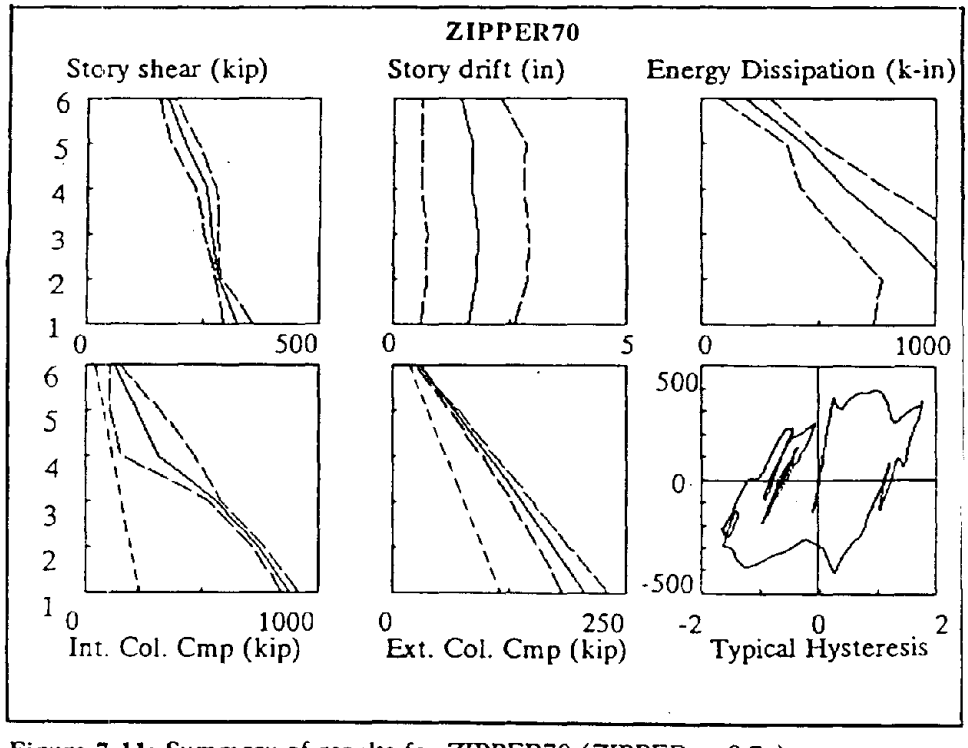

Figure 7-11: Summary of results for ZIPPER70 (ZIPPER at 0.7g)

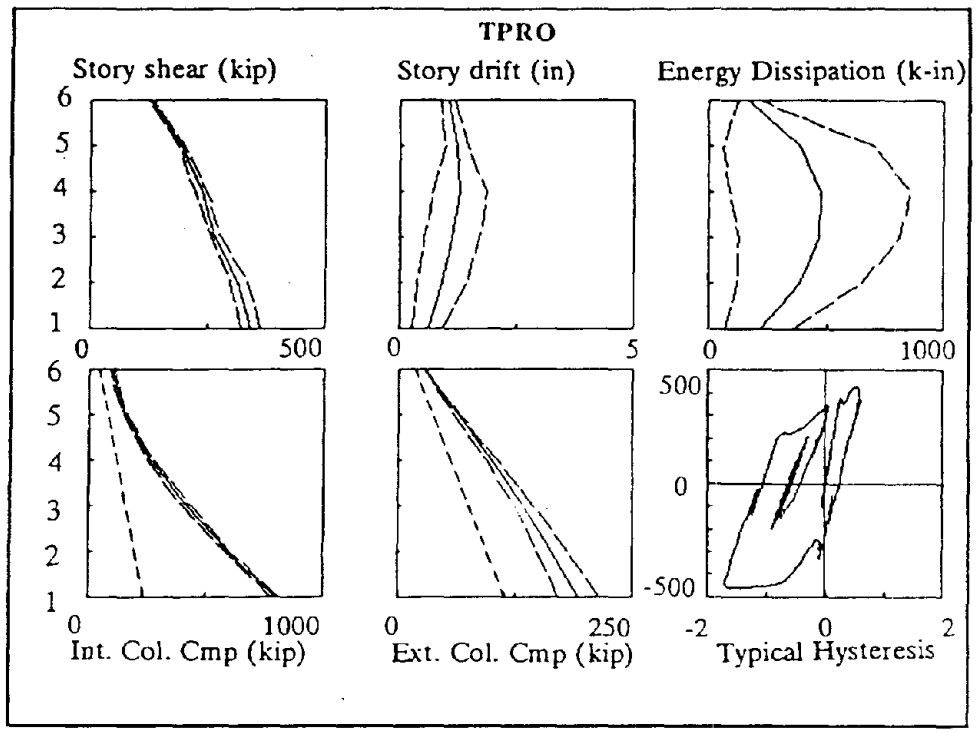

Figure 7-12: Summary of results for TPRO ("proportional braces" in TBTG)

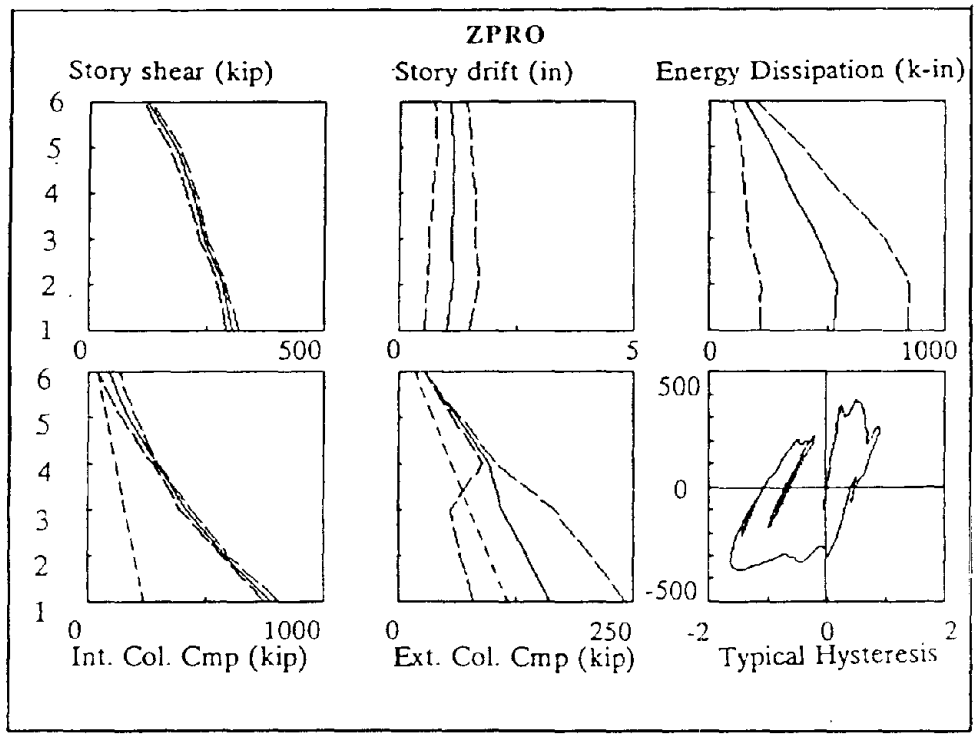

Figure 7-13: Summary of results for ZPRO ("proportional braces" in ZIPPER)

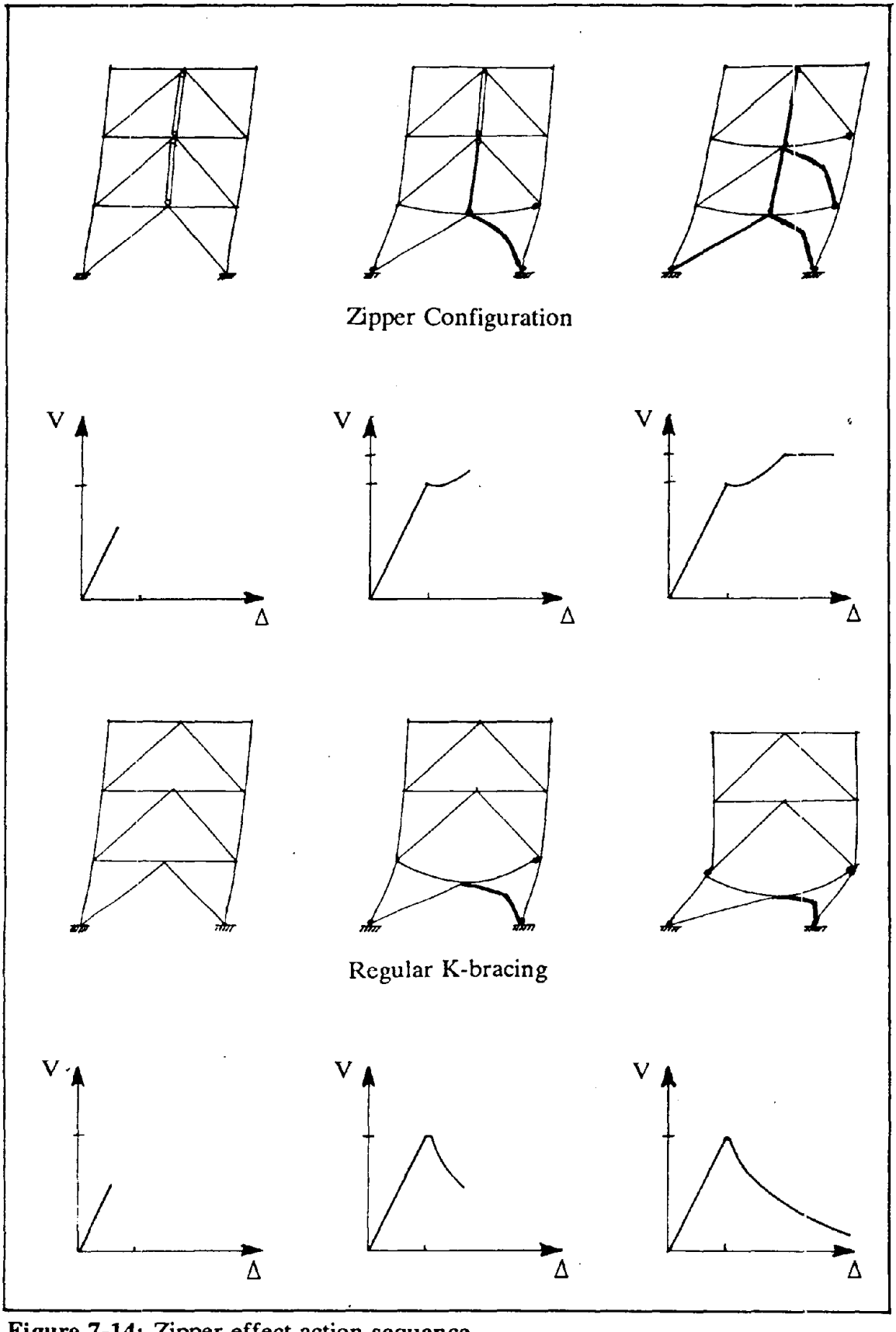

Figure 7-14: Zipper effect action sequence

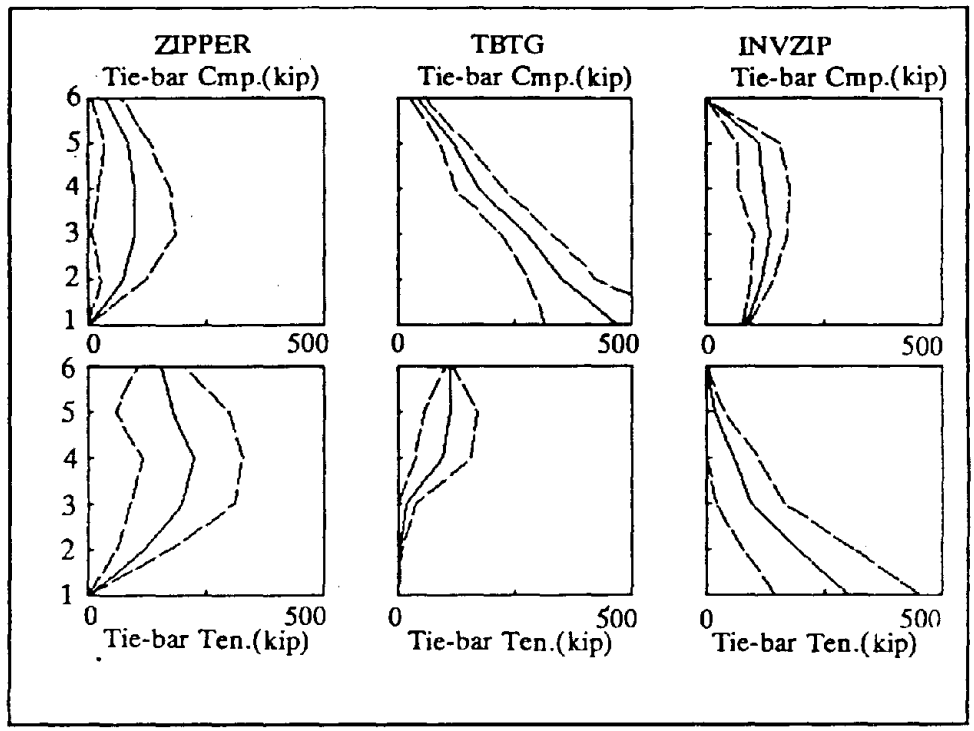

Figure 7-15-a: Distribution of tie-bar forces, part-I

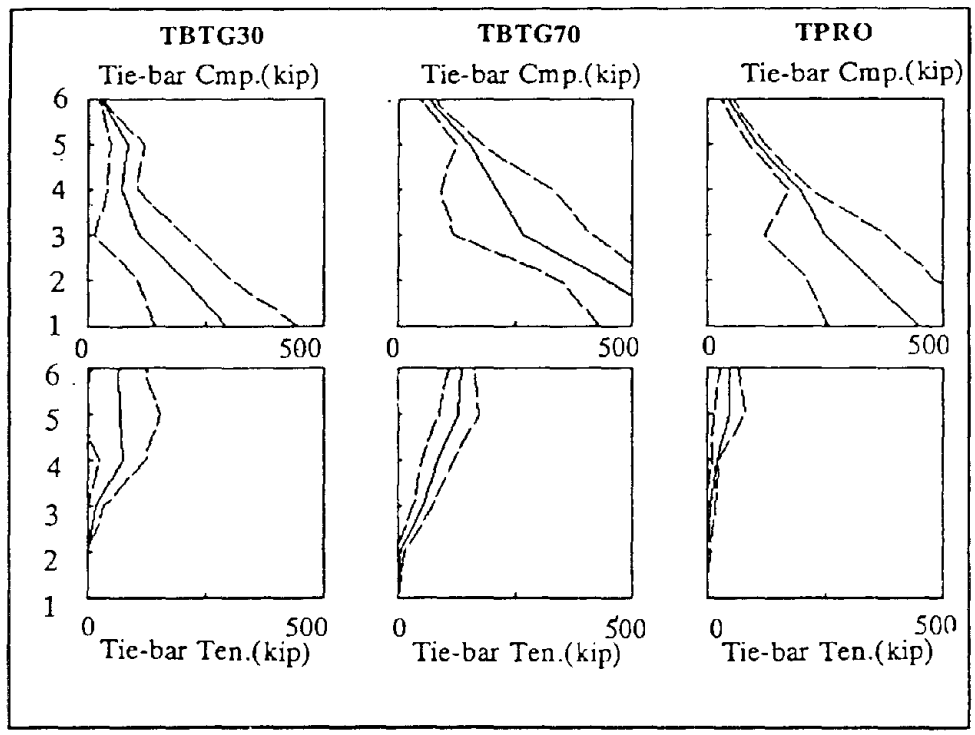

Figure 7-15-b: Distribution of tie-bar forces, part-II

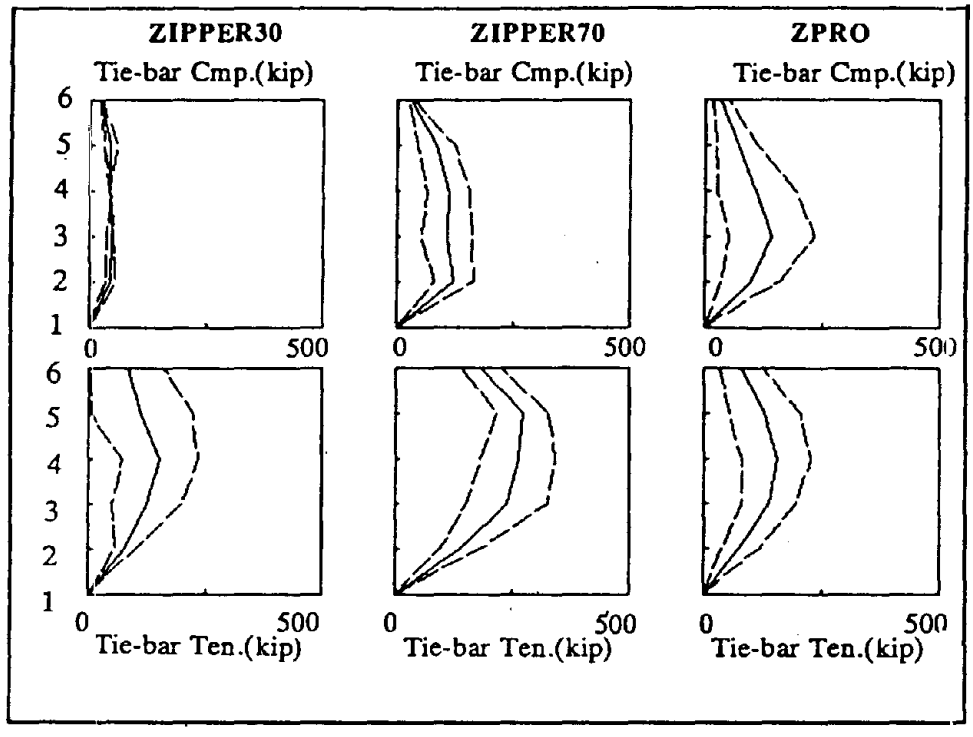

Figure 7-15-c: Distribution of tie-bar forces, part-III

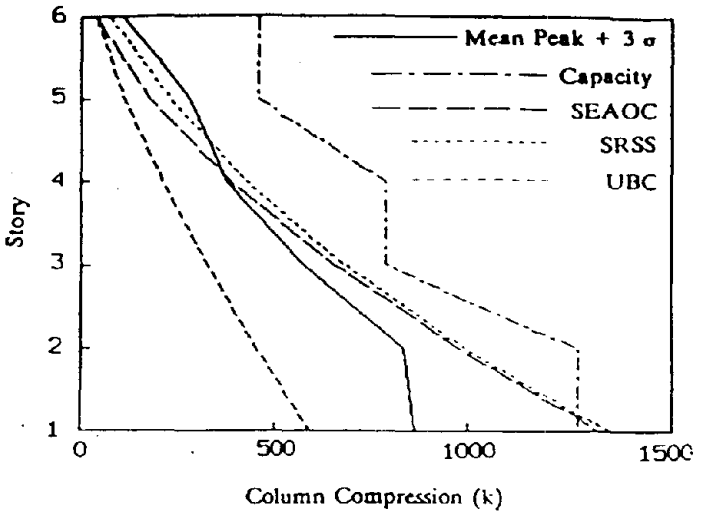

Figure B-1: Interior Column Compression for KREG

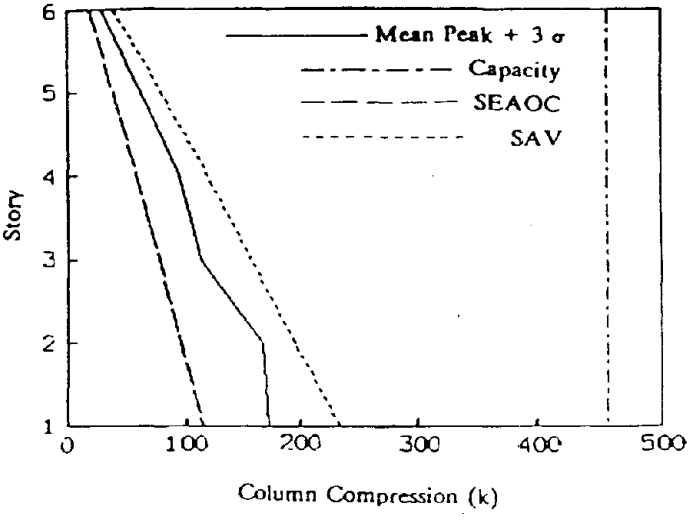

Figure B-2: Exterior Column Compression for KREG

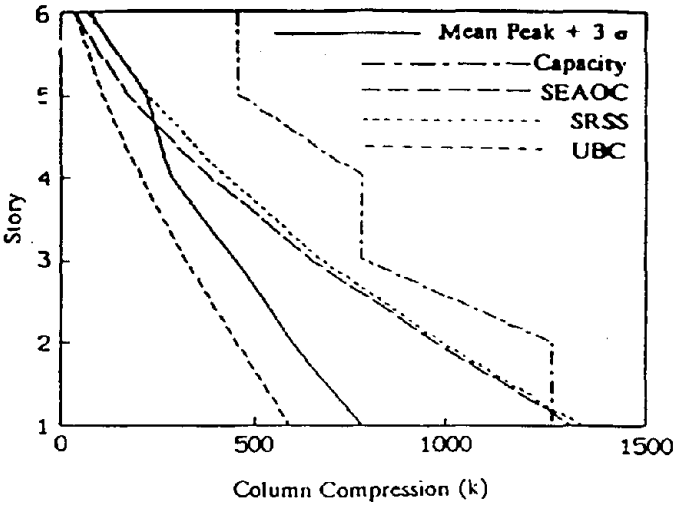

Figure B-3: Interior Column Compression for KSTO

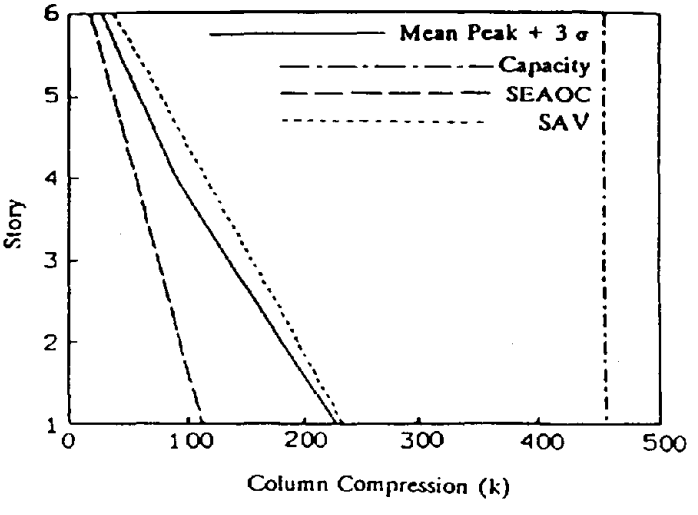

Figure B-4: Exterior Column Compression for KSTO

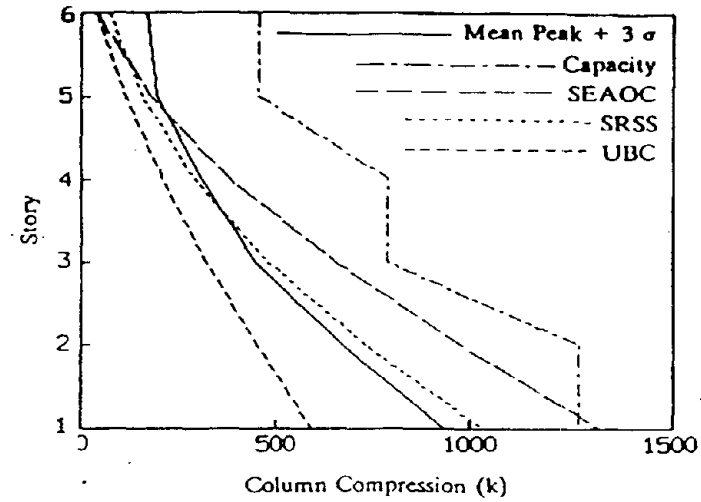

Figure B-5: Interior Column Compression for KPRO

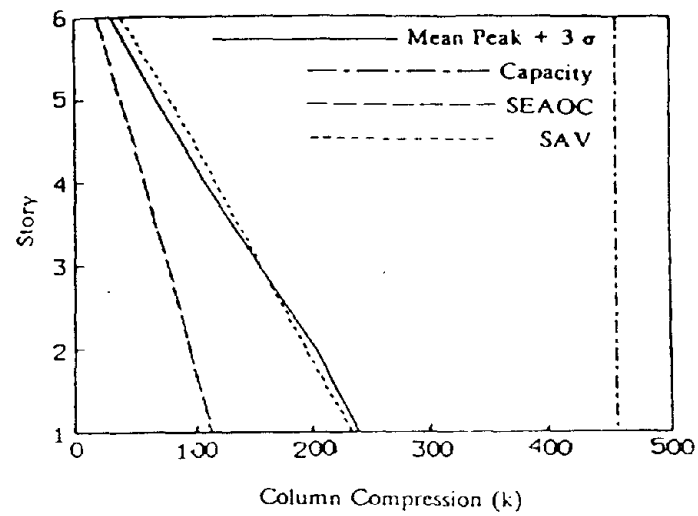

Figure B-6: Exterior Column Compression for KPRO

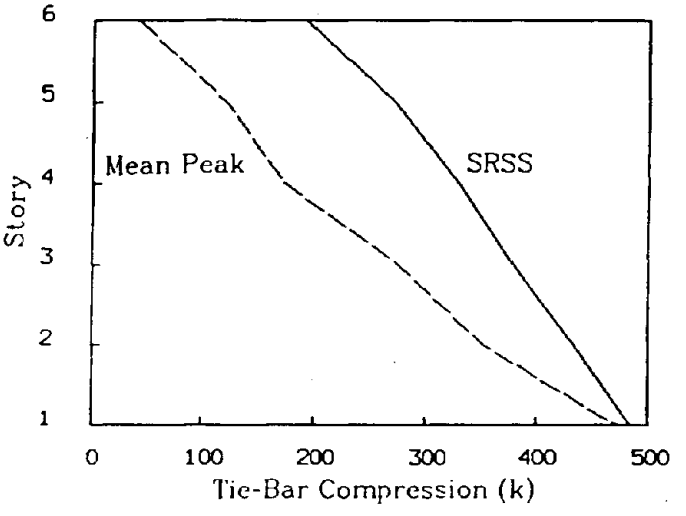

Figure C-1: Tie-Bar Compression for TBTG

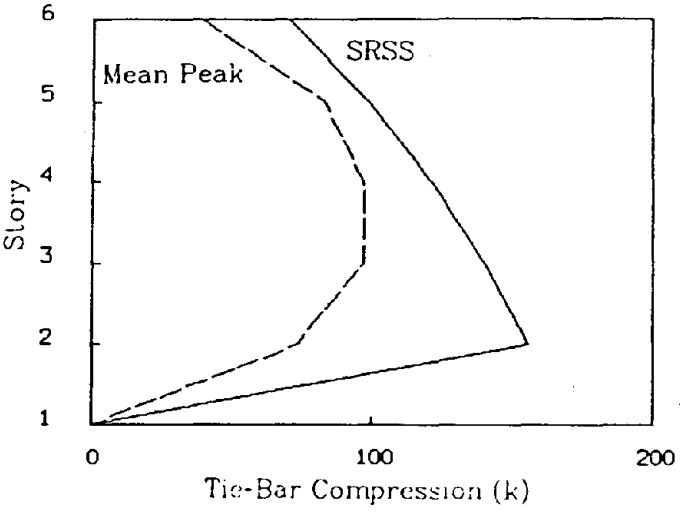

Figure C-2: Tie-Bar Compression for ZIPPER

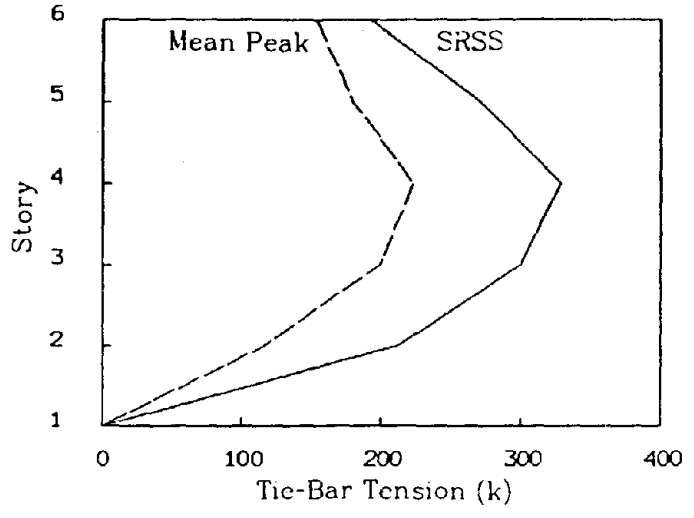

Figure C-3: Tie-Bar Tension for ZIPPER

EARTHQUAKE ENGINEERING RESEARCH CENTER REPORT SERIES

EERC reports are available from the National Information Service for Earthquake Engineering(NISEE) and from the National Technical Information Service(NTIS). Numbers in parentheses are Accession Numbers assigned by the National Technical Information Service; these are followed by a price code. Contact NTIS, 5285 Port Royal Road, Springfield Virginia, 22161 for more information. Reports without Accession Numbers were not available from NTIS at the time of printing. For a current complete list of EERC reports (from EERC 67-1) and availablity information, please contact University of California, EERC, NISEE, 1301 South 46th Street, Richmond, California 94804.

UCB/EERC-80/01 "Earthquake Response of Concrete Gravity Dams Including Hydrodynamic and Foundation Interaction Effects," by Chopra, A.K., Chakrabarti, P. and Gupta, S., January 1980, (AD-A087297)A10.

UCB/EERC-80/02 "Rocking Response of Rigid Blocks to Earthquakes," by Yim, C.S., Chopra, A.K. and Penzien, J., January 1980, (PB80 166 002)A04.

UCB/EERC-80/03 "Optimum Inelastic Design of Seismic-Resistant Reinforced Concrete Frame Structures," by Zagajeski, S.W. and Bertero, V.V., January 1980, (PB80 164 635)A06.

UCB/EERC-80/04 "Effects of Amount and Arrangement of Wall-Panel Reinforcement on Hysteretic Behavior of Reinforced Concrete Walls," by Iliya, R. and Bertero, V.V., February 1980, (PB81 122 525)A09.

UCB/EERC-80/05 "Shaking Table Research on Concrete Dam Models," by Niwa, A. and Clough, R.W., September 1980, (PB81 122 368)A06.

UCB/EERC-80/06 "The Design of Steel Energy-Absorbing Restrainers and their Incorporation into Nuclear Power Plants for Enhanced Safety (Vol 1a): Piping with Energy Absorbing Restrainers: Parameter Study on Small Systems," by Powell, G.H., Oughourlian, C. and Simons, J., June 1980.

UCB/EERC-80/07 "Inelastic Torsional Response of Structures Subjected to Earthquake Ground Motions," by Yamazaki, Y., April 1980, (PB81 122 327)A08.

UCB/EERC-80/08 "Study of X-Braced Steel Frame Structures under Earthquake Simulation," by Ghanaat, Y., April 1980, (PB81 122 335)A11.

UCB/EERC-80/09 "Hybrid Modelling of Soil-Structure Interaction," by Gupta, S., Lin, T.W. and Penzien, J., May 1980, (PB81 122 319)A07.

UCB/EERC-80/10 "General Applicability of a Nonlinear Model of a One Story Steel Frame," by Sveinsson, B.I. and McNiven, H.D., May 1980, (PB81 124 877)A06.

UCB/EERC-80/11 "A Green-Function Method for Wave Interaction with a Submerged Body," by Kioka, W., April 1980, (PB81 122 269)A07.

UCB/EERC-80/12 "Hydrodynamic Pressure and Added Mass for Axisymmetric Bodies.," by Nilrat, F., May 1980, (PB81 122 343)A08.

UCB/EERC-80/13 "Treatment of Non-Linear Drag Forces Acting on Offshore Platforms," by Dao, B.V. and Penzien, J., May 1980, (PB81 153 413)A07.

UCB/EERC-80/14 "2D Plane/Axisymmetric Solid Element (Type 3-Elastic or Elastic-Perfectly Plastic)for the ANSR-II Program," by Mondkar, D.P. and Powell, G.H., July 1980, (PB81 122 350)A03.

UCB/EERC-80/15 "A Response Spectrum Method for Random Vibrations," by Der Kiureghian, A., June 1981, (PB81 122 301)A03.

UCB/EERC-80/16 "Cyclic Inelastic Buckling of Tubular Steel Braces," by Zayas, V.A., Popov, E.P. and Mahin, S.A., June 1981, (PB81 124 885)A10.

UCB/EERC-80/17 "Dynamic Response of Simple Arch Dams Including Hydrodynamic Interaction," by Porter, C.S. and Chopra, A.K., July 1981, (PB81 124 000)A13.

UCB/EERC-80/18 "Experimental Testing of a Friction Damped Aseismic Base Isolation System with Fail-Safe Characteristics," by Kelly, J.M., Beucke, K.E. and Skinner, M.S., July 1980, (PB81 148 595)A04.

UCB/EERC-80/19 "The Design of Steel Energy-Absorbing Restrainers and their Incorporation into Nuclear Power Plants for Enhanced Safety (Vol.1B): Stochastic Seismic Analyses of Nuclear Power Plant Structures and Piping Systems Subjected to Multiple Supported Excitations," by Lee, M.C. and Penzien, J., June 1980, (PB82 201 872)A08.

UCB/EERC-80/20 "The Design of Steel Energy-Absorbing Restrainers and their Incorporation into Nuclear Power Plants for Enhanced Safety (Vol 1C): Numerical Method for Dynamic Substructure Analysis," by Dickens, J.M. and Wilson, E.L., June 1980.

UCB/EERC-80/21 "The Design of Steel Energy-Absorbing Restrainers and their Incorporation into Nuclear Power Plants for Enhanced Safety (Vol 2): Development and Testing of Restraints for Nuclear Piping Systems," by Kelly, J.M. and Skinner, M.S., June 1980.

UCB/EERC-80/22 "3D Solid Element (Type 4-Elastic or Elastic-Perfectly-Plastic) for the ANSR-II Program," by Mondkar, D.P. and Powell, G.H., July 1980, (PB81 123 242)A03.

UCB/EERC-80/23 "Gap-Friction Element (Type 5) for the Ansr-II Program," by Mondkar, D.P. and Powell, G.H., July 1980, (PB81 122 285)A03.

UCB/EERC-80/24 "U-Bar Restraint Element (Type 11) for the ANSR-II Program," by Oughourlian, C. and Powell, G.H., July 1980, (PB81 122 293)A03.

UCB/EERC-80/25 "Testing of a Natural Rubber Base Isolation System by an Explosively Simulated Earthquake," by Kelly, J.M., August 1980, (PB81 201 360)A04.

UCB/EERC-80/26 "Input Identification from Structural Vibrational Response," by Hu, Y., August 1980, (PB81 152 308)A05.

UCB/EERC-80/27 "Cyclic Inelastic Behavior of Steel Offshore Structures," by Zayas, V.A., Mahin, S.A. and Popov, E.P., August 1980, (PB81 196 180)A15.

UCB/EERC-80/28 "Shaking Table Testing of a Reinforced Concrete Frame with Biaxial Response," by Oliva, M.G., October 1980, (PB81 154 304)A10.

UCB/EERC-80/29 "Dynamic Properties of a Twelve-Story Prefabricated Panel Building," by Bouwkamp, J.G., Kollegger, J.P. and Stephen, R.M., October 1980, (PB82 138 777)A07.

UCB/EERC-80/30 "Dynamic Properties of an Eight-Story Prefabricated Panel Building," by Bouwkamp, J.G., Kollegger, J.P. and Stephen, R.M., October 1980, (PB81 200 313)A05.

UCB/EERC-80/31 "Predictive Dynamic Response of Panel Type Structures under Earthquakes," by Kollegger, J.P. and Bouwkamp, J.G., October 1980, (PB81 152 316)A04.

UCB/EERC-80/32 "The Design of Steel Energy-Absorbing Restrainers and their Incorporation into Nuclear Power Plants for Enhanced Safety (Vol 3): Testing of Commercial Steels in Low-Cycle Torsional Fatigue," by Spanner, P., Parker, E.R., Jongewaard, E. and Dory, M., 1980.

UCB/EERC-80/33 "The Design of Steel Energy-Absorbing Restrainers and their Incorporation into Nuclear Power Plants for Enhanced Safety (Vol 4): Shaking Table Tests of Piping Systems with Energy-Absorbing Restrainers," by Stiemer, S.F. and Godden, W.G., September 1980, (PB82 201 880)A05.

UCB/EERC-80/34 "The Design of Steel Energy-Absorbing Restrainers and their Incorporation into Nuclear Power Plants for Enhanced Safety (Vol 5): Summary Report," by Spencer, P., 1980.

UCB/EERC-80/35 "Experimental Testing of an Energy-Absorbing Base Isolation System," by Kelly, J.M., Skinner, M.S. and Beucke, K.E., October 1980, (PB81 154 072)A04.

UCB/EERC-80/36 "Simulating and Analyzing Artificial Non-Stationary Earth Ground Motions," by Nau, R.F., Oliver, R.M. and Pister, K.S., October 1980, (PB81 153 397)A04.

UCB/EERC-80/37 "Earthquake Engineering at Berkeley - 1980," by , September 1980, (PB81 205 674)A09.

UCB/EERC-80/38 "Inelastic Seismic Analysis of Large Panel Buildings," by Schricker, V. and Powell, G.H., September 1980, (PB81 154 338)A13.

UCB/EERC-80/39 "Dynamic Response of Embankment, Concrete-Gavity and Arch Dams Including Hydrodynamic Interation," by Hall, J.F. and Chopra, A.K., October 1980, (PB81 152 324)A11.

UCB/EERC-80/40 "Inelastic Buckling of Steel Struts under Cyclic Load Reversal.," by Black, R.G., Wenger, W.A. and Popov, E.P., October 1980, (PB81 154 312)A08.

UCB/EERC-80/41 "Influence of Site Characteristics on Buildings Damage during the October 3,1974 Lima Earthquake," by Repetto, P., Arango, I. and Seed, H.B., September 1980, (PB81 161 739)A05.

UCB/EERC-80/42 "Evaluation of a Shaking Table Test Program on Response Behavior of a Two Story Reinforced Concrete Frame," by Blondet, J.M., Clough, R.W. and Mahin, S.A., December 1980, (PB82 196 544)A11.

UCB/EERC-80/43 "Modelling of Soil-Structure Interaction by Finite and Infinite Elements," by Medina, F., December 1980, (PB81 229 270)A04.

UCB/EERC-81/01 "Control of Seismic Response of Piping Systems and Other Structures by Base Isolation," by Kelly, J.M., January 1981, (PB81 200 735)A05.

UCB/EERC-81/02 "OPTNSR- An Interactive Software System for Optimal Design of Statically and Dynamically Loaded Structures with Nonlinear Response," by Bhatti, M.A., Ciampi, V. and Pister, K.S., January 1981, (PB81 218 851)A09.

UCB/EERC-81/03 "Analysis of Local Variations in Free Field Seismic Ground Motions," by Chen, J.-C., Lysmer, J. and Seed, H.B., January 1981, (AD-A099508)A13.

UCB/EERC-81/04 "Inelastic Structural Modeling of Braced Offshore Platforms for Seismic Loading," by Zayas, V.A., Shing, P.-S.B., Mahin, S.A. and Popov, E.P., January 1981, (PB82 138 777)A07.

UCB/EERC-81/05 "Dynamic Response of Light Equipment in Structures," by Der Kiureghian, A., Sackman, J.L. and Nour-Omid, B., April 1981, (PB81 218 497)A04.

UCB/EERC-81/06 "Preliminary Experimental Investigation of a Broad Base Liquid Storage Tank," by Bouwkamp, J.G., Kollegger, J.P. and Stephen, R.M., May 1981, (PB82 140 385)A03.

UCB/EERC-81/07 "The Seismic Resistant Design of Reinforced Concrete Coupled Structural Walls," by Aktan, A.E. and Bertero, V.V., June 1981, (PB82 113 358)A11.

UCB/EERC-81/08 "Unassigned," by Unassigned, 1981.

UCB/EERC-81/09 "Experimental Behavior of a Spatial Piping System with Steel Energy Absorbers Subjected to a Simulated Differential Seismic Input," by Stiemer, S.F., Godden, W.G. and Kelly, J.M., July 1981, (PB82 201 898)A04.

UCB/EERC-81/10 "Evaluation of Seismic Design Provisions for Masonry in the United States," by Sveinsson, B.I., Mayes, R.L. and McNiven, H.D., August 1981, (PB82 166 075)A08.

UCB/EERC-81/11 "Two-Dimensional Hybrid Modelling of Soil-Structure Interaction," by Tzong, T.-J., Gupta, S. and Penzien, J., August 1981, (PB82 142 118)A04.

UCB/EERC-81/12 "Studies on Effects of Infills in Seismic Resistant R/C Construction," by Brokken, S. and Bertero, V.V., October 1981, (PB82 166 190)A09.

UCB/EERC-81/13 "Linear Models to Predict the Nonlinear Seismic Behavior of a One-Story Steel Frame," by Valdimarsson, H., Shah, A.H. and McNiven, H.D., September 1981, (PB82 138 793)A07.

UCB/EERC-81/14 "TLUSH: A Computer Program for the Three-Dimensional Dynamic Analysis of Earth Dams," by Kagawa, T., Mejia, L.H., Seed, H.B. and Lysmer, J., September 1981, (PB82 139 940)A06.

UCB/EERC-81/15 "Three Dimensional Dynamic Response Analysis of Earth Dams," by Mejia, L.H. and Seed, H.B., September 1981, (PB82 137 274)A12.

UCB/EERC-81/16 "Experimental Study of Lead and Elastomeric Dampers for Base Isolation Systems," by Kelly, J.M. and Hodder, S.B., October 1981, (PB82 166 182)A05.

UCB/EERC-81/17 "The Influence of Base Isolation on the Seismic Response of Light Secondary Equipment," by Kelly, J.M., April 1981, (PB82 255 266)A04.

UCB/EERC-81/18 "Studies on Evaluation of Shaking Table Response Analysis Procedures," by Blondet, J. M., November 1981, (PB82 197 278)A10.

UCB/EERC-81/19 "DELIGHT.STRUCT: A Computer-Aided Design Environment for Structural Engineering," by Balling, R.J., Pister, K.S. and Polak, E., December 1981, (PB82 218 496)A07.

UCB/EERC-81/20 "Optimal Design of Seismic-Resistant Planar Steel Frames," by Balling, R.J., Ciampi, V. and Pister, K.S., December 1981, (PB82 220 179)A07.

UCB/EERC-82/01 "Dynamic Behavior of Ground for Seismic Analysis of Lifeline Systems," by Sato, T. and Der Kiureghian, A., January 1982, (PB82 218 926)A05.

UCB/EERC-82/02 "Shaking Table Tests of a Tubular Steel Frame Model," by Ghanaat, Y. and Clough, R.W., January 1982, (PB82 220 161)A07.

UCB/EERC-82/03 "Behavior of a Piping System under Seismic Excitation: Experimental Investigations of a Spatial Piping System supported by Mechanical Shock Arrestors," by Schneider, S., Lee, H.-M. and Godden, W. G., May 1982, (PB83 172 544)A09.

UCB/EERC-82/04 "New Approaches for the Dynamic Analysis of Large Structural Systems," by Wilson, E.L., June 1982, (PB83 148 080)A05.

UCB/EERC-82/05 "Model Study of Effects of Damage on the Vibration Properties of Steel Offshore Platforms," by Shahrivar, F. and Bouwkamp, J.G., June 1982, (PB83 148 742)A10.

UCB/EERC-82/06 "States of the Art and Pratice in the Optimum Seismic Design and Analytical Response Prediction of R/C Frame Wall Structures," by Aktan, A.E. and Bertero, V.V., July 1982, (PB83 147 736)A05.

UCB/EERC-82/07 "Further Study of the Earthquake Response of a Broad Cylindrical Liquid-Storage Tank Model," by Manos, G.C. and Clough, R.W., July 1982, (PB83 147 744)A11.

UCB/EERC-82/08 "An Evaluation of the Design and Analytical Seismic Response of a Seven Story Reinforced Concrete Frame," by Charney, F.A. and Bertero, V.V., July 1982, (PB83 157 628)A09.

UCB/EERC-82/09 "Fluid-Structure Interactions: Added Mass Computations for Incompressible Fluid," by Kuo, J.S.-H., August 1982, (PB83 156 281)A07.

UCB/EERC-82/10 "Joint-Opening Nonlinear Mechanism: Interface Smeared Crack Model," by Kuo, J.S.-H., August 1982, (PB83 149 195)A05.

UCB/EERC-82/11 "Dynamic Response Analysis of Techi Dam," by Clough, R.W., Stephen, R.M. and Kuo, J.S.-H., August 1982, (PB83 147 496)A06.

UCB/EERC-82/12 "Prediction of the Seismic Response of R/C Frame-Coupled Wall Structures," by Aktan, A.E., Bertero, V.V. and Piazzo, M., August 1982, (PB83 149 203)A09.

UCB/EERC-82/13 "Preliminary Report on the Smart 1 Strong Motion Array in Taiwan," by Bolt, B.A., Loh, C.H., Penzien, J. and Tsai, Y.B., August 1982, (PB83 159 400)A10.

UCB/EERC-82/14 "Shaking-Table Studies of an Eccentrically X-Braced Steel Structure," by Yang, M.S., September 1982, (PB83 260 778)A12.

UCB/EERC-82/15 "The Performance of Stairways in Earthquakes," by Roha, C., Axley, J.W. and Bertero, V.V., September 1982, (PB83 157 693)A07.

UCB/EERC-82/16 "The Behavior of Submerged Multiple Bodies in Earthquakes," by Liao, W.-G., September 1982, (PB83 158 709)A07.

UCB/EERC-82/17 "Effects of Concrete Types and Loading Conditions on Local Bond-Slip Relationships," by Cowell, A.D., Popov, E.P. and Bertero, V.V., September 1982, (PB83 153 577)A04.

UCB/EERC-82/18 "Mechanical Behavior of Shear Wall Vertical Boundary Members: An Experimental Investigation," by Wagner, M.T. and Bertero, V.V., October 1982, (PB83 159 764)A05.

UCB/EERC-82/19 "Experimental Studies of Multi-support Seismic Loading on Piping Systems," by Kelly, J.M. and Cowell, A.D., November 1982.

UCB/EERC-82/20 "Generalized Plastic Hinge Concepts for 3D Beam-Column Elements," by Chen, P. F.-S. and Powell, G.H., November 1982, (PB83 247 981)A13.

UCB/EERC-82/21 "ANSR-II: General Computer Program for Nonlinear Structural Analysis," by Oughourlian, C.V. and Powell, G.H., November 1982, (PB83 251 330)A12.

UCB/EERC-82/22 "Solution Strategies for Statically Loaded Nonlinear Structures," by Simons, J.W. and Powell, G.H., November 1982, (PB83 197 970)A06.

UCB/EERC-82/23 "Analytical Model of Deformed Bar Anchorages under Generalized Excitations," by Ciampi, V., Eligehausen, R., Bertero, V.V. and Popov, E.P., November 1982, (PB83 169 532)A06.

UCB/EERC-82/24 "A Mathematical Model for the Response of Masonry Walls to Dynamic Excitations," by Sucuoglu, H., Mengi, Y. and McNiven, H.D., November 1982, (PB83 169 011)A07.

UCB/EERC-82/25 "Earthquake Response Considerations of Broad Liquid Storage Tanks," by Cambra, F.J., November 1982, (PB83 251 215)A09.

UCB/EERC-82/26 "Computational Models for Cyclic Plasticity, Rate Dependence and Creep," by Mosaddad, B. and Powell, G.H., November 1982, (PB83 245 829)A08.

UCB/EERC-82/27 "Inelastic Analysis of Piping and Tubular Structures," by Mahasuverachai, M. and Powell, G.H., November 1982, (PB83 249 987)A07.

UCB/EERC-83/01 "The Economic Feasibility of Seismic Rehabilitation of Buildings by Base Isolation," by Kelly, J.M., January 1983, (PB83 197 988)A05.

UCB/EERC-83/02 "Seismic Moment Connections for Moment-Resisting Steel Frames.," by Popov, E.P., January 1983, (PB83 195 412)A04.

UCB/EERC-83/03 "Design of Links and Beam-to-Column Connections for Eccentrically Braced Steel Frames," by Popov, E.P. and Malley, J.O., January 1983, (PB83 194 811)A04.

UCB/EERC-83/04 "Numerical Techniques for the Evaluation of Soil-Structure Interaction Effects in the Time Domain," by Bayo, E. and Wilson, E.L., February 1983, (PB83 245 605)A09.

UCB/EERC-83/05 "A Transducer for Measuring the Internal Forces in the Columns of a Frame-Wall Reinforced Concrete Structure," by Sause, R. and Bertero, V.V., May 1983, (PB84 119 494)A06.

UCB/EERC-83/06 "Dynamic Interactions Between Floating Ice and Offshore Structures," by Croteau, P., May 1983, (PB84 119 486)A16.

UCB/EERC-83/07 "Dynamic Analysis of Multiply Tuned and Arbitrarily Supported Secondary Systems," by Igusa, T. and Der Kiureghian, A., July 1983, (PB84 118 272)A11.

UCB/EERC-83/08 "A Laboratory Study of Submerged Multi-body Systems in Earthquakes," by Ansari, G.R., June 1983, (PB83 261 842)A17.

UCB/EERC-83/09 "Effects of Transient Foundation Uplift on Earthquake Response of Structures," by Yim, C.-S. and Chopra, A.K., June 1983, (PB83 261 396)A07.

UCB/EERC-83/10 "Optimal Design of Friction-Braced Frames under Seismic Loading," by Austin, M.A. and Pister, K.S., June 1983, (PB84 119 288)A06.

UCB/EERC-83/11 "Shaking Table Study of Single-Story Masonry Houses: Dynamic Performance under Three Component Seismic Input and Recommendations," by Manos, G.C., Clough, R.W. and Mayes, R.L., July 1983, (UCB/EERC-83/11)A08.

UCB/EERC-83/12 "Experimental Error Propagation in Pseudodynamic Testing," by Shiing, P.B. and Mahin, S.A., June 1983, (PB84 119 270)A09.

UCB/EERC-83/13 "Experimental and Analytical Predictions of the Mechanical Characteristics of a 1/5-scale Model of a 7-story R/C Frame-Wall Building Structure," by Aktan, A.E., Bertero, V.V., Chowdhury, A.A. and Nagashima, T., June 1983, (PB84 119 213)A07.

UCB/EERC-83/14 "Shaking Table Tests of Large-Panel Precast Concrete Building System Assemblages," by Oliva, M.G. and Clough, R.W., June 1983, (PB86 110 210/AS)A11.

UCB/EERC-83/15 "Seismic Behavior of Active Beam Links in Eccentrically Braced Frames," by Hjelmstad, K.D. and Popov, E.P., July 1983, (PB84 119 676)A09.

UCB/EERC-83/16 "System Identification of Structures with Joint Rotation," by Dimsdale, J.S., July 1983, (PB84 192 210)A06.

UCB/EERC-83/17 "Construction of Inelastic Response Spectra for Single-Degree-of-Freedom Systems," by Mahin, S. and Lin, J., June 1983, (PB84 208 834)A05.

UCB/EERC-83/18 "Interactive Computer Analysis Methods for Predicting the Inelastic Cyclic Behaviour of Structural Sections," by Kaba, S. and Mahin, S., July 1983, (PB84 192 012)A06.

UCB/EERC-83/19 "Effects of Bond Deterioration on Hysteretic Behavior of Reinforced Concrete Joints," by Filippou, F.C., Popov, E.P. and Bertero, V.V., August 1983, (PB84 192 020)A10.

UCB/EERC-83/20 "Correlation of Analytical and Experimental Responses of Large-Panel Precast Building Systems," by Oliva, M.G., Clough, R.W., Velkov, M. and Gavrilovic, P., May 1988.

UCB/EERC-83/21 "Mechanical Characteristics of Materials Used in a 1/5 Scale Model of a 7-Story Reinforced Concrete Test Structure," by Bertero, V.V., Aktan, A.E., Harris, H.G. and Chowdhury, A.A., October 1983, (PB84 193 697)A05.

UCB/EERC-83/22 "Hybrid Modelling of Soil-Structure Interaction in Layered Media," by Tzong, T.-J. and Penzien, J., October 1983, (PB84 192 178)A08.

UCB/EERC-83/23 "Local Bond Stress-Slip Relationships of Deformed Bars under Generalized Excitations," by Eligehausen, R., Popov, E.P. and Bertero, V.V., October 1983, (PB84 192 848)A09.

UCB/EERC-83/24 "Design Considerations for Shear Links in Eccentrically Braced Frames," by Malley, J.O. and Popov, E.P., November 1983, (PB84 192 186)A07.

UCB/EERC-84/01 "Pseudodynamic Test Method for Seismic Performance Evaluation: Theory and Implementation," by Shing, P.-S.B. and Mahin, S.A., January 1984, (PB84 190 644)A08.

UCB/EERC-84/02 "Dynamic Response Behavior of Kiang Hong Dian Dam," by Clough, R.W., Chang, K.-T., Chen, H.-Q. and Stephen, R.M., April 1984, (PB84 209 402)A08.

UCB/EERC-84/03 "Refined Modelling of Reinforced Concrete Columns for Seismic Analysis," by Kaba, S.A. and Mahin, S.A., April 1984, (PB84 234 384)A06.

UCB/EERC-84/04 "A New Floor Response Spectrum Method for Seismic Analysis of Multiply Supported Secondary Systems," by Asfura, A. and Der Kiureghian, A., June 1984, (PB84 239 417)A06.

UCB/EERC-84/05 "Earthquake Simulation Tests and Associated Studies of a 1/5th-scale Model of a 7-Story R/C Frame-Wall Test Structure," by Bertero, V.V., Aktan, A.E., Charney, F.A. and Sause, R., June 1984, (PB84 239 409)A09.

UCB/EERC-84/06 "R/C Structural Walls: Seismic Design for Shear," by Aktan, A.E. and Bertero, V.V., 1984.

UCB/EERC-84/07 "Behavior of Interior and Exterior Flat-Plate Connections subjected to Inelastic Load Reversals," by Zee, H.L. and Moehle, J.P., August 1984, (PB86 117 629/AS)A07.

UCB/EERC-84/08 "Experimental Study of the Seismic Behavior of a Two-Story Flat-Plate Structure," by Moehle, J.P. and Diebold, J.W., August 1984, (PB86 122 553/AS)A12.

UCB/EERC-84/09 "Phenomenological Modeling of Steel Braces under Cyclic Loading," by Ikeda, K., Mahin, S.A. and Dermitzakis, S.N., May 1984, (PB86 132 198/AS)A08.

UCB/EERC-84/10 "Earthquake Analysis and Response of Concrete Gravity Dams," by Fenves, G. and Chopra, A.K., August 1984, (PB85 193 902/AS)A11.

UCB/EERC-84/11 "EAGD-84: A Computer Program for Earthquake Analysis of Concrete Gravity Dams," by Fenves, G. and Chopra, A.K., August 1984, (PB85 193 613/AS)A05.

UCB/EERC-84/12 "A Refined Physical Theory Model for Predicting the Seismic Behavior of Braced Steel Frames," by Ikeda, K. and Mahin, S.A., July 1984, (PB85 191 450/AS)A09.

UCB/EERC-84/13 "Earthquake Engineering Research at Berkeley - 1984," by , August 1984, (PB85 197 341/AS)A10.

UCB/EERC-84/14 "Moduli and Damping Factors for Dynamic Analyses of Cohesionless Soils," by Seed, H.B., Wong, R.T., Idriss, I.M. and Tokimatsu, K., September 1984, (PB85 191 468/AS)A04.

UCB/EERC-84/15 "The Influence of SPT Procedures in Soil Liquefaction Resistance Evaluations," by Seed, H.B., Tokimatsu, K., Harder, L.F. and Chung, R.M., October 1984, (PB85 191 732/AS)A04.

UCB/EERC-84/16 "Simplified Procedures for the Evaluation of Settlements in Sands Due to Earthquake Shaking," by Tokimatsu, K. and Seed, H.B., October 1984, (PB85 197 887/AS)A03.

UCB/EERC-84/17 "Evaluation of Energy Absorption Characteristics of Highway Bridges Under Seismic Conditions - Volume I and Volume II (Appendices)," by Imbsen, R.A. and Penzien, J., September 1986.

UCB/EERC-84/18 "Structure-Foundation Interactions under Dynamic Loads," by Liu, W.D. and Penzien, J., November 1984, (PB87 124 889/AS)A11.

UCB/EERC-84/19 "Seismic Modelling of Deep Foundations," by Chen, C.-H. and Penzien, J., November 1984, (PB87 124 798/AS)A07.

UCB/EERC-84/20 "Dynamic Response Behavior of Quan Shui Dam," by Clough, R.W., Chang, K.-T., Chen, H.-Q., Stephen, R.M., Ghanaat, Y. and Qi, J.-H., November 1984, (PB86 115177/AS)A07.

UCB/EERC-85/01 "Simplified Methods of Analysis for Earthquake Resistant Design of Buildings," by Cruz, E.F. and Chopra, A.K., February 1985, (PB86 112299/AS)A12.

UCB/EERC-85/02 "Estimation of Seismic Wave Coherency and Rupture Velocity using the SMART 1 Strong-Motion Array Recordings," by Abrahamson, N.A., March 1985, (PB86 214 343)A07.

UCB/EERC-85/03 "Dynamic Properties of a Thirty Story Condominium Tower Building," by Stephen, R.M., Wilson, E.L. and Stander, N., April 1985, (PB86 118965/AS)A06.

UCB/EERC-85/04 "Development of Substructuring Techniques for On-Line Computer Controlled Seismic Performance Testing," by Dermitzakis, S. and Mahin, S., February 1985, (PB86 132941/AS)A08.

UCB/EERC-85/05 "A Simple Model for Reinforcing Bar Anchorages under Cyclic Excitations," by Filippou, F.C., March 1985, (PB86 112 919/AS)A05.

UCB/EERC-85/06 "Racking Behavior of Wood-framed Gypsum Panels under Dynamic Load," by Oliva, M.G., June 1985.

UCB/EERC-85/07 "Earthquake Analysis and Response of Concrete Arch Dams," by Fok, K.-L. and Chopra, A.K., June 1985, (PB86 139672/AS)A10.

UCB/EERC-85/08 "Effect of Inelastic Behavior on the Analysis and Design of Earthquake Resistant Structures," by Lin, J.P. and Mahin, S.A., June 1985, (PB86 135340/AS)A08.

UCB/EERC-85/09 "Earthquake Simulator Testing of a Base-Isolated Bridge Deck," by Kelly, J.M., Buckle, I.G. and Tsai, H.-C., January 1986, (PB87 124 152/AS)A06.

UCB/EERC-85/10 "Simplified Analysis for Earthquake Resistant Design of Concrete Gravity Dams," by Fenves, G. and Chopra, A.K., June 1986, (PB87 124 160/AS)A08.

UCB/EERC-85/11 "Dynamic Interaction Effects in Arch Dams," by Clough, R.W., Chang, K.-T., Chen, H.-Q. and Ghanaat, Y., October 1985, (PB86 135027/AS)A05.

UCB/EERC-85/12 "Dynamic Response of Long Valley Dam in the Mammoth Lake Earthquake Series of May 25-27, 1980," by Lai, S. and Seed, H.B., November 1985, (PB86 142304/AS)A05.

UCB/EERC-85/13 "A Methodology for Computer-Aided Design of Earthquake-Resistant Steel Structures," by Austin, M.A., Pister, K.S. and Mahin, S.A., December 1985, (PB86 159480/AS)A10 .

UCB/EERC-85/14 "Response of Tension-Leg Platforms to Vertical Seismic Excitations," by Liou, G.-S., Penzien, J. and Yeung, R.W., December 1985, (PB87 124 871/AS)A08.

UCB/EERC-85/15 "Cyclic Loading Tests of Masonry Single Piers: Volume 4 - Additional Tests with Height to Width Ratio of 1," by Sveinsson, B., McNiven, H.D. and Sucuoglu, H., December 1985.

UCB/EERC-85/16 "An Experimental Program for Studying the Dynamic Response of a Steel Frame with a Variety of Infill Partitions," by Yanev, B. and McNiven, H.D., December 1985.

UCB/EERC-86/01 "A Study of Seismically Resistant Eccentrically Braced Steel Frame Systems," by Kasai, K. and Popov, E.P., January 1986, (PB87 124 178/AS)A14.

UCB/EERC-86/02 "Design Problems in Soil Liquefaction," by Seed, H.B., February 1986, (PB87 124 186/AS)A03.

UCB/EERC-86/03 "Implications of Recent Earthquakes and Research on Earthquake-Resistant Design and Construction of Buildings," by Bertero, V.V., March 1986, (PB87 124 194/AS)A05.

UCB/EERC-86/04 "The Use of Load Dependent Vectors for Dynamic and Earthquake Analyses," by Leger, P., Wilson, E.L. and Clough, R.W., March 1986, (PB87 124 202/AS)A12.

UCB/EERC-86/05 "Two Beam-To-Column Web Connections," by Tsai, K.-C. and Popov, E.P., April 1986, (PB87 124 301/AS)A04.

UCB/EERC-86/06 "Determination of Penetration Resistance for Coarse-Grained Soils using the Becker Hammer Drill," by Harder, L.F. and Seed, H.B., May 1986, (PB87 124 210/AS)A07.

UCB/EERC-86/07 "A Mathematical Model for Predicting the Nonlinear Response of Unreinforced Masonry Walls to In-Plane Earthquake Excitations," by Mengi, Y. and McNiven, H.D., May 1986, (PB87 124 780/AS)A06.

UCB/EERC-86/08 "The 19 September 1985 Mexico Earthquake: Building Behavior," by Bertero, V.V., July 1986.

UCB/EERC-86/09 "EACD-3D: A Computer Program for Three-Dimensional Earthquake Analysis of Concrete Dams," by Fok, K.-L., Hall, J.F. and Chopra, A.K., July 1986, (PB87 124 228/AS)A08.

UCB/EERC-86/10 "Earthquake Simulation Tests and Associated Studies of a 0.3-Scale Model of a Six-Story Concentrically Braced Steel Structure," by Uang, C.-M. and Bertero, V.V., December 1986, (PB87 163 564/AS)A17.

UCB/EERC-86/11 "Mechanical Characteristics of Base Isolation Bearings for a Bridge Deck Model Test," by Kelly, J.M., Buckle, I.G. and Koh, C.-G., November 1987.

UCB/EERC-86/12 "Effects of Axial Load on Elastomeric Isolation Bearings," by Koh, C.-G. and Kelly, J.M., November 1987.

UCB/EERC-87/01 "The FPS Earthquake Resisting System: Experimental Report," by Zayas, V.A., Low, S.S. and Mahin, S.A., June 1987.

UCB/EERC-87/02 "Earthquake Simulator Tests and Associated Studies of a 0.3-Scale Model of a Six-Story Eccentrically Braced Steel Structure," by Whittaker, A., Uang, C.-M. and Bertero, V.V., July 1987.

UCB/EERC-87/03 "A Displacement Control and Uplift Restraint Device for Base-Isolated Structures," by Kelly, J.M., Griffith, M.C and Aiken, I.D., April 1987.

UCB/EERC-87/04 "Earthquake Simulator Testing of a Combined Sliding Bearing and Rubber Bearing Isolation System," by Kelly, J.M. and Chalhoub, M.S., 1987.

UCB/EERC-87/05 "Three-Dimensional Inelastic Analysis of Reinforced Concrete Frame-Wall Structures," by Moazzami, S. and Bertero, V.V., May 1987.

UCB/EERC-87/06 "Experiments on Eccentrically Braced Frames with Composite Floors," by Ricles, J. and Popov, E., June 1987.

UCB/EERC-87/07 "Dynamic Analysis of Seismically Resistant Eccentrically Braced Frames," by Ricles, J. and Popov, E., June 1987.

UCB/EERC-87/08 "Undrained Cyclic Triaxial Testing of Gravels-The Effect of Membrane Compliance," by Evans, M.D. and Seed, H.B., July 1987.

UCB/EERC-87/09 "Hybrid Solution Techniques for Generalized Pseudo-Dynamic Testing," by Thewalt, C. and Mahin, S.A., July 1987.

UCB/EERC-87/10 "Ultimate Behavior of Butt Welded Splices in Heavy Rolled Steel Sections," by Bruneau, M., Mahin, S.A. and Popov, E.P., July 1987.

UCB/EERC-87/11 "Residual Strength of Sand from Dam Failures in the Chilean Earthquake of March 3, 1985," by De Alba, P., Seed, H.B., Retamal, E. and Seed, R.B., September 1987.

UCB/EERC-87/12 "Inelastic Seismic Response of Structures with Mass or Stiffness Eccentricities in Plan," by Bruneau, M. and Mahin, S.A., September 1987.

UCB/EERC-87/13 "CSTRUCT: An Interactive Computer Environment for the Design and Analysis of Earthquake Resistant Steel Structures," by Austin, M.A., Mahin, S.A. and Pister, K.S., September 1987.

UCB/EERC-87/14 "Experimental Study of Reinforced Concrete Columns Subjected to Multi-Axial Loading," by Low, S.S. and Moehle, J.P., September 1987.

UCB/EERC-87/15 "Relationships between Soil Conditions and Earthquake Ground Motions in Mexico City in the Earthquake of Sept. 19, 1985," by Seed, H.B., Romo, M.P., Sun, J., Jaime, A. and Lysmer, J., October 1987.

UCB/EERC-87/16 "Experimental Study of Seismic Response of R. C. Setback Buildings," by Shahrooz, B.M. and Moehle, J.P., October 1987.

UCB/EERC-87/17 "The Effect of Slabs on the Flexural Behavior of Beams," by Pantazopoulou, S.J. and Moehle, J.P., October 1987.

UCB/EERC-87/18 "Design Procedure for R-FBI Bearings," by Mostaghel, N. and Kelly, J.M., November 1987.

UCB/EERC-87/19 "Analytical Models for Predicting the Lateral Response of R C Shear Walls: Evaluation of their Reliability," by Vulcano, A. and Bertero, V.V., November 1987.

UCB/EERC-87/20 "Earthquake Response of Torsionally-Coupled Buildings," by Hejal, R. and Chopra, A.K., December 1987.

UCB/EERC-87/21 "Dynamic Reservoir Interaction with Monticello Dam," by Clough, R.W., Ghanaat, Y. and Qiu, X-F., December 1987.

UCB/EERC-87/22 "Strength Evaluation of Coarse-Grained Soils," by Siddiqi, F.H., Seed, R.B., Chan, C.K., Seed, H.B. and Pyke, R.M., December 1987.

UCB/EERC-88/01 "Seismic Behavior of Concentrically Braced Steel Frames," by Khatib, I., Mahin, S.A. and Pister, K.S., January 1988.